Contribution à l'étude paléomagnétique des roches déformées

Jean-Pascal Cogné

J. P. COGNÉ

ISSN 0755-978X
ISBN 2-905532-16-5

contribution à l'étude paléomagnétique de roches déformées

MEMOIRES ET DOCUMENTS
du Centre Armoricain d'Etude Structurale des Socles
n° 17
CAESS
Rennes 1987

MEMOIRES ET DOCUMENTS
DU
CENTRE ARMORICAIN D'ETUDE STRUCTURALE DES SOCLES

N°17

J.P. COGNE

Contribution à l'étude paléomagnétique des roches déformées.

Thèse d'Etat présentée devant l'Université de Rennes I
le 25 Septembre 1987

Centre Armoricain d'Etude Structurale des Socles
LP CNRS n°4661
Université de Rennes I
Campus de Beaulieu
F-35042 - RENNES Cédex
(France)

1987

ISSN : 0755-978 X

ISBN : 2-905532-16-5

Centre Armoricain d'Etude Structurale des Socles
LP CNRS n°4661
Université de Rennes I - Campus de Beaulieu
F-35042 - RENNES Cédex (France)

J.P. COGNE (1987)

Contribution à l'étude paléomagnétique des roches déformées.

Mém. Docum. Centre Arm. Et. Struct. Socles, Rennes, 17 ; 204 p.

AVANT-PROPOS.

Ce mémoire est organisé suivant trois parties principales. La première, où est exposée une synthèse des résultats obtenus, comprend une trentaine de pages rédigées en Français. De manière à faciliter la compréhension de cet exposé par les lecteurs non francophones, une traduction en Anglais de ce texte constitue la deuxième partie. La liste bibliographique, commune à ces deux textes, est donnée en fin de deuxième partie. Enfin, la troisième partie comprend un ensemble de dix annexes constituées par les photocopies d'articles parus, sous presse ou en préparation, sur lesquels s'appuie la discussion de synthèse. Une table des matières simplifiée correspondant à ces trois parties est donnée ci-dessous.

This memoir is organized following three main parts. The first one gives a synthesis and discussion of obtained results. This section is written in French. In order to help understanding of this synthesis by non french-speaking readers, an English translation is provided in a second part which is ended by the references list, common to both sections. The discussions of the synthesis are developed with constant reference to ten articles (published, in press or in prep.) given in Annexes 1 to 10 which form the third part. The relevant simplified content list is given below.

CONTRIBUTION A L'ETUDE PALEOMAGNETIQUE DE ROCHES DEFORMEES.

ANNEXE 3. J.P. COGNE. **Strain-induced AMS in the granite of Flamanville and its effects upon TRM acquisition.** Accepté à Geophys. J. R. astron. Soc.

ANNEXE 4. J.P. COGNE. **Experimental and numerical modeling of IRM rotation in deformed synthetic samples.** Accepté à Earth Planet. Sci. Lett.

ANNEXE 5. J.P. COGNE, H. PERROUD. M.P. TEXIER and N. BONHOMMET. **Strain reorientation of hematite and its bearing upon remanent magnetization.** Tectonics 5, 5, 753-767, 1986.

ANNEXE 6. J.P. COGNE, D. GAPAIS. **Passive rotation of hematite during deformation : a comparison of simulated and natural redbeds fabrics.** Tectonophysics, 121, 365-372, 1986.

ANNEXE 7. J.P. COGNE, H. PERROUD. **Strain removal applied to paleomagnetic directions in an orogenic belt : the permian red slates of the Alpes Maritimes,France.** Earth Planet.Sci. Let. 72, 125-140, 1985.

ANNEXE 8. J.P. COGNE. **Paleomagnetic direction obtained by strain removal in the Pyrenean Permian redbeds at the "Col du Somport" (France).** Earth Planet. Sci. Lett., 85, 162-172, 1987.

ANNEXE 9. **Déformation, anisotropie de susceptibilité magnétique et paléomagnétisme des séries rouges de la formation de Pont-Réan (Bretagne centrale, France).**

ANNEXE 10. J.P. COGNE, H. PERROUD. **Unstraining paleomagnetic vectors: the current state of debate.** Eos Trans., 68, 34, 705, 1987.

INTRODUCTION.

Mise à part l'hypothèse de la nature dipolaire persistante du champ magnétique terrestre, l'utilisation du vecteur aimantation rémanente en terme de marqueur géodynamique est subordonnée à deux conditions fondamentales (1) le parallélisme du vecteur aimantation et du vecteur champ magnétique au moment de l'acquisition; (2) la stabilité de l'aimantation rémanente depuis l'acquisition jusqu'à nos jours. On sait que la première condition est remplie si la roche est initialement isotrope, ou du moins faiblement anisotrope. En fait, c'est surtout à la vérification de la deuxième hypothèse que s'adresse l'ensemble des techniques mises en oeuvre par la méthodologie du paléomagnétisme moderne. On peut diviser les types d'instabilité de l'aimantation en deux grands ensembles. D'une part, il y a tout ce qui concerne un réajustement de la mémoire magnétique par réaimantation partielle ou totale au cours d'évènements thermiques ou chimiques. L'étude de la nature de l'aimantation rémanente naturelle, de ses composantes, de ses porteurs, de son âge etc..., s'appuie sur un ensemble de techniques et de tests qui constituent la plus grande part de l'analyse paléomagnétique. Elles comprennent la décomposition vectorielle des ARN par désaimantations progressives par paliers, la mesure de paramètres caractéristiques du contenu magnétique de la roche (la susceptibilité, ainsi que sa variation avec la température, par exemple) ainsi qu'une série de tests: test de contact, du pli, du conglomérat etc.... Dans le meilleur des cas, cette analyse permet de déterminer une direction moyenne d'aimantation rémanente pour une formation donnée, d'en argumenter l'âge, et d'en déduire la position d'un pôle géomagnétique virtuel.

Un deuxième type d'instabilité de l'aimantation est lié aux déviations induites par la déformation, au sens large, et plus particulièrement par le plissement des séries sédimentaires. Jusqu'à maintenant les corrections structurales des vecteurs paléomagnétiques en zone plissée reposent principalement sur la correction de pendage classique. Celle-ci consiste à appliquer au vecteur aimantation, une rotation d'angle égal au pendage du plan de stratification, autour de l'horizontale de ce plan. La comparaison des distributions de vecteurs échantillonnés dans les deux flancs d'un pli, avant et après cette correction, permet de leur attribuer un âge relatif par rapport à l'âge du plissement: antétectonique si le groupement des vecteurs est meilleur après la correction de pendage, post-tectonique s'il est meilleur avant. Une troisième situation existe lorsque les vecteurs ne sont groupés ni avant ni après correction de pendage, mais tendent à se regrouper au cours du déplissement. On suppose alors qu'elles ont été acquises au cours du plissement et on leur donne le nom d'aimantations syntectoniques. Ce test concernant l'âge relatif de l'aimantation et du plissement est connu sous le nom de test du pli et a été proposé par Graham (1949).

Si l'on se réfère à l'analyse géométrique de la déformation (translation, rotation, distorsion; Ramsay 1967) la correction de pendage consiste donc à ne considérer que la rotation rigide autour d'un axe horizontal dans l'ensemble de la déformation; rigoureusement cela n'est applicable que dans le cas de plis concentriques à axe horizontal, et sans déformation interne. Avec le développement récent des études paléomagnétiques en zone orogénique, cet algorithme s'est rapidement avéré insuffisant. Dans

un premier temps, il a été montré qu'il fallait tenir compte de la géométrie du plissement pour la détermination d'une direction d'aimantation rémanente antétectonique dans des formations plissées avec un axe incliné, ou en plusieurs phases, etc. (McDonnald 1980, Bonhommet et al. 1981, Perroud & Cobbold 1984, par exemple). Il ne s'agit cependant que d'améliorations de l'estimation de la rotation rigide totale, valides à condition de supposer que les relations angulaires vecteur aimantation/plan de stratification n'ont pas été altérées au cours des processus de plissement. Une telle condition peut etre vérifiée en l'absence totale de déformation interne; cependant il ne s'agit pas du cas général. On sait en effet que, parmi d'autres mécanismes, la déformation interne ductile peut induire des rotations de minéraux de forme anisotrope, qui aboutissent au développement d'orientations préférentielles soit de forme, soit de réseau et se traduisent par exemple par le développement d'une schistosité. Du point de vue paléomagnétique, ce mécanisme est primordial, dans la mesure où une rotation des minéraux porteurs de l'aimantation antétectonique peut être considérée comme une cause majeure de déviation de l'aimantation rémanente. Cette cause a été évoquée à de multiples reprises pour expliquer des distributions anormales de vecteurs aimantation (cf. par ex. Van den Ende 1977, Kligfield et al. 1981, Perroud 1983, Rosenbaum 1986), cependant les effets précis de la déformation interne sur l'aimantation rémanente restent mal connus. La question qui se pose, et à laquelle l'ensemble des travaux réunis dans ce mémoire tente d'apporter une réponse, est la suivante: "existe-t-il une cohérence dans les effets de la déformation interne sur l'aimantation rémanente des roches, et par conséquent, quelles sont les possibilités et limitations d'études paléomagnétiques en zone déformée ?". Les éléments de réponse que l'on tentera d'apporter à ce vaste problème sont divisés en trois parties.

Au travers de l'étude structurale, paléomagnétique et de l'anisotropie de susceptibilité magnétique du granite de Flamanville, le premier chapitre traite du problème de l'acquisition d'une aimantation rémanente par un matériau où une déformation antérieure à cette acquisition a induit une forte anisotropie du milieu.

Le problème des effets de la déformation interne accompagnant le plissement, sur l'orientation de l'aimantation rémanente antétectonique sera abordé au chapitre II. La caractérisation de ces effets sera discutée à partir des résultats de simulations analogiques et numériques, et d'études paléomagnétiques de séries rouges déformées.

Enfin, la possibilité de corriger les déviations de l'aimantation rémanente antétectonique dans les séries rouges déformées, est argumentée dans le troisième chapitre.

L'argumentation et les discussions développées au cours de ces trois chapitres s'appuient sur les résultats d'études qui ont fait l'objet de publications. Les photocopies de ces articles ou des manuscrits sont rassemblées dans les Annexes 1 à 10.

CHAPITRE I. AIMANTATION ACQUISE PAR UN MATERIAU ANISOTROPE: l'ATR dans le granite de Flamanville.

I.1. Anisotropie de susceptibilité et déformation.

En général, l'expression anisotropie de susceptibilité magnétique traduit la variabilité directionnelle de l'aimantation induite en champ faible dans un volume de roche donné. L'intensité de l'aimantation induite en champ faible est une fonction linéaire de l'intensité du champ magnétique et peut s'écrire sous la forme:

$$M_1 = k_{11} H_1 + k_{12} H_2 + k_{13} H_3$$
$$M_2 = k_{21} H_1 + k_{22} H_2 + k_{23} H_3$$
$$M_3 = k_{31} H_1 + k_{32} H_2 + k_{33} H_3$$

ou, $M_i = k_{ij} H_j \qquad i, j = 1,2,3$

avec M_i: composantes cartésiennes du vecteur aimantation induite

H_j: composantes cartésiennes du vecteur champ magnétique

k_{ij}: tenseur symétrique 3x3 cartésien de second ordre appelé tenseur d'anisotropie de susceptibilité magnétique (ASM). Ce tenseur possède trois valeurs propres réelles k_1, k_2 et k_3 qui sont les susceptibilités principales.

D'après Hrouda (1982), les causes de l'anisotropie de susceptibilité magnétique dans les roches sont habituellement résumées de la manière suivante:

(1) Alignement de forme des grains ferromagnétiques
(2) Alignement des réseaux de grains à forte anisotropie magnétocristalline
(3) Alignement de domaines magnétiques
(4) "chainage" de grains magnétiques
(5) Anisotropie due à contraintes
(6) Anisotropie d'échange.

Parmi celles-ci, les causes (1) et (2) sont considérées comme les causes dominantes controlant l'anisotropie de susceptibilité magnétique des roches.

La mesure de l' ASM d'une roche est donc, au même titre que d'autres types de mesures (goniométrie de texture en diffractométrie X par exemple), une mesure de la fabrique d'une roche. L'orientation préférentielle soit de forme, soit de réseau, des minéraux magnétiques est controlée par des processus classiques de dépot et compaction dans les roches sédimentaires, mise en place sous contrainte des roches effusives, déformation ductile pour tous les types de roches. L'anisotropie de susceptibilité magnétique peut, à ce titre, être utilisée comme outil d'analyse structurale pour à peu près tous les types de roches.

Un nombre important d'études a été consacré à cet aspect des relations entre anisotropie de susceptibilité magnétique et déformation (voir la revue par Hrouda (1982)). Elles ont en général montré que la déformation interne totale controle le développement de l'ASM, tant du point de vue de l'orientation des directions principales que des variations de forme et d'intensité de l'ellipsoide d'ASM (voir en particulier les travaux de Wood et al. 1976, Hrouda 1976, 1979, 1980, Rathore 1979, Elwood & Whitney 1980, Wagner et al. 1981, Kligfield et al. 1983, Rathore et al. 1983, parmi

d'autres). Une étude expérimentale récente des effets de la déformation interne sur l'ASM d'échantillons synthétiques à magnétite, a permis a Borradaile & Alford (1987) de confirmer de manière détaillée cette analyse. Les résultats les plus significatifs sont les suivants. (1) A partir d'une fabrique magnétique préexistante, la déformation interne induit un réajustement de l'ASM dont l'axe minimum tend à se paralleliser avec l'axe d'élongation minimum de la déformation. (2) L'ASM garde cependant une mémoire de la fabrique initiale; cela signifie qu'elle ne reflète pas le dernier incrément de déformation, mais bien la déformation totale (voir à ce sujet l'évolution de la fabrique magnétique décrite dans les séries rouges du Sud de Rennes en Annexe 9). (3) Enfin, l'anisotropie de susceptibilité croît avec l'intensité de la déformation, au moins jusqu'aux 35% de raccourcissement homogène obtenus par ces auteurs. Dans le cas général, il n'apparait cependant toujours pas raisonnable de calibrer la déformation interne en terme d'anisotropie de susceptibilité.

Les résultats de nos propres investigations conduites dans ce sens sur le granite de Flamanville sont reportés Annexe 1. Les conclusions à ce travail sont tout à fait similaires à celles d'études semblables: il existe une bonne correlation entre les directions de déformation interne et les directions des susceptibilités principales d'une part, et entre les valeurs de déformation interne et les valeurs des susceptibilités principales, d'autre part. En l'absence de lois théoriques sur les relations déformation/ASM, cette dernière correlation ne peut être qu'empirique. Ce point est discuté en Annexe 1. On peut cependant souligner que si les valeurs des susceptibilités ne permettent pas de dériver directement des valeurs de déformation interne sans un contrôle minimum de ces dernières, les variations relatives de ces susceptibilités au travers d'une zone sont, elles, directement reliées aux variations de déformation dans cette zone. Cela signifie que l'ASM peut constituer un moyen rapide, efficace et précis pour étudier des gradients de déformation, élément somme toute le plus significatif dans le cadre d'études structurales régionales.

I.2. Anisotropie de susceptibilité magnétique et anisotropie d'aimantation rémanente: l'exemple du granite de Flamanville.

La propriété élémentaire de l'ASM est que dans un milieu anisotrope le vecteur aimantation n'est pas parallèle au vecteur champ. Cette propriété vérifiée dans le cas de l'aimantation induite (c'est ce qui constitue la base meme de la mesure de l'anisotropie de susceptibilité), est généralement considérée comme importante en paléomagnétisme, dans la mesure où l'aimantation rémanente acquise par un matériau anisotrope ne reflète plus nécéssairement la direction du champ magnétique terrestre ancien. Cependant, bien que ce problème soit reconnu comme important, très peu de développements théoriques ont été faits pour tenter d'établir les relations entre anisotropie de susceptibilité et anisotropie d'aimantation rémanente. Seules les déviations de l'aimantation thermorémanente (ATR) dans les roches à magnétite polydomaine ont fait l'objet de développements en 2 dimensions (applicables uniquement aux ellipsoides de révolution) que l'on trouve dans Nagata (1961), ou Stacey & Banerjee (1974), par exemple. Plus récemment, Stephenson et al. (1986) ont montré qu'il existait théoriquement une relation linéaire entre les valeurs propres du tenseur d'ASM et celles du tenseur d'ATR et également du tenseur d'aimantation rémanente isotherme (ARI).

Cependant, si cette relation linéaire a des justifications théoriques , elle nécessite ici aussi d'être établie pour chaque type de roche étudié.

Dans le cadre général de l'étude des effets de la déformation sur l'aimantation rémanente, et celui, plus particulier des déviations de l'ATR acquise postérieurement à la déformation, j'ai été amené à proposer un développement théorique en 3 dimensions des relations entre tenseur d'anisotropie de susceptibilité magnétique et tenseur d'anisotropie d'ATR dans les roches à magnétite polydomaine en assemblage anisotrope. Ce développement est donné en Annexe 2. Une relation simple a été mise en évidence entre ces deux tenseurs, montrant que ceux-ci ont les mêmes vecteurs propres et que les rapports de leurs valeurs propres suivent une relation quadratique du type $M_i/M_j \approx (k_i/k_j)^2$ où k_i sont les susceptibilités principales, et M_i les valeurs propres du tenseur d'anisotropie d'ATR. On a donc là, contrairement au cas ASM/déformation, une relation théorique directe entre les deux tenseurs. Une mesure de l'ASM permet par conséquent une estimation directe de l'ordre de grandeur du tenseur d'anisotropie d'ATR. Des acquisitions d'ATR sur des échantillons de roches à forte ASM ont permis de vérifier cette corrélation.

Enfin, l'étude paléomagnétique du granite anisotrope de Flamanville, présentée en Annexe 3, m'a permis, d'une part de montrer que l'anisotropie de susceptibilité magnétique était accompagnée par des déviations significatives de l'aimantation thermorémanente primaire de ce granite, et d'autre part, de vérifier qu'à partir des mesures d'ASM, il est possible d'estimer un tenseur normalisé d'anisotropie d'ATR qui, après inversion, permet de calculer une direction de paléochamp fiable en utilisant ces ATR déviées.

I.3. Conclusions.

Les principales conclusions liées à ces travaux sont déjà données dans les Annexes 1 à 3. On peut cependant insister sur les points suivants.

On notera qu'en ce qui concerne les déviations de l'ATR, on n'a jamais eu à prendre position sur les mécanismes de déformation. Il suffit en effet que l'ASM existe (et qu'elle n'évolue plus) au moment où l'ATR est acquise, pour qu'il existe des déviations de celle-ci. On peut donc penser que si l'on est capable d'établir les relations théoriques entre l'aimantation induite et les différents types d'aimantation rémanente, l'anisotropie de susceptibilité magnétique peut fournir une estimation de l'anisotropie de l'aimantation rémanente, quel que soit le processus physique du développement de l'orientation préférentielle des minéraux porteurs de l'aimantation. C'est ce raisonnement à 2 niveaux ((1) la déformation est la cause de l'ASM, mais (2) c'est l'ASM qui permet de déterminer l'anisotropie d'aimantation rémanente) qui fait la différence fondamentale entre l'étude de l'aimantation acquise après déformation et l'étude de l'aimantation acquise avant déformation puis déviée, cas où il n'existe plus nécessairement de relation simple entre ASM et déviation de l'aimantation.

Par ailleurs, bien que la présente étude n'ait porté que sur l'ATR des magnétites polydomaines, son domaine d'application est probablement assez large en paléomagnétisme du fait du caractère courant de ce porteur magnétique. Quoi qu'il en soit, on ne peut se permettre de négliger l'effet de l'ASM, et un controle systématique de celle-ci apparait nécessaire lors d'études paléomagnétiques en zone déformée.

CHAPITRE II. DEFORMATION ET AIMANTATION REMANENTE ANTETECTONIQUE.

II.1. Introduction.

La caractérisation des effets de la déformation interne sur l'aimantation rémanente antétectonique constitue la part majeure du travail présenté dans ce mémoire. La plupart des résultats obtenus sont publiés ou sont en voie de l'etre. Les photocopies de ces articles sont réunies dans les Annexes 4 à 9, et une synthèse est donnée en Annexe 10.

La nécessité d'étudier les effets de la déformation interne sur l'aimantation rémanente antétectonique est apparue récemment, parallèlement à l'établissement d'autres méthodologies liées au développement du paléomagnétisme en zone orogénique. Bien que la déformation interne soit généralement considérée comme source majeure de perturbation de la mémoire magnétique d'une roche, et que quelques investigations ponctuelles aient été publiées (Van den Ende 1977, Ozima 1980, Kligfield et al. 1981, Facer 1983, Rosenbaum 1986, Anson & Kodama 1987), aucune caractérisation approfondie n'a été proposée. De ce fait, des critères établis en vue de simplifier les problèmes ont guidé notre approche. Ces quelques critères peuvent être résumés de la manière suivante: (1) Une direction paléomagnétique de référence (à l'état non déformé) doit être connue pour les séries naturelles étudiées. (2) L'aimantation rémanente antétectonique ne doit pas avoir été effacée par la déformation. (3) Seul un mécanisme de rotation des particules magnétiques doit pouvoir être envisagé. (4) La déformation totale homogène de chaque site d'échantillonnage paléomagnétique doit pouvoir être quantifiée. (5) Il doit exister des variations de l'intensité de la déformation, et des directions des axes principaux de la déformation par rapport à celles de l'aimantation rémanente antétectonique de référence.

Compte tenu de ces contraintes, des séries pélitiques rouges modérément déformées ont été choisies comme objet naturel d'étude. La forme anisométrique des cristaux d'hématite permet de supposer qu'ils subissent des rotations au cours de la déformation, et leur mémoire magnétique est stable. Le plan de stratification des séries sédimentaire supposé initialement horizontal, est un bon marqueur de la rotation rigide, et la présence fréquente dans les séries rouges de zones elliptiques décolorées (taches de réduction) fournit de bons marqueurs de la déformation interne. Cependant, avant de présenter les résultats des études paléomagnétiques et structurales de séries naturelles déformées (Annexes 7, 8 et 9), on détaillera les résultats expérimentaux de simulations analogiques (Annexe 4) et numériques (Annexe 5), où les effets de la rotation de cristaux d'hématite, induite par la déformation interne, sur l'aimantation rémanente ont été modélisés.

II.2. Les modèles.

II.2.1. Simulation analogique et simulation numérique.

Les quelques simulations analogiques dont les résultats ont été publiés dans la littérature permettaient de penser que la déformation continue d'échantillons aimantés s'accompagne de déviations de l'aimantation rémanente, dont l'angle avec l'axe de raccourcissement tend à croître avec le taux de déformation (Blow & Hamilton 1978, Ozima 1980, Morash & Bonhommet

1981). Cependant, le mécanisme physique induisant ces déviations n'a jamais été totalement contraint bien qu'il soit globalement attribué à des rotations des porteurs magnétiques.

Reprenant et complétant les expériences de Morash (1981), j'ai réalisé une modélisation analogique par raccourcissement coaxial d'échantillons artificiels constitués de plasticine contenant de la poudre d'hématite en cristaux anisométriques aplatis. Les variations en direction, intensité et groupement d'une aimantation rémanente isotherme (ARI), en fonction des taux de raccourcissement, ont été étudiées. Les résultats sont reportés en Annexe 4, où ils sont comparés avec les résultats d'une simulation numérique. Cette simulation numérique (Annexe 5) consiste à étudier le comportement de la somme vectorielle de N micromoments magnétiques, chaque micromoment étant porté par une particule planaire se comportant en plan passif durant la déformation (modèle de March, 1932). Cette comparaison a montré que les résultats provenant de ces deux simulations sont identiques. Cependant du point de vue des mécanismes de rotations des grains, cette identité de résultats est paradoxale et nécessite d'etre discutée.

II.2.2. Rotation rigide de particules planaires et rotation passive de plans.

Avant d'examiner en détail ce paradoxe, il convient de redéfinir les différents mécanismes de rotations envisageables à l'échelle du grain. J'en distinguerai 3 principaux. Pour les deux premiers, on modélise la "particule" par un ellipsoide ayant un contraste de viscosité donné avec la matrice. Le cas général a été étudié par Bilby et al. (1975), on ne considerera que les cas extrêmes suivants: (1) le contraste de viscosité est nul, la particule se déforme de manière homogène avec la matrice; c'est ce qu'on appelle strictement le comportement passif. Un bon exemple d'un tel comportement nous est donné par les taches de réduction dans les séries rouges, la forme de ces taches fournissant une mesure de la déformation de l'ensemble du volume matrice + taches. (2) Le contraste de viscosité est infini; on parle alors de particules rigides et la rotation de ces particules lors de la déformation est qualifiée de rotation rigide des particules. Il est clair que les particules d'hématite contenues dans une matrice de plasticine (Annexe 4) correspondent de près à ce modèle. (3) Pour le troisième mécanisme, les particules allongées sont modélisées comme les lignes et les particules aplaties comme des plans et durant la déformation elles se comportent comme des lignes et des plans passifs suivant le modèle de March (1932). Ce modèle, nommé par Owens (1974) "line/plane model" est celui qui a été utilisé pour la rotation des particules de la simulation numérique (Annexe 5). Un rappel des équations de transformation des lignes et plans passifs a été fait à l'occasion de l'étude paléomagnétique des séries rouges des Alpes Maritimes (Annexe 7).

Il n'y a, à priori, pas de raison que la rotation de particules rigides et la rotation de lignes ou plans passifs soient identiques dans le cas général. Pourtant, du point de vue de l'aimantation, j'ai obtenu des résultats similaires en simulation numérique (Annexe 5), où le mécanisme (3) était modélisé, et en simulation analogique (Annexe 4) où le mécanisme (2) est le plus probable. Si on interprète le comportement de l'aimantation comme résultant de la rotation des grains, il faut admettre que les rotations des grains dues à ces deux mécanismes sont ici similaires. C'est ici que réside le paradoxe évoqué plus haut.

Pour tenter d'expliquer cette identité de rotation, j'ai effectué une comparaison en deux dimensions des rotations de particules rigides et des

rotations de lignes passives. A partir des équations générales proposées par Bilby et al. (1975), P. Cobbold et D. Gapais ont établi les équations correspondant à quelques conditions aux limites particulières. Parmi celles-ci, la rotation due à un raccourcissement coaxial ("Pure Shear" en 2-D) d'un grain elliptique ayant un contraste de viscosité infini avec la matrice qui le contient, peut s'écrire (D. Gapais, comm. pers.):

$$\tan \Phi = (\lambda_1/\lambda_2)^x . \tan \Phi_o \qquad (1)$$

où Φ_o est l'angle initial entre le grand axe du grain elliptique et l'axe d'allongement de la déformation et Φ cet angle après déformation. L'exposant 'x' est fonction de l'ellipticité du grain et s'écrit :

$$x = \frac{1/R^2 - 1}{1/R^2 + 1}$$

où R est le rapport axial de la particule elliptique. Rappelons pour mémoire que la rotation de la ligne passive dans ce cas particulier peut s'écrire

$$\tan \Phi = (\lambda_2/\lambda_1) . \tan \Phi_o \qquad (2)$$

On remarquera que lorsque $R \to \infty$, $x \to -1$ et la première expression se réduit à la seconde. En déformation coaxiale 2-D, on peut donc définir la ligne passive comme une particule elliptique rigide de longueur infinie. Afin d'estimer la limite d'ellipticité à partir de laquelle on peut assimiler la particule rigide à une ligne passive, les courbes correspondant à l'équation (1) ci-dessus ont été tracées pour différentes valeurs initiales Φ_o , à rapport axial R croissant, et pour différentes intensités de déformation λ_1/λ_2 de 1.5 à 10 (Fig. II.1). On peut constater que, quelle que soit la valeur de λ_1/λ_2, la rotation de particules rigides devient très rapidement identique à celle de lignes passives (traits fins sur les diagrammes). A partir d'un rapport axial de 3 pour la particule rigide, la différence de rotation de celle-ci et de la ligne passive est en général inférieure à 5°. Cela signifie que, en déformation par raccourcissement coaxial, les particules rigides peuvent être assimilées à des lignes ou des plans passifs à partir d'une anisotropie de forme modérée. Le fait que les particules planaires utilisées en simulation analogique ont un rapport epaisseur:longueur de 1:20 à 1:30 permet probablement d'expliquer la similitude des résultats obtenus par simulations numériques et simulations analogiques du comportement de l'aimantation (Annexes 4 et 5).

Il faut cependant noter que cette analyse ne s'applique strictement que dans le cas de déformations coaxiales. En ce qui concerne les déformations fortement non coaxiales, cisaillement simple par exemple, seules d'autres simulations et études de séries naturelles déformées permettraient d'en envisager les conséquences sur l'aimantation rémanente.

II.2.3. Rotation des porteurs magnétiques et rotation de l'aimantation rémanente.

Pour compléter cette analyse on doit finalement considérer, non plus le mécanisme de rotation des grains, mais en quoi ce mécanisme induit une rotation cohérente de l'aimantation rémanente mesurable (=somme des micromoments portés par les grains). Ce point a été particulièrement discuté dans l'exposé des résultats de la simulation analogique (Annexe 4). On peut en résumer l'analyse de la manière suivante. Du fait de la forte anisotropie magnétocristalline de l'hématite, seules les particules dont le plan basal

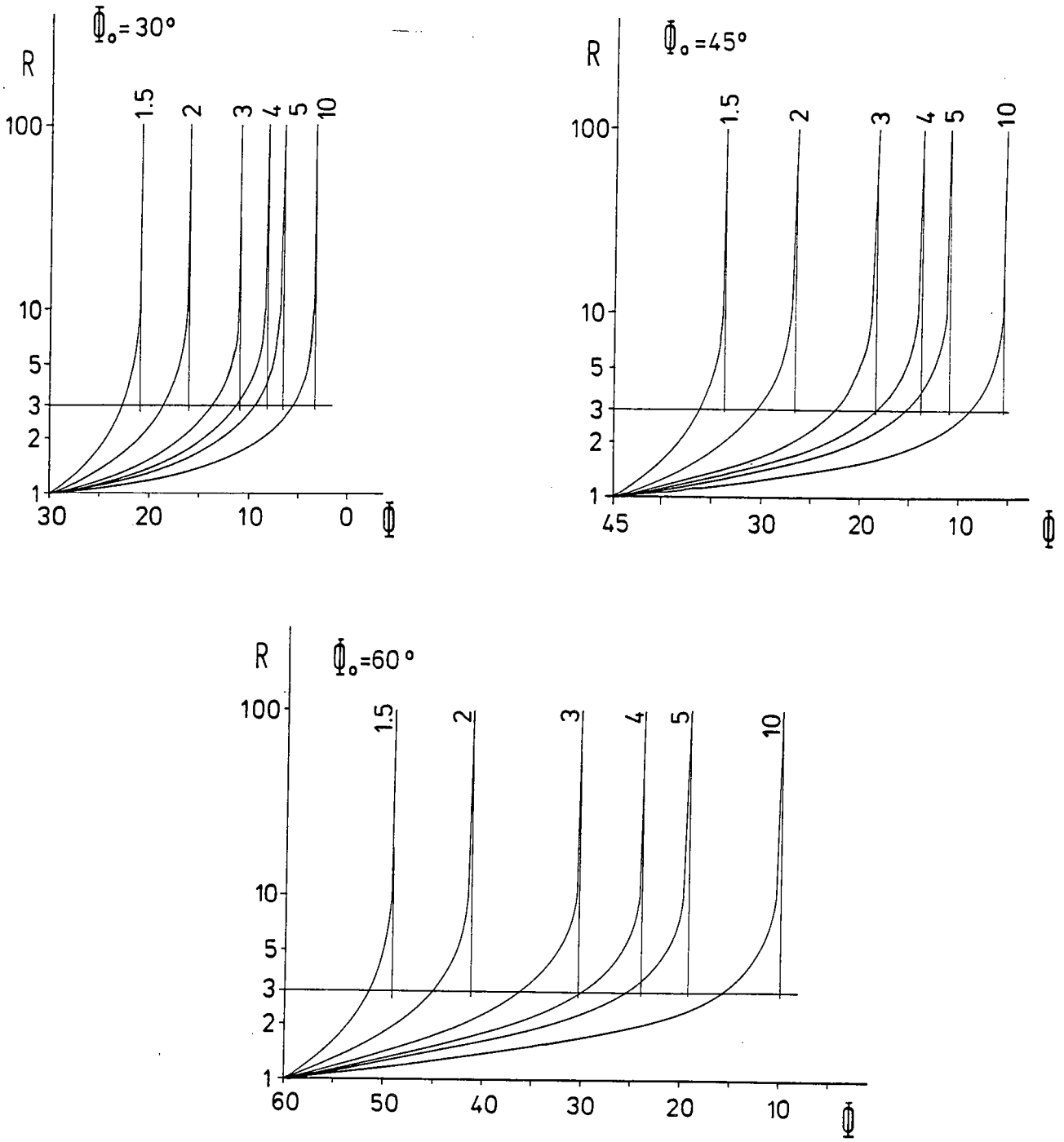

Fig.II.1 : Variations de l'angle Φ entre le grand axe d'une particule elliptique rigide et l'axe d'allongement de la déformation (λ_1) en fonction du rapport d'ellipticité R de la particule. Trois cas d'angle initial Φ_o = 30°, 45° et 60° ont été considérés. Chaque courbe correspond à une intensité de déformation, exprimée par le rapport λ_1/λ_2 croissant de 1.5 à 10. Les traits fins verticaux donnent la déviation de la ligne matérielle pour ces valeurs de déformation.

contient le vecteur champ magnétique acquerront un moment magnétique significatif dans la rémanence totale. En schématisant à l'extrême, les autres particules auront une contribution négligeable à la rémanence, et leur rotation ultérieure, un effet négligeable sur la déviation de la rémanence. Les micromoments "significatifs" étant contenus dans les plans "passifs" auront eux-mêmes un comportement passif lors de la déformation: (1) stabilité lors d'un raccourcissement orthogonal à leur position moyenne. (2) Déviation symétrique autour de la direction de raccourcissement lorque celle-ci est parallèle à leur position moyenne initiale; il en résulte une baisse de l'intensité de l'aimantation mesurable à l'échelle de l'échantillon, et une augmentation de la dispersion initiale pour plusieurs échantillons (ces deux phénomènes sont d'ailleurs liés), la direction moyenne de l'aimantation d'un bloc restant stable. (3) Déviation plus ou moins homogène des micromoments passifs provoquant une déviation globale de l'aimantation résultante vers le plan d'aplatissement. Le comportement de l'aimantation rémanente mesurable apparait donc globalement comparable au comportement de chaque micromoment. Cependant, la rotation passive de chaque micromoment n'induit pas nécéssairement un comportement exactement passif de la somme vectorielle. Les écarts du comportement de l'aimantation rémanente au comportement de la ligne passive sont discutés au Chapitre III.

Cette analyse fait ressortir deux points: pour que l'aimantation soit déviée lors de la déformation, il faut (1) que les minéraux magnétiques possèdent une anisotropie de forme suffisante pour pouvoir subir des rotations, (2) que les minéraux magnétiques aient une anisotropie d'acquisition de l'aimantation liée à cette anisotropie de forme. Ces conditions sont remplies pour l'hématite (anisotropie magnétocristalline importante liée au plan basal des cristaux d'hématite planaire), et peuvent etre suspectées dans le cas de magnétite en aiguille, ou l'anisotropie de forme contraint l'aimantation à s'aligner avec l'axe du grain.

II.3. Etudes paléomagnétiques de séries rouges déformées.

L'étude des effets de la déformation interne sur l'orientation de l'aimantation rémanente antétectonique a été menée sur 3 formations rouges déformées: les séries rouges Permiennes des Alpes Maritimes (Annexe 7), les séries rouges Permiennes des Pyrénées au Col du Somport (Annexe 8), les séries rouges Ordoviciennes de la formation de Pont-Réan, Bretagne Centrale (Annexe 9).

Dans toutes ces séries, la déformation interne a pu être quantifiée en chaque site d'échantillonnage à l'aide des mesures de rapports axiaux et d'orientation de taches de réduction elliptiques.

Dans le cas des séries rouges des Alpes Maritimes, on a pu montrer que la déformation interne était accompagnée d'une rotation progressive des minéraux d'hématite. Celle-ci a été quantifiée par l'étude des orientations préférentielles d'axes {104} de l'hématite par goniométrie de texture en diffractométrie X. Une comparaison de ces fabriques avec des fabriques simulées suivant un modèle de rotation passive des minéraux planaires a montré que ce mécanisme rend convenablement compte des fabriques naturelles d'hématite dans ces séries. Cette analyse est détaillée en Annexe 6.

En ce qui concerne les séries rouges du Sud de Rennes, les mesures d'anisotropie de susceptibilité ont également été interprétées en terme de rotation progressive de l'hématite, sans toutefois pouvoir affirmer le caractère exactement passif de cette rotation (Annexe 9).

D'importantes recristallisations secondaires d'hématite ont été constatées dans les séries rouges Permiennes du Col du Somport. Celles-ci ont été gênantes sur deux points essentiels. D'une part elles ont empêché de tester le contrôle de la déformation sur l'orientation préférentielle des hématites primaires (Annexe 6); d'autre part, les réaimantations dues à ces recristallisations ont rendu difficile la détermination de la direction d'aimantation rémanente antétectonique et, par conséquent, impossible une analyse détaillée des effets de la déformation interne sur celle-ci (Annexe 8).

Par contre, une telle analyse a pu être faite dans les deux autres exemples étudiés. Elle a permis de montrer qu'il existe une bonne cohérence dans le comportement de l'aimantation rémanente antétectonique vis-à-vis de la déformation.

II.4. Synthèse et discussion.

II.4.1. Distribution intrasite et distribution intersite des aimantations à l'état déformé.

Une première synthèse des effets de la déformation interne sur l'orientation et le groupement de l'aimantation rémanente est presentée en Annexe 10. A l'époque où cet article était rédigé, je ne disposais ni de l'analyse des résultats de la simulation analogique (Annexe 4) ni de celle des résultats de l'étude paléomagnétique complémentaire des séries rouges Ordoviciennes de la Formation de Pont-Réan (Annexe 9). Ces deux dernières études s'intègrent néanmoins parfaitement bien à l'analyse globale du problème donné en Annexe 10, et confirment cette analyse.

L'ensemble des études présentées ici (Annexes 4 à 10) permet de caractériser l'effet de la déformation interne sur l'aimantation rémanente antétectonique. Cet effet peut être décrit par un phénomène fondamental, la déviation du vecteur aimantation vers le plan d'aplatissement de la déformation. Dans cette description, le vecteur aimantation est défini à l'échelle du spécimen couramment mesurable. A l'intérieur d'un site d'échantillonnage, défini comme le volume maximum dans lequel on peut considérer que la déformation est homogène, la déviation mesurable à l'échelle de chaque échantillon aura des conséquences diverses sur l'évolution de la direction moyenne et de sa dispersion, qui dépendront essentiellement des relations angulaires initiales entre direction d'aimantation et direction de raccourcissement. Divers cas ont été envisagés lors des simulations analogiques (Annexe 4) et les effets constatés à l'échelle des blocs de plasticine ("hand-samples") se sont trouvés vérifiés à l'échelle des sites de déformation homogène des études paléomagnétiques (en particulier Annexes 7 et 9).

Il me semble ici particulièrement important d'insister sur un point de méthodologie. Dans l'étude de la déformation finie, il est généralement admis que l'analyse de domaines à déformation hétérogène se fait par l'étude de domaines suffisamment petits pour que la déformation puisse y être considérée comme homogène (Cf. Ramsay 1967). Il en va de même en ce qui concerne l'étude des effets de la déformation interne sur l'aimantation rémanente. Avant de chercher à analyser la distribution des directions d'aimantation au travers d'une série plissée (domaine de déformation typiquement hétérogène), il convient tout d'abord d'étudier et de caractériser les effets de la déformation interne homogène. C'est cette démarche qui a permis de comparer les résultats des simulations analogiques aux dispersions et déviations

intrasites des aimantations naturelles. La distribution inter-site in-situ des directions d'aimantation dépend ensuite de la distribution de la déformation interne au travers de la zone plissée, et peut donc être extrêmement variable: suivant un grand cercle dans les Alpes Maritimes (cf en particulier figures 9 et 10 Annexe 7), fisherienne dans la Formation de Pont-Réan (Annexe 9), grossièrement sur un petit cercle au Col du Somport (Annexe 8). Il n'apparait donc pas raisonnable d'essayer de caractériser, dans le cas général, la distribution des aimantations à l'échelle d'une série plissée avec déformation interne.

II.4.2. Déviation de l'aimantation et test du pli.

Malgré les réserves émises ci-dessus en ce qui concerne une caractérisation globale des effets de la déformation à l'échelle d'une série plissée, il existe cependant un effet de première importance à cette échelle, qui est la modification de l'angle initial entre aimantation et plan de stratification. De ce fait, le test du pli, en tant que test statistique, est inutilisable dans son acceptation courante. Il a été montré que les aimantations antétectoniques peuvent présenter une évolution caractéristique d'aimantations syntectoniques, dans le cas des séries rouges des Alpes-Maritimes (Annexe 7), ou même post-tectoniques dans le cas de la formation de Pont-Réan (Annexe 9), au cours du déplissement classique. Ces appréciations qualitatives, basées sur la comparaison des distributions avant et après correction de pendage, peuvent être précisées par l'étude de l'évolution du paramètre 'k' (Fisher, 1953) des groupements, en fonction des pourcentages de déplissement progressif par paliers ('stepwise unfolding'). Cette méthode a été proposée récemment par Scotese & Van Der Voo (1983) qui montrent que dans le cas d'une réaimantation syntectonique, le paramètre de précision 'k' passe par une valeur maximale au cours du déplissement progressif. Depuis cette démonstration, un certain nombre d'auteurs ont utilisé cette méthode, et considéré l'obtention d'un 'kmax' avant 100% de déplissement comme un argument définitif en faveur d'un âge syntectonique de l'aimantation (voir par exemple, McCabe et al. 1983, Miller & Kent 1986 a et b, Kent & Opdyke 1985, parmi d'autres).

L' application de cette méthode aux données paléomagnétiques des séries rouges des Alpes Maritimes et de la Formation de Pont-Réan, donne les résultats illustrés Fig.II.2 (d'après les données des Annexes 7 et 9). On constate que pour les 3 groupes de données, les paramètres 'k' de groupement passent par un maximum au cours du déplissement progressif, à environ 30% de déplissement pour le groupe I des Alpes-Maritimes (Cf. Annexe 7), 45% pour le groupe II, 25% pour les données de la Formation de Pont-Réan. L'évolution des groupements de ces données devrait par conséquent conduire, du point de vue purement statistique, à l'interprétation erronée d'aimantations syn- à post-tectoniques.

Cet aspect des résultats des études paléomagnétiques de séries rouges déformées rejoint deux analyses théoriques récentes de Van der Pluijm (1986, 1987) et Kodama (1986 a et b, 1987). Sur la base de modèles simples 2-D du comportement de l'aimantation en cours de plissement avec déformation interne, ces auteurs remettent en cause l'interprétation syntectonique des aimantations basée sur l'évolution des groupements de données au cours du déplissement progressif par rotations rigides partielles. Il est ainsi démontré que l'argument statistique (augmentation du paramètre 'k' de groupement pour un pourcentage donné de déplissement) ne constitue pas à lui seul une démonstration de l'âge syntectonique d'une aimantation, bien qu'il

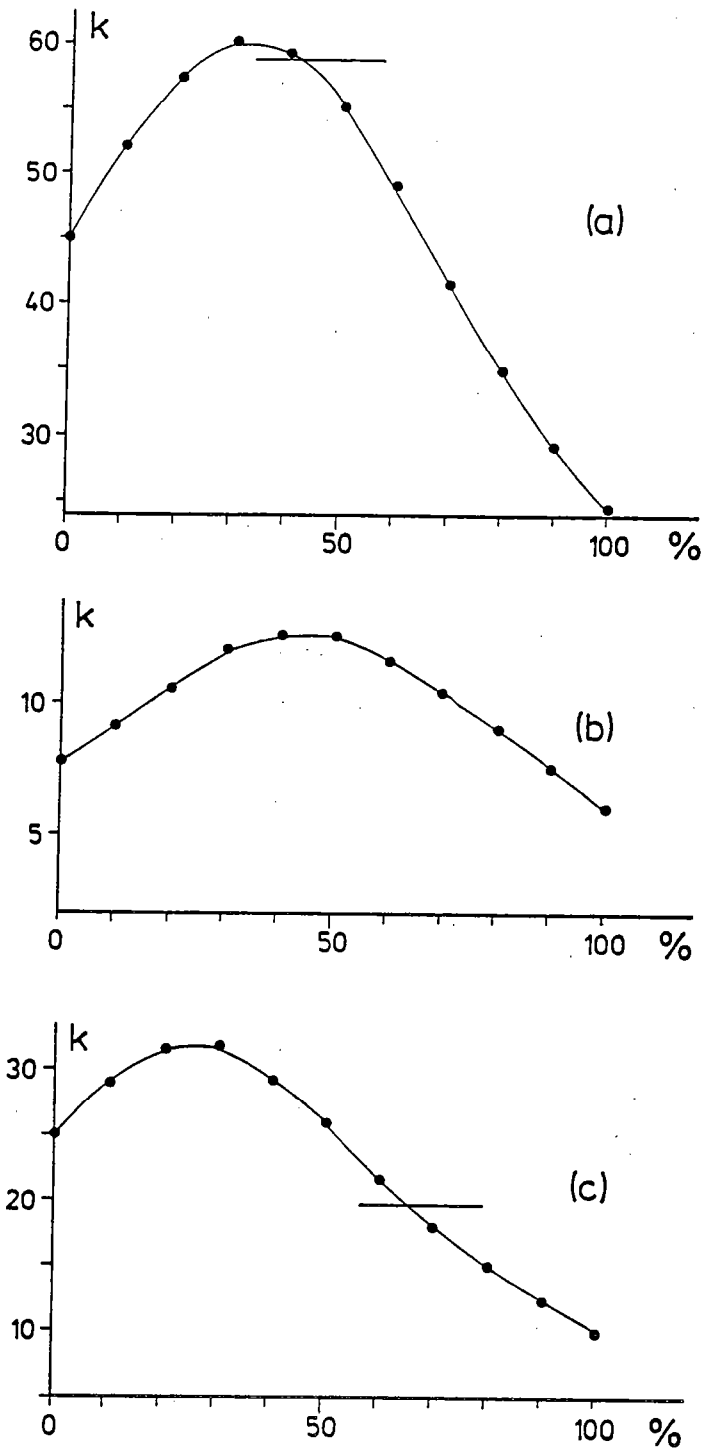

Fig.II.2: Evolution du paramètre k (Fisher 1953) de groupement des distributions intersites dans les séries rouges déformées, en fonction du pourcentage (%) de déplissement; (a) groupe I des Alpes Maritimes (cf. Annexe 7); (b) groupe II des Alpes Maritimes; (c) Formation de Pont-Réan (Annexe 9). Les traits fins horizontaux en (a) et (c) indiquent le seuil de probabilité à 95% au-dessus duquel les valeurs de k sont significativement supérieures au paramètre k des données à 100% de déplissement (i.e. corrigées du pendage).

soit une condition nécéssaire pour cette interprétation. En effet, il faut de plus démontrer l'absence de déformation interne liée au plissement. Ici également, la mesure de l'anisotropie de susceptibilité magnétique doit permettre de vérifier aisément l'existence, ou non, d'une orientation préférentielle des porteurs magnétiques accompagnant les processus de plissement.

II.5. Conclusion.

La déformation progressive des séries rouges étudiées s'accompagne, indépendemment des recristallisations, d'une rotation progressive des minéraux planaires d'hématite. Cette réorientation progressive de l'hématite, dont le plan basal tend à s'aligner dans la schistosité, a été vérifiée par mesure des orientations préférentielles d'axes {104} de l' hématite par goniométrie de texture en diffractométrie X, ou par mesure de l'anisotropie de susceptibilité.

L'aimantation rémanente, schématisée par la somme vectorielle des micromoments portés par chaque particule, subit des déviations et des changements de groupement qui ont été caractérisés à l'aide de simulations en raccourcissement coaxial. Les caractéristiques des distributions de vecteurs aimantation lors de ces simulations ont été retrouvées lors des études paléomagnétiques de séries naturelles. On peut résumer les effets de la déformation sur l'aimantation en un seul phénomène fondamental: la déviation du vecteur aimantation élémentaire (= mesurable dans le plus petit volume possible) vers le plan d'aplatissement. On peut ensuite envisager les conséquences logiques de ce comportement, sur l'évolution en groupement et direction de populations de vecteurs, en fonction de leurs relations angulaires initiales avec les axes de la déformation interne homogène.

A partir de cette cohérence dans la description des effets de la déformation interne homogène sur l'aimantation rémanente antétectonique, on est finalement amené à se poser la question de la possibilité de corriger les déviations de l'aimantation, dans le but d'estimer la direction de champ magnétique ambiant lors de l'acquisition.

CHAPITRE III : DEFORMATION INVERSE DE L'AIMANTATION REMANENTE ANTETECTONIQUE.

III.1. L'algorithme et son application.

L'analyse des déviations de l'aimantation rémanente et des dispersions intrasites qui en résultent, m'a conduit, lors de l'étude paléomagnétique des séries rouges des Alpes Maritimes (Annexe 7), à poser l'hypothèse de base du traitement de déformation inverse des vecteurs aimantations: la distribution des vecteurs aimantations à l'état déformé, ainsi que les variations de cette distribution en fonction de la déformation, sont comparables aux distributions de lignes passives, ou lignes matérielles, dans ces conditions de déformation. A partir de cette observation, on peut tenter de corriger les déviations du vecteur aimantation, en utilisant les lois de comportement de la ligne passive suivant le modèle de March (1932).

Une nuance importante est à noter ici: on ne suppose pas que le vecteur aimantation est une ligne matérielle (ligne joignant deux points matériels du volume considéré), ce qui est évidemment un modèle irréaliste, mais on constate que les déviations du vecteur aimantation sont analogues à celles de lignes matérielles, au moins dans les cas étudiés. La déformation inverse des directions d'aimantation suivant l'hypothèse du modèle de March (1932) est décrite en détail Annexe 7, rappelée Annexe 8, 9 et discutée Annexe 10. Le principe général en est le suivant. L'orientation finale d'une ligne passive dépend uniquement de son orientation initiale et de la déformation totale. Cette dernière peut, par conséquent, être décomposée en 2 de ses composantes géométriques classiques (Ramsay, 1967): une déformation interne et une rotation rigide. La troisième composante, la translation rigide n'intervient pas dans ce problème. La correction appliquée aux vecteurs aimantations s'effectue donc en deux temps (Fig. III.1 et Annexe 7): (1) déformation inverse du vecteur aimantation à l'aide du tenseur de déformation interne inverse, (2) rotation rigide inverse par correction de pendage classique de la stratification elle-meme corrigée de la déformation interne.

Cette correction a été appliquée avec succès aux aimantations rémanentes antétectoniques des 3 exemples naturels étudiés. Elle a permis de corriger les fortes dispersions intrasites des vecteurs aimantations dans les cas où la déformation avait un tel effet (Annexe 7); elle a toujours permis, après déformation inverse complète, de déterminer une direction moyenne d'aimantation antétectonique sur l'ensemble de la formation plissée, bien que les critères classiques de déplissement eussent du conduire au rejet de ces séries (Annexes 7,8 et 9).

III.2. Discussion: estimation des sources d'erreur.

Malgré ces résultats globalement positifs, l'application de cette correction de déformation interne n'a pas toujours été aisée. Cela est particulièrement sensible dans le cas des Pyrénées (Annexe 8). On peut classer les sources d'erreur en deux ensembles: (1) Imprécisions et erreurs sur la détermination des paramètres du problème (aimantation, déformation). (2) Inexactitude de la loi de comportement proposée (hypothèse de la ligne passive). Ces deux points ont été abordés lors des études paléomagnétiques des séries rouges Pyrénéennes (Annexe 8) et du Sud de Rennes (Annexe 9), et

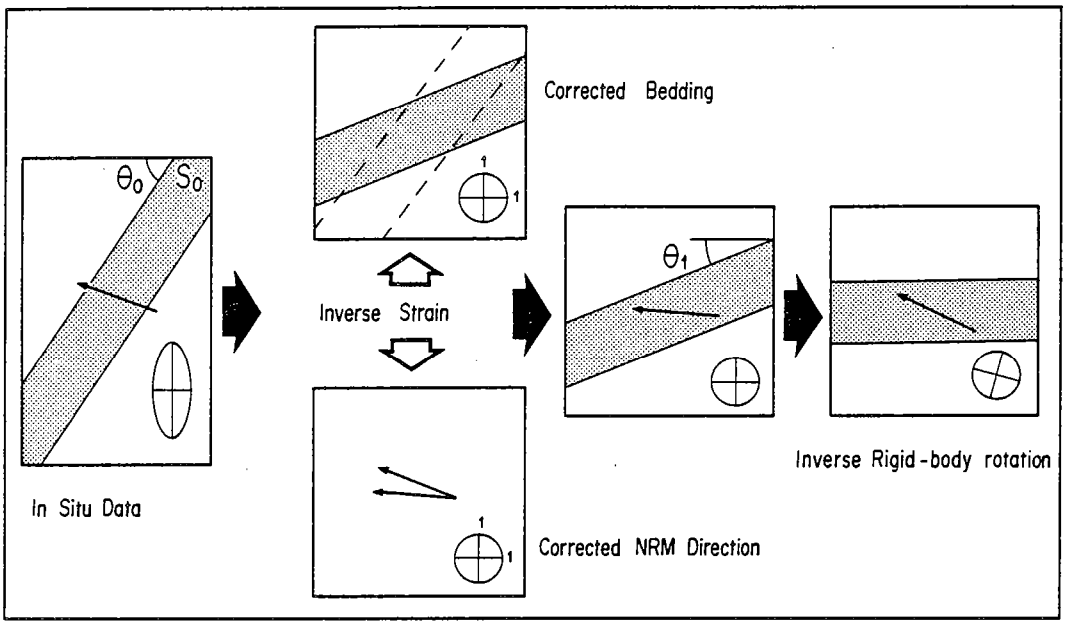

Fig. III.1 : Illustration schématique de la déformation inverse des directions d'aimantation (Cf. Annexe 7).

lors de la discussion de synthèse dans l'Annexe 10. On peut en faire la revue suivante.

III.2.1 Imprécisions sur les paramètres.

Sans en négliger l'importance, je ne m'attarderai pas ici sur les problèmes posés par l'analyse paléomagnétique, c'est à dire, la décomposition vectorielle des aimantations rémanentes naturelles et la détermination des composantes primaires. Les techniques d'analyse paléomagnétiques et leurs limitations font désormais partie de la méthodologie du paléomagnétisme moderne (cf. Perroud, 1985). Des problèmes plus spécifiques à mon travail sont liés à la détermination de la déformation totale ayant affecté les vecteurs aimantations. Ainsi qu'il a été noté ci-dessus, l'hypothèse du comportement passif permet de décomposer la déformation totale en (1) déformation interne, (2) rotation rigide.

-(1) La déformation interne est déterminée par la mesure, sur le terrain, de l'orientation de la schistosité (plan d'aplatissement) et de la linéation d'étirement (direction d'élongation maximum λ_1). Dès ce stade, il peut exister des erreurs non négligeables, dont une illustration est donnée par la comparaison des directions structurales et des susceptibilités magnétiques principales en Annexe 9. D'autre part, les élongations suivant les directions principales sont estimées d'après les mesures des rapports de marqueurs elliptiques (ici, des taches de réduction). Ici aussi, on peut établir l'ordre de grandeur des barres d'erreur autour des rapports axiaux moyens, mais ce n'est pas là, en fait, que réside la plus grande indétermination sur la déformation interne affectant les vecteurs aimantation. Le problème est plutôt de distinguer, dans la déformation totale reflétée par la forme finie des taches de réduction, la part de déformation d'origine tectonique de celle d'origine sédimentaire (fabrique initiale due à la compaction). En effet, partant de l'hypothèse raisonnable que l'aimantation des séries rouges étudiées ici est principalement d'origine chimique, acquise par deshydratation des hydroxydes de fer durant la compaction et la diagénèse, seule la déformation d'origine tectonique déviera ces aimantations. Utiliser le tenseur de déformation totale, estimé d'après la mesure de marqueurs qui ont pu enregistrer la compaction et la déformation, dans le but de corriger ces déviations, pourra introduire des erreurs significatives dans le traitement de déformation inverse. Ce problème est parfaitement illustré dans le cas des Pyrénées (Annexe 8). Il y a été montré, d'une part qu'une composante de compaction importante avait été enregistrée par les taches de réduction, et d'autre part, qu'il était nécessaire de supprimer cette composante pour obtenir un résultat correct en déformation inverse du vecteur aimantation.

-(2) En ce qui concerne la rotation rigide, elle est estimée d'après la direction et le pendage du plan de stratification après déformation inverse de ce dernier.En considérant que la stratification était horizontale au moment de l'acquisition de l'aimantation, on a donc là une bonne indication de la rotation rigide autour d'un axe horizontal. Cela reste cependant la seule composante de rotation rigide que l'on puisse déterminer à l'échelle d'un site de déformation homogène. Ce traitement discret, site par site, du déplissement interdit toute estimation de la rotation rigide autour d'axes verticaux. Cette limitation (évoquée en Annexes 8 et 9) est inhérente à la méthode employée, et seule une déformation inverse tridimensionnelle à l'échelle de la formation plissée, telle que celle proposée par Percevault (1983) par exemple, permettrait de respecter la compatibilité aux limites des

volumes dédéformés. Enfin, l'hypothèse même de l'horizontalité de la stratification à l'état initial peut être remise en cause, ainsi qu'il a été suspecté sur la base des résultats paléomagnétiques par Perroud et al. (1986) sur la formation rouge du Moulin de Chateaupanne, ou dans la présente étude, sur la Formation de Pont Réan (Annexe 9). On peut cependant noter que ce dernier point n'est pas spécifique au problème des séries plissées avec déformation interne, et qu'il peut être rencontré lors de toute correction de pendage classique.

Notons pour finir que des erreurs dans la mesure des directions structurales (schistosité, stratification, etc...) peut conduire à des situations d'instabilité dans la correction appliquée aux aimantations. Cela est particulièrement sensible dans le cas des séries rouges du Sud de Rennes (Annexe 9), où la direction moyenne d'aimantation est très proche du plan de schistosité. Suivant que la direction d'aimantation se situe d'un coté ou de l'autre du plan, la correction induira une rotation dans un sens ou dans l'autre et pourra éventuellement être erronée du seul fait de l'imprécision des mesures. Bien qu'il en ait été donné une autre explication en Annexe 9, un tel effet peut être suspecté dans le cas des données des 4 sites éliminés dans le calcul final de l'aimantation moyenne après déformation inverse de cette formation. La correction actuelle discrète ne permet pas de contrôler ces instabilités induites par les erreurs de mesures sur les données structurales.

III.2.2. Simulation analogique et hypothèse de la ligne passive.

C'est sur un tout autre plan que se situe l'autre source envisageable d'erreur de correction. Elle pourrait être due à une possible inadéquation de la loi théorique reliant aimantation et déformation interne. Le comportement passif de l'aimantation a été postulé d'après l'analyse globale des distributions de vecteurs dans le cas des Alpes Maritimes. Cela a ensuite été vérifié au moins dans le cas de la Formation de Pont-Réan, et suspecté pour les Pyrénées. Bien que dans l'ensemble il y ait une bonne compatibilité, il apparait difficile de tester l'exacte correspondance entre déviations de lignes passives et déviations de vecteurs aimantation dans des exemples naturels. La meilleure possibilité qui nous est offerte d'estimer la différence de comportement entre vecteur aimantation et ligne passive est d'utiliser les résultats des simulations. J'ai donc comparé les déviations de l'ARI lors des simulations analogiques (Annexe 4) aux déviations théoriques de lignes matérielles suivant le modèle de March (1932). Les résultats sont illustrés Fig.III.2, où la différence de déviations entre l'ARI et la ligne passive est représentée en fonction du pourcentage de raccourcissement (% R) pour les différents angles initiaux θ_0 entre ARI et raccourcissement (λ_3) envisagés en Annexe 4. La différence Δ, égale à la différence d'inclinaisons dans la terminologie de l'Annexe 4, est calculée de manière à ce qu'une différence positive exprime une déviation de la ligne passive supérieure à celle de l'ARI. On peut faire les observations suivantes: (1) dans les deux cas de conditions initiales (isotrope, ou initialement raccourci de 30%), lorsque l'ARI est parallèle ($\theta_0=0^o$) ou orthogonale ($\theta_0=90^o$) à λ_3, ni la ligne passive, ni la direction moyenne d'ARI ne sont déviées (cf. Annexe 4). La différence reste donc proche de 0. Celà peut paraitre élémentaire mais on peut conclure que dans ces cas particuliers il n'existe pas de différence entre une ligne passive et le vecteur aimantation. Cette observation s'applique également lorsque l'ARI est "proche" de λ_3 ($\theta_0=5^o$). (2) Dans les cas d'angle initial θ_0 intermédiaire, la déviation de la ligne passive est

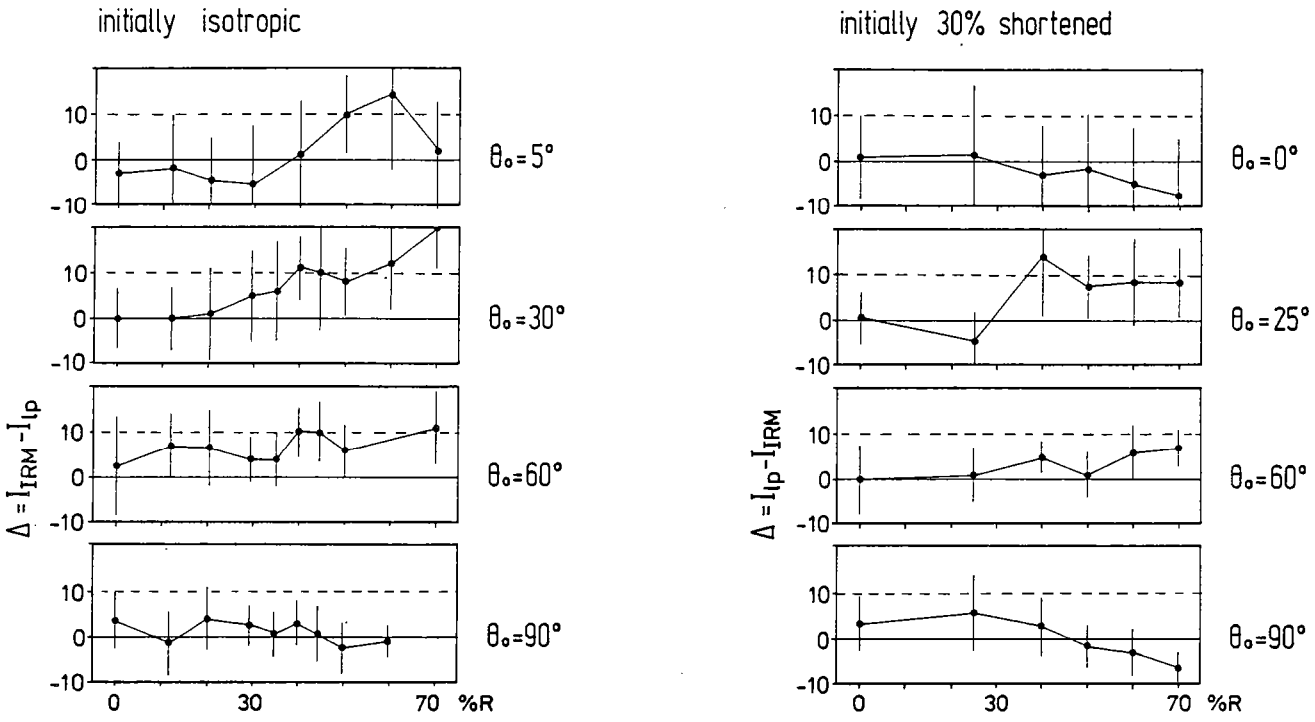

Fig.III.2 : Différence de déviation Δ entre la ligne passive et l'ARI des simulations analogiques de l'Annexe 4, en fonction du pourcentage de raccourcissement (% R), et pour différents angles θ_o entre direction de raccourcissement et ARI initiale moyenne. A gauche: échantillons initialement isotropes; à droite: échantillons initialement raccourcis de 30% (Cf. Annexe 4).

pratiquement toujours supérieure à celle de l'ARI. On remarquera cependant que la différence de déviation Δ est inférieure à 10^{o} pour tous les cas jusqu'à 50% de raccourcissement, et, dans le cas d'échantillons initialement raccourcis de 30%, jusqu'à 70% de raccourcissement. Par ailleurs, ces derniers échantillons présentent en moyenne des différences de déviation inférieures à celles des échantillons initialement isotropes. On peut donc estimer que, dans les limites du modèle utilisé, les déviations de l'aimantation rémanente, quoique inférieures, sont proches des déviations théoriques de la ligne matérielle; une fabrique initiale semble, de plus, améliorer cette similitude.

Ces observations m'amènent à reformuler de la manière suivante la loi théorique du comportement de l'aimantation rémanente: la direction initiale et la direction finale, après déformation, de l'aimantation rémanente, sont liées par un "tenseur de déviation" symétrique d'ordre 2, dont les vecteurs propres sont identiques aux vecteurs propres du tenseur de déformation interne, et dont les valeurs propres sont proches des valeurs propres du tenseur de déformation interne. Cette formulation permet de modifier l'expression de l'hypothèse du comportement de l'aimantation rémanente antétectonique: plutôt que d'assimiler le comportement du vecteur aimantation au comportement d'une ligne passive, il me semble préférable de dire que l'on assimile le tenseur de déviation du vecteur aimantation au tenseur de déformation interne. Si la première formulation (ligne passive) offre l'avantage de la simplicité d'expression, la seconde est plus rigoureuse du point de vue des mécanismes. Quoiqu'il en soit, ces deux formulations traduisent strictement la même expression mathématique de l'hypothèse utilisée.

Il faut finalement noter que si les différences de déviation entre l'ARI de la simulation analogique et la ligne matérielle sont de l'ordre de 5 à 10^{o}, il est difficile de prévoir quelle est la portée de cet écart dans le cas des séries naturelles. Les résultats positifs obtenus lors des diverses "déformations inverses" du vecteur aimantation semblent cependant montrer qu'assimiler le tenseur de déviation de l'aimantation au tenseur de déformation interne constitue une hypothèse de travail correcte.

En conclusion à cette revue des sources d'erreur dans l'estimation de la correction à appliquer aux aimantation déviées par la déformation, on peut retenir les points suivants :

(1) On est capable de mettre des barres d'erreur sur la mesure des différentes données du problème (aimantation, directions structurales, rapports axiaux des marqueurs elliptiques de déformation etc...).

(2) On sait que l'estimation de la rotation rigide est en soi assez approximative.

(3) Assimiler le "tenseur de correction de déformation interne" au tenseur inverse de déformation est, bien que globalement correct, également une approximation.

(4) Malgré la connaissance que l'on a des diverses sources d'erreurs et d'approximation, l'application actuelle discrète (direction d'aimantation par direction d'aimantation) de l'algorithme de déformation inverse des aimantations antétectoniques ne permet pas de prendre en compte et d'utiliser ces incertitudes, dans le but d'optimiser la détermination finale de la direction moyenne d'aimantation rémanente antétectonique, à l'échelle de la série plissée.

Il parait donc judicieux d'établir une méthode permettant une estimation de la direction paléomagnétique antétectonique, basée non plus sur le calcul de la moyenne d'estimations ponctuelles, mais sur la recherche de la solution correspondant au mieux à toutes les données et à leurs incertitudes.

III.3. Application de la méthode d'inversion non-linéaire généralisée, à la détermination d'une direction d'aimantation antétectonique dans une série plissée avec déformation interne.

L'exposé ci-dessous est une application de la solution généralisée au problème inverse non-linéaire suivant le critère des moindres carrés, proposée par Tarantola et Valette (1982). Le caractère général de la formulation proposée par ces auteurs, en a permis l'application à des domaines aussi divers que la détermination des paramètres de diffusion haute température dans les cristaux (Sotin et Poirier, 1984), ou la résolution de tenseurs de contrainte à partir de mesures de stries sur plans de faille (Angelier et al, 1982), par exemple.

La solution, suivant cette méthode, du problème posé par la détermination de la direction d'aimantation antétectonique à partir d'aimantations rémanentes déviées, passe par une reformulation rigoureuse de la loi physique considérée et de ses paramètres.

III.3.1. Hypothèse de base.

A partir de l'analyse faite au Chapitre II et ci-dessus en III.1, l'aimantation M mesurée après déformation, peut être reliée à sa direction initiale H, par un tenseur T de la manière suivante :

$$M_i = T_{ij}.H_j \qquad i,j=1,2,3 \qquad (1)$$

Le tenseur de déviation totale T_{ij} pour une aimantation M_i donnée, peut être décomposé en un tenseur de déviation due à la rotation rigide R (la seule prise en compte habituellement en paléomagnétisme), et un tenseur de déviation S due à la déformation interne homogène et qui est, suivant ce qui a été discuté ci-dessus, estimé par le tenseur de déformation interne lui-même.

$$T_{ij} = S_{ik}.R_{kj} \qquad (2)$$

Les équations (1) et (2) définissent la loi physique du système aimantation antétectonique, déformation, aimantation mesurée.

III.3.2. Les paramètres du problème.

***-Tenseur de déviation T.**

(i) Tenseur S.

Pour décrire les directions principales de ce tenseur, on utilise la mesure de trois angles indépendants: la direction de l'horizontale par rapport au Nord géographique (Strike: Sc) et le pendage (Dip: Dc) du plan de schistosité, et l'angle que fait la linéation d'étirement avec l'horizontale dans ce plan (Pitch: Px) (la direction Sc est choisie de manière à ce que le pendage soit vers le bas dans la direction $Sc+90^o$).

A partir de ces 3 angles, on détermine les cosinus directeurs des vecteurs propres du tenseur S:

-Direction d'élongation minimum λ_3 (normale à S_1) :

$$\begin{cases} Z_1 = -\sin Sc.\sin Dc \\ Z_2 = \cos Sc.\sin Dc \\ Z_3 = -\cos Dc \end{cases} \qquad (3)$$

-Direction d'élongation maximum λ_1 (linéation d'étirement) :

$$\begin{cases} X_1 = \cos Sc.\cos Px - \sin Sc.\cos Dc.\sin Px \\ X_2 = \sin Sc.\cos Px + \cos Sc.\cos Dc.\sin Px \\ X_3 = \sin Dc.\sin Px \end{cases} \qquad (4)$$

La direction d'élongation intermédiaire λ_2 (Y_1, Y_2, Y_3) est définie par le produit vectoriel des 2 précédents. Les composantes cartésiennes des vecteurs propres de S ainsi déterminée, on peut construire la matrice a_{ij} des cosinus directeurs de S:

$$a = \begin{pmatrix} X_1 & Y_1 & Z_1 \\ X_2 & Y_2 & Z_2 \\ X_3 & Y_3 & Z_3 \end{pmatrix} \qquad (5)$$

Les valeurs propres λ_1, λ_2 et λ_3 du tenseur S sont déterminées soit d'après les moyennes des rapports axiaux de marqueurs elliptiques tels que les taches de réduction, ou par ajustement d'abaque Rf/Φ de Dunnet (1969), l'avantage de la moyenne arithmétique étant de pouvoir calculer un écart-type sur le lot de données. On peut alors construire le tenseur diagonal S'_{ij}:

$$S' = \begin{pmatrix} \lambda_1 & 0 & 0 \\ 0 & \lambda_2 & 0 \\ 0 & 0 & \lambda_3 \end{pmatrix} \qquad (6)$$

et finalement, construire S_{ij} dans le repère géographique :

$$S_{ij} = a_{ik}.a_{jl}.S'_{kl} \qquad i,j,k,l = 1,2,3 \qquad (7)$$

(ii). Tenseur R.

Ainsi qu'il a été discuté plus haut, la rotation rigide est estimée d'après la direction et le pendage de la stratification après déformation inverse de celle-ci. La mesure élémentaire est donc celle de la direction (Strike: Sb) et du pendage (Dip: Db) du plan de stratification à l'état final.

On définit la normale à la stratification:

$$\begin{cases} n_x = -\sin Sb.\sin Db \\ n_y = \cos Sb.\sin Db \\ n_z = -\cos Db \end{cases} \qquad (8)$$

La normale à la stratification dédéformée est donnée par (Cf. Owens 1974 et Annexe 7):

$$n'_i = S_{ij}.n_j \qquad i,j = 1,2,3 \qquad (9)$$

ce qui permet de définir la direction (Sb') et le pendage (Db'), du plan de stratification à l'état non déformé. On peut ainsi construire la matrice de rotation, avec un axe horizontal dans la direction Sb' et un angle de rotation égal à Db'. Cette matrice est égale à

$$R=\begin{pmatrix} \cos^2 Sb'+\sin^2 Sb'.\cos Db' & \cos Sb'.\sin Sb'.(1-\cos Db') & \sin Sb'.\sin Db' \\ \cos Sb'.\sin Sb'.(1-\cos Db') & \sin^2 Sb'+\cos^2 Sb'.\cos Db' & -\cos Sb'.\sin Db' \\ -\sin Sb'.\sin Db' & \cos Sb'.\sin Db' & \cos Db' \end{pmatrix} \qquad (10)$$

N.B: R est ici la matrice de rotation rigide, et non la matrice de rotation rigide inverse, ou de "correction de pendage".

Afin d'éviter des calculs supplémentaires en passant des coordonnées n'_x, n'_y et n'_z du pôle de la stratification dédéformée aux angles direction (Sb') et pendage (Db') de celle-ci, on peut exprimer R_{ij} directement en fonction des coordonnées de n' normalisée, obtenue d'après (9):

$$R=\begin{pmatrix} \frac{n'^2_y-n'^2_x.n'_z}{1-n'^2_z} & \frac{n'_x.n'_y}{n_z-1} & -n'_x \\ \frac{n'_x.n'_y}{n'_z-1} & \frac{n'^2_x-n'^2_y.n'_z}{1-n'^2_z} & -n'_y \\ n'_x & n'_y & -n'_z \end{pmatrix} \qquad (11)$$

N.B: L'expression (11) de R_{ij} est obtenue d'après (10) et les équations (8).

(iii) Tenseur de déviation totale T.

A partir des expressions (7) de S_{ij} et (11) de R_{ij}, on construit le tenseur T suivant (2):

$$T_{ij} = S_{ik}.R_{kj}$$

La construction de ce tenseur repose donc sur la mesure de 8 paramètres:

Sc: direction du plan de schistosité
Dc: pendage " "
Px: "Pitch" de la linéation d'étirement dans S_1
λ_1, λ_2, λ_3: déformations principales
Sb: direction du plan de stratification
Db: pendage " "

En supposant une distribution Gaussienne des erreurs sur chacune de ces mesures, on peut établir un écart-type autour de celles-ci. En ce qui concerne les angles, cet écart-type peut être estimé d'après la précision de lecture des instruments de mesure, et/ou, d'après les observations de terrain sur la qualité des objets mesurés. Pour les valeurs λ_i, les écarts-type sont établis d'après ceux calculés sur les rapports moyens λ_1/λ_2 λ_2/λ_3 etc. On peut cependant, compte tenu de la discussion sur l'identité tenseur de déformation/tenseur de déviation faite ci-dessus, choisir volontairement un domaine de variation plus grand que celui découlant strictement des mesures.

***-Aimantation rémanente déviée M.**

L'aimantation rémanente M à l'état déformé est définie par deux angles (on ne tient pas compte du module |M| du vecteur), analogues aux angles polaires classiques: la déclinaison "d" et l'inclinaison "i". L'estimation de ces paramètres résulte de l'analyse vectorielle de l'évolution du vecteur aimantation au cours de traitements de désaimantation progressive. Ici

également, on peut se fixer des barres d'erreur qui dépendront de la qualité des mesures, de la qualité des trajectoires de désaimantation etc...

***-Direction d'aimantation antétectonique H.**

Le vecteur H est également défini par deux paramètres, la déclinaison D et l'inclinaison I. Ces paramètres, uniques pour l'ensemble des aimantations déviées et des tenseurs T correspondants, sont les inconnues de notre problème.

III.3.3. Le problème inverse.

Soit (D_o, I_o) une estimation a priori (indépendante de la série de mesures) du vecteur H, et (σ_o^D, σ_o^I) les écarts-type sur cette estimation a priori. Si on ne possède aucune information a priori sur H, on prendra un écart-type infini (très large). Soit $(d_o, i_o, Sc_o, Dc_o, Px_o, \lambda_{1o}, \lambda_{2o}, \lambda_{3o}, Sb_o, Db_o)^k$ les données (aimantation et déformation) correspondant à la $k^{ième}$ aimantation déviée et $(\sigma_o^d, \sigma_o^i, \sigma_o^{Sc}, \sigma_o^{Dc}, \ldots, \sigma_o^{Db})^k$ les écarts-type correspondants (k est un indice, non un exposant). Il est clair qu'aucune direction H(D,I) ne vérifie exactement (1) pour toutes les aimantations et déformations considérées. On cherchera à définir une direcrion H(D,I), et une série de "données corrigées" $(d, i, Sc, Dc, Px, \ldots, Db)^k$ vérifiant au mieux (1):

$$M_i = T_{ij}.H_j \qquad (1)$$

et on choisira la solution qui minimise la somme

$$S = \left(\frac{D-D_o}{\sigma_o^D}\right)^2 + \left(\frac{I-I_o}{\sigma_o^I}\right)^2 + \sum_{k=1}^{N} \left[\left(\frac{d-d_o}{\sigma_o^d}\right)^2_k + \left(\frac{i-i_o}{\sigma_o^i}\right)^2_k + \left(\frac{Sc-Sc_o}{\sigma_o^{Sc}}\right)^2_k + \left(\frac{Dc-Dc_o}{\sigma_o^{Dc}}\right)^2_k + \ldots \ldots\ldots\ldots + \left(\frac{Db-Db_o}{\sigma_o^{Db}}\right)^2_k \right] \qquad (12)$$

où N est le nombre d'aimantations déviées mesurées. L'équation (1) et la minimisation de S (12) établissent le problème inverse.

III.3.4. Solution du problème inverse.

On définit les vecteurs colonnes suivants

$$X_o = \begin{bmatrix} \begin{pmatrix} d_o \\ i_o \\ Sc_o \\ Dc_o \\ Px_o \\ . \\ . \\ Db_o \end{pmatrix} 1 \\ . \\ . \\ . \\ \begin{pmatrix} d_o \\ i_o \\ Sc_o \\ Dc_o \\ Px_o \\ . \\ . \\ Db_o \end{pmatrix} N \\ D_o \\ I_o \end{bmatrix} \qquad X = \begin{bmatrix} \begin{pmatrix} d \\ i \\ Sc \\ Dc \\ Px \\ . \\ . \\ Db \end{pmatrix} 1 \\ . \\ . \\ . \\ \begin{pmatrix} d \\ i \\ Sc \\ Dc \\ Px \\ . \\ . \\ Db \end{pmatrix} N \\ D \\ I \end{bmatrix} \qquad (13)$$

On définit C_o, matrice de covariance des valeurs a priori de X_o. Suivant l'hypothèse des erreurs indépendantes sur les données, C_o est une matrice diagonale contenant les variances respectives sur les éléments de X_o.

L'inversion doit définir le vecteur X le plus probable, compatible avec les erreurs expérimentales et verifiant les N équations:

$$f^k(X)=|M^k - T^k.H|^2=0 \qquad k = 1,N \qquad (14)$$

où $|M^k - T^k.H|$ est le module du vecteur différence $D_i=M_i^k-T_{ij}^k.H_j$, et M^k et T^k sont fonction de $(d,i,Sc,Dc,Px,...,Db)^k$ suivant la section III.3.2.

Suivant cette notation la solution

$$f(X) = 0 \qquad (15)$$

est obtenue par la minimisation de

$$S = (X-X_o)^t.C_o^{-1}.(X-X_o) \qquad (16)$$

On notera que les équations (14) et la condition (16) sont equivalentes à (1) et (12) respectivement.

Tarantola et Valette (1982) ont démontré que la solution de ce problème non-linéaire suivant le critère des moindres carrés, est obtenue par l'algorithme itératif :

$$X_{n+1}= X_o+C_o.F_n^t.(F_n.C_o.F_n^t)^{-1}.[F_n.(X_n-X_o)-f(X_n)] \qquad (17)$$

où F est la matrice des dérivées partielles

$$(F_n)_{ij} = \left(\frac{\partial f^i}{\partial X_j}\right)_{X=X_n} \qquad (18)$$

La matrice C de covariance de la solution X peut être obtenue approximativement par une formule utilisant une approximation linéaire (Tarantola et Valette 1982)

$$C \approx C_o-C_o.F^t.(F.C_o.F^t)^{-1}.F.C_o \qquad (19)$$

où les dérivées partielles sont prises au point solution X.

Dérivées partielles de $f^k(X)$

Dans un but de simplification de l'exposé ci-dessous, on renomme le vecteur M^k par A, et le vecteur $T^k.H$ par B.

On peut alors reécrire l'équation (14) sous la forme explicite:

$$f^k(X) = (A_1-B_1)^2+(A_2-B_2)^2+(A_3-B_3)^2 \qquad (20)$$

où
$$\left|\begin{array}{l} A_1 = \cos d^k.\cos i^k \\ A_2 = \sin d^k.\cos i^k \\ A_3 = \sin i^k \end{array}\right. \qquad (21)$$
coordonnées cartésiennes de M^k

et
$$\left|\begin{array}{l} B_1 = T_{11}^k.X+T_{12}^k.Y+T_{13}^k.Z \\ B_2 = T_{21}^k.X+T_{22}^k.Y+T_{23}^k.Z \\ B_3 = T_{31}^k.X+T_{32}^k.Y+T_{33}^k.Z \end{array}\right. \qquad (22)$$

avec
$$\left|\begin{array}{l} X = \cos D.\cos I \\ Y = \sin D.\cos I \\ Z = \sin I \end{array}\right.$$
coordonnées cartésiennes de H

et $T_{ij}^k = g(Sc^k, Dc^k, Px^k, \lambda_1^k, \lambda_2^k, \lambda_3^k, Sb^k, Db^k)$

En utilisant cette notation, les dérivées de f^k par rapport aux paramètres définissant H(D,I) sont :

$$\frac{\partial f^k}{\partial D} = \frac{\partial (A_1-B_1)^2}{\partial D} + \frac{\partial (A_2-B_2)^2}{\partial D} + \frac{\partial (A_3-B_3)^2}{\partial D}$$

$$= 2\Big\{-(A_1-B_1).\left[T_{11}^k(-\sin D.\cos I)+T_{12}^k(\cos D.\cos I)\right]$$
$$-(A_2-B_2).\left[T_{21}^k(-\sin D.\cos I)+T_{22}^k(\cos D.\cos I)\right]$$
$$-(A_3-B_3).\left[T_{31}^k(-\sin D.\cos I)+T_{32}^k(\cos D.\cos I)\right]\Big\}$$

$$= 2\sum_{i=1}^{3}(A_i-B_i).\left[T_{i1}^k.Y-T_{i2}^k.X\right]$$

De la même manière, on arrive à

$$\frac{\partial f^k}{\partial I} = 2\sum_{i=1}^{3}(A_i-B_i)\left[T_{i1}^k(\cos D.\sin I)+T_{i2}^k(\sin D.\sin I)-T_{i3}^k(\cos I)\right]$$

Les dérivées de f^k par rapport aux données sont

$$\frac{\partial f^k}{\partial d^k} = \frac{\partial (A_1-B_1)^2}{\partial d^k} + \frac{\partial (A_2-B_2)^2}{\partial d^k}$$

$$= 2(A_1-B_1).(-\sin d^k.\cos i^k)+2(A_2-B_2).(\cos d^k.\sin i^k)$$

$$= 2\left[A_1.(A_2-B_2)-A_2.(A_1-B_1)\right]$$

et

$$\frac{\partial f^k}{\partial i^k} = 2\Big[(A_3-B_3).(\cos i^k)$$
$$-(A_2-B_2).(\sin d^k.\sin i^k)$$
$$-(A_1-B_1).(\cos d^k.\sin i^k)\Big]$$

Les dérivées de f^k par rapport aux données définissant T^k n'ont pas de solution analytique évidente, elles seront calculées numériquement.

Enfin, si les données concernant deux aimantations déviées sont indépendantes, les dérivées de f^k par rapport à $(d,i,Sc,Dc,\ldots,Db)^j$ sont nulles pour $j \neq k$.

III.3.5. Conclusion.

Cet exposé montre qu'il est relativement aisé d'adapter la solution générale au problème inverse du type de celle proposée par Tarantola et Valette (1982) au problème de la détermination d'une direction d'aimantation antétectonique à partir de directions d'aimantations déviées par la déformation. Cependant, en l'absence d'applications numériques de cet algorithme, il est difficile de discuter de manière détaillée son pouvoir de résolution. Quoi qu'il en soit, seule une formulation de ce type autorise la prise en compte des erreurs sur les paramètres autres que les aimantations, et à ce titre le résultat final aura une meilleure justification en terme de probabilité, que la détermination actueile par moyennes de "directions corrigées" de manière discrète.

III.4. Conclusions.

En conclusion au problème de la correction des déviations dues à la déformation interne dans les séries rouges, on peut retenir les points essentiels suivants :

(1) L'analyse des déviations de l'ARI dans le modèle analogique, et de l'ARN dans les séries rouges étudiées montre que la direction initiale, connue ou supposée, et la direction finale, après déformation, du vecteur aimantation sont reliées par un "tenseur de déviation" dont une estimation approximative est donnée par le tenseur de déformation interne. Cette définition du "tenseur de déviation" est exactement analogue à l'hypothèse "ligne passive" pour le vecteur aimantation.

(2) A partir de cette hypothèse, le tenseur inverse de déformation interne a été utilisé comme tenseur de correction des déviations induites par la déformation interne. Les résultats positifs obtenus pour les 3 exemples de séries rouges traités montrent d'une part que c'est une hypothèse de travail correcte, et d'autre part, qu'il est par conséquent possible de retrouver une direction de champ magnétique primaire à partir d'aimantations déviées par la déformation.

(3) Après ce premier stade d'analyse et de vérification des hypo- thèses, il apparait cependant nécessaire d'établir une méthode de correction prenant en compte les erreurs expérimentales sur les mesures de tous les paramètres impliqués dans ce problème (aimantation et déformation), ainsi que les incertitudes théoriques sur la loi physique du système. Une telle formulation a été proposée.

(4) Finalement, il faut noter que l'algorithme de déformation inverse proposé ici n'a pas de caractère universel et ne peut etre utilisé aveuglément. Son utilisation est subordonnée à une analyse soigneuse des relations entre déformation et directions d'aimantation, qui, seule, peut justifier l'hypothèse de comportement utilisée.

CONCLUSIONS

La conclusion la plus élémentaire que l'on puisse tirer de cet ensemble d'investigations est le fait que la déformation interne ductile, dans la mesure où elle résulte dans le développement d'orientations préférentielles des porteurs magnétiques, induit nécéssairement des déviations de l'aimantation rémanente naturelle de la roche: déviation de l'aimantation acquise par le matériau déformé, déviation de l'aimantation antétectonique portée par des minéraux anisotropes. Cette observation préliminaire implique la nécessité de prendre en considération l'existence de déformation interne, toujours possible lors d'études paléomagnétiques en zone orogénique. Les études paléomagnétiques de séries rouges déformées présentées ici ont montré que cela est particulièrement critique dans l'interprétation des résultats du test de pli: sur le seul argument de l'évolution des groupements, les aimantations auraient pu être interprétées comme syntectoniques dans le cas des Alpes Maritimes, syn- à post-tectoniques dans la formation de Pont-Réan. Il apparait par conséquent nécessaire d'assortir l'argument statistique de l'évolution des groupements, d'une discussion sur l'absence de déformation interne. L'étude de l'anisotropie de susceptibilité magnétique, en tant qu'image de l'orientation préférentielle des minéraux magnétiques, parait constituer le meilleur moyen d'argumenter cette discussion.

A un niveau supérieur d'analyse, il a été montré que ces déviations sont cohérentes: écart de l'ATR à la direction de champ cohérente avec les directions d'ASM, elle-meme contrôlée par la déformation interne, dans l'exemple du granite de Flamanville; cohérence des distributions intra et inter-sites des aimantations antétectonique avec les directions principales de déformation interne, dans le cas des séries rouges plissées avec déformation interne. Dans le premier cas, une relation théorique entre tenseur d'anisotropie de susceptibilité magnétique et tenseur d'anisotropie d'aimantation thermorémanente a été établie. La démarche suivie pour établir cette relation met en valeur l'utilisation nouvelle de la mesure de l'ASM en tant qu'estimateur direct des déviations de l'aimantation rémanente. Dans le cas précis du granite de Flamanville, le but final, à savoir la détermination d'une direction de champ magnétique par l'étude paléomagnétique de roches déformées, a été atteint.

En ce qui concerne les effets de la déformation interne sur l'aimantation rémanente antétectonique, il a été montré par modélisation analogique et numérique, qu'un mécanisme de rotation des particules magnétiques rend convenablement compte des fabriques cristallines et magnétiques des séries pélitiques étudiées. Les effets d'une telle rotation sur l'orientation de l'aimantation rémanente ont été caractérisés par simulation analogique pour quelques conditions aux limites simples, et sont globalement identiques aux effets observés dans les séries naturelles étudiées. Dans la limite de ces exemples, la déviation de l'aimantation rémanente s'est révélée similaire à la déviation de la ligne matérielle (modèle de March, 1932), ce qui m'a amené à proposer une correction fondée sur ce modèle de comportement. La discussion de cette hypothèse et des résultats obtenus mène à la conclusion que, quoique approximatif, le modèle de comportement passif de l'aimantation rémanente dans les séries rouges

déformées constitue la meilleure possibilité actuelle d'estimer une direction d'aimantation antétectonique à partir d'aimantations rémanentes déviées par la déformation.

Dans la mesure où la loi de comportement apparait proche du comportement observé, il semble, de plus, préférable de tenter d'améliorer le traitement numérique global des données, plutôt que d'améliorer la loi théorique elle-même.

Finalement, les résultats obtenus ici permettent de répondre par l'affirmative à un certain nombre de questions d'ordre général: question de l'existence, ou non, de déviations significatives de l'aimantation acquise par les roches anisotropes ou ultérieurement déformées; question de la cohérence de ces déviations; question de la possibilité de caractériser les effets de la déformation interne sur l'orientation de l'aimantation. A la question finale de la possibilité d'effectuer des études paléomagnétiques en zones déformées, la réponse est également affirmative, au moins dans la limite des exemples étudiés, et sous réserve de l'analyse détaillée et de la compréhension des mécanismes de déviation de l'aimantation.

En revanche, il subsiste un certain nombre de problèmes; problème général de l'utilisation du test du pli en zone orogénique; problème des limites, non atteintes ici, des corrections proposées; problème des mécanismes dans d'autres régimes de déformation (fortement non coaxiale, par exemple), pour d'autre types de roches et d'autres porteurs magnétiques.

Seules des simulations et études paléomagnétiques supplémentaires permettront d'apporter des éléments de réponse à ces questions. Cependant, le caractère globalement positif des résultats obtenus ici devrait stimuler la poursuite des recherches dans cette voie.

PALEOMAGNETIC STUDY OF DEFORMED ROCKS.

An English translation of

CONTRIBUTION A L'ETUDE PALEOMAGNETIQUE DE ROCHES DEFORMEES.

By

Jean-Pascal COGNE

State **THESIS** defended at Rennes, September 25, 1987

PALEOMAGNETIC STUDY OF DEFORMED ROCKS.

ANNEXES.

ANNEX 3. J.P. COGNE. **Strain-induced AMS in the granite of Flamanville and its effects upon TRM acquisition.** Accepted in Geophys. J. R. astron. Soc.

ANNEX 4. J.P. COGNE. **Experimental and numerical modeling of IRM rotation in deformed synthetic samples.** Accepted in Earth Planet. Sci. Lett.

ANNEX 5. J.P. COGNE, H. PERROUD. M.P. TEXIER and N. BONHOMMET. **Strain reorientation of hematite and its bearing upon remanent magnetization.** Tectonics 5, 5, 753-767, 1986.

ANNEX 6. J.P. COGNE, D. GAPAIS. **Passive rotation of hematite during deformation : a comparison of simulated and natural redbeds fabrics.** Tectonophysics, 121, 365-372, 1986.

ANNEX 7. J.P. COGNE, H. PERROUD. **Strain removal applied to paleomagnetic directions in an orogenic belt : the permian red slates of the Alpes Maritimes,France.** Earth Planet.Sci. Let. 72, 125-140, 1985

ANNEX 8. J.P. COGNE. **Paleomagnetic direction obtained by strain removal in the Pyrenean Permian redbeds at the "Col du Somport" (France).** Earth Planet. Sci. Lett., 85, 162-172, 1987.

ANNEX 9. **Déformation, anisotropie de susceptibilité magnétique et paléomagnétisme des séries rouges de la formation de Pont-Réan (Bretagne centrale, France).**

ANNEX 10. J.P. COGNE, H. PERROUD. **Unstraining paleomagnetic vectors: the current state of debate.** Eos Trans. Amer. Geophys. Union, 68, 34, 705, 1987.

INTRODUCTION.

Apart from the basic hypothesis of the dipolar nature of the Earth magnetic field, using of paleomagnetic vectors in geodynamic problems relies on two main assumptions: (1) the parallelism between the magnetic field vector and the magnetization vector, and (2) the stability of remanent magnetization since its acquisition until now. The first condition is met if the rock is initially isotropic, or at least, weakly anisotropic. In fact, the paleomagnetic methodology mainly aims at verifying the second hypothesis. Reasons for instability can be divided into two main groups. The first one deals with the problem of magnetic memory resetting during thermal or chemical events, leading to partial or total remagnetizations. All the techniques (stepwise demagnetization procedures and components analysis, rock magnetism experiments, etc...) and the tests (fold test, contact test, conglomerate test etc..) that are used in paleomagnetism, generally leads to an argumentation of NRM nature, origin and age of a given rock formation.

A second kind of magnetization instability is due to deformation in a large sense, and particularly to the deviating effect of folding processes in orogenic zones. Up to now, structural corrections of paleomagnetic directions have relied on the classical bedding tilt correction. A comparison of vector distributions before and after this correction allows a test of pre-, syn- or post-tectonic age of magnetization.

If we consider the geometrical description of deformation (translation, rotation, distorsion; Ramsay 1967), the classical tilt correction only takes into account the component of rigid-body rotation around horizontal axes in the total deformation. Strictly, this could only be applied in the case of concentrical folds with horizontal axes, without any internal deformation, or strain. With the recent development of paleomagnetism within orogenic zones, such an algorithm appeared to be unsufficient. At first, some improvements were made in order to take into account more complicated fold geometries such as superimposed folds, or inclined fold axes, etc..(e.g. see McDonnald 1980, Bonhommet et al. 1981, Perroud & Cobbold 1984). However, these are improvements in the total rigid-body rotation estimates, which are valid only if it can be assumed that angular relationships between magnetic vectors and bedding plane have not been changed during folding. Such an assumption may be valid in the total lack of internal deformation, but such is not the general case. Amongst other mechanism, it is well admitted that ductile strain may induce a rotation of particles, leading to the development of mineral preferred orientations. This mechanism is important in paleomagnetism, because a rotation of magnetic carriers can be considered as a major cause of pretectonic magnetization deviations. This has been suspected in the cases of anomalous behaviour of magnetization distributions (e.g. see Van den Ende 1977, Kligfield et al. 1981, Perroud, 1983, Rosenbaum 1986). However, exact effects of strain upon remanent magnetization are poorly understood. The basic question that is to be asked and that I try to answer here is: "Is there any coherent effect upon remanent magnetization of rocks, and thus, what are the possibilities and limitations of paleomagnetic investigations within deformed areas?". Tentative answers given here are divided into three parts.

Through the structural, paleomagnetic and anisotropy of magnetic susceptibility studies of the granite of Flamanville, the magnetization acquisition by a (pre-)deformed rock is envisaged in the first chapter.

The problem of the effects of strain ocurring during folding processes upon a pretectonic remanent magnetization is considered in the second chapter. The characterization of these effects will be discussed through results of analogic and numerical simulations, and paleomagnetic studies of deformed redbeds.

Finally, an argumentation of the possibilities of correcting paleomagnetic vector deviations induced by strain is given in the third chapter.

Discussions developped along these 3 chapters are based upon results from published studies. Copies of these publications or manuscripts are given in Annexes 1 to 10.

CHAPTER I: MAGNETIZATION ACQUIRED BY AN ANISOTROPIC MATERIAL: TRM in the granite of Flamanville.

I.1. Anisotropy of magnetic susceptibility and deformation.

Generally, the directional variability of induced magnetization in a weak magnetic field is what is named anisotropy of magnetic susceptibility (AMS). Weak field magnetization is a linear function of field strength and is written as:

$$M_1 = k_{11}.H_1 + k_{12}.H_2 + k_{13}.H_3$$
$$M_2 = k_{21}.H_1 + k_{22}.H_2 + k_{23}.H_3$$
$$M_3 = k_{31}.H_1 + k_{32}.H_2 + k_{33}.H_3$$

or, $M_i = k_{ij}.H_j \qquad i, j = 1,2,3$

with M_i: cartesian coordinates of induced magnetization vector.

H_j: cartesian coordinates of magnetic field vector.

k_{ij}: second order symmetrical cartesian tensor, the AMS tensor. This tensor has three real eigenvalues, k_1, k_2, k_3, the principal susceptibilities.

Following Hrouda (1982), causes for AMS are generally summarized as follows:

(1) Shape alignment of ferromagnetic grains.
(2) Lattice alignment of crystals with magnetocrystalline anisotropy.
(3) Magnetic domains alignment.
(4) Stringing together of magnetic grains.
(5) Stress-induced anisotropy.
(6) Exchange anisotropy.

Amongst them, AMS in natural rocks is considered as being mainly controlled by (1) and (2). Measuring AMS in a rock thus yields an estimation of its fabric, just as other methods do (texture goniometry by X-ray diffractometry, for example), and this can be used as a structural tool for almost all rock types.

An abundent litterature is devoted to this subject (see the review by Hrouda 1982). Such studies have generally shown that total strain of rocks controls AMS development, in the direction of its principal susceptibilities, as well as in the variations of shape and intensity of AMS ellipsoid (see for example Wood et al. 1976, Hrouda 1976, 1979, 1980, Rathore 1979, Elwood & Whitney 1980, Wagner et al. 1981, Kligfield et al. 1983, Rathore et al. 1983, amongst others). A recent experimental study of strain effects upon AMS within magnetite-bearing synthetic samples, allowed Borradaile & Alford (1987) to confirm this analysis in a detailed way. (1) From a preexisting AMS, strain induces a rotation of AMS principal directions, and k_3 becomes rapidly parallel to λ_3. (2) However, AMS keeps a memory of its initial state. This means that AMS is not controlled by the last strain increment, but by the total deformation (about this subject, see also the magnetic fabric evolution we describe in the case of the Pont-Réan Formation in Annex 9). (3) Anisotropy degree increases with strain intensity, at least up to the 35% of homogeneous shortening obtained by these authors. However it does not appear to be reasonnable to exactly calibrate strain from AMS measurements in the general case.

The results of our own investigations on this subject in the granite of Flamanville are given in Annex 1. Our conclusions are identical to those of similar works: there is a good correlation between strain and AMS directions and between natural strain values and principal susceptibility differences. Although this last correlation is quite empirical (see discussion in Annex 1), the correlation between strain and AMS intensities shows that a good estimation of deformation gradients through a deformed area can be directly obtained from AMS measurements.

I.2. Anisotropy of magnetic susceptibility and anisotropy of remanent magnetization: the example of the Flamanville granite.

AMS is generally considered as important in paleomagnetism, because in anisotropic media, the remanent magnetization at the time of acquisition is not necessarily parallel to the ancient magnetic field direction. However, relationships between AMS and remanent magnetization anisotropy are not known. Only theoretical 2-D developments, dealing with TRM in anisotropic assemblages of multidomain (MD) magnetites have been given by Nagata (1961), or Stacey & Banerjee (1974), for example. More recently, Stephenson et al. (1986) have shown that a theoretical linear relationsip exists between AMS, IRM and TRM anisotropy tensors eigenvalues. However, if such correlations are theoretically justified, they need, just as in the case of strain and AMS correlations, to be established for every rock type studied.

From currently admitted theories of TRM acquisition by assemblages of MD magnetites, a simple relationship has been established between AMS tensor and TRM anisotropy tensor. Following this development, given in Annex 2, these tensors have the same eigenvectors, and their eigenvalue ratios should follow a relation of the type $M_i/M_j \approx (k_i/k_j)^2$. This theoretical relationship has been verified by experimental tests held on 2 sets of strongly anisotropic rock samples.

Finally, the paleomagnetic study of the anisotropic granite of Flamanville (Annex 3) allowed to give an application of this correlation. It has been shown that AMS is accompanied by significative and consistent deviations of primary TRM. It was verified that from AMS measurements, it was possible to estimate an inverse TRM anisotropy tensor, allowing the computation of the paleofield direction from these deviated TRM

I.3. Conclusions.

Main conclusions have already been drawn in Annexes 1 to 3. We can however stress the following points.

We can note that for TRM deviations in the Flamanville granite, we never had to consider the deformation mechanisms. Independently from its causes, this is the occurence of AMS itself which results in TRM deviations. We can therefore think that if we are able to establish the theoretical relationships between induced magnetization and the different types of remanent magnetization, the measurement of AMS can provide a direct estimate of remanent magnetization anisotropy, whatever the mechanisms of magnetic carriers preferred orientation development could be. This conception makes the fundamental difference between the study of remanence acquired after deformation, and the study of magnetization acquired before deformation, and then deviated by strain. In this latter case there is, in effect, no more direct relationships between AMS and remanence deviations.

Although only TRM in MD magnetite assemblages has been considered here, the application of this theory is probably wide, owing to the large occurence of such a magnetic carrier. Nevertheless, AMS effects cannot be neglected, and a systematic check of AMS appears desirable when performing paleomagnetic studies within deformed areas.

CHAPTER II. DEFORMATION AND PRETECTONIC REMANENT MAGNETIZATION.

II.1. Introduction.

The characterization of strain effects upon pretectonic remanent magnetization forms the main part of the work presented here. Most of the results obtained are published or planned to be published. Copies of these articles are given in Annexes 4 to 9, and a synthesis is given in Annex 10.

Although strain is generally recognized as a major cause of NRM perturbations (see for example Van den Ende 1977, Ozima 1980, Kligfield et al. 1981, Facer 1983, Rosenbaum 1986, Anson & Kodama 1987), no thorough characterization has yet been undertaken. For this reason, some simplifying criteria have been established here. (1) A reference paleomagnetic direction (at the undeformed state) must be known. (2) The pretectonic remanent magnetization must not be totally erased during deformation. (3) magnetic particles should only suffer a rotation mechanism. (4) We have to measure the total strain within each of the paleomagnetic sampling site. (5) We want variations of strain intensity, and of angular relationships between principal strain directions and initial direction of the pretectonic remanent magnetization.

From these constraints, moderately deformed redbed formations were chosen. The anisotropic shape of hematite crystals allows to think that they undergo some rotations during strain processes. The magnetic memory of hematite is admitted to be stable. The bedding plane of sedimentary formations is generally admitted to be a good paleo-horizontal indicator, and in redbeds, the occurence of elliptical decolorated areas (reduction spots) provides good quality strain markers.

However, before considering the results obtained from natural series (Annexes 7, 8 and 9), we detail the results of analogic models (Annex 4) and numerical models (Annex 5), where the effects of magnetic particle rotations induced by strain, upon remanent magnetization have been simulated.

II.2. The models.

II.2.1. Analogic simulation and numerical simulation.

The few results of analogic simulations that are found in the litterature allowed to think that deformation of magnetized synthetic samples is accompanied by a rotation of magnetization away from the shortening direction (e.g. Blow & Hamilton 1978, Ozima 1980, Morash & Bonhommet 1981). However, the physical mechanism allowing such a rotation has never been fully constrained, although it is generally attributed to some rotations of magnetic carriers.

I thus reconsidered and completed the experiments of Morash (1981), and performed a series of coaxial shortening experiments with Plasticine samples containing anisometric hematite particles. The analysis of variations in direction, intensity and grouping of IRM with respects to strain directions and intensity, is given in Annex 4. The results are compared with results from a numerical simulation (Annex 5), where the magnetization is modeled as the vector sum of N micromoments, each micromoment being carried by a planar particle modeled as a passive plane (model of March 1932) during deformation. The results from these 2 simulations are shown to be identical. However, such

an identity is quite paradoxal, with respects to particle rotation mechanisms, and needs to be discussed.

II.2.2. Rigid rotation of planar particles and passive rotation of planes.

Before entering this discussion, we have to redefine three possible rotation mechanisms. For the first and the second one, the particle is modeled as an ellipsoid embedded in a homogeneously deforming matrix with a given viscosity contrast. The general case has been studied by Bilby et al. (1975), but we consider the following extreme cases: (1) There is no viscosity contrast and thus, the particle deforms homogeneously with the matrix; this is strictly what is named the passive behaviour. An example of this behaviour is given by the reduction spots within redbeds. (2) The viscosity contrast is infinite: the particle is defined as a rigid particle, and its rotation during deformation of the matrix is a rigid rotation. Clearly, hematite particles embedded in a plasticine matrix (Annex 4) closely follow this model. (3) For the third mechanism, elongated particles are modeled as lines, and planar particles are modeled as planes. During deformation, they behave as passive lines and planes, following the model of March (1932). This model, which has been given the name of "line/plane model" by Owens (1974), has been used for the numerical simulation of Annex 5.

There is no immediate reason for having identical rotations of rigid particles and passive lines and planes. However, we obtained similar results in numerical simulation, where the mechanism (3) was modeled, and in analogic simulation, where the mechanism (2) is the most probable. This is the paradox alluded above.

In order to explain this, I carried out a comparison in 2 dimensions between rigid rotations of elliptical particles and rotations of passive lines. From the general equations of Bilby et al. (1975), P. Cobbold and D. Gapais (pers. comm.) have established equations for few limiting conditions. Amongst them, the rotation of rigid particles during a coaxial shortening can be written:

$$\tan \Phi = (\lambda_1/\lambda_2)^x . \tan \Phi_o \qquad (1)$$

where Φ_o is the initial angle between the long axis of elliptical grain and the maximum elongation axis of strain, and Φ this angle after deformation. The exponent 'x' is a function of the grain ellipticity and is written as:

$$x = \frac{1/R^2 - 1}{1/R^2 + 1}$$

where R is the axial ratio of the particle. The rotation of a passive line in this particuliar case is written as:

$$\tan \quad = (\lambda_2/\lambda_1).\tan \qquad (2)$$

We can note that when R converges toward ∞, x converges toward -1, and eqn.(1) becomes eqn.(2). In coaxial 2-D deformation, the passive line can thus be defined as a rigid particle of infinite length. In order to estimate the limit of ellipticity above which a rigid particle can be considered as a passive line, curves of equation (1) have been drawn (Fig.II.1) as the variations of Φ as a function of R, for different strain values λ_1/λ_2, and for different initial values of Φ_o . It can be seen that for an ellipticity greater than 3, the difference between rigid particle rotations and passive line rotations (thin lines in the diagrams) is lower than 5^o. Since the hematite particles of analogic simulations (Annex 4) have a normal:length

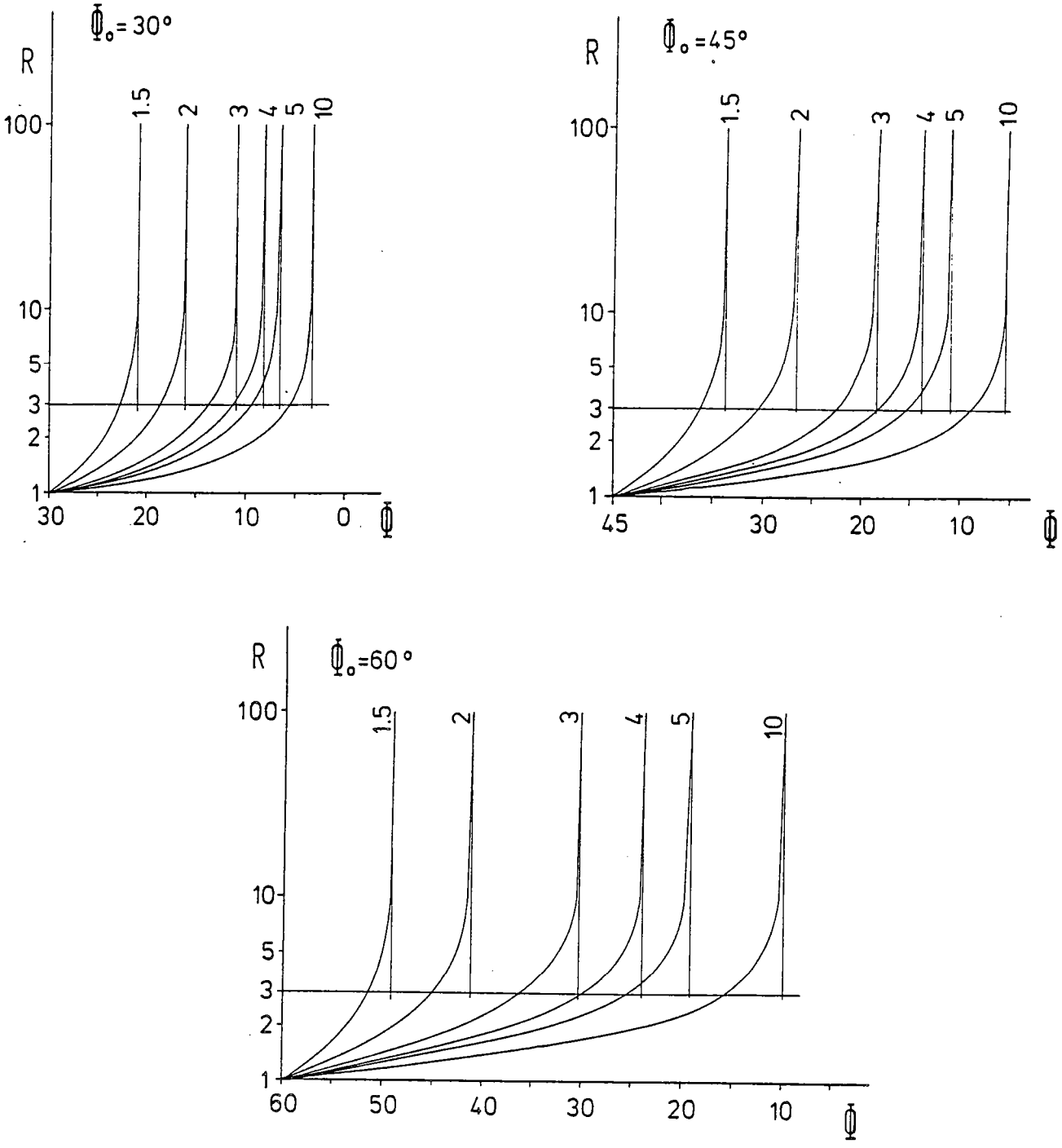

Fig.II.1: Variations of the angle Φ between the long axis of a rigid elliptical particle and the strain maximum elongation axis (λ_1), as a function of the particle ellipticity ratio R. Three cases with initial Φ_o =30°, 45° and 60° have been considered. Each curve is drawn for a given intensity of strain, expressed as the ratio $\lambda 1/\lambda 2$, increasing from 1.5 to 10. Vertical thin lines are the material line deviations for these strain values.

ratio of 1:20 to 1:30, this probably explains the similarity between results from analogic and numerical simulations.

we finally have to note that such an analysis only applies in the considered case of coaxial shortening. The effects of strongly non-coaxial deformations should only be known from other simulations.

II.2.3. Rotation of magnetic carriers and rotation of remanent magnetization.

(N.B.: In the original French version of the text, this section is approximately a translation of the analysis given in the section '4. interpretation and conclusions' of Annex 4. English readers can refer to this section.)

II.3. Paleomagnetic studies of deformed redbeds.

The effects of strain upon pretectonic remanent magnetization have been studied within three red formations: the Permian redbeds of the Alpes-Maritimes (Annex 7), the Pyrenean Permian redbeds at the 'Col du Somport' (Annex 8), and the Ordovician redbeds of the Pont-Réan Formation, Central Brittany (Annex 9).

In each of these formations strain was estimated by measuring the orientation and axial ratios of elliptical reduction spots.

In the Alpes-Maritimes redbeds, X-ray texture goniometry was used to study the progressive development of hematite preferred orientations (Annex 6). A comparison of these fabrics with fabrics simulated following a model of passive plane rotation of hematite, has shown that such a mechanism can account for natural fabrics in these redbeds.

In the Pont-Réan Formation too, a progressive rotation of hematite during deformation has been inferred from AMS measurements (Annex 9). However AMS results did not allow to assess the exactly passive behaviour of hematite.

Secondary recrystallisation of hematite did not allow to check the reorientation processes of hematite in the Pyrenean redbeds (Annex 6). Moreover, they resulted in a strong overprint of the primary pretectonic remanent magnetization component by a secondary one, leading to difficulties in analysing the effects of strain upon primary remanence (Annex 8).

In contrast, such an analysis could be performed in the two other examples. It results in a consistent description of strain effects upon pretectonic remanent magnetization.

II.4. Synthesis and discussion.

II.4.1. Within-site distribution and between-site distribution of magnetization at the deformed state.

A first synthesis of strain effects upon remanent magnetization is given in Annex 10. When writing this article, results from analogic simulations (Annex 4) and from the paleomagnetic study of the Pont-Réan formation (Annex 9) were not yet available. We can however note that these late studies perfectly fit the analysis of Annex 10.

The compilation of studies given in Annexes 4 to 10 allows to describe the effect of strain upon pretectonic remanent magnetization as one basic phenomenon: the deviation of the magnetic vector towards the strain flattening plane. In this description, the magnetic vector is defined at the scale of usually measurable specimen. Within a sampling site, defined as the largest volume in which strain can be considered as homogeneous, this deviation measured at the specimen scale will have various effects on mean

direction and its grouping, depending upon initial angular relationships between magnetization direction and shortening direction. Various situations have been described in the analogic simulations, and the effects observed at the hand-sample scales have been recovered in the paleomagnetic studies of natural rocks (particularly Annexes 7 and 9).

It seems to be important to stress here a point of methodology. In the sudies of finite strain, it is usually admitted that the study of heterogeneously deformed regions can be done through the study of small domains where strain can be considered as homogeneous (see Ramsay 1967). Such a partition should be applied in studying the effects of strain upon remanent magnetization. Before analysing paleomagnetic vector distributions through folded areas (which are typical heterogeneously deformed domains), we must study and understand the effects of homogeneous strain. This allowed us to compare the simulation results with within-site deviations and dispersions in natural formations. The in-situ between-site distributions then depend upon strain distribution over the folded area and can thus be extremely variable: along a great circle in the Alpes-Maritimes redbeds (see Fig. 9 and 10 in Annex 7), Fisherian in the Pont-Réan formation (Annex 9), more or less on a small circle in the Pyrenean redbeds (Annex 8).

II.4.2. Magnetization deviation and the fold test.

Notwithstanding the above comments, there is one general effect of strain, of first importance at the scale of a folded area, that is the general modification of angular relationships between magnetization vector and bedding plane. This leads to anomalous results with respect to the classical fold test. During classical unfolding, pretectonic magnetizations have shown evolutions that are characteristic of syntectonic remagnetizations in the case of the Alpes-Maritimes redbeds, or post-tectonic remagnetizations in the Pont-Réan formation. This can be illustrated by drawing the evolution of the precision parameter 'k' (Fisher 1953) as a function of unfolding percentages during stepwise unfolding. This has been proposed by Scotese & Van der Voo (1983), to show that in the case of synfolding remagnetizations, the data cluster before 100% unfolding. Since this time, an increasing number of workers has used this method, and interpreted 'kmax' at a given percentage of unfolding as an argument for a synfolding age of magnetization (e.g. see McCabe et al. 1983, Kent & Opdyke 1985, Miller & Kent 1986 a and b).

Application of this method to our data from Annexes 7 and 9 gives the result of Fig.II.2. It is obvious that in the 3 considered cases, the precision parameter 'k' reaches a maximum before total unfolding. Without any other analysis, these data should have thus been interpreted as syntectonic remagnetizations.

These results corroborate some recent theoretical analyses of Van der Pluijm (1986, 1987) and Kodama (1986 a and b, 1987). From simple 2-D models of magnetization behaviour during folding with strain, these authors criticize synfolding interpretations only inferred from this statistical test. It is shown here that, in effect, the statistical argument is, although necessary, not a sufficient condition for such an interpretation. The lack of strain during folding processes must also be argumented. It is thought that AMS measurements should provide a check of possible strain-induced preferred orientations of magnetic carriers.

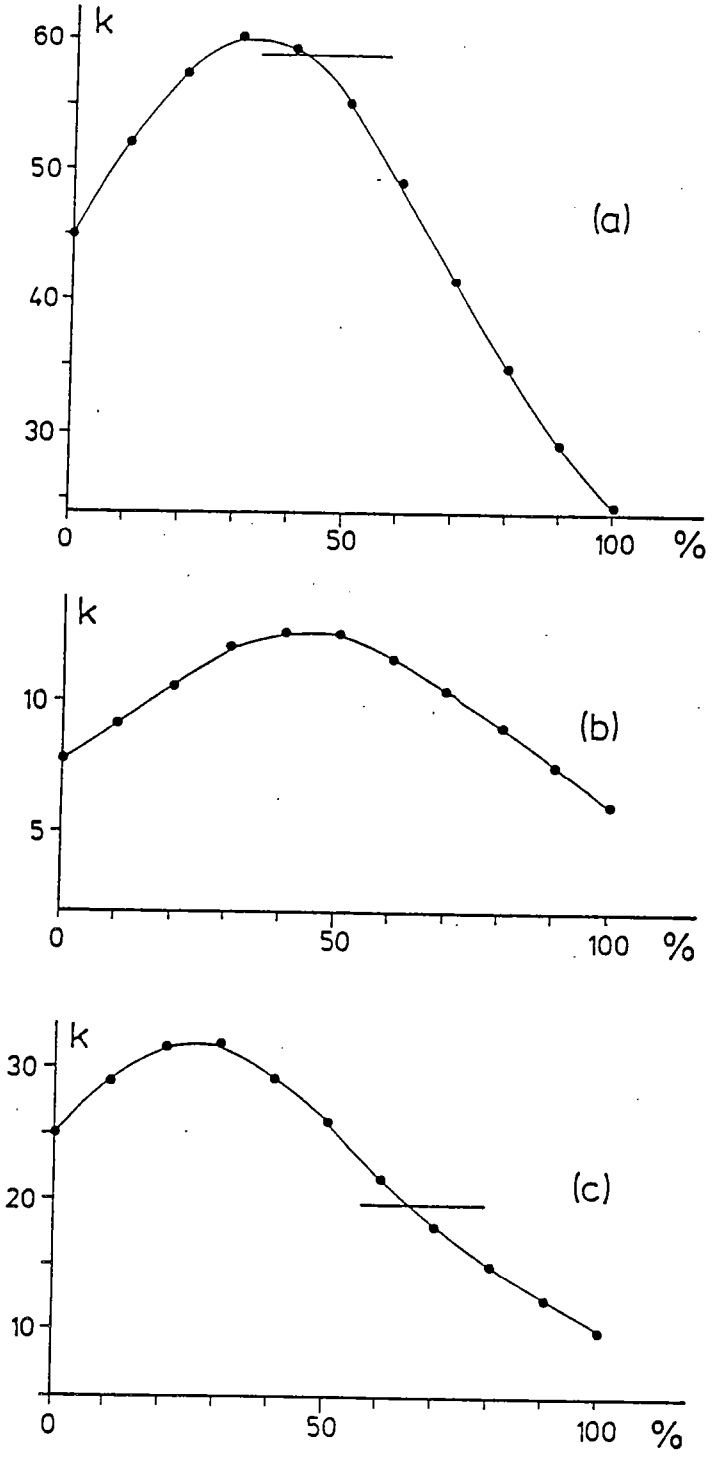

Fig.II.2: Evolution of the precision parameter 'k' (Fisher 1953) of the between-site distributions in the folded redbeds, as a function of unfolding percentage (%). (a) Group I in the Alpes-Maritimes redbeds (see Annex 7); (b) Group II in the Alpes-Maritimes redbeds; (c) redbeds of the Pont-Réan formation (Annex 9). Horizontal thin lines in (a) and (c) indicate the 95% probability level above which parameters 'k' are significantly greater than in the 100% unfolded state (tilt-corrected).

II.5. Conclusions.

Apart from some recrystallizations, the progressive deformation of redbeds is accompanied by a progressive rotation of planar hematite particles. This has been verified by the study of hematite fabrics through texture goniometry or AMS measurements.

The remanent magnetization, modeled as the vector sum of micromoments carried by each particle, is rotated and its grouping is changed in a way that has been described through results of simulations in simple coaxial shortening. The characteristic effects described from the simulations have been observed in natural deformed rock units. Strain effects can be summarized as one basic phenomenon, the deviation of measurable magnetization towards the strain flattening plane. The effects upon mean directions and grouping of vector population can then be logically envisaged, by considering their initial angular relationships with strain directions at the site scale.

From this consistent description of strain effects upon remanent magnetization, we can now consider the possibility of correcting paleomagnetic vectors for strain-induced deviations, in order to estimate the magnetic field direction at the time of acquisition.

CHAPTER III. STRAIN REMOVAL APPLIED TO PRETECTONIC REMANENT MAGNETIZATION

III.1. The algorithm and its application.

The analysis of paleomagnetic data from the Alpes-Maritimes (Annex 7) led me to establish the basic hypothesis for the strain removal technique applied to paleomagnetic vectors: magnetization vector distributions at the deformed state, as well as the variations of these distributions with respect to strain, are consistent with the distributions of passive lines, or material lines, in these strain conditions. From this observation, one can try to correct paleomagnetic vectors for these deviations, by using the strain response model of March (1932) for material lines.

It is important to stress here that we do not consider the paleomagnetic vector as being a material line (a line joining 2 material points of the volume), which is indeed an irrealistic assumption, but we observe that paleomagnetic vector deviations are analogous to material line deviations, at least for the studied cases. The strain removal technique applied to paleomagnetic vectors is described in Annex 7, recalled in Annexes 8 and 9, and discussed in Annex 10. The final orientation of a material line only depends upon its initial orientation and the total deformation. The latter can thus be decomposed into its 2 classical components (Ramsay 1967): a strain part, and a rigid-body rotation part. The third component, the rigid translation, has no influence in this problem. The correction applied to paleomagetic vectors is thus done in two steps (Fig.III.1 and Annex 7): (1) inverse strain by applying the inverse strain tensor to the vector, (2) inverse rigid-body rotation by a classical tilt correction, but from the unstrained bedding coordinates.

This correction has been successfully applied to the pretectonic paleomagnetic vectors of the 3 studied natural redbed units. It allowed to correct for the large within-site dispersion when strain had such an effect (Annex 7). After the total inverse deformation, it always allowed to recover a mean pretectonic direction of magnetization, although the application of classical criteria should have lead to reject these data.

III.2. Discussion: an estimation of the causes of errors.

Although these results appear to be quite positive, the application of this correction was not always easy. Possible error causes can be separated into 2 main groups: (1) experimental errors in estimating the parameters of the problem (magnetization, deformation), (2) theoretical error on the strain response model (passive line hypothesis). These two points have been discussed in the paleomagnetic studies of the Pyrenean redbeds (Annex 8) and of the Pont-Réan Formation (Annex 9), and also in the synthesis discussion of Annex 10. We can give the following review.

III.2.1. Experimental errors on parameters.

Without neglecting their importance, I shall not discuss here problems of paleomagnetic analysis (separation of magnetic vectors, determination of primary components, etc..). Paleomagnetic techniques and their limitations are now quite well established, and make the methodology of modern paleomagnetism (see Perroud 1985). More specific problems appear in the

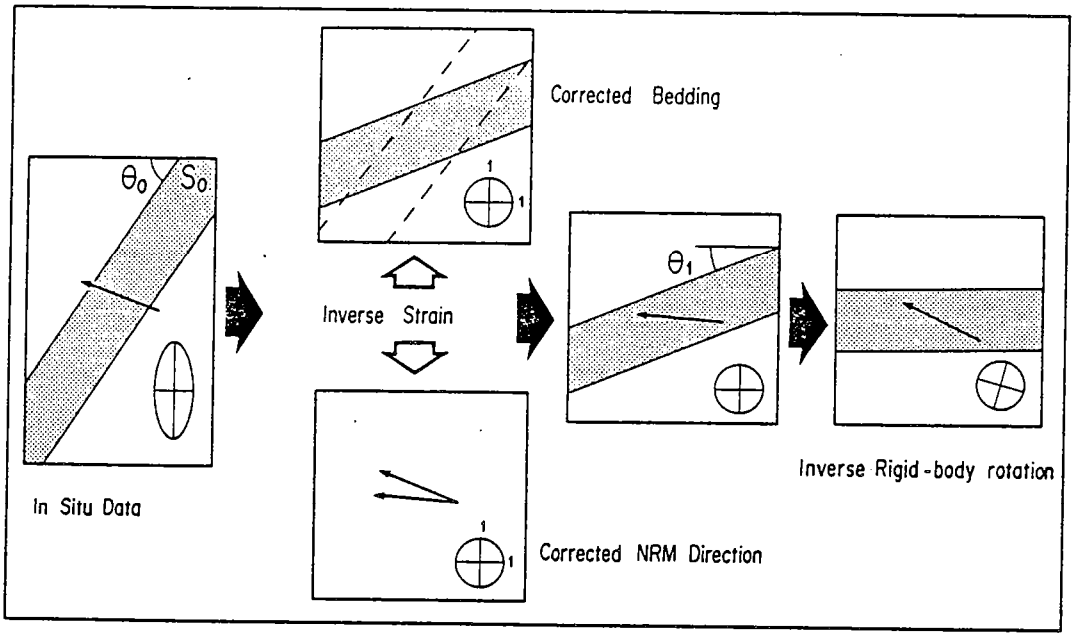

Fig.III.1: Schematic illustration of the strain removal technique applied to pretectonic directions of magnetization (after Annex 7).

present work, mainly dealing with the estimation of total deformation that affects paleomagnetic vectors. As noted above, the passive line hypothesis allows to separate total deformation into (1) a strain part and (2) a rigid body rotation part.

-(1) The strain tensor is estimated from field measurements of the cleavage plane strike and dip, the direction of stretching lineation, and the axial ratios of elliptical strain markers. Here, as in all other physical measurements, there are some experimental errors around the estimated value. A good example is given by the comparison between strain and AMS principal directions in the Pont-Réan Formation (Annex 9). However a more important problem is to estimate the exact part of deformation affecting the paleomagnetic vectors, from the measured total deformation. This is illustrated by the example of the Pyrenean redbeds, in which it has been shown that reduction spots have recorded both a compaction and a tectonic deformations. From the reasonable assumption that magnetization is of chemical origin, acquired during compaction and diagenesis, only the tectonic part of the total strain recorded by the reduction spots will have a deviating effect on magnetization vectors. Using of the total strain tensor in order to correct deviated vectors can thus induce significant errors in the final results. In the case of the Pyrenean redbeds, it has been shown that it was necessary to remove the compactionnal part from total deformation, before applying the strain removal technique to the primary paleomagnetic vectors.

-(2) The rigid-body rotation is estimated from the strike and dip of the unstrained bedding plane. Assuming that the bedding plane was initially horizontal, this yields a good estimation of the rigid-body rotation part around the horizontal axis. However, this estimation, at the scale of homogeneously deformed sites, does not allow any estimation of rotations around vertical axes. This limitation is inherent in the used technique, and only 3-D inverse deformation at the scale of the folded area (see e.g. Percevault 1983) could allow such estimations. Finally, we can also question the basic hypothesis of the initially horizontal attitude of the bedding plane (see for example Perroud et al. 1986, and also our results in the Pont-Réan formation in Annex 9).

We can finally noté that some instability situations in the correction of paleomagnetic vectors can arise from errors in measuring structural directions (cleavage, bedding..). This is well illustrated in the case of the Pont-Réan Formation, where the mean direction of magnetization is very close to the cleavage plane. Some slight variations in the direction of the cleavage plane are sufficient for the vectors to be on one side or the other of this plane, and thus, the applied correction will induce a rotation in one sense or the other, leading to spurious results in one situation. Such an effect can be suspected in the case of the 4 eliminated data in Annex 9. The current mean of applying strain removal does not allow to control such instabilities.

III.2.2. The analogic simulation and the passive line hypothesis.

Another suspected major cause of error in applying the strain removal technique could be due to significant differences between the paleomagnetic vectors behaviour and the passive line behaviour. The passive behaviour of magnetization has been postulated from the analysis of results from the paleomagnetic study of the Alpes-Maritimes redbeds. It has been then verified, at least in the case of the Pont-Réan Formation, and suspected in

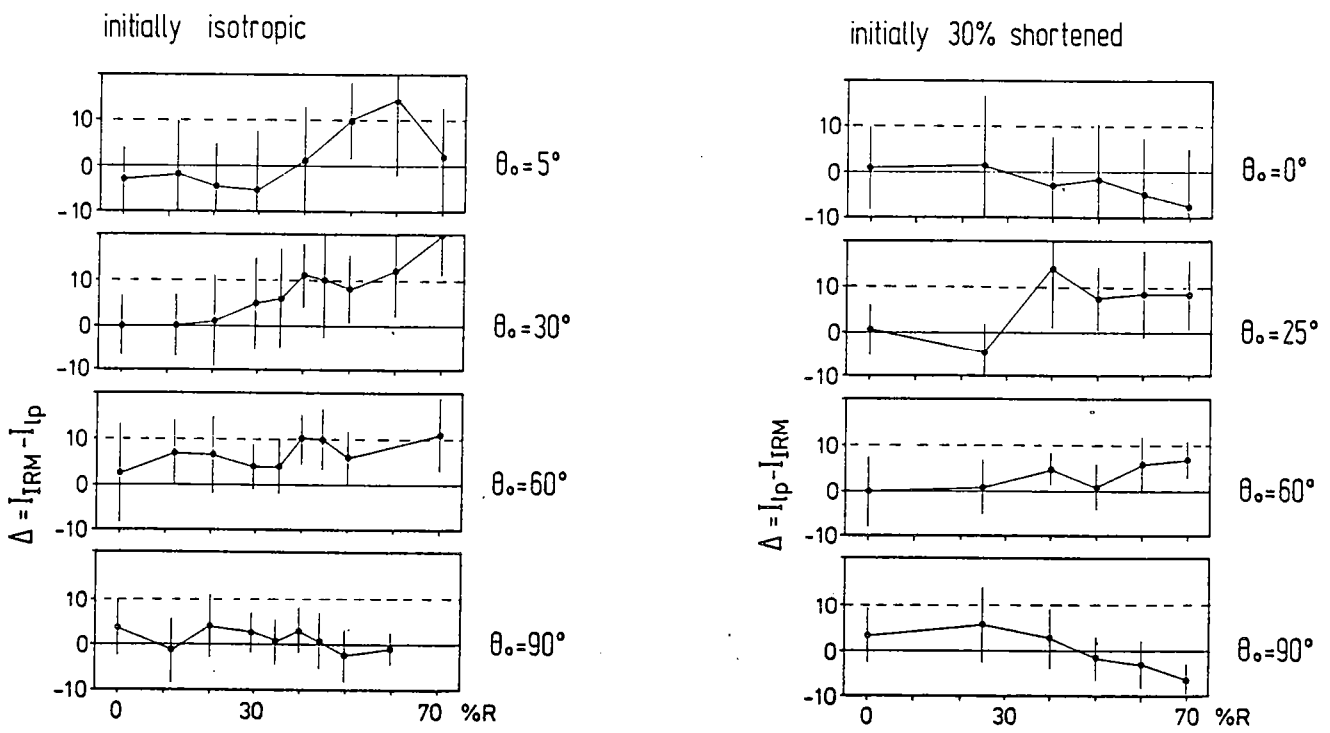

Fig.III.2: Deviation differences Δ between the passive line and IRM of analogic simulations of Annex 4, as a function of shortening percentages (%R), and for various angles θ_0 between shortening direction and initial mean IRM. Left: initially isotropic samples; right: initially 30% shortened samples (see Annex 4).

the Pyrenean redbeds. However it appears quite difficult to check the exact fitness of this model within natural series. Our best chance to estimate differences in behaviour between passive lines and magnetic vectors, is to use the results of the simulations. A comparison of IRM deviations of the analogic simulation (Annex 4) with the theoretical deviations of passive lines following the model of March (1932) is given in Fig.III.2. In this figure, the difference between passive lines deviations and IRM deviations are expressed as a function of shortening percentages (%R), for various initial angles θ_0 between initial IRM direction and shortening (λ_3) direction. The difference Δ, which is the difference in inclination in the terminology of Annex 4, is computed so that a positive difference expresses a deviation of passive line greater than the deviation of IRM. We can make the following observations: (1) in both cases of initial conditions (isotropic, or initially 30% shortened), when initial IRM is parallel ($\theta_0=0^o$) or orthogonal ($\theta_0=90^o$) to λ_3, neither IRM, nor the passive line are deviated. The difference thus stays close to 0. It is thus concluded that in these particuliar cases, there is no difference between passive line and IRM behaviours. This observation also applies in the case where IRM is initially close to λ_3 ($\theta_0=5^o$). (2) In all other cases of intermediate θ_0, the passive line deviation is practically always greater than IRM deviation. We can however note that the difference in deviation Δ is lower than 10^o for all the cases, up to 50% of shortening, and in the case of initially 30% shortened specimens, up to 70% of shortening. Moreover, these latter specimens show generally smaller differences than the initially isotropic specimens. We can thus say that, within the limits of the simulation, IRM deviations are close to the theoretical deviations of material lines. Furthermore, an initial fabric seems to improve this similitude.

These remarks lead me to give another formulation of the magnetic vector behaviour law: the initial direction and the final direction, at the deformed state, are connected through a second-order symmetrical "deviation tensor". Its eigenvectors are identical to the strain tensor eigenvectors, and its eigenvalues are close to the strain tensor eigenvalues. This formulation allows to give another expression of the basic hypothesis: rather than modelling the magnetic vector as a material line, it seems better to say that the deviation tensor of paleomagnetic vectors is conveniently estimated by the strain tensor. Although both expressions result in exactly the same mathematical formulation, the second one appears more strict with respect to the mechanisms.

We can finally note that, if differences in deviation are about 5^o to 10^o in the simulations, it is quite difficult to estimate the consequences of this difference within natural series. However, the positive results obtained by applying the strain removal technique in the 3 studied redbeds formations, allow to think that estimating the deviation tensor from the measured strain tensor is a quite good working hypothesis.

In conclusion to this review of causes of errors in applying corrections to deviated remanent magnetization vectors, we can stress the following points:

(1) We are able to put error bars on the measures of the various parameters of the problem.

(2) We know that the estimation of rigid-body rotation is approxi- mative.

(3) Although quite correct, the estimation of the deviation tensor from the strain tensor is also an approximation.

(4) Although we have a certain knowledge of these causes of errors, the discrete application of the strain removal algorithm does not allow to take these incertitudes into account.

In order to improve the final estimation of the pretectonic direction of magnetization, it appears necessary to develop a numerical method allowing the determination of a solution that takes into account all the data and their incertitudes.

III.3. Application of the generalized nonlinear inversion to the determination of the pretectonic direction of magnetization within strained folded beds.

The following is an application of the solution to the generalized nonlinear inverse problem using the least-squares criterion as proposed by Tarantola & Valette (1982). The solution, following this method, to the problem of paleomagnetic vectors deviated by strain, needs to redefine strictly our physical system and its parameters.

III.3.1. Basic assumption.

From the analyses given in Chapter II and above, section III.1, the magnetization M, measured at the deformed state, can be connected to its initial direction H through a tensor T in the following way:

$$M_i = T_{ij}.H_j \qquad i,j=1,2,3 \qquad (1)$$

The total deviation tensor T_{ij} for a given magnetization M_i can be decomposed into a part of deviation induced by a rigid-body rotation R (which is the only part usually considered in paleomagnetism), and a tensor S of the deviation induced by strain. Following the above discussion, S is estimated as being the strain tensor.

$$T_{ij} = S_{ik}.R_{kj} \qquad (2)$$

Equations (1) and (2) define the physical system: pretectonic magnetization, deformation, measured magnetization.

III.3.2. The parameters of the problem.

***-Deviation tensor T.**

(i) Tensor S.

Principal directions of this tensor are defined by the measure of 3 independant angles: The strike (Sc) and the dip (Dc) of the cleavage plane (S_1), and the pitch (Px) of the stretching lineation within this plane. The direction of Sc is determined so that the plane dips downward in the direction Sc+90°.

From the measure of these 3 angles, the direction cosine of the eigenvectors of S are determined as:

-Direction of minimum elongation λ_3 (normal to S_1) :

$$\begin{cases} Z_1 = -\sin Sc.\sin Dc \\ Z_2 = \cos Sc.\sin Dc \\ Z_3 = -\cos Dc \end{cases} \qquad (3)$$

-Direction of maximum elongation λ_1 (stretching lineation) :

$$\begin{cases} X_1 = \cos Sc.\cos Px - \sin Sc.\cos Dc.\sin Px \\ X_2 = \sin Sc.\cos Px + \cos Sc.\cos Dc.\sin Px \\ X_3 = \sin Dc.\sin Px \end{cases} \qquad (4)$$

The direction of intermediate elongation λ_2 (Y_1,Y_2,Y_3) is defined as the vector product of the 2 others. The cartesian coordinates of the eigenvectors of S are then used to construct the transformation matrix a_{ij}:

$$a = \begin{pmatrix} X_1 & Y_1 & Z_1 \\ X_2 & Y_2 & Z_2 \\ X_3 & Y_3 & Z_3 \end{pmatrix} \qquad (5)$$

The eigenvalues λ_1, λ_2 et λ_3 of S are estimated from the mean axial ratios of elliptical markers, or by fitting with Rf/Φ graphs of Dunnet (1969). The advantage of an arithmetical mean is to provide a standard deviation around the mean value. We can then construct the diagonal tensor S'_{ij}:

$$S' = \begin{pmatrix} \lambda_1 & 0 & 0 \\ 0 & \lambda_2 & 0 \\ 0 & 0 & \lambda_3 \end{pmatrix} \qquad (6)$$

and finally obtain S_{ij} in the geographical system of coordinates:

$$S_{ij} = a_{ik}.a_{jl}.S'_{kl} \qquad i,j,k,l = 1,2,3 \qquad (7)$$

(ii). Tensor R.

As discussed above, the rigid body rotation is estimated from the unstrained bedding plane. The basic parameters are thus the strike (Sb) and the dip (Db) of the bedding plane in the deformed state.

The normal to bedding is defined as:

$$\begin{cases} n_x = -\sin Sb.\sin Db \\ n_y = \cos Sb.\sin Db \\ n_z = -\cos Db \end{cases} \qquad (8)$$

And the normal to the unstrained bedding is obtained from (see Owens 1974 and Annex 7):

$$n'_i = S_{ij}.n_j \qquad i,j = 1,2,3 \qquad (9)$$

which allows to obtain the strike (Sb′) and the dip (Db′) of the undeformed bedding plane. We can thus construct the rotation tensor, with a horizontal axis in the Sb′ direction, and Db′ as the rotation angle. This tensor is:

$$R = \begin{pmatrix} \cos^2 Sb' + \sin^2 Sb'.\cos Db' & \cos Sb'.\sin Sb'.(1-\cos Db') & \sin Sb'.\sin Db' \\ \cos Sb'.\sin Sb'.(1-\cos Db') & \sin^2 Sb' + \cos^2 Sb'.\cos Db' & -\cos Sb'.\sin Db' \\ -\sin Sb'.\sin Db' & \cos Sb'.\sin Db' & \cos Db' \end{pmatrix} \qquad (10)$$

N.B: R is the rigid-body rotation tensor, and not the inverse rigid-body rotation, or "tilt-correction", tensor.

In order to avoid unnecessary computing, we can express R directly from the normalized coordinates of n' following (9):

$$R = \begin{pmatrix} \frac{n'_y{}^2 - n'_x{}^2 . n'_z}{1 - n'_z{}^2} & \frac{n'_x . n'_y}{n'_z - 1} & -n'_x \\ \frac{n'_x . n'_y}{n'_z - 1} & \frac{n'_x{}^2 - n'_y{}^2 . n'_z}{1 - n'_z{}^2} & -n'_y \\ n'_x & n'_y & -n'_z \end{pmatrix} \qquad (11)$$

N.B: The expression (11) of R_{ij} is obtained from (10) and (8).

(iii) Total deviation tensor T.

From expressions (7) of S_{ij} and (11) of R_{ij}, T is constructed following (2):

$$T_{ij} = S_{ik} . R_{kj}$$

This tensor is thus constructed from the measure of 8 parameters:

Sc: strike of the cleavage plane
Dc: dip " "
Px: pitch of the stretching lineation within S_1
λ_1, λ_2, λ_3: principal strains
Sb: strike of the bedding plane
Db: dip " "

By assuming a gaussian distribution of errors in the estimation of each of these parameters, we can establish a standard deviation around each of them. For the angles, these standard deviations can be inferred both from the precision of the instrument and from field observations. For the λ_i values, standard deviations are derived from those of the mean ratios λ_1/λ_2, λ_2/λ_3 etc..However, taking into account the above discussion about the identity strain tensor/deviation tensor, we can choose greater standard deviation than those resulting directly from measurements.

***-Deviated remanent magnetization M.**

The remanent magnetization M is defined by two angles (the modulus |M| is not considered), the declination "d" and inclination "i". The estimation of these parameters is performed through vector analysis of magnetic vector trajectories during stepwise demagnetizations. Here too, we can choose error bars depending on the quality of measurements, the quality of demagnetization trajectories etc..

***-Pretectonic direction of magnetization H.**

The vector H is also defined by two angles, the declination "D" and inclination "I". These parameters are uniques for all the deviated remanent magnetizations and the relevant tensors T, and are the basic unknowns of our problem.

III.3.3. The inverse problem.

Let (D_o, I_o) be an a-priori estimate (independent of our set of measurements) of the vector H, and (σ_o^D, σ_o^I) the standard deviation of this a-priori estimate. If we have no a-priori information on H, we will

accordingly take an infinite (very large) a priori standard deviation. Let $(d_o, i_o, Sc_o, Dc_o, Px_o, \lambda_{1o}, \lambda_{2o}, \lambda_{3o}, Sb_o, Db_o)^k$ be the data and $(\sigma_o^d, \sigma_o^i, \sigma_o^{Sc}, \sigma_o^{Dc}, \ldots, \sigma_o^{Db})^k$ the standard deviations for the magnetization number k (k is an index, not an exponent). Clearly, there is no direction H(D,I) exactly verifying (1) for all the considered magnetizations and deformations. We aim at defining a direction H(D,I) and a set of "corrected data" $(d, i, Sc, Dc, Px, \ldots, Db)^k$ which are compatible with equation (1):

$$M_i = T_{ij}.H_j \qquad (1)$$

and we will choose the solution which minimizes the sum:

$$S = \left(\frac{D-D_o}{\sigma_o^D}\right)^2 + \left(\frac{I-I_o}{\sigma_o^I}\right)^2 + \sum_{k=1}^{N} \left[\left(\frac{d-d_o}{\sigma_o^d}\right)_k^2 + \left(\frac{i-i_o}{\sigma_o^i}\right)_k^2 + \left(\frac{Sc-Sc_o}{\sigma_o^{Sc}}\right)_k^2 + \left(\frac{Dc-Dc_o}{\sigma_o^{Dc}}\right)_k^2 + \ldots\ldots\ldots\ldots + \left(\frac{Db-Db_o}{\sigma_o^{Db}}\right)_k^2 \right] \qquad (12)$$

where N is the number of deviated magnetizations considered in the problem. Equation (1) and minimization of S given by (12) state the inverse problem.

III.3.4. Solution of the inverse problem.

We introduce the following vectors:

$$X_o = \begin{bmatrix} \begin{pmatrix} d_o \\ i_o \\ Sc_o \\ Dc_o \\ Px_o \\ \cdot \\ \cdot \\ Db_o \end{pmatrix}_1 \\ \cdot \\ \cdot \\ \cdot \\ \begin{pmatrix} d_o \\ i_o \\ Sc_o \\ Dc_o \\ Px_o \\ \cdot \\ \cdot \\ Db_o \end{pmatrix}_N \\ D_o \\ I_o \end{bmatrix} \qquad X = \begin{bmatrix} \begin{pmatrix} d \\ i \\ Sc \\ Dc \\ Px \\ \cdot \\ \cdot \\ Db \end{pmatrix}_1 \\ \cdot \\ \cdot \\ \cdot \\ \begin{pmatrix} d \\ i \\ Sc \\ Dc \\ Px \\ \cdot \\ \cdot \\ Db \end{pmatrix}_N \\ D \\ I \end{bmatrix} \qquad (13)$$

C_o is the covariance matrix of the a-priori values X_o. Under the hypothesis of independant errors, this matrix is diagonal and contains the respective variances of the elements of X_o.

The inversion must yield the most probable vector X compatible with the experimental errors and obeying the N equations:

$$f^k(X) = |M^k - T^k.H|^2 = 0 \qquad k = 1,N \qquad (14)$$

where $|M^k - T^k.H|$ is the modulus of the difference vector $D_i = M_i^k - T_{ij}^k.H_j$, and M^k and T^k are function of $(d,i,Sc,Dc,Px,\ldots,Db)^k$ following the section III.3.2.

Following this notation the solution

$$f(X) = 0 \qquad (15)$$

is defined by the minimization of

$$S = (X-X_0)^t.C_0^{-1}.(X-X_0) \qquad (16)$$

Note that equations (14) and condition (16) are equivalent to (1) and (12) resp.

Tarantola & Valette (1982) have shown that the solution of this nonlinear least-squares problem is obtained by the iterative algorithm:

$$X_{n+1}= X_0+C_0.F_n^t.(F_n.C_0.F_n^t)^{-1}.[F_n.(X_n-X_0)-f(X_n)] \qquad (17)$$

where F is the partial derivatives matrix:

$$(F_n)_{ij} = \left(\frac{\partial f^i}{\partial x_j}\right)_{X=X_n} \qquad (18)$$

When the solution X has been obtained, the covariance matrix of the solution, C, can be approximately obtained by a formula involving a linear approximation (Tarantola et Valette 1982)

$$C \approx C_0-C_0.F^t.(F.C_0.F^t)^{-1}.F.C_0 \qquad (19)$$

where the partial derivatives are taken at point X.

Partial derivatives of $f^k(X)$

In order to simplify the following expressions, vector M^k is named A, and vector $T^k.H$ is named B.

We can thus rewrite the equation (14) in the explicit form:

$$f^k(X) = (A_1-B_1)^2+(A_2-B_2)^2+(A_3-B_3)^2 \qquad (20)$$

where
$$\left|\begin{array}{l} A_1 = \cos d^k.\cos i^k \\ A_2 = \sin d^k.\cos i^k \\ A_3 = \sin i^k \end{array}\right. \qquad (21)$$
cartesian coordinates of M^k

and
$$\left|\begin{array}{l} B_1 = T_{11}^k.X+T_{12}^k.Y+T_{13}^k.Z \\ B_2 = T_{21}^k.X+T_{22}^k.Y+T_{23}^k.Z \\ B_3 = T_{31}^k.X+T_{32}^k.Y+T_{33}^k.Z \end{array}\right. \qquad (22)$$

with
$$\left|\begin{array}{l} X = \cos D.\cos I \\ Y = \sin D.\cos I \\ Z = \sin I \end{array}\right.$$
cartesian coordinates of H

and $T_{ij}^k = g(Sc^k, Dc^k, Px^k, \lambda_1^k, \lambda_2^k, \lambda_3^k, Sb^k, Db^k)$

Using this notation, derivatives of f^k with respect to the parameters defining H(D,I) are:

$$\frac{\partial f^k}{\partial D} = \frac{\partial (A_1-B_1)^2}{\partial D} + \frac{\partial (A_2-B_2)^2}{\partial D} + \frac{\partial (A_3-B_3)^2}{\partial D}$$

$$= 2\Big\{-(A_1-B_1).\left[T_{11}^k(-\sin D.\cos I)+T_{12}^k(\cos D.\cos I)\right]$$
$$-(A_2-B_2).\left[T_{21}^k(-\sin D.\cos I)+T_{22}^k(\cos D.\cos I)\right]$$
$$-(A_3-B_3).\left[T_{31}^k(-\sin D.\cos I)+T_{32}^k(\cos D.\cos I)\right]\Big\}$$

$$= 2\sum_{i=1}^{3}(A_i-B_i).\left[T_{i1}^k.Y-T_{i2}^k.X\right]$$

In a similar way, one obtains:

$$\frac{\partial f^k}{\partial I} = 2\sum_{i=1}^{3}(A_i-B_i)\left[T_{i1}^k(\cos D.\sin I)+T_{i2}^k(\sin D.\sin I)-T_{i3}^k(\cos I)\right]$$

Derivatives of f^k with respect to data are:

$$\frac{\partial f^k}{\partial d^k} = \frac{\partial (A_1-B_1)^2}{\partial d^k} + \frac{\partial (A_2-B_2)^2}{\partial d^k}$$

$$= 2(A_1-B_1).(-\sin d^k.\cos i^k)+2(A_2-B_2).(\cos d^k.\sin i^k)$$

$$= 2\left[A_1.(A_2-B_2)-A_2.(A_1-B_1)\right]$$

and

$$\frac{\partial f^k}{\partial i^k} = 2\Big[(A_3-B_3).(\cos i^k)$$
$$-(A_2-B_2).(\sin d^k.\sin i^k)$$
$$-(A_1-B_1).(\cos d^k.\sin i^k)\Big]$$

Derivatives of f^k with respect to the data that define T^k have no evident analytical solution, they will be numerically computed.

Finally, if data for two magnetizations are independent, partial derivatives of f^k with respect to $(d,i,Sc,Dc,\ldots,Db)^j$ are null for $j \neq k$.

III.3.5. Conclusion.

The above paragraphs show that it is quite easy to adapt the kind of general solution to inverse problem as proposed by Tarantola & Valette (1982), to the problem of recovering a pretectonic direction of magnetization from deviated ones within strained beds. However, without numerical applications of this algorithm, it is difficult to discuss its resolution. Nevertheless, such a formulation is the only mean to take into account all experimental errors on data, and in this way, the final result should have a better justification in terms of probability than the current determination by the mean of discrete "corrected directions".

III.4. Conclusions.

To conclude on the problem of correcting paleomagnetic directions from strain-induced deviations within redbeds, we can retain the following points:

(1) The analysis of IRM deviations in analogic simulations, and of NRM within redbeds shows that the known or suspected initial direction of magnetization is connected to its final direction, after deformation, through a "deviation tensor" which can be approximately estimated as being the strain tensor. This definition of the deviation tensor is analogous to the passive line hypothesis for paleomagnetic vectors.

(2) From this hypothesis, the inverse strain tensor can be used as a correction tensor for strain-induced deviations of paleomagnetic vectors. Positive results obtained by applying this technique on 3 natural examples shows that this is a good working hypothesis, and thus that it is possible to recover a mean pretectonic direction of magnetization from deviated remanent vectors.

(3) After this first step in establishing the hypothesis and testing it, it appears however necessary to improve the numerical treatments, in order to consider all experimental errors on the parameters implied in this problem. Such a formulation has been proposed.

(4) Finally, it must be noted that the proposed algorithm is not universal, and cannot be applied without a strict analysis of deformation and magnetization interrelationships. Only such an analysis should allow to justify the applied behaviour model.

CONCLUSIONS.

From the set of investigations presented here, the most basic conclusion that can be drawn is that ductile strain, as far as it results in the development of magnetic carriers preferred orientations, necessarily induces some deviations of the natural remanent magnetization: deviation of magnetization acquired by deformed rocks, deviation of pretectonic magnetization carried by anisometric crystals. This preliminary observation implies the necessity to take into account the occurence of strain, always possible when paleomagnetically studying formations within orogenic belts. The paleomagnetic studies of deformed redbeds we have given here, show that these deviations are particularly crucial for the interpretation of the fold test: with only the statistical argument of distribution evolutions during unfolding, the magnetizations should have been interpreted as synfolding in the Alpes- Maritimes redbeds, and syn- to post-folding in the Pont-Réan Formation. It therefore appears necessary to complete the statistical argument with a discussion on the total lack of strain. The study of the anisotropy of magnetic susceptibility, since it reflects the preferred orientation of magnetic minerals, is probably the best argument in this discussion.

At a second level of analysis, it has been shown that these deviations are consistent: consistency of TRM divergence from the field direction with respect to AMS directions, itself being controlled by strain, in the granite of Flamanville; consistency of within-site and between-site distributions with respect to strain directions, in the strained and folded redbeds. In the first case, a theoretical relationship has been established between AMS and TRM anisotropy tensors. The way of establishing this relationship allows to stress the original using of AMS measurements as a direct estimator of remanent magnetization deviations. In the granite of Flamanville, we have attained our end, that is, the determination of a paleofield direction through the paleomagnetic study of significantly deformed rocks.

For the problem of strain effects upon pretectonic remanent magnetization, simulations have shown that a mechanism of hematite rotation conveniently accounts for the development of observed crystallographic and magnetic fabrics within deformed pelitic redbeds. Within the limits of these examples, the deviation of paleomagnetic vectors appear roughly similar to passive lines deviation following the model of March (1932). This allowed to propose a correction based on this behaviour model. The discussion of this hypothesis, and the obtained results lead me to the conclusion that, although approximative, this model is our best chance to estimate a pretectonic direction of magnetization from remanent directions deviated by strain within redbeds.

Since the behaviour model is very close to the observed behaviour, it furthermore appears better to improve the numerical treatment of data, rather than to try to improve the behaviour model itself.

Finally, the results we obtained here allow to give a positive answer to some general questions: question on the deviating effects of strain within

deformed rocks; question on the consistency of these deviations; question on the possibility to characterize the effects of strain upon remanent magnetization. To the final question on the possibility of performing paleomagnetic studies within deformed areas, the answer is also affirmative, at least in the limits of the studied examples, and under the condition of a detailed and carefull analysis of strain and magnetization relationships, and of a sufficient understanding of magnetization deviation mechanisms.

In contrast, some problems remain; general problem of the fold test interpretation in orogenic zones; problem of the limitations to the proposed strain corrections; problem of mechanisms for other deformation styles (strongly non-coaxial, for example), other rock units with other magnetic carriers.

Only further investigations could help to solve such problems. However, the positive results we obtained appear stimulating for the development of research in this widely open field.

REFERENCES.

ANGELIER, J., TARANTOLA, A., VALETTE, B., MANOUSSIS, S., 1982. Inversion of field data in fault tectonics to obtain the regional stress. I - Single phase fault populations: a new method of computing the stress tensor. Geophys. J. R. Astron. Soc., 69, 607-621.

ANSON, G.L. & KODAMA, K.P., 1987. Compaction-induced inclination shallowing of the post-depositional remanent magnetization in a synthetic sediment. Geophys. J. R. Astron. Soc., 88, 673-692.

BIBLY, B.A., ESHELBY, J.D., KUNDU, A.K., 1975. The change of shape of a viscous ellipsoidal region embedded in a slowly deforming matrix having a different viscosity. Tectonophysics, 28, 265-274.

BLOW, R.A., HAMILTON, M., 1978. Effect of compaction on the acquisition of a detrital remanent magnetization in fine-grained sediments. Geophys. J. R. Astron. Soc., 52, 13-23.

BONHOMMET, N., COBBOLD, P.R., PERROUD, H., RICHARDSON, A. 1981. Paleomagnetism and cross-folding in a key area of the Asturian Arc (Spain). J. Geophys. Res., 86, B3, 1873-1887.

BORRADAILE, G. & ALFORD, C., 1987. Relationship between magnetic susceptibility and strain in laboratory experiments. Tectonophysics, 133, 121-135.

DUNNET, D., 1969. A technique of finite strain analysis using elliptical particles. Tectonophysics, 7, 117-136.

ELLWOOD, B.B. & WHITNEY,J.A., 1980. Magnetic fabric of the Elberton granite, Northeast Georgia. J. Geophys. Res., 85, 1481-1486.

FACER, R.A., 1983. Folding, strain and Graham's fold test in palaeomagnetic investigations. Geophys. J. R. Astron. Soc., 72, 165-171.

GRAHAM, J.W., 1949. The stability and significance of magnetism in sedimentary rocks. J. Geophys. Res., 54, 131-167.

HROUDA, F., 1976. A model for the orientation process of ferromagnetic minerals in slates. Earth Planet. Sci. Lett., 33, 107-110.

HROUDA, F., 1979. The strain interpretation of magnetic anisotropy in rocks of the Nisky Jezenik Mountains (Czechoslovakia). Sb. Geol. Ved, 16, 27-62.

HROUDA, F., 1980. Magnetocrystalline anisotropy of rocks and massive ores : a mathematical model study and its fabric implications. J. Struc. Geol., 2, 459-462.

HROUDA, F., 1982. Magnetic anisotropy of rocks and its application in Geology and Geophysics. Geophys. Surv., 5, 37-82.

KENT, D.V. et OPDYKE, N.D., 1985. Multicomponent magnetizations from the Mississippian Mauch Chunk Formation of the central Appalachians and their tectonic implications. J. Geophys. Res., 90, 5371-5383.

KLIGFIELD, R., OWENS, W.H., LOWRIE, W., 1981. Magnetic susceptibility anisotropy, strain, and progressive deformation in permian sediments from the Maritime Alps (France). Earth Planet. Sci. Lett., 55, 181-189.

KLIGFIELD, R., LOWRIE, W., HIRT, A., SIDDANS, A.W.B., 1983. Effect of progressive deformation on remanent magnetization of Permian redbeds from the Alpes Maritimes (France). Tectonophysics, 97, 59-85.

KODAMA, K.P., 1986a. The effect of deformation on the fold test. Eos Trans., 67, 268.

KODAMA, K.P., 1986b. Effect of flexural slip on Fisherian distributions: Implications for the fold test, Eos Trans., 67, 924.

KODAMA, K.P., 1987. Remanence rotation due to rock strain during folding and the stepwise application of the fold test. Submitted to J. Geophys. Res.

Mc CABE, C., VAN DER VOO, R., PEACOR, D.R., SCOTESE, C.R. et FREEMAN, R., 1983. Diagenetic magnetite carries ancient yet secondary remanence in some Paleozoic carbonates. Geology, 11, 221-223.

Mc DONALD, W.D., 1980. Net tectonic rotation, apparent tectonic rotation and the structural tilt correction in paleomagnetic studies. J. Geophys. Res., 85, 3657-3669.

MARCH, A., 1932. Mathematische theorie der regelung nach der korngestalt bei affiner deformation. Z. Krist., 81, 285-297.

MORASH, A., 1981. Paleomagnetisme et deformation. Mem. D.E.A., Rennes, 24p.

MORASH, A. BONHOMMET, N., 1981. Deviation of I.R.M. during simple shortening experiments. Abs. 4th IAGA Scientific Assembly Edimburgh, I13-12, 252.

MILLER, J.D. et KENT, D.V., 1986a. Synfolding and prefolding magnetizations in the Upper Devonian Catskill Formation of eastern Pennsylvania: Implications for the tectonic history of Acadia. J. Geophys. Res., 91, 12791-12803.

MILLER, J.D. et KENT, D.V., 1986b. Paleomagnetism of the Upper Devonian Catskill Formation from the southern limb of the Pennsylvania salient: Possible evidence of oroclinal rotation. Geophys. R. Lett., 13, 1173-1176.

NAGATA, T., 1961. Rock magnetism. Mazuren, Tokyo, 350p.

OWENS, W.H., 1974. Mathematical model studies on factors affecting the magnetic anisotropy of deformed rocks. Tectonophysics, 24, 115-131.

OZIMA, M., 1980. Effects of a plastic deformation on the remanent magnetization of a Cu-Co alloy. Earth Planet. Sci. Lett., 47, 121-123.

PERCEVAULT, M.N., 1983. Problème inverse en déformation finie. Application au segment Hercynien de Bretagne Centrale. Thèse 3ème Cycle, Rennes, 137 pp.

PERROUD, H., 1983. Paleomagnetism of paleozoic rocks from the Cabo de Penas, Asturia, Spain. Geophys. J. Astron. Soc., 75, 201-215.

PERROUD, H., 1985. Paléomagnétisme dans l'Arc Ibéro-Armoricain et l'Orogénèse Varisque en Europe Occidentale. Thèse d'Etat, Rennes.

PERROUD, H., COBBOLD, P.R., 1984. L'aimantation rémanente comme marqueur de la déformation: exemple d'un pli à axe incliné dans les séries rouges siluro-dévoniennes à Cabrillanes, Asturies (Espagne). Bull. Soc. Géol. France, XXVI, 1, 169-184.

PERROUD, H., BONHOMMET, N. et THEBAULT, J.P., 1986. Paleomagnetism of the Ordovician Moulin de Chateaupanne formation, Vendée, France. Geophys. J. R. astr. Soc. 85, 573-582.

RAMSAY, J.G., 1967. Folding and fracturing of rocks. Mc Graw-Hill, New-York, 568pp.

RATHORE, J.S., 1979. Magnetic susceptibility anisotropy in the Cambrian slate belt of North Wales and correlation with strain. Tectonophysics, 24, 115-136.

RATHORE, J.S., COURRIOUX, G., CHOUKROUNE, P., 1983. Study of ductile shear zones (Galicia, Spain) using texture goniometry and magnetic fabric methods. Tectonophysics, 98, 87-109.

ROSENBAUM, J.G., 1986. Paleomagnetic directional dispersion produced by plastic deformation in a thick Miocene welded tuff, southern Nevada: implications for welding temperatures. J. Geophys. Res., 91, 12817-12834.

SCOTESE, C.R., VAN DER VOO, R., 1983. Paleomagnetic dating of the Alleghenian folding. Eos Trans., 64, 218.

SOTIN, C., POIRIER, J.P., 1984. Analysis of high-temperature creep experiments by generalized non linear inversion. Mech. Mat., 3, 311-317.

STACEY, F.D. & BANERJEE, S.K., 1974. The physical principles of rock magnetism. Elsevier, Amsterdam, 195 pp.

STEPHENSON, A., SADIKUN, S., POTTER, D.K., 1986. A theoretical and experimental comparison of the anisotropies of magnetic susceptibility and remanence in rocks and minerals. Geophys. J. R. Astron. Soc., 84, 185-200.

TARANTOLA, A., VALETTE, B., 1982. Generalized nonlinear inverse problem solved using the least squares criterion. Rev. Geophys. Space Phys., 20, 219-232.

VAN DEN ENDE C., 1977. Paleomagnetism of permian red beds of the Dome de Barrot (S. France). Thèse Utrecht, 171 pp.

VAN DER PLUIJM, B.A., 1986. Superimposed bulk homogeneous strain and the fold test. Eos Trans., 67, 268.

VAN DER PLUIJM, B.A., 1987. Grain scale deformation and the fold-test evaluation of syn-folding remagnetization. Geophys. R. Lett., 14, 155-157.

WAGNER, J.J., HEDLEY,I.G., STEEN, D., TINKLER, C. & VUAGNAT, M., 1981. Magnetic anisotropy and fabric of some progressively deformed ophiolitic gabbros. J. Geophys. Res., 86, 307-315.

WOOD, D.S., OERTEL, G., SINGH, J. and BENNETT H.F., 1976. Strain and anisotropy in rocks. Phil. Trans. R. Soc. Lond., A.283, 27-42.

ANNEXE 1.

J.P. COGNE, H. PERROUD. **The anisotropy of the magnetic susceptibility as a strain gauge in the Flamanville granite, NW France.** Phys. Earth Planet. Int. in press.

ANISOTROPY OF MAGNETIC SUSCEPTIBILITY AS A STRAIN GAUGE IN THE FLAMANVILLE GRANITE, NW FRANCE.

J.P.COGNE and H.PERROUD
C.A.E.S.S. Laboratoire de Géophysique Interne, Institut de Géologie,
Université de Rennes 1, Campus de Beaulieu, 35042 Rennes CEDEX (FRANCE)

Abstract

The relationship between strain and anisotropy of magnetic susceptibility (A.M.S.) has been investigated in the Carboniferous Flamanville granite in the Armorican Massif, NW France. We measured the axial ratios of elliptical inclusions and the orientation of cleavage planes at 8 sites around the granite margin. Measurements of A.M.S. were made on 73 specimens using a Schonstedt spinner magnetometer. A.M.S. measurements are shown to provide accurate predictions of cleavage and lineation directions, even where these structures are difficult to measure in the field. The strain and A.M.S. ellipsoids show similar regional variations in shape and intensity, and a good correlation between the lengths of the principal axes. Finally, our data are consistent with the hypothesis that the Flamanville granite was syntectonically emplaced during late stages of the Hercynian orogeny.

INTRODUCTION

The Flamanville granitic pluton was intruded into an Upper Proterozoic-Lower Paleozoic basement during the late phases of the Hercynian orogeny. Whereas the pluton shows no sign of deformation in its central part, there is a clear structural foliation parallel to the margins, suggesting these severely deformed during emplacement. The pluton has been the object of structural studies by Martin (1953), Ledru and Brun (1977) and Brun (1981). A paleomagnetic reconnaissance by Van der Voo and Klootwijk (1972) yielded AMS results with a good fit between principal directions of AMS and strain. This encouraged us to perform a more detailed study. The occurence of deformed xenoliths (Martin, 1953) allowed us to estimate strain intensity and thus to attempt to correlate the strain and susceptibility ellipsoids quantitatively, following similar works by others (Kneen, 1976; Wood et al., 1976; Hrouda, 1979; Rathore, 1979; Kligfield et al., 1981, 1983; amongst others). The purpose of this paper is therefore to report new structural and magnetic data we obtained on this pluton and to discuss their relationships and implications with respect to its emplacement.

GEOLOGICAL SETTING AND SAMPLING SITES.

Being intrusive in the Paleozoic formations of the Siouville syncline in Normandy, France (Fig. 1), the granite massif of Flamanville was at first considered as ending the Hercynian structural history of the region (Martin, 1953). However, a detailed study of cleavage development in the Siouville syncline (Ledru and Brun, 1977) has shown that it is controlled by the thermal anomaly due to granite intrusion. Regionally, the cleavage trajectories trend E-W in the country rocks, but locally they bend around the margins of the Flamanville pluton. The locally subcircular cleavage pattern grades into the regional schistosity, except at one locality, east of the

pluton, where there is an isotropic point, or triple point, of cleavage directions (i.e. a point of no finite strain; Ramsay, 1967; Brun, 1983). By symmetry, a second triple point is probably situated offshore, west of the granite. The structural and metamorphic data are interpreted as resulting from the interference of two synchronous processes, diapiric emplacement of granite and Hercynian regional deformation.

In the granite, there is a steeply dipping planar foliation parallel to the margins, except in the southern part, where foliation surfaces crosscut the contact with the country rocks. According to Martin (1953), the foliation is mainly due to coplanar orientation of mafic minerals. Nine sampling sites (A to I ; Fig.1) were chosen around the well-exposed western border of the massif, at localities where markers were available for strain measurement.

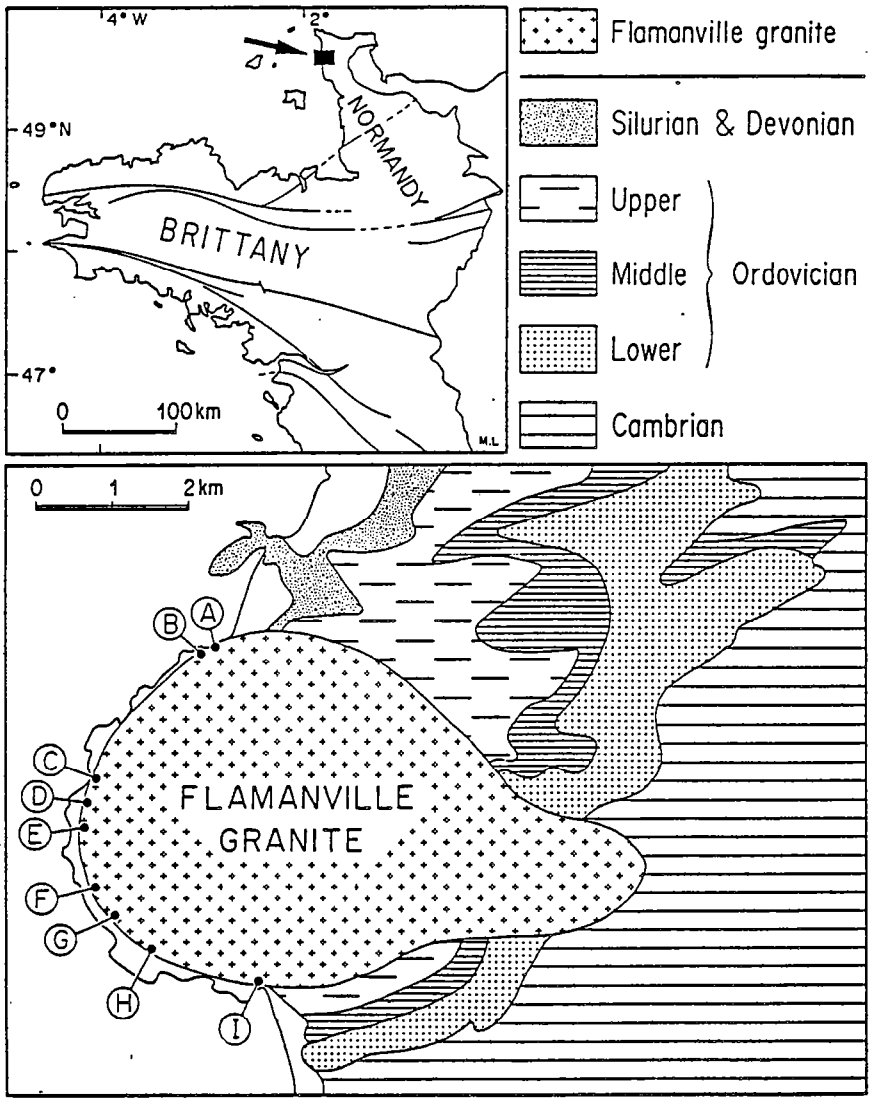

Fig. 1 - Upper : location map of the Flamanville area in the Armorican Massif, Normandy, France. Lower : Schematic geological map of the Flamanville massif. Dots labelled A to I are the sampling sites of this study.

STRAIN ESTIMATES.

At each site (except G), xenoliths systematically show ellipsoidal shapes, their long axes lying within the foliation surfaces. The xenoliths were used to estimate a mean finite strain at site scale. As noted by Martin (1953), long axes of inclusions tend to lie at random in the flattening plane ($\lambda_1 \lambda_2$) and it was therefore difficult (in some sites, impossible) to determine the stretching direction in this plane. Nevertheless,since the lineation in the country rocks is almost horizontal (Brun, 1981), and the granite appears to be syntectonic, the stretching lineation in the granite was assumed to have the same shallow plunge, for the purposes of field measurement. We generally considered subhorizontal joint planes, perpendicular to the foliation planes ($\lambda_1\lambda_2$) , as being the $\lambda_1\lambda_3$ planes and the subvertical ones, perpendicular to the two others, as the $\lambda_2\lambda_3$ planes. Moreover, the foliation plane was not always a plane of easy splitting (particularly in site G) and a measure of this plane may not be as accurate as desirable. The mean axial ratios of the elliptical inclusions has been estimated from arithmetic means of the measurements within each of the principal planes. Declination and inclination of stretching (λ_1) and shortening (λ_3) directions, mean axial ratios .and strain parameters are listed in Table I. Foliation planes represented by their poles in fig. 2a, strike parallel to the wall of the body and systematically dip towards the centre of the massif. In all the sites, the strain ellipsoid is of the flattening type with low values of shape parameter K (Flinn, 1965), close to an oblate strain ellipsoid.

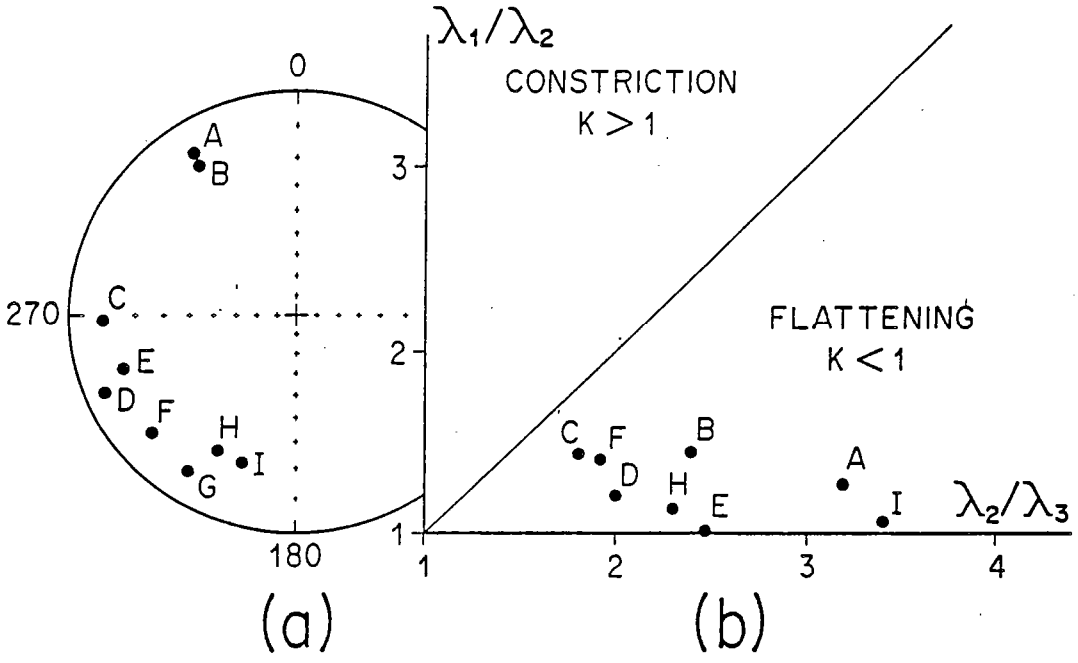

Fig. 2 - Strain data :(a) Stereoplots in the lower hemisphere showing the orientation of the mean poles to cleavage (λ_3). (b) Flinn diagram (1965) of the mean strains of sites A to I. $K = (\lambda_1/\lambda_2-1)/(\lambda_2/\lambda_3-1)$.

ANISOTROPY OF MAGNETIC SUSCEPTIBILITY (A.M.S.).

Measurements of A.M.S.

The A.M.S. measurements were made with a Schonstedt spinner magnetometer, in the manner described by Collinson (1983) : a 40 A/m vertical field is applied to the spinning sample, whilst the horizontal fluxgate measures the component of magnetization perpendicular to the field and the spinning axis. The magnetization measured is due to both remanent magnetization and anisotropic induced magnetization. The periodic signal is sampled 8 times during each spin and the data are transferred to a PDP 11 micro-computer for reduction. By combining the 8 readings, both remanent and induced magnetization components can be estimated since they have different periodicities. Accumulation of results from several spins controls the signal to noise ratios for both magnetizations.In order to fully determine the

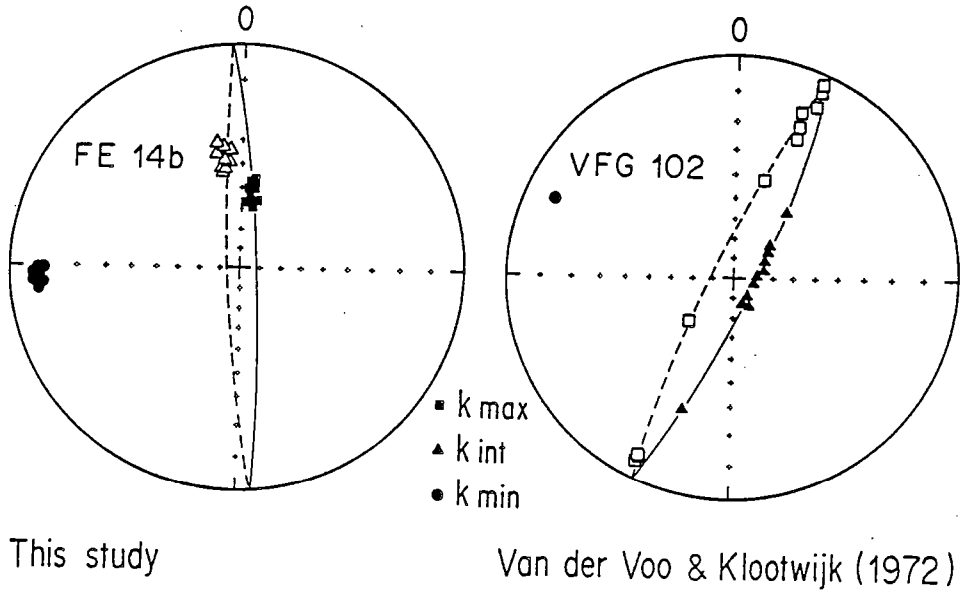

Fig. 3 - Orientation of the principal susceptibility axes of two individual specimens (from different localities) measured after successive steps of A.F. demagnetization. Left: this study, measurements made with a spinner magnetometer. Right: results obtained by Van der Voo and Klootwijk (1972, Fig. 6b) by measuring with an astatic magnetometer. Stereographic projections. Closed (open) symbols : projection in the lower (upper) hemisphere. Squares: kmax. Triangles: kint. Circles: kmin

susceptibility tensor, kzz (i.e. the susceptibility along the Z-axis of the sample) is measured with a susceptibility meter (Digico or Bartington).

A more difficult problem is the calibration of the Schonstedt magnetometer, especially since electronic amplification and filtering produce phase offset and amplitude attenuation which are frequency dependent. For our study, the magnetometer was calibrated using an artificial sample, composed of iron needles, carefully oriented along the sample axes of a wooden cylinder. The sample was measured along these axes using the Bartington susceptibility meter, and the values obtained were used to calibrate the Schonstedt magnetometer.

Finally, to check the influence of remanent magnetization on our results, we have progressively demagnetized some samples, using alternating fields up to 100 mT and measuring A.M.S. at each step. We have observed no variation of A.M.S. during each entire experiment (Fig.3, left) and we conclude, therefore, that A.M.S. measurements with the Schonstedt are not significantly perturbed by the second harmonic of the remanent magnetization signal, as suggested by Collinson (1983). Such was not the case for the results of Van der Voo and Klootwijk (1972) (Fig.3 right) who used an astatic magnetometer, and we can therefore consider our apparatus as being at least as accurate as the astatic magnetometer when dealing with fairly intense anisotropic induced magnetization. However, the measurement of low susceptibilities or low anisotropy has proved to be impossible, due to the effect of sample shape when the sample is too close to the fluxgate sensor. The measured signal should be strong enough to be detectable when the sample is at a distance of at least two or three times its diameter from the fluxgate.

Results.

In the nine sites distributed around the granite body, 66 cores with a diameter of 25mm and 60 to 100mm long were drilled and oriented in situ, using magnetic and sun compasses. The cores were cut in the laboratory to yield 93 samples, with standard shapes of 25 mm diameter x 24 mm length. The kzz component of the susceptibility tensor of these specimens was measured using a Digico bulk susceptibility meter. Twenty specimens were eliminated from the A.M.S. measurements because their low volume susceptibility ($<10^{-3}$SI= 10^{-4}G/Oe cgs) was too weak to be measured with the spinner magnetometer. All the specimens of site H are in this category, and we have no results for this site. For the 73 remaining samples, the kzz component is in the range 0.3-0.8 10^{-2} SI. The eigenvectors of the susceptibility tensor give the orientation of the maximum (kmax), intermediate (kint) and minimum (kmin) susceptibility axes, and its eigenvalues give the magnitude of kmax, kint, kmin, from which are derived the shape and intensity parameters of the ellipsoid. At each site, a mean susceptibility tensor has been computed by summation of the n tensors measured. Diagonalization of this tensor provides the mean directions and parameters which are shown in Table II.

In all specimens, the susceptibility ellipsoid is triaxial and oblate (Fig. 4a). There is a measurable ellipticity in the kmax.kint plane and, thus, there is a magnetic lineation in this plane. The total degree of anisotropy, expressed as % An = (kmax/kmin - 1) x 100, is high, ranging from 10 to 35% (Fig. 4b). These results are in good agreement with those obtained by Van der Voo and Klootwijk (1972). The principal directions of

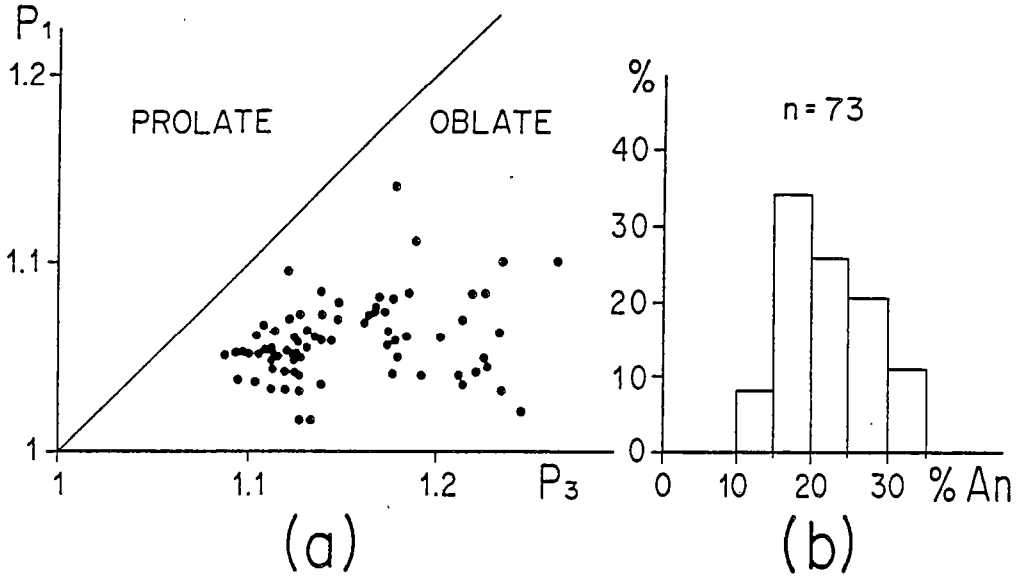

Fig. 4 - A.M.S. data: (a) Flinn diagram (1965) for all measured specimens. P1 = kmax/kint , P3 = kint/kmin. (b) Frequency plot of the anisotropy percentages for the 73 specimens. %An = (kmax/kmin - 1)*100.

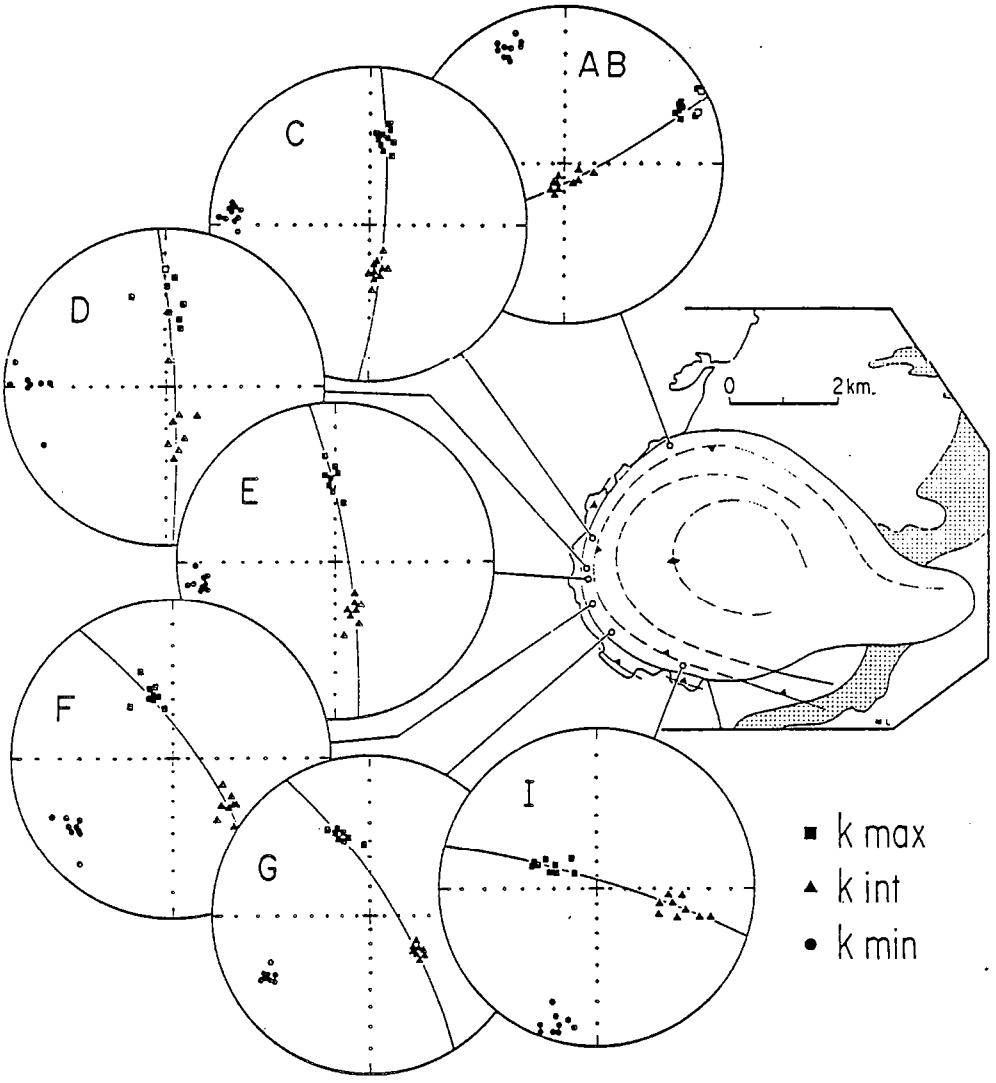

Fig. 5 - Magnetic fabric data from the investigated sites. The best fit kmax.kint planes are drawn. The dotted lines in the schematic map are the cleavage trajectories (after Martin, 1953). Same symbols and conventions as in Fig. 3

susceptibility from each site are shown in figure 5. They show good within-site consistency. The kmin axes are systematically inclined down to the west (NW to SW) direction. The corresponding kmax.kint planes dip steeply towards the centre and strike parallel to the margins of the pluton. The magnetic lineation is well defined within each site, with a good cluster of kmax directions in the kmax.kint plane. The plunge of the within-site mean kmax axes progressively increases from north to south, from 15 to 55 .

Forty specimens out of these 73 were also measured using the Bartington magnetic susceptibility meter. The measurements were made in six different positions (three sample axes plus three diagonals), sufficient for the susceptibility tensor to be estimated. No significant differences were observed between the two data sets, on the basis of either shape and intensity of susceptibility ellipsoids or directions of their axes.

CORRELATION OF STRAIN ELLIPSOID AND MAGNETIC SUSCEPTIBILITY ELLIPSOID.

As expected, both ellipsoids have similar orientations. The angle between the pole to cleavage (λ_3, Table I) and the pole to the mean magnetic foliation (kmin, Table II) is generally less than 10°, except at sites D and G where this angle is greater than 20°. This is not surprising, since greater difficulties were encountered at these sites in estimating the strike and dip of the cleavage plane.

Although no clear stretching lineation is observable in the field, due to the low λ_1/λ_2 ratio displayed by the elliptical xenoliths, A.M.S. measurements show a weak but well-defined magnetic lineation . The within-site cluster of the kmax directions (obvious in figure 5) together with the non-random between-site distribution of these axes suggest they are related to a structural lineation.

Following other studies, an attempt has been made to express the magnetic anisotropy in quantitative terms of finite strain. From the published case histories on this subject, two main expressions have been used to correlate A.M.S. and strain. On the one hand, Kneen (1976), Wood et al. (1976), Rathore (1979) and Rathore et al. (1983) favour the following relationship:

$$k_1/k_2 = [(1+e_1)/(1+e_2)]^x$$
$$k_2/k_3 = [(1+e_2)/(1+e_3)]^x \qquad (1)$$

with various results for the value of exponent 'x'. On the other hand, Hrouda (1979) and Kligfield et al. (1981, 1983) favour relationship of the form:

$$(k_1-k_2)/k_0 = y \ln[(1+e_1)/(1+e_2)]$$
$$(k_2-k_3)/k_0 = y \ln[(1+e_2)/(1+e_3)] \qquad (2)$$

where k_0 is either $(k_1+k_2+k_3)/3$ (Kligfield et al., 1981), or $(k_1k_2k_3)^{1/3}$ (Kligfield et al., 1983).

The choice between these two sets of formulae is not straightforward, since there does not appear to be any theoretical reason for preferring a log/log relation rather than a linear/log relation or even a linear/linear one. Furthermore, since we usually deal with anisotropy lower than 30%, we have $(k_1-k_2)/k_0 \approx \ln(k_1/k_2)$ and $(k_2-k_3)/k_0 \approx \ln(k_2/k_3)$ (Hrouda, 1982). Thus, both expressions are equivalent in the range of experimental error. We follow Kligfield et al. (1983) in computing the linear regression between the

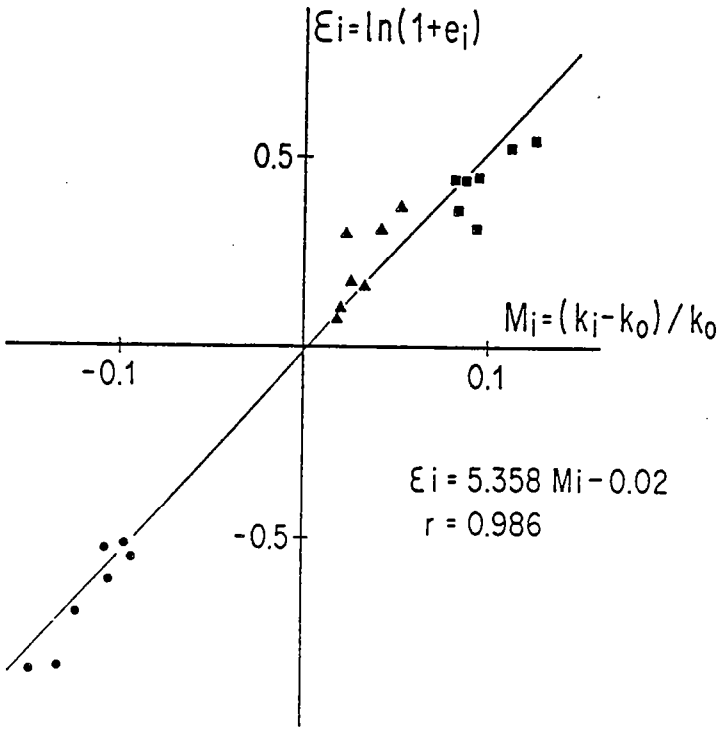

Fig. 6 - Mean logarithmic strains (ε_i) vs. mean principal susceptibility differences (M_i). Same symbols for kmax, kint, kmin as in figure 3. The line represents the best fit line through the experimental points.

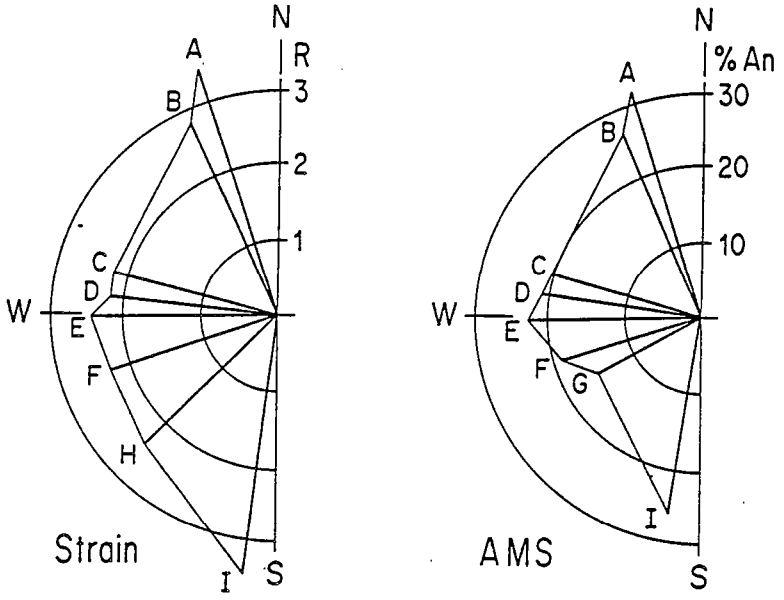

Fig. 7 - Mean strain intensities R (left) and mean anisotropy percentages %An (right) from the studied sites represented as a function of site location around the schematic half-circle shape of the western border of the Flamanville granite

logarithmic strains ($\varepsilon_i = \ln (1+e_i)$; i=1,2,3) and the related principal susceptibility differences ($M_i = (k_i - k_0)/ k_0$; $k_0 = (kmax.kint.kmin)^{1/3}$; i = 1,2,3) (Fig.6). A strong positive correlation is obtained, $\varepsilon_i = 5.358\ M_i - 0.022$, with a correlation coefficient r = 0.986 (n=21). In the ideal case, the residual term (-0.022) should be zero, but it appears small enough to be neglected. This correlation strongly suggests that A.M.S. ellipsoid shape and intensity variations are directly related to strain variations. From the good quality of this correlation, it seems therefore possible to estimate the strain in any other point of the granite body even if there are no direct strain markers.

Finally, the correlation between strain and A.M.S. intensities is illustrated in figure 7, where strain intensity R and %An are plotted for the various site locations around the quasi-circular western border of the Flamanville granite. Strain intensity increases, from the Western border of the body, towards either the north or the south. This strain gradient is accompagnied by a similar variation in anisotropy of magnetic susceptibility percentages. Note the lack of A.M.S. data at site H and of strain data at site G. Although the two sites are different, each shows AMS or strain values intermediate those of western and southern sites.

CONCLUSIONS.

From our study, we draw conclusions at two levels. First, strain tensor and A.M.S. tensors may be correlated not only in the directions of their eigenvectors but also in the variations of magnitude of their eigenvalues. The A.M.S. technique is probably more accurate in the determination of the flattening strain plane direction. Moreover, a consistent magnetic lineation is found in each site, although it was not possible to find a well defined stretching lineation in the field. The good correlation that exists between the logarithmic strains and the principal susceptibility differences, shows that the degree and shape of susceptibility anisotropy is controlled by strain. It seems therefore possible to derive strain from A.M.S. measurements in all points of the granite body. All these fit the well admitted idea that A.M.S. not only provides a complementary tool in structural analysis but may be considered itself as a good strain marker, providing there is a minimum number of classical strain markers to allow the correlation to be established and controlled.

The geological interpretation of our data with respect to the emplacement of the Flamanville granite also supports the idea of a syntectonic diapir proposed by Ledru and Brun (1977). The strain and anisotropy percentage, as they increase from the western sites towards the northern and southern borders of the pluton, probably result from the superimposition of a N-S regional shortening (E-W regional schistosity) upon a radial shortening due to ballooning during pluton emplacement (Brun, 1983). The dip of the cleavage towards the centre of the Flamanville pluton shows that the current erosion surface is situated slightly below the plane of maximum width of the body. The effect of diapiric emplacement alone should have produced downdip stretching lineations in this zone (Brun, 1983). Here too, our intermediate inclination of magnetic lineations may be the result of the superimposition of a shallow regional stretching in the country rocks (Brun, 1981) upon the downdip stretching produced by diapiric emplacement. The structural and AMS studies reported here, thus provide additional

arguments for the synchronism between granite intrusion and regional Hercynian deformation in the Flamanville area.

Site	Shortening (λ_3)		Stretching (λ_1)		Principal strains			Shape	Intensity
	De	I	De	I	λ_1	λ_2	λ_3	K	R
A	328.0	10.0	237.0	7.0	1.725	1.360	0.426	0.123	3.459
B	327.0	14.0	57.0	0.0	1.704	1.184	0.495	0.316	2.829
C	268.0	10.0	358.0	0.0	1.552	1.081	0.595	0.532	2.252
D	247.0	6.0	337.5	0.0	1.434	1.181	0.590	0.214	2.214
E	252.0	13.5	342.0	0.0	1.361	1.346	0.545	0.007	2.478
F	229.5	11.0	323.0	17.0	1.561	1.108	0.578	0.446	2.326
G	213.5	9.0	303.5	0.0	-	-	-	-	-
H	209.5	19.0	299.5	0.0	1.437	1.260	0.552	0.110	2.423
I	199.5	18.0	100.0	27.5	1.569	1.472	0.433	0.027	3.468

Table I: Mean site strain data for the Flamanville granite. Shortening and stretching down-plunge directions are given by their declination (De) and inclination (I). Principal strains λ_i are $1+e_i$ where e_i is the elongation along each axis. Strains are computed assuming no volume change, i.e. $\lambda_1.\lambda_2.\lambda_3=1$. Shape (Flinn, 1965) is $K=(\lambda_1/\lambda_2-1)/(\lambda_2/\lambda_3-1)$. Intensity (Watterson, 1968) is $R=\lambda_1/\lambda_2+\lambda_2/\lambda_3-1$.

Site	N	Kmax		Kmin		P1	P3	%An	Principal susceptibility difference		
		De	I	De	I				M 1	M 2	M 3
A	7	65.0	14.4	332.1	11.2	1.078	1.221	31.6	0.124	0.042	- 0.146
B	4	62.7	-3.8	333.6	13.3	1.082	1.169	26.5	0.110	0.026	- 0.122
C	11	9.9	33.2	274.5	8.1	1.066	1.128	20.3	0.087	0.019	- 0.097
D	8	3.4	36.1	267.3	8.4	1.047	1.158	21.2	0.083	0.034	- 0.107
E	10	357.4	38.2	259.6	9.7	1.069	1.143	22.2	0.093	0.023	- 0.105
F	10	340.5	45.0	234.8	15.2	1.060	1.125	19.3	0.081	0.020	- 0.093
G	14	342.2	34.5	238.6	18.8	1.042	1.107	15.3	0.063	0.020	- 0.078
I	9	296.2	54.7	196.8	6.6	1.040	1.212	26.1	0.094	0.052	- 0.132

Table II: Mean site A.M.S. data for the Flamanville granite. N is the number of susceptibility ellipsoid determinations in each site. Direction of principal susceptibility axes (kmax, kmin) is given by declination (De) and inclination (I). P1=kmax/kint, P3=kint/kmin. %An=(kmax/kmin-1)*100. $M_i=(k_i-k_0)/k_0$ with $k_0=(kmax.kint.kmin)^{1/3}$, i=1, 2, 3 = kmax, kint, kmin.

REFERENCES.

Brun, J.P., 1981. Instabilités gravitaires et déformation de la croute continentale. Application au développement des domes et des plutons. Thèse, Rennes, 197 pp.

Brun, J.P., 1983. Isotropic points and lines in strain fields. J. Struct. Geol., 5, 3/4: 321-327.

Collinson, D.W., 1983. Methods in rock magnetism and palaeomagnetism. Chapman and Hall ed., London, 499 pp.

Flinn, D., 1965. On the symmetry principle and the deformation ellipsoid. Geol. Mag., 102: 36-45.

Hrouda, F., 1979. The strain interpretation of magnetic anisotropy in rocks of the Nizky Jezenik Mountains (Czechoslovakia). Sbor. Geol. Ved., UG16: 27-62

Hrouda, F., 1982. Magnetic anisotropy of rocks and its application in Geology and Geophysics. Geophys. Surv., 5: 37-82.

Kligfield, R., Owens, W.H., and Lowrie, W., 1981. Magnetic susceptibility anisotropy, strain, and progressive deformation in Permian sediments from the Maritime Alps (France). Earth Planet. Sci. Lett., 55: 181-189.

Kligfield, R., Lowrie, W., Hirt, A., and Siddans, A.W.B., 1983. Effect of progressive deformation on remanent magnetization of Permian redbeds from the Alpes Maritimes (France). Tectonophysics, 97: 59-85.

Kneen, S.J., 1976. The relationship between the magnetic and strain fabrics of some Haematite-bearing Welsh Slates. Earth Planet. Sci. Lett., 31: 413-416.

Ledru, P., Brun, J.P., 1977. Utilisation des fronts et des trajectoires de schistosité dans l'étude des relations entre tectonique et intrusion granitique : exemple du granite de Flamanville (Manche). C. R. Acad. Sc. Paris, 285, Série D: 1199-1202.

Martin, N.R., 1953. The structure of the granite massif of Flamanville, Manche, North-West France. Quarterly J. Geol. Soc. of London, 432, C VIII, 4: 311-341.

Ramsay, J.G., 1967. Folding and fracturing of rocks. Mc Graw Hill Ed., New-York, 568 pp.

Rathore, J.S., 1979. Magnetic susceptibility anisotropy in the Cambrian slate belt of north Wales and correlation with strain. Tectonophysics, 53: 83-97.

Rathore, J.S., Courrioux, G., and Choukroune, P., 1983. Study of ductile shear zones (Galicia, Spain) using texture goniometry and magnetic fabric methods. Tectonophysics, 98: 87-109.

Van der Voo, R., Klootwijk, C.T., 1972. Paleomagnetic reconnaissance study of the Flamanville granite with a special reference to the anisotropy of its susceptibility. Geol. en Mijnbouw 51 (6): 609-617.

Watterson, J., 1968. Homogeneous deformation of the gneisses of Vesterland, South West Greenland. Gron. Geol. Unterso. Bull., 78.

Wood, D.S., Oertel, G., Singh, J., and Bennet, H.F., 1976. Strain and anisotropy in rocks. Phil. Trans. R. Soc. London, Ser. A, 283: 27-42.

ANNEXE 2.

J.P. COGNE. **TRM deviations in anisotropic assemblages of multidomain magnetites.** Geophys. J. R. astron. Soc., in press.

TRM DEVIATIONS IN ANISOTROPIC ASSEMBLAGES OF MULTIDOMAIN MAGNETITE.

J.P. Cogné. Laboratoire de Géophysique Interne, CAESS, Campus de Beaulieu, Université de Rennes 1, 35042 Rennes Cedex, France.

Short Title: AMS induced TRM deviations.

Summary.

Anisotropic assemblages of multidomain magnetite particles develop an anisotropy of magnetic susceptibility (AMS), which in turn induces deviations of thermo-remanent magnetization (TRM) from the field direction. From the theories of multidomain TRM acquisition, it is shown that the TRM anisotropy tensor has its eigenvalue ratios (T_i) related to the principal weak-field susceptibility ratios (P_i) by the order of magnitude $T_i \approx P_i^2$. This relation has been experimentally verified on two sets of highly anisotropic rock samples. The exponent has been determined to be 1.94 in the samples from a Peruvian gabbro, and 1.81 in those from the granite of Flamanville (NW France). Accounting for experimental difficulties in determining the TRM anisotropy tensors, these exponents are judged to agree well with the expected one. It is therefore stressed that AMS measurements provide a good means of evaluating the magnetic field direction from deviated TRM directions, providing magnetic carriers are mainly multidomain magnetites.

Key words: magnetic susceptibility anisotropy, TRM anisotropy, paleomagnetism, anisotropic rocks.

1 - Introduction.

The anisotropy of the magnetic susceptibility (AMS) induced by the preferred orientation of magnetic minerals within anisotropic rocks is a well known phenomenon. This has been the subject of considerable study, mainly in order to relate this physical property of geological materials with crustal strain processes (see Hrouda 1982, for a review). On the other hand, very little is known about the effect of AMS upon remanent magnetization acquisition, and in particular, about the thermoremanent magnetization (TRM) deviations due to anisotropy from the ambient field. As a matter of fact, most paleomagnetic investigations have until recently been made on unmetamorphosed essentially isotropic rocks, and therefore this problem has not been considered as critical. However, in order to determine quantitatively the kinematics of orogenic belts, paleomagnetic studies have recently been extended to deformed regions, and it becomes necessary to obtain paleomagnetic results from rock units which can have suffered from appreciable strain processes. Since strain is obviously a major cause of remanent vector deviations, our understanding of the effects of strain upon remanent magnetization must be developed. This problem can be separated into two main aspects, depending upon the relative chronology between magnetization acquisition and deformation of the rock unit.

Our aim in this paper is to estimate the deviations of a TRM acquired by anisotropic rocks (that is to say, where strain processes predate magnetization acquisition), where the magnetic carriers are predominantly multidomain magnetite grains. From the currently accepted TRM acquisition theory in multidomain magnetite assemblages, it is shown that the order of magnitude of the eigenvalue ratios of the TRM anisotropy tensor can be derived from the weak field AMS measurements. This is then experimentally

verified by giving TRM to 2 sets of anisotropic specimens from a granite and a gabbro, where the magnetic mineralogy has been checked. The positive results of the experiments suggest the possibility of using deviated TRM directions in order to recover the field direction within natural anisotropic rock units.

2 - Theoretical basis.

Following the notation of Schmidt & Clark (1985), the thermoremanent magnetization in isotropic assemblages of multidomain magnetite-bearing rocks may be taken to be of the form:

$$J_{TRM}(To) = J_{TRM}(Tb).J_S(To)/J_S(Tb).[1+N\varkappa_i(To)]^{-1} \qquad (1)$$

where

- $J_{TRM}(Tb)$ is the magnetization at blocking temperature.
- $J_S(To)/J_S(Tb)$ is the ratio of the spontaneous magnetizations at room viz. blocking temperatures
- $\varkappa_i$ is the intrinsic susceptibility
- N is the demagnetizing factor; this parameter depends upon the shape of the body, and is isotropic for a sphere.

An equivalent expression is given by Stacey & Banerjee (1974) with $J_{TRM}(Tb)=H/N$ where H is the inducing field at the blocking temperature. Equation (1) then becomes:

$$J_{TRM}(To)=[N^{-1}.(1+N\varkappa_i)^{-1}.J_S(To)/J_S(Tb)].H \qquad (2)$$

Thus, weak field remanence can be regarded as proportionnal to the applied field. If now, the grain assemblage becomes anisotropic, that is, for example, if there exists a preferred orientation of the long axes of elongated magnetite grains, the magnetization strength will be directionally dependent within the rock specimen. Therefore, the TRM components in a given cartesian frame can be expressed as a function of magnetic field components, and (2) rewritten as:

$$J_i = M_{ij}\, H_j \qquad i, j = 1,2,3 \qquad (3)$$

where M_{ij} is a 3 x 3 second order symmetrical cartesian tensor, which will be called the TRM anisotropy tensor, and the eigenvalues of which have a form analogous to (2):

$$M_j = N_j^{-1}.(1+N_j\varkappa_i)^{-1}.J_S(To)/J_S(Tb) \qquad j=1,2,3 \qquad (4)$$

(Note that index "i" for $\varkappa$ stands for intrinsic susceptibility)

Following the concept of Stacey & Banerjee (1974) of the equivalent ellipsoid, that is the ellipsoid which would have the net anisotropy of the grains assemblage under consideration, N_j is the demagnetizing factor along the j^{th} principal direction of this anisotropic assemblage.

Multiplying (4) by $\varkappa_i/\varkappa_i$, this may be rewritten as

$$M_j = \frac{1}{N_j} \cdot \frac{\varkappa_i}{1+N_j\varkappa_i} \left[\frac{1}{\varkappa_i} \cdot J_s(T_o)/J_s(Tb)\right] \qquad (5)$$

$\frac{\varkappa_i}{1+N_j\varkappa_i}$ is the apparent susceptibility k_j. For high intrinsic susceptibility $\varkappa_i$, which is the case of magnetite, the value of the apparent susceptibility k approaches 1/N, that is

$$k_j \approx \frac{1}{N_j} \qquad (6)$$

therefore, (5) becomes

$$M_j \approx k_j^2 \left[\frac{1}{\varkappa_i} \cdot J_s(T_o)/J_s(T_b) \right] \qquad (7)$$

The ratio of spontaneous magnetizations $J_s(To)/J_s(Tb)$, as well as the intrinsic susceptibility x_i, are intrinsic properties of the magnetite grain assemblage being considered and thus are not directionally dependent. Therefore, if we take any pair of eigenvalues of the tensor M_{ij}, we should have

$$\frac{M_i}{M_j} \approx \left(\frac{k_i}{k_j}\right)^2$$

This last equation means that, under the assumption that both anisotropy of magnetic susceptibility (AMS) and thermoremanent magnetization (TRM) are due to polydomain magnetite assemblages in a rock, the measurement of weak field AMS allows an easy estimation of the order of magnitude of the TRM anisotropy eigenvalue ratios, their eigenvectors being identical.

Then, by normalizing these eigenvalues, for example by the sum $M_1+M_2+M_3$, it is possible to construct a normalized TRM anisotropy tensor equal to M_{ij} of expression (3) except for an unknown multiplicative constant. Note that the change in direction of an initial vector (say H_j) to a final one (J_i) is governed by the eigenvalue ratios of the tensor, while the change of modulus is controlled by the eigenvalue magnitudes. Therefore, since the aim of this work is to estimate a field direction H from deviated TRM directions, and not the strength of the field in itself, the unknown constant may be neglected and will not be taken into consideration in the following.

3 - Discussion.

All the above developments are based upon two main assumptions. The first one is that $k \approx 1/N$ (equation 6). This approximation mainly relies on the approximation that $Nx_i \ll 1$ at all temperatures. After Schmidt & Clark (1985), the value of $\varkappa_i$ for 50 μm magnetite grains can be estimated to be $\varkappa_i \sim 17$ at room temperature, and increases by a factor ~ 90 by heating at 470°C. Therefore, the above approximation appears quite correct. The second assumption, which derives from the first one, is that the apparent susceptibility ratios k_i/k_j are weakly dependent upon temperature, allowing to make the final approximation:

$$\frac{N_j \cdot (1 + N_j \varkappa_i)}{N_i \cdot (1 + N_i \varkappa_i)} \approx \left(\frac{k_i}{k_j}\right)^2$$

where k_i are measured at room temperature. In order to check the discrepancy between apparent susceptibility ratios at room and high temperature, we have computed these ratios, depending upon the demagnetizing factor ratios Ny/Nx for perfectly oblate and prolate ellipsoids. In an ellipsoid of revolution, Ne=0.5(1- Np) (Collinson, 1983), where Ne (Np) is the equatorial (polar) demagnetizing factor. Using this relationship, values of kmax/kmin have been calculated as $(1+N_y x_i)/(1+N_x x_i)$, where Nx is the equatorial (polar) demagnetizing factor in the case of prolate (oblate) ellipsoid, and $\varkappa_i$ the intrinsic susceptibility. We have used intrinsic susceptibility values of 17 and 1270 (SI) at respectively room and 470° C temperatures, as estimated by Schmidt & Clark (1985) for 50 μm multidomain magnetite. Results are illustrated in figure 1. As can be seen in this figure, at the reasonably high value of kmax/kmin(To) of 1,5 (that is, 50% of magnetic susceptibility anisotropy) the value at 470°C should be about 1.6, an increase of only 7%, in both the prolate and oblate case. It seems therefore that the

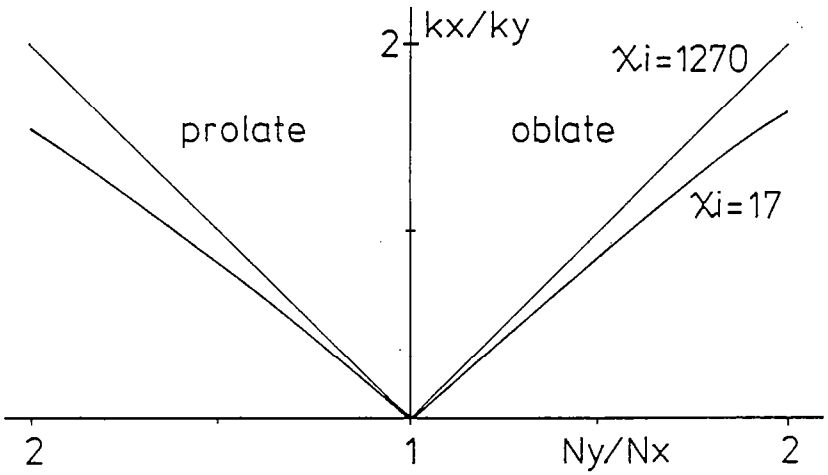

Fig. 1 - Curves of principal susceptibility ratios vs. shape factor ratios for prolate and oblate ellipsoids of revolution. Heavy (light) curve for intrinsic susceptibility κ_i = 17 (1270). Data for intrinsic susceptibility are after Schmidt & Clark (1985).

approximation of temperature independence of the susceptibility ratios should be correct in the range of experimental determinations of anisotropy induced TRM deviations.

It can be further noted that expressions (3) an (8) are nothing but a 3-D development of some expressions that can be found, for example, in a slightly different form in Nagata (1961; p.174). This author constructed a 2-D curve of TRM deviations as a function of susceptibility ratios, from an approximation similar to $M_1/M_2 \approx (k_1/k_2)^2$. It appeared to be in fair agreement with the experimental data of Uyeda et al. (1963), obtained by giving a TRM to discs of polycrystalline magnetite with varied dimension ratios.

In order to check the relations (3) and (8), a series of experimental tests has been carried on two sets of polydomain magnetite-bearing anisotropic rock samples.

4. Experimental tests.

4 .1 TECHNIQUES AND PROCEDURES.

Two sets of 12 specimens of rock samples from the Flamanville granite (NW France) and a Peruvian gabbro, were given a TRM along each of three perpendicular axes in the specimen, in a manner similar to that described by Stephenson et al. (1986). The cartesian components of each TRM then measured give a line of the TRM anisotropy tensor, i.e.

Field	along	X	axis	gives	Mxx	Mxy	Mxz
"	"	Y	"	"	Myx	Myy	Myz
"	"	Z	"	"	Mzx	Mzy	Mzz

In order to avoid as far as possible chemical changes during successive heating steps, the specimens were heated under a vacuum lower than 10^{-2} Torr, using the paleointensity ovens system described by Salis (1986). A complete TRM acquisition in one direction of the sample is achieved by heating it above its Curie point, here 640°C, and then by cooling it in a controlled magnetic field of 60 μT, the order of magnitude of the Earth Magnetic Field. The complete TRM acquired successively along the X, Y and Z axes was repeated along -X, -Y, -Z. This allowed a test of the stability of TRM acquisition during the six heating steps. Furthermore, this provides two estimates of the diagonal terms of tensor **M** and four estimates of the non diagonal, symmetrical terms, allowing an averaging of the specimen axes orientation error which has been estimated to be typically $\pm 5°$.

TRM acquired at each step was measured using a Digico spinner magnetometer, and the magnetic mineralogy stability was checked by measuring the stability of the weak-field room-temperature magnetic susceptibility anisotropy between each step. This was measured using a Bartington-MS2 susceptibility meter with a special sample holder allowing various position of the sample in the sensor.

The magnetic mineralogy was checked by Curie point determinations of the corresponding rock powders, using a computer-monitored vertical high-field Curie balance. Here too, the experiments were made under a vacuum lower than 10^{-2} Torr, the powders being placed into sealed quartz 1 cm^3 containers. All the thermomagnetic curves presented below are corrected for various parameters such as diamagnetic susceptibility of the quartz containers, thermal modification of heated air buoyancy, and room temperature. Also low field, low temperature susceptibility measurements were made to check the

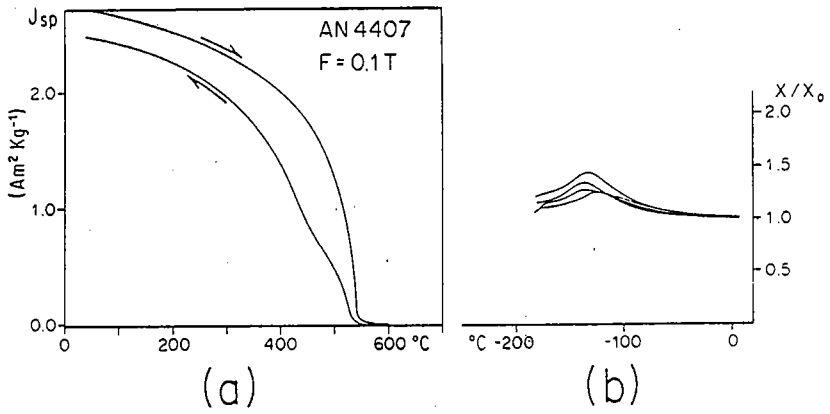

Fig. 2 - Thermomagnetic (a) and low temperature susceptibility (b) curves for the Peruvian gabbro specimens. In (a), F is the field, arrows indicate heating and cooling.

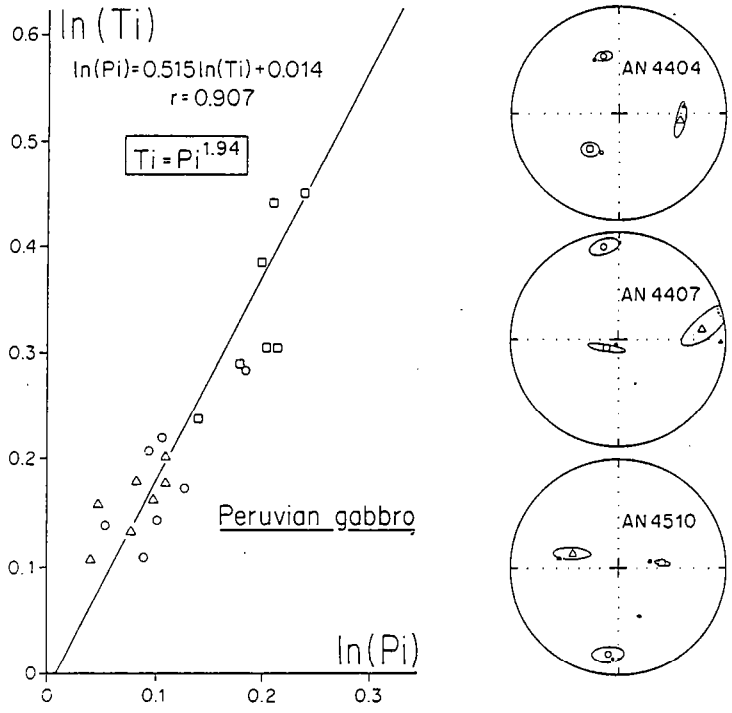

Fig. 3 - Comparison of TRM anisotropy and AMS in the Peruvian gabbro. Left: logarithms of TRM anisotropy eigenvalue ratios (Ti) vs. logarithms of principal susceptibility ratios (Pi). The best-fit line over the experimental points is drawn, and regression coefficients are given. Squares: max/min ratios; circles: int/min; triangles: max/int. Right: equal area projections in the lower hemisphere, for 3 specimens, of the principal susceptibilities (open symbols) with their ellipses of 95% confidence (after Jelinek 1978), and TRM anisotropy tensor eigenvalues (closed symbols). Squares: maximum values; triangles: intermediate; circles: minimum.

domain state of the magnetites. Some standard cylindrical paleomagnetic rock specimens were plunged into liquid nitrogen after they had been embedded in a magnetically amorphous silicone matrix, in order to place a thermocouple in a fixed position along the specimen surface and to provide a minimum thermal insulation of the sample periphery. After about 1 hour of cooling, the specimens were allowed to reheat to room temperature. Susceptibility changes with temperature were then continuously (about one susceptibility and one temperature sampling per 2s) measured with the Bartington MS2 susceptibility meter coupled to a computer. The results of these tests are the following.

4.2 THE GABBROS

The typical thermomagnetic and low temperature susceptibility curves for these specimens are drawn in fig.2. The decay of saturation magnetization (fig.2a) points to a Curie point of about 560°C, close to the pure magnetite Curie temperature. On the other hand no paramagnetism is observable. The low temperature susceptibility curve (fig.2b) shows a peak at about -140°C, which is described by Senanayake & McElhinny (1981, 1982) as characteristic of samples containing predominantly multidomain pure magnetite or magnetite-rich titanomagnetites ($x < 0.15$).

Measurements of the anisotropy of magnetic susceptibility give high bulk susceptibilities, in the range of 3 to 10.10^{-2}SI (in dimensionless volumetric SI units). This value is high enough for the influence of any paramagnetic components to be neglected. The anisotropy is high, with anisotropy percentages, defined as (kmax/kmin-1) x 100, of 18 to 25%. The anisotropy of magnetic susceptibility remains stable after the successive heating steps. From the twelve determinations of TRM anisotropy tensors, five were rejected on the basis of excessive chemical change during heating, which leads to incompatibilities between the two determinations of each TRM anisotropy tensor (different values for diagonal terms, different eigenvectors for the two tensors etc...). For the seven remaining specimens, the TRM anisotropy tensor has been determined by averaging the two estimates. The eigenvectors of this tensor fit the eigenvectors of the mean AMS tensor within a few degrees, as shown in the three examples of figure 3 (right). In this figure, the mean AMS tensor eigenvectors are represented with their ellipses of 95% confidence, following the second order tensor statistics of Jelinek (1978), derived from Hext (1963). The eigenvalues of AMS and TRM anisotropy tensors are displayed in Table 1. The estimation of the exponent of the power law (8) established above, has been done by computing the linear regression between $\ln(P_i)$ and $\ln(T_i)$ (fig. 3;left). P_i are : $P_1=k_1/k_2$, $P_2=k_1/k_3$, $P_3=k_2/k_3$; T_i are : $T_1=M_1/M_2$, $T_2=M_1/M_3$, $T_3=M_2/M_3$, where the indices 1, 2, 3 in k and M, indicate maximum, intermediate and minimum values respectively.

The parameters appear to correlate strongly (r=0,907) and the regression line is

$$\ln(P_i) = 0.515 \ln(T_i) + 0.014.$$

In the exponential form, this expression becomes

$$T_i = (1.0072\ P_i)^{1.94}$$

which can be approximated as

$$T_i \approx P_i^{1.94}$$

From this example, the theoretical relations (3) and (8) are therefore experimentally well verified.

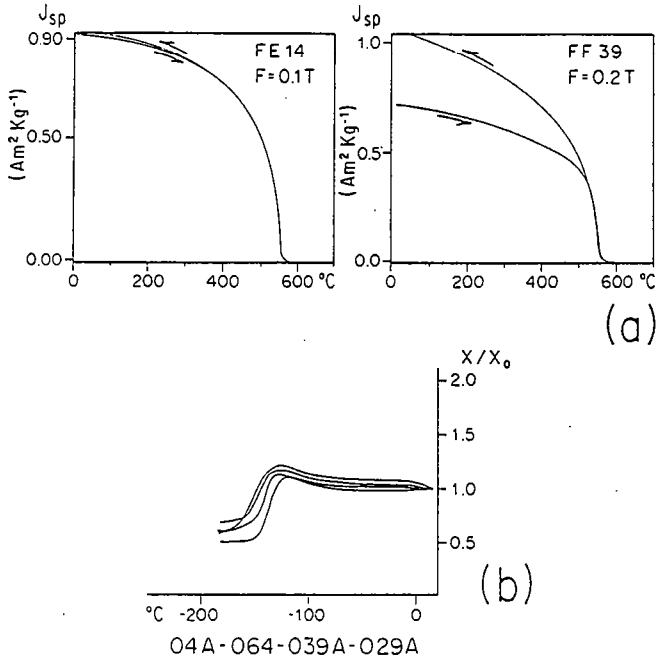

Fig. 4 - Thermomagnetic (a) and low temperature susceptibility (b) curves for the Flamanville granite specimens. In both thermomagnetic curves (a), F is the field, arrows indicate heating and cooling.

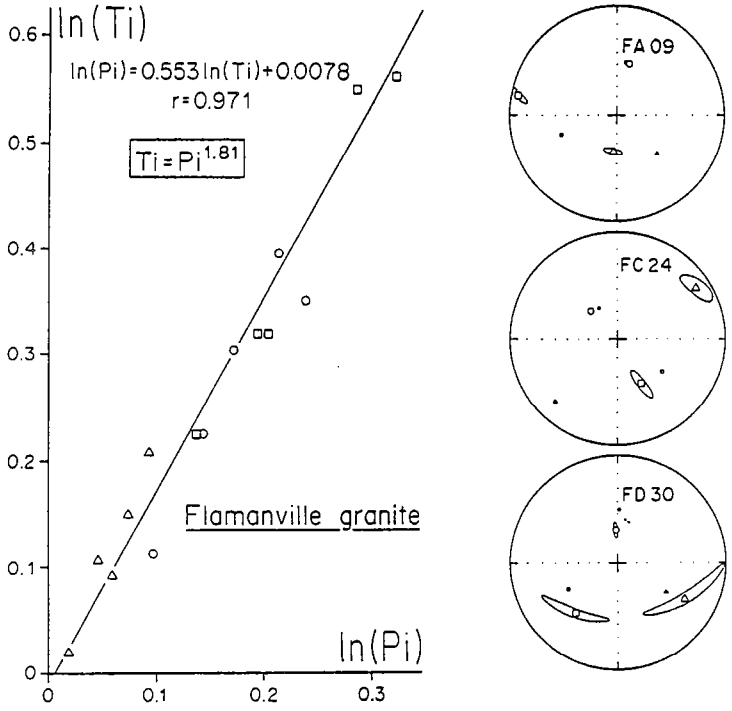

Fig. 5 - Comparison of TRM anisotropy and AMS of the Flamanville granite samples. Same diagrams, symbols and conventions as in Fig. 3.

4.3 THE FLAMANVILLE GRANITE

The series of tests conducted on the specimens of the highly anisotropic granite of Flamanville (Van der Voo & Klootwijk 1972; Cogné & Perroud in press) is the same as in the previous case. The Curie balance experiments give thermomagnetic curves (fig.4a) showing Curie points at about 560° C, close to the Curie point of pure magnetite. One further observation can be done on these curves. While in some cases, they show a perfect reversibility in cooling down to the room temperature (fig.4a, spec. FE 14), this is generally not the case (fig. 4a, spec FF 39). This indicates slight chemical or physical changes produced in the rocks by heating. The low-temperature susceptibility curves (fig. 4b) show a less typical path than in the previous case. However, the susceptibility peak at -140°C remains and it is therefore inferred that the ferromagnetic phase in these rocks is dominated by multidomain magnetites.

The anisotropy of the magnetic susceptibility in the Flamanville granite has been the subject of regional studies (Van der Voo & Klootwijk 1972; Cogné & Perroud in press). They have shown that apparent susceptibilities are high (0.3 - 0.8 10^{-2} SI) and that preferred orientation of elongated magnetite grains develop a strong anisotropy of magnetic susceptibility, with anisotropy percentages ranging from 15 to 35%. It can be further noted that the AMS ellipsoids are all of the flattened type with, in general, weak k_1/k_2 ratios.

Due to the chemical or physical modifications of the magnetic content of the rocks during heating which have affected a number of our specimens, a good TRM anisotropy estimation was obtained on only five of them. The comparison of the eigenvectors of AMS and TRM anisotropy tensors in each specimen is illustrated by three examples in fig.5 (right). What is obvious in this figure is that only k_3 and M_3 fit well, k_1, k_2, M_1 and M_2 being distributed in the perpendicular plane. Due to the low k_1/k_2 ratios, well illustrated by the elongated shape of the ellipses of 95% confidence in spec. FD 30 of fig.5, it is however assumed that the AMS and TRM anisotropy tensors do not significantly differ in their principal directions. The eigenvalues of both tensors are displayed in Table 2. As in the previous case, the linear regression has been computed between the logarithm of principal susceptibility ratios (P_i) and the logarithm of the TRM anisotropy eigenvalue ratios (T_i) (fig. 5; left). These parameters strongly correlate, with r = 0.971 and the equation of the best fit line is found as

$$\ln(P_i) = 0.553 \ln(T_i) + 0.0078$$

This can be rearranged as

$$T_i = (1.0043\ P_i)^{1.81}$$

and approximated as

$$T_i \approx P_i^{1.81}$$

Here too, the experimental determination of exponent 1.81, appears well consistent with the theoretical quadratic relationship (8).

5. Conclusion.

Although limited to the case of multidomain magnetite-bearing rocks, the above development shows that TRM deviations in such anisotropic rocks can easily be estimated by measuring their anisotropy of initial magnetic susceptibility. Indeed, the established quadratic relationship between the eigenvalue ratios is an approximation, and this cannot be considered as an

exact theoretical contribution to the theories of multidomain TRM processes. However, the tests carried out on natural anisotropic rock specimens show that the experimentally determined exponents fit quite well with the expected one. We therefore stress that (1) multidomain TRM can be significantly deviated from the ambient field where it is acquired ; (2) a systematic check for anisotropy state by measurement of AMS is desirable when paleomagnetically studying rock units within strained regions ; (3) these measurements should allow estimates of TRM deviations, and (4) it is therefore possible to compute a reliable field direction from such deviated TRM directions by using an inverse TRM anisotropy tensor estimated from the AMS tensor determinations.

In order to check how far this correction can be conveniently applied in practice, a paleomagnetic study of the anisotropic granite of Flamanville (NW France) is planned.

Acknowledgments.

Dr. M. Prévot has provided helpful comments. Colleagues at Rennes are acknowledged, A. Chauvin performed low temperature susceptibility experiments, P. Roperch provided the Peruvian gabbro specimens. This is a contribution of LP CNRS n°4661.

N°	TRM (A/m)			AMS ($\times 10^{-1}$ SI)		
	M_1	M_2	M_3	k_1	k_2	k_3
4404C	10.092	8.846	7.427	0.425	0.393	0.342
4407C	13.533	11.457	8.620	0.775	0.736	0.611
4410D	29.467	26.510	23.089	1.088	1.044	0.943
4501D	21.710	18.118	14.642	0.850	0.762	0.692
4503C	19.253	16.335	14.174	0.933	0.844	0.761
4504C	20.009	16.729	15.004	0.812	0.744	0.679
4510C	18.152	14.598	11.708	0.756	0.676	0.611

Table 1. TRM anisotropy and AMS data for the Peruvian gabbro specimens. M_1, M_2, M_3 are the TRM anisotropy eigenvalues. These are the magnetization components in A/m along the three principal axes, acquired by cooling in vacuum from 640°C down to room temperature, in a 60 μT field. k_1, k_2, k_3 are the mean principal susceptibilities, obtained by 6 measurements, one between each heating step.

No	TRM ($\times 10^{-1}$ A/m)			AMS ($\times 10^{-2}$ SI)		
	M_1	M_2	M_3	k_1	k_2	k_3
FA04B	9.529	7.705	5.422	1.366	1.230	0.965
FB09A	11.376	9.767	6.572	1.414	1.314	1.061
FC24	10.045	9.114	7.262	0.834	0.784	0.680
FD30A	2.171	2.131	1.574	0.795	0.777	0.653
FF37A	4.729	4.237	3.776	0.503	0.482	0.437

Table 2. TRM anisotropy and AMS data for the Flamanville granite specimens. Same legend as in Table 1.

REFERENCES

Cogné, J.P. & Perroud, H. Anisotropy of magnetic susceptibility as a strain gauge in the Flamanville granite, Phys. Earth Planet. Int., In Press.

Collinson, D.W., 1983. Methods in rock magnetism and palaeomagnetism, Chapman & Hall, London, 499 pp.

Hext, G.R., 1963, The estimation of second-order tensors with related tests and designs, Biometrika, 50, 353-373.

Hrouda, F., 1982. Magnetic anisotropy of rocks and its application in geology and geophysics, Geophys. Surv., 5, 37-82.

Jelinek, V., 1978. Statistical processing of anisotropy of magnetic susceptibility measured on groups of specimens, Studia Geoph. et Geod., 22, 50-62.

Nagata, T., 1961. Rock magnetism, Maruzen, Tokyo, 350 pp.

Salis, J.S., 1986. Variation séculaire du champ magnétique terrestre, direction et paléointensité, sur la période 7000-70000 ans BP, dans la chaine des Puys, Thèse Univ. Rennes, 192 pp.

Schmidt, P.W. & Clark, D.A., 1985. Step-wise and continuous thermal demagnetization and theories of thermoremanence, Geophys. J. R. astron. Soc., 83, 731-751.

Senanayake, W.E. & MacElhinny, M.W., 1981. Hysteresis and susceptibility characteristics of magnetites and titanomagnetites: interpretation of results from basaltic rocks, Phys. Earth Planet. Int., 26, 47-55.

Senanayake, W.E. & MacElhinny, M.W., 1982. The effects of heating on low-temperature and hysteresis properties of basalts, Phys. Earth Planet. Int., 30, 317-321.

Stacey, F.D. & Banerjee, S.K., 1974. The physical principles of rock magnetism, Elsevier, Amsterdam, 195 pp.

Stephenson, A., Sadikun, S. & Potter, D.K., 1986. A theoretical and experimental comparison of the anisotropies of magnetic susceptibility and remanence in rocks and minerals, Geophys. J. R. astr. Soc., 84, 185-200.

Uyeda, S., Fuller, M.D., Belshé, J.C. & Girdler, R.W., 1963. Anisotropy of magnetic susceptibility of rocks and minerals, J. Geophys. Res., 68, 279-291.

Van Der Voo, R. & Klootwijk, C.T., 1972. Paleomagnetic reconnaissance study of the Flamanville granite with a special reference to the anisotropy of its susceptibility, Geol. en Mijn., 51, 609-617.

ANNEXE 3.

J.P. COGNE. **Strain-induced AMS in the granite of Flamanville and its effects upon TRM acquisition.** Accepté à Geophys. J. R. astron. Soc.

STRAIN-INDUCED AMS IN THE GRANITE OF FLAMANVILLE AND ITS EFFECTS UPON TRM ACQUISITION.

J.P. COGNE. C.A.E.S.S., Laboratoire de Géophysique Interne, Université de Rennes 1, 35042 Rennes-Cedex, France.

Abbreviated title: AMS and TRM in the Flamanville granite.

Summary. A palaeomagnetic study of the Carboniferous granite of Flamanville (NW France) has been conducted in order (1) to examine the possible deviating effects of the anisotropy of magnetic susceptibility (AMS) upon TRM acquisition in strained rocks, and (2) to test the possibility of correcting these deviations by using the relationships between AMS and TRM anisotropy tensors previously proposed for multidomain TRM (Cogné 1987). In each of the 9 sampled sites, a weak TRM is recovered, after thermal and AF cleaning, from a strong present-day field VRM overprinting. This TRM, predominantly carried by multidomain magnetite, is consistent with the known Carboniferous magnetic field direction in the Armorican Massif. However, TRM mean-site declinations present a large between-site dispersion, which is shown to be related to a deviating effect of AMS in each site. An attempt is thus made to correct for these deviations by using the inverse TRM anisotropy tensor deduced from AMS measurements. This clusters the data, and allows a paleofield direction to be defined with better accuracy. The result obtained is $D=205^0$ $I=18^0$ $\propto_{95}=5.5^0$. Finally, we emphasize the possibility of using deviated TRM acquired by anisotropic rocks within strained regions, in order to compute a reliable paleofield direction.

Key words: Strain, anisotropy, susceptibility, remanent magnetization, palaeomagnetism.

1. Introduction.

During the last decade, palaeomagnetism has been recognized as a powerfull tool with which to study the tectonic history of orogenic belts (Van der Voo & Chanell 1980). This recognition was accompanied by improvements in the methods of studying rock magnetization, including multicomponent magnetization analysis, K-Ar dating of components, rock magnetism experiments etc... Until recently these developments were focused on the remagnetization effects of metamorphism or reheating of rock units, and on the mean of recovering primary magnetization directions in such materials. However, one of the more difficult problems, and perhaps at present the less studied, is the problem of the effects of deformation upon the orientation of palaeomagnetic vectors. This has two main aspects, depending upon the relative chronology between deformation and magnetization acquisition ages. The questions are (1) of what is the effect of deformation upon a predating (primary) magnetization direction and (2) by how much a magnetization acquired by anisotropic strained rocks can be deviated from the ambient magnetic field.

In partial answer to the first question, the effects of deformation upon primary pretectonic magnetization have recently been described within some deformed redbeds, or by the way of numerical simulations (Cogné & Perroud

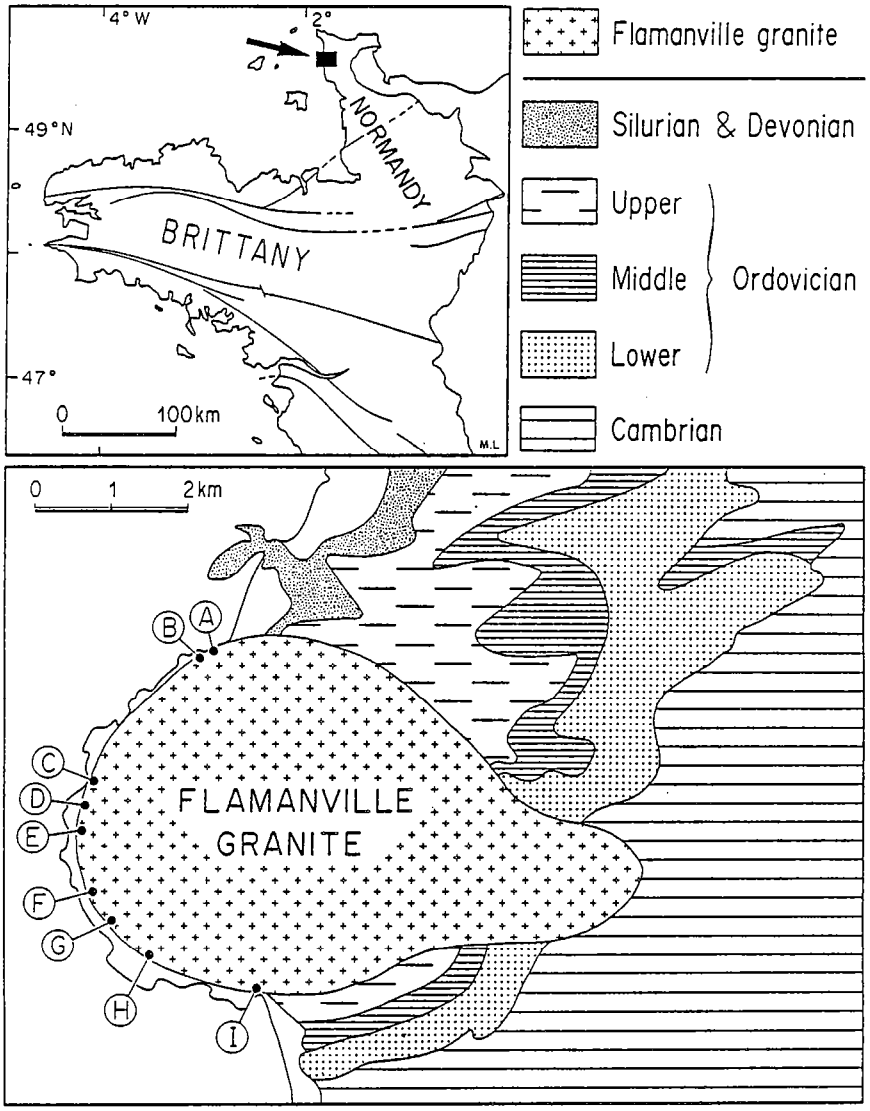

Fig. 1: Upper: location map of the Flamanville area in the Armorican Massif, Normandy, France. Lower: schematic geological map of the Flamanville Massif. Dots labelled A to I are the sampling sites of this study.

1985, Cogné et al. 1986). A new method of unstraining palaeomagnetic vectors has been proposed by Cogné & Perroud (1985).

The second aspect of the problem has so far been less studied. It is well established that magnetic anisotropy due to particle alignment may cause the natural remanent magnetization (NRM) of rocks to be deflected away from the field direction when remanence is acquired (Nagata 1961, Uyeda et al. 1963, Fuller 1963). For this reason, strongly anisotropic rocks are generally avoided for palaeomagnetic studies. Stephenson et al. (1986) have established theoretical relationships between the anisotropies of magnetic susceptibility (AMS), thermoremanent magnetization (TRM) and isothermal remanent magnetization (IRM). Restricting ourselves to the case of TRM in multidomain magnetite-bearing rocks, we have shown that TRM and susceptibility anisotropy tensors are simply related by a quadratic relationship between the ratios of their eigenvalues (Cogné 1987). This theoretical relationship has been verified by experiments on anisotropic rock samples.

In order to study the deviations of TRM from the ambient field in a naturally anisotropic rock unit, and to emphasize the possibility of computing a reliable field direction from such deviated remanence directions, a joint study of strain, anisotropy of magnetic susceptibility, and remanence has been conducted in the Hercynian granite of Flamanville (France).

2. Geological setting and sampling sites.

The Carboniferous (308±07 Ma, Vidal 1980) Flamanville granitic pluton was intruded into the Paleozoic formations of the Siouville syncline in Normandy, France (Fig.1). At first considered as ending the Hercynian structural history of the region (Martin 1953), this pluton has been shown to be syntectonic by Ledru & Brun (1977), and Brun (1981). Their detailed study of the Siouville syncline has shown that the cleavage development in the country rocks is controlled by the thermal anomaly due to granite intrusion. The regionally E-W trending cleavage trajectories bend around the margins of the Flamanville pluton. The locally subcircular cleavage pattern grades into the regional schistosity except at a triple point of cleavage direction (i.e. a point of no finite strain ; Ramsay 1967) situated east of the pluton. These features were interpreted by Brun (1981) as resulting from the interference of synchronous diapiric emplacement and Hercynian regional deformation.

In the granite itself, there is a steeply dipping foliation plane parallel to the pluton margin, except in the southern part, where foliation crosscuts the contact with the country rocks. Mainly due to the coplanar orientation of mafic minerals (Martin 1953), the foliation induces an anisotropy of the magnetic susceptibility (AMS). This was first studied by Van der Voo & Klootwijk (1972) who have shown that anisotropy percentages are high and that the magnetic foliation plane (k_1k_2 plane) is parallel to the granite margins. In our study of AMS and strain relationships in this granite (Cogné & Perroud 1987), we found that strain (as estimated from elliptical xenoliths measurements in the field) and AMS ellipsoids are related not only in the direction, but also in the magnitude of their principal axes. Additionally, we showed the existence of a strain gradient from the western border of the granitic body towards the northern and southern ones, accompanied by similar variations of AMS intensities. We concluded that this was consistent with a synchronism of regional deformation and diapiric emplacement of the pluton.

The sampling sites of the present study are the same as in the previous one (Cogné & Perroud 1987): 9 sites (A to I, Fig.1) have been sampled around

the well-exposed western border of the pluton. 66 cores were sampled using a portable drill, and oriented in-situ with magnetic and sun compasses. The cores were cut in the laboratory to yield 125 specimens.

3. Anisotropy of the magnetic susceptibility.

From the 125 specimens, 93 had the optimum shape of 25mm diameter x 22 mm length for susceptibility anisotropy measurement (Noltimier 1971). The measurements of AMS were made with a Schonstedt DSM-1 spinner magnetometer as described previously (Cogné & Perroud 1987). Twenty of these 93 specimens were eliminated from the AMS measurements because their bulk susceptibility was too low ($<10^{-3}$ SI) for their anisotropies to be accurately measured with the spinner magnetometer. All the specimens of site H are in this category. The k_{zz} component of the susceptibility tensor (i.e., the susceptibility along the axis of the cylindrical specimen, measured with a Bartington MS-2 susceptibility meter) of the 73 remaining specimens is high, ranging from 0.3 to 1.0×10^{-2} SI. From the N measured specimens at each site, a mean normalized susceptibility tensor has been computed by using the tensor statistics of Jelinek (1978) derived from Hext (1963). Following this anlysis, each tensor determined by a measurement is normalized by its mean susceptibility $(k_1+k_2+k_3)/3$, in order to eliminate the effects of the fluctuating specimen bulk susceptibility upon the estimation of the site mean tensor. The mean tensor and its confidence limits are then estimated by summing the N normalized tensors of a site and computing the relevant covariance matrix, from which are derived the variance (σ^2) of the normalized principal susceptibilities and the semi-angles (a,b) of the ellipse of confidence at the 95% probability level around the principal directions. To complete the description of AMS, the mean-site bulk susceptibility is calculated as $k=(k_1+k_2+k_3)/3$, where k_1, k_2, k_3 are the eigenvalues of the unnormalized mean tensor of the site. These parameters are displayed in Table 1, and illustrated on Fig.2 and 3.

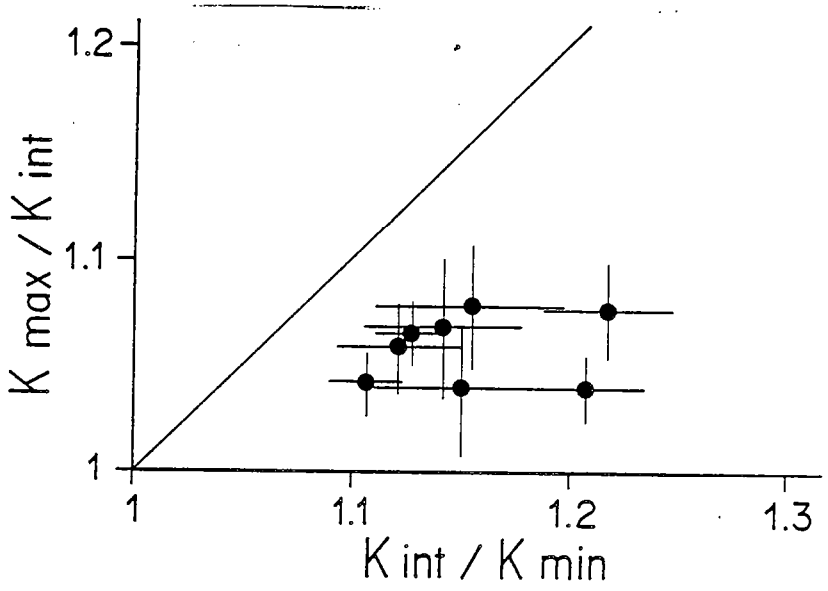

Fig. 2: Flinn (1965) diagram of mean-site AMS data. Each point represents the mean AMS of a site with error bars derived from the standard deviation of mean k_1, k_2 and k_3 of Table 1.

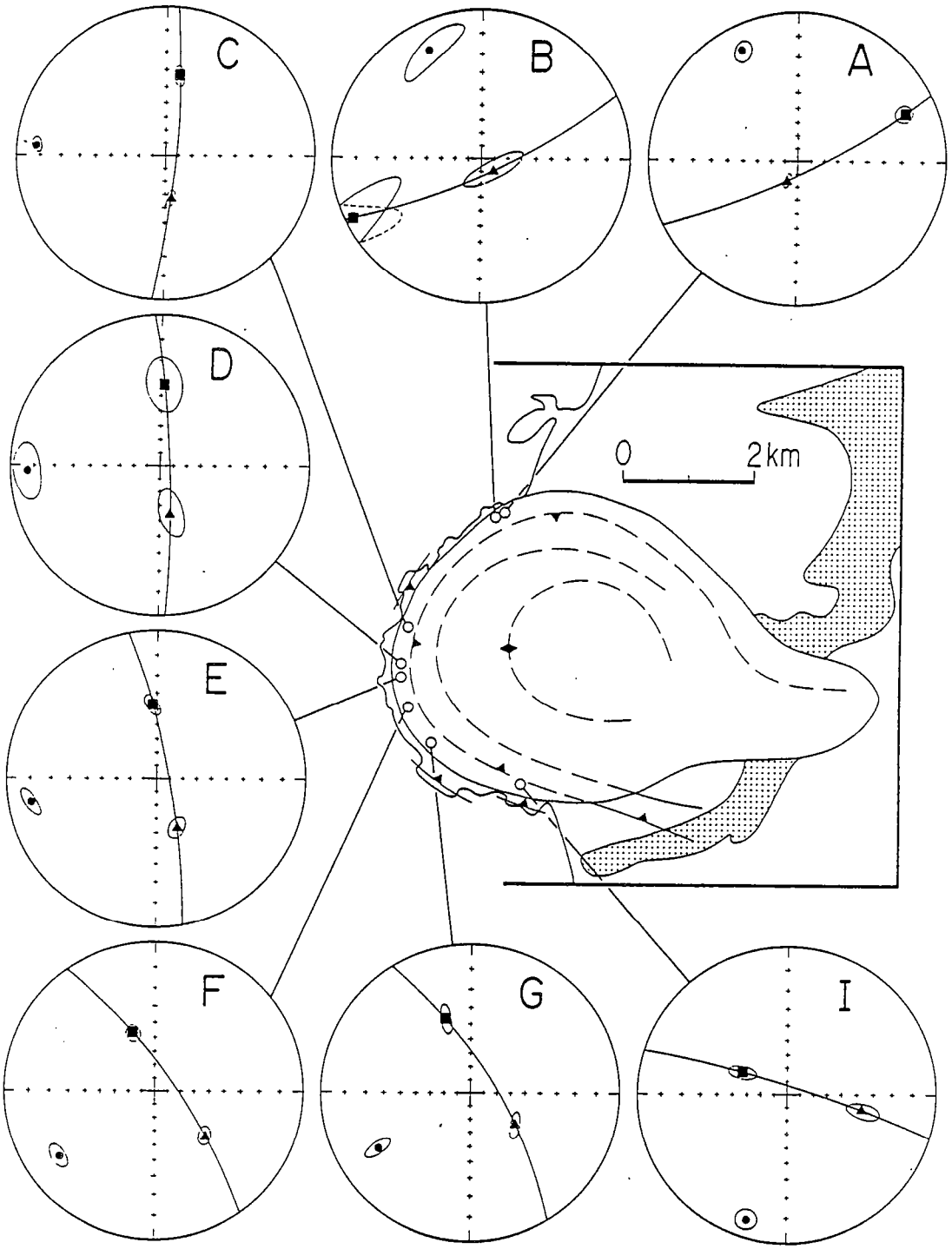

Fig. 3: Stereoplots of mean-site principal susceptibility directions with their ellipses of 95% confidence (Jelinek 1978). Squares: k_1; triangles: k_2; circles: k_3. The mean k_1k_2 magnetic foliation planes are drawn. Stereographic projections in the lower hemisphere.

From Table 1, it can be seen that both susceptibility and anisotropy are high. In a Flinn (1965) diagram (Fig.2), the data are in the flattened ellipsoid area. The principal susceptibility directions are in general well defined (Fig.3). Note that in site B, the large ellipses of confidence are mainly due to the small number (4) of AMS determinations. The steeply dipping magnetic foliation planes (k_1k_2 planes) follow the granitic body contour (Fig.3) from NE-SW striking (site A) to about an E-W trending (site I), through N-S directions. The directional variability, together with the high anisotropy therefore offer a particuliarly favourable situation in which to study the possible deviation effects of AMS upon TRM acquisition.

4. Palaeomagnetic analysis.

Natural remanent magnetizations (NRM's) have been measured with a Schonstedt spinner magnetometer. Before demagnetization, a short-period viscosity test (Thellier & Thellier 1959) was carried out. Alternating field (AF) and thermal (Th) demagnetizations were performed with Schonstedt equipment, with companion specimens being subjected to different treatments. Orthogonal projections of the demagnetization results were used to determine the direction of magnetization components (Zijderveld 1967). Curie point determinations were obtained from thermomagnetic analyses done with a Brucker Curie balance. Low-temperature susceptibility experiments were done with a Bartington MS-2 susceptibility meter.

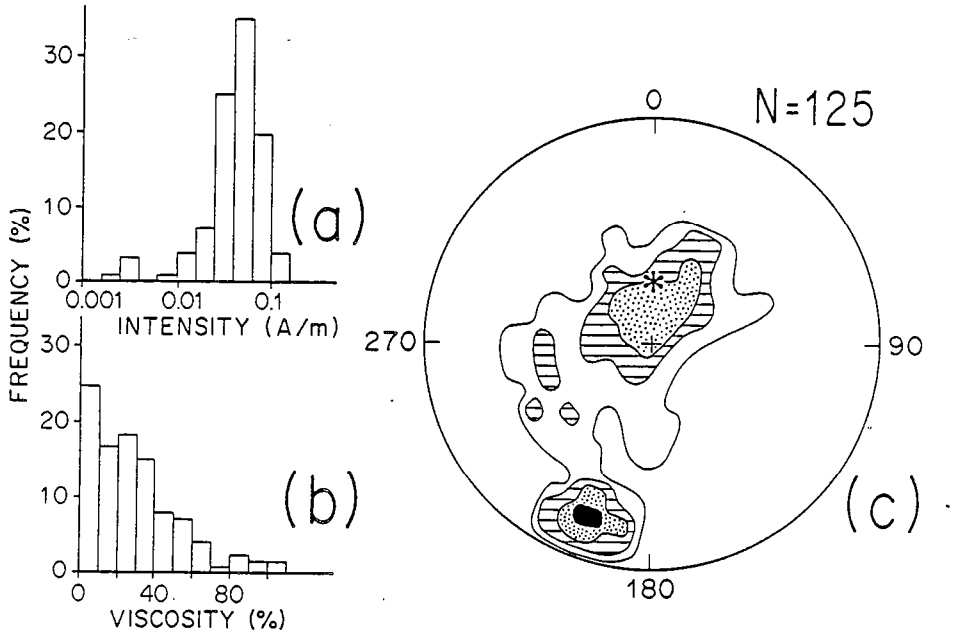

Fig. 4: (a) Frequency plot of NRM intensities observed in the Flamanville samples. (b) Frequency of viscosity coefficients (Thellier & Thellier 1959). (c) Point-density equal-area projection in the lower hemisphere of NRM directions (before demagnetization); contours are 1, 2.5, 5, 10 and 20% of the data in 1% of the hemisphere surface; star is the present-day dipole field direction in the Flamanville area.

NRM intensities (Fig.4a) are quite homogeneous, in the range 0.01-0.1 Am^{-1}. A small group of specimens has intensities of about 0.001 Am^{-1}. The short period (8 days) viscosity coefficients (Fig.4b) are generally high, only 41% of specimens have a viscosity coefficient lower than 20%. In fig. 4c, the NRM directions are shown in a density plot which underlines the bipolar distribution of these directions. A first group shows southeasterly declinations, with shallow inclinations. This is consistent with the known Carboniferous field direction in the Armorican Massif (Perroud 1985). A second group clusters near the present day axial dipole field direction (star in Fig. 4c). One can note that inclinations are slightly higher than that of the dipole field. Due to the generally steeply dipping magnetic foliation plane and the high degree of anisotropy in this granite , on the one hand, and the high visosity coefficients, on the other hand, this may be interpreted as a deviation effect of magnetic susceptibility anisotropy upon a viscous remanent magnetization which overprints the Carboniferous TRM. However, the question of secondary magnetization deviations will not be developed here, since we are mainly interested in the deviating effects of AMS upon primary TRM directions.

113 specimens were subjected to stepwise AF and thermal demagnetizations. Some typical demagnetization curves in orthogonal projections (Zijderveld 1967) are shown in Fig.5 and 6. In a few samples, in

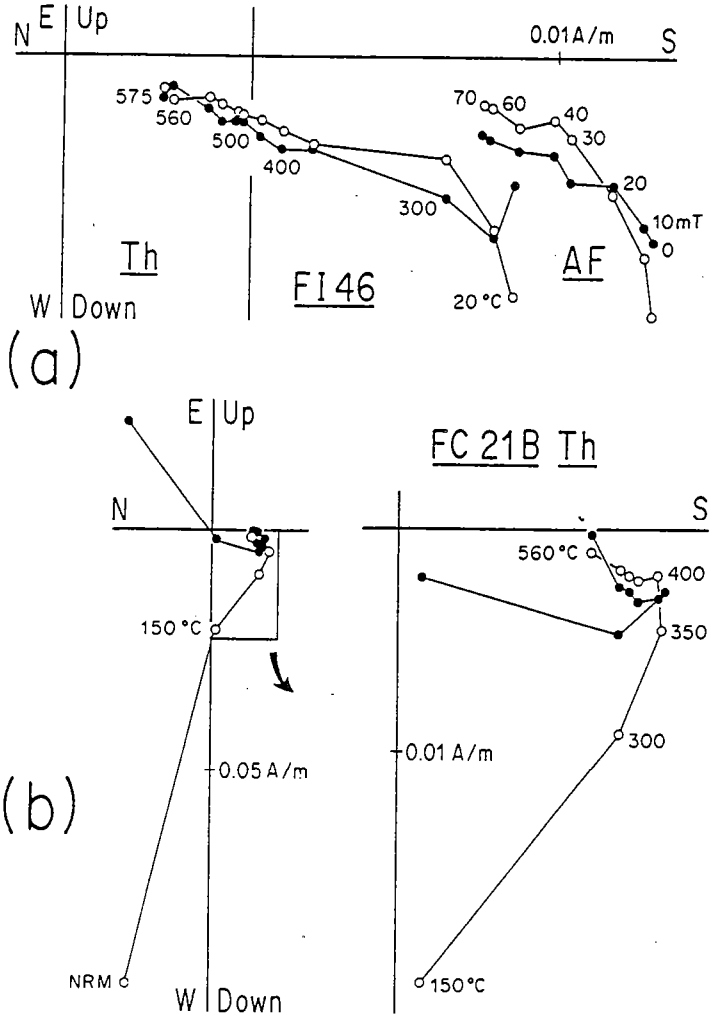

Fig. 5: Alternating field (AF) and thermal (Th) demagnetization curves in orthogonal projections (Zijderveld 1967) in the in-situ coordinates. Open (closed) symbols: projections onto the vertical (horizontal) plane. Temperature steps indicated in °C, AF in mT. (a) and (b): see text.

which viscosity coefficients are low, a single component of magnetization was observed in thermal as well as in AF demagnetization (Fig.5a). It has a southerly to southwesterly declination with shallow inclinations. The unblocking temperatures, are in the range of 500 to 560°C, typical of magnetite. However, in most of our specimens, this component is overprinted by another one which presents high inclinations (Fig. 5b), conforming to the present day geomagnetic field in France, and thus assumed to be of recent origin. This secondary component generally represents more than 80% of the total NRM intensity. This made it difficult, and sometimes impossible, to determine the direction of the weak primary magnetization component (Fig.6a).

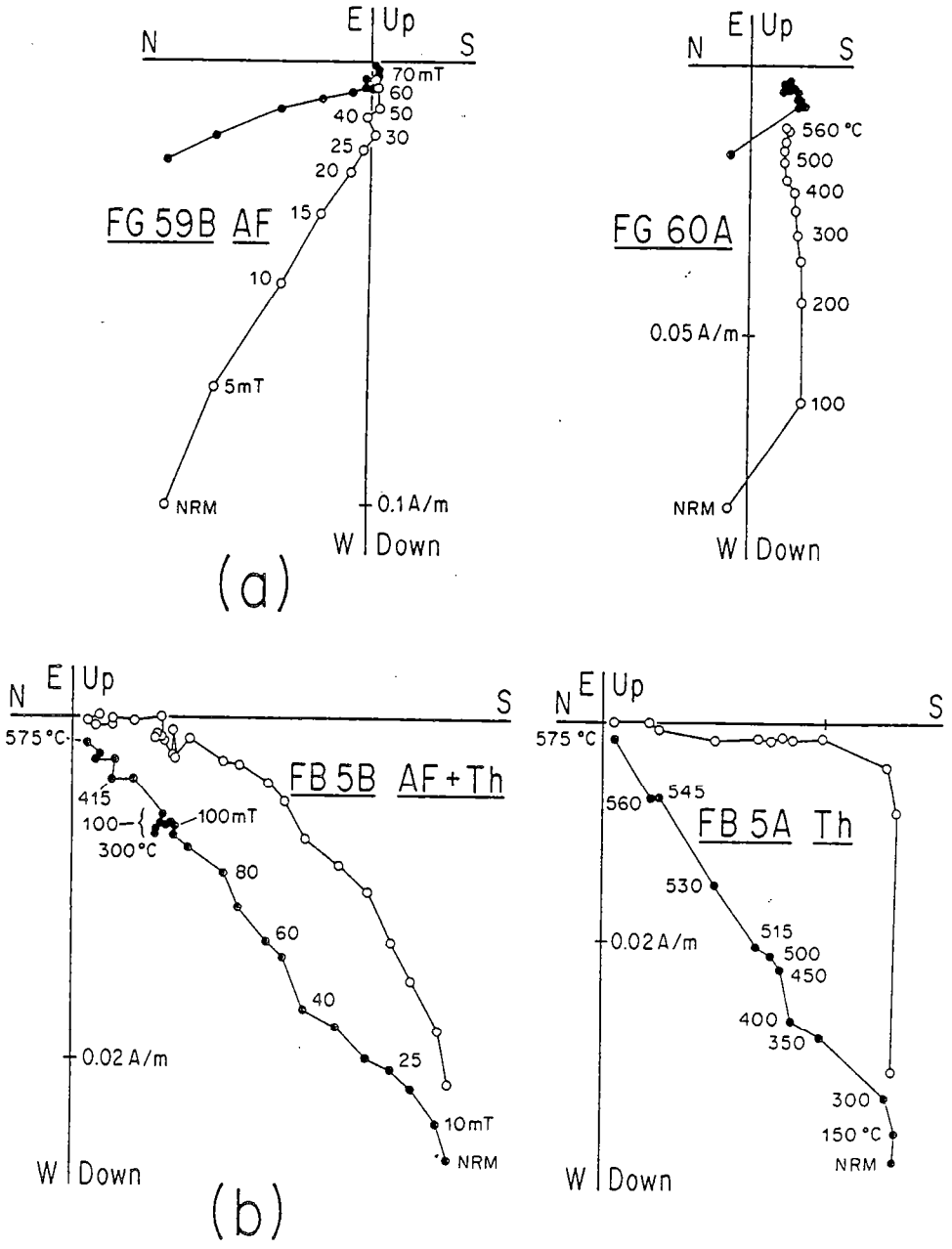

Fig. 6: Same caption as in Fig.5. (a) and (b): see text.

Finally, it is to be noticed that AF demagnetization was generally less efficient than thermal demagnetization for separating these components. This is illustrated in Fig.6b, where one of the specimens of a core was demagnetized by thermal treatment, the other by alternating field. It is clear that the AF demagnetization alone (specimen FB 5B) does not allow the separation of the components which is achieved at temperatures over 300°C in thermal demagnetization (specimen FB 5A). In the first case, we had to follow the AF by a thermal treatment to achieve the cleaning of primary characteristic magnetization. Due to the difficulties thus encountered, only 77 from the 113 demagnetization curves allowed an accurate determination of the characteristic remanent magnetization (ChRM), defined as the high temperature or coercivity linear portions of the demagnetization curves. The in-situ ChRM directions are shown for each site in Fig.7, their within site means are given in Table 2 and illustrated in Fig.7. They are generally gently inclined in a SSW direction except for site G, where ChRM's show a clear trend towards the northerly steeply inclined present-day dipole field direction. This is thought to be due to a poor separation of the components and therefore all the data of this site have been rejected from the final analysis. This observation applies for site C as well, since palaeomagnetic data of this site cluster in 2 groups. Only the 6 shallowest magnetic vectors

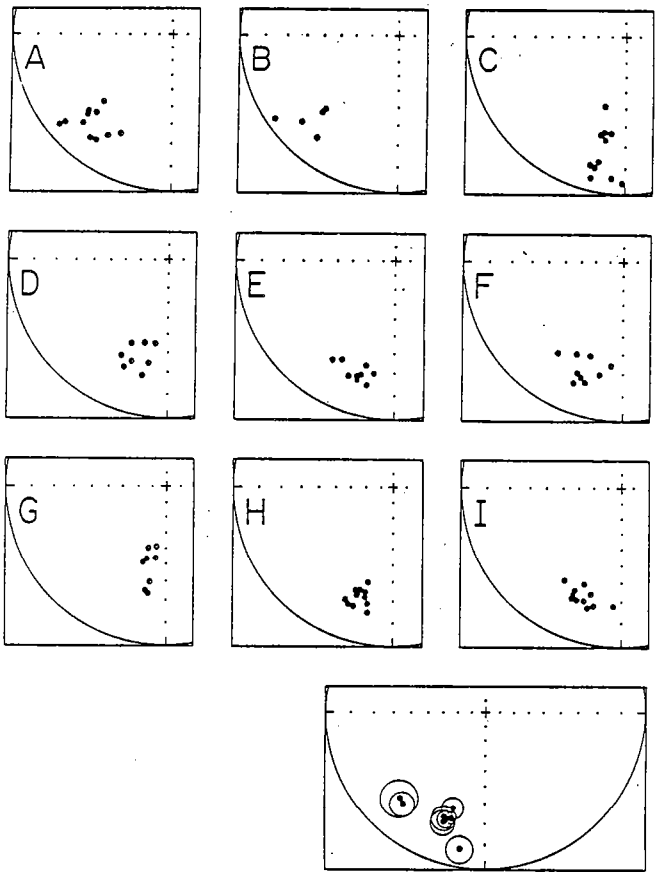

Fig. 7: Site-by-site projections of characteristic remanent magnetization (ChRM) directions isolated by thermal and AF demagnetization. Lower: mean-site ChRM directions with their circles of 95% confidence (see Table 2). Stereographic projections in the lower hemisphere.

have been taken into account for the computation of the site C mean given in Table 2.

Although homogeneous in inclination, the mean site directions show a significant dispersion in declination (Fig.7 lower). However, before detailing the analysis of this dispersion, it is necessary to identify the magnetic carrier of the remanent magnetization.

5. Rock magnetism.

5.1. IRM ACQUISITION.

One specimen of each site was given an IRM in progressively increasing magnetizing fields. Saturation was typically reached in fields of 0.05 -0.15 T (Fig.8a). This range of saturating field is characteristic of magnetite (Dunlop 1972). A higher coercivity phase is sometimes present, as shown by the coercivity spectrum of specimen FI 47 in Fig. 8a. This suggests the presence of hematite, but also of pyrrhotite. However, if this is related to the low unblocking temperature remanence components observed in thermal demagnetization, it seems unlikely that hematite bears a significant part of the remanent magnetization.

5.2. THERMOMAGNETIC EXPERIMENTS.

Curie points of some rock powders from the granite of Flamanville were determined by using a computer-monitored vertical high-field Curie balance. The powders were placed into sealed $1cm^3$ quartz containers, under a vacuum lower than 10^{-2} Torr. The thermal decay of saturation magnetization (Fig. 8b) is typical of magnetite, with a Curie point at about 560°C. Although the curves can be reversible in temperature as shown by specimen FE 14 of Fig.8b, the heating experiments often result in a significant increase in the saturation magnetization intensity (specimen FF 39 Fig.8b) which can reach twice its initial value when cooling down to room temperature. Such an irreversibility can be due either to the inversion of maghemites (O'Reilly 1984), or also to magnetite produced by the breakdown of sulphides (pyrite) above 350°.

5.3. LOW TEMPERATURE SUSCEPTIBILITY.

The evolution of the susceptibility from liquid nitrogen temperature up to room temperature is shown in Fig.8c. The curves clearly exhibit a peak at about -140°C. This peak is associated with the low temperature transition when the magnetocrystalline anisotropy constant k_1 vanishes. According to Senanayake & McElhinny (1981, 1982), this is characteristic of samples containing predominantly multidomain (MD) magnetites or magnetite-rich titanomagnetites. It is therefore inferred that the magnetic content of the Flamanville granite is dominated by MD magnetite grains. This is in good agreement with the conclusions of Van Der Voo & Klootwijk (1972).

5.4. INTERPRETATION.

From this series of experiments, we appear to have two main phases of magnetic minerals. The presence of fine-grained pyrrhotite could explain the high coercivity phase seen in IRM acquisition curves, the unblocking temperatures lower than 350°C of the steeply dipping remanent magnetization component, and the resistance of this component against AF treatment (Fig.5 and 6) (Kligfield & Channel 1981). The magnetization component carried by this phase is therefore inferred to be a secondary long term viscous remanent magnetization (VRM) which overprints the primary magnetization of the granite. The presence of other suspected phases, such as hematite or

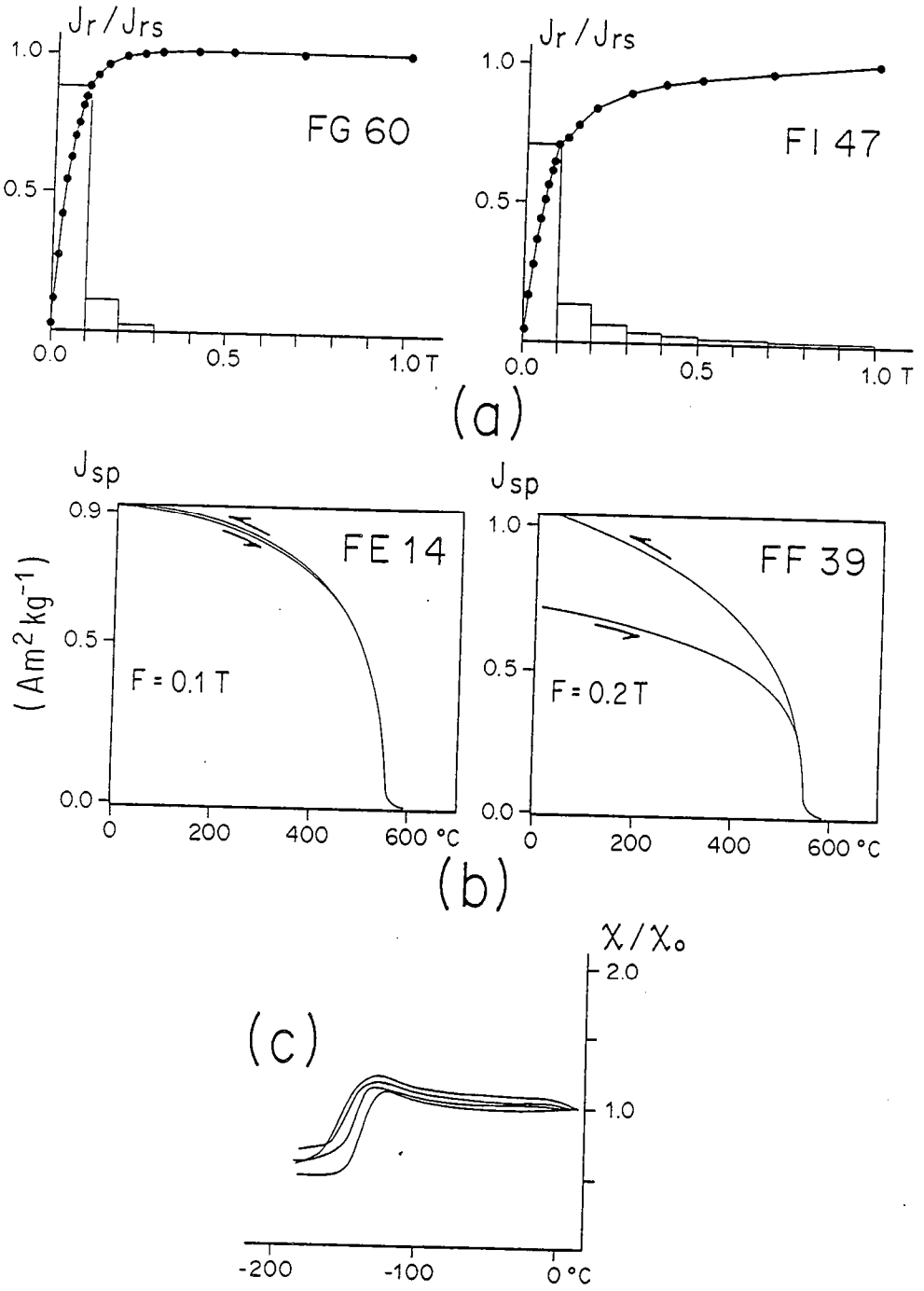

Fig. 8: (a) IRM acquisition curves in the Flamanville granite samples; IRM intensities (J_r) normalized to the saturation remanence (J_{rs}) vs. field strength in T. (b) Thermomagnetic curves: saturation magnetization (J_{sp}) in Am^2kg^{-1} vs temperature in ^oC; arrows indicate heating and cooling, F is the field in T. (c) Evolution of low temperature susceptibility, normalized to the room temperature susceptibility.

maghemite, cannot strictly be eliminated, but their contribution to the remanence is thought to be negligible.

The second magnetic phase is magnetite or magnetite-rich titanomagnetite, with 0.1-0.2 T coercivities and a Curie point at 560°C. The low temperature susceptibility curves show that the magnetite grains are predominantly in the MD state. The highest unblocking temperature magnetization components isolated by thermal demagnetization are associated with this phase. Owing to the nature of the magnetic carrier and to the igneous origin of the granite, as well as to the lack of thermal event since its emplacement, the ChRM's shown in Fig.7 and Table 2 are assumed to be primary TRM's acquired by the granite when cooling in the Carboniferous magnetic field.

6. Estimates of the paleofield direction from deviated TRM.

6.1. TRM DEVIATIONS ANALYSIS.

As commented on above, mean-site TRM directions show a large between site dispersion although individual directions are quite well clustered within each site. It is unlikely that this dispersion results from an inadequate separation of TRM and VRM components, since that would, principally, induce a scatter in inclination, as shown in sites C and G (Fig.7) for example.

In fact, if we take into account the high anisotropy of magnetic susceptibility described above, the most conceivable hypothesis to explain this dispersion is that TRM's are deviated by AMS away from the magnetic field direction. In order to test this hypothesis, a comparison of magnetic foliation plane (k_1k_2 plane) direction, TRM direction and an assumed Carboniferous magnetic field direction has been made at each site. The magnetic field reference direction (D=206.5°, I=10.5°) has been computed for the studied area location from the 280 -330 Ma Virtual Geomagnetic Pole (327°E, 31°S), of the Armorican Massif, as reviewed by Perroud (1985). Since TRM's and field vectors have shallow inclinations, and the k_1k_2 planes dip steeply, only their declinations and strikes are represented for simplicity in the horizontal plane in Fig.9. From this figure, it is clear that TRM systematically deviates from the ambient field direction towards the magnetic foliation plane. It can further be noted that the amount of deviation depends upon the angle between the field direction and the k_1k_2 plane, and upon the degree of anisotropy: in site I where the field direction is close to the normal to the k_1k_2 plane, the deviation appears very small, unsignificant with respect to the TRM determination error and the field direction uncertainties. On the other hand, sites A and B, where anisotropy percentages are the highest, show greater divergence than sites D and E although the angular relationships between field and k_1k_2 planes are similar in these 4 sites. All these observations lead us to assume that AMS is actually the most probable cause of the between-site TRM dispersion in the granite of Flamanville.

6.2. MAGNETIC FIELD DIRECTION ESTIMATE.

Until now the problem of correcting TRM deviations induced by AMS has not been considered as critical, since it is generally agreed that below a given degree of anisotropy, TRM deflections are not significant for paleomagnetism. For Nagata (1961) and Stacey & Banerjee (1974), an anisotropy percentage of 5% is the limiting value for an allowed maximum TRM deviation of 3°. A more recent investigation of the problem was reported by Stephenson

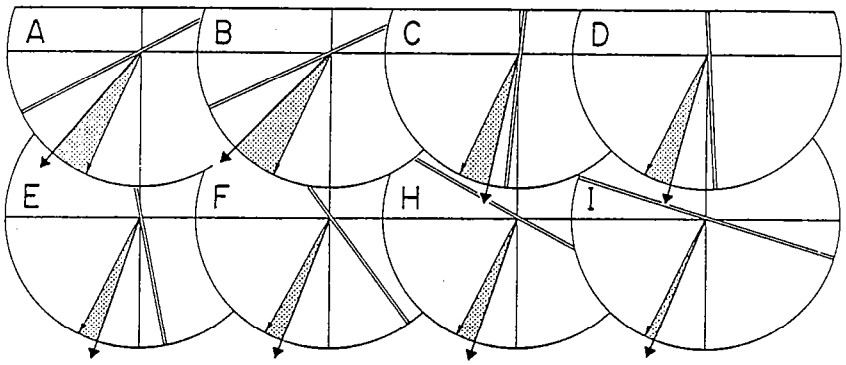

Fig. 9: 2-D comparison of k_1k_2 plane strikes (double lines), mean-site TRM directions (long arrows) and the Carboniferous reference field direction (short arrows). The dotted areas underline the deviation of TRM away from the field.

et al. (1986). They express the cartesian coordinates J_i of the TRM as a function of those of the field H_j through the TRM anisotropy tensor $\mathbf{M}_{ij}$, as $J_i=\mathbf{M}_{ij}.H_j$ (i,j= 1,2,3). They show that the eigenvalues of the TRM anisotropy tensor are linearly related to the AMS tensor eigenvalues, and also to the eigenvalues of a low-field IRM anisotropy tensor, defined in the same manner. The coefficients of the correlation between the normalized principal values of these ellipsoids mainly depend upon the size of the magnetite grains, and need therefore to be determined for each rock sample studied.

From currently accepted theory of multidomain TRM (Nagata 1961, Stacey & Banerjee 1974, Schmidt & Clark 1985) I have recently shown (Cogné 1987) that in anisotropic multidomain magnetite assemblages, the order of magnitude of the TRM anisotropy eigenvalue ratios is expected to be the square of the principal susceptibility ratios.

Briefly, if we express the TRM components as above $J_i= \mathbf{M}_{ij}.H_j$, the eigenvaiues, or principal values, of $\mathbf{M}_{ij}$ are M_i (i=1,2,3), and the ratio of any pair of M_i is found to be

$$\frac{M_i}{M_j} = \frac{N_j}{N_i} \cdot \frac{1 + N_j\varkappa_0}{1 + N_i\varkappa_0}$$

where N_i is the demagnetizing factor in the i^{th} direction and $\varkappa_0$ the intrinsic isotropic susceptibility. Assuming $\varkappa_0$ as sufficiently high to approximate the initial susceptibility k as $k\approx 1/N$, this reduces to $M_i/M_j\approx (k_i/k_j)^2$

This relationship has been well verified by a series of TRM acquisition experiments performed on two sets of rock samples containing predominantly multidomain magnetite and having high AMS (Cogné 1987). It was therefore decided to use this relationship in order to estimate the magnetic field direction from the deviated TRM of the granite of Flamanville.

In each site, the TRM anisotropy tensor was estimated from the mean AMS tensor (Table 1) in the following manner: their eigenvectors are identical; according to the above relationship, the ratios M_1/M_2 and M_2/M_3 has been calculated as $(k_1/k2)^2$ and $(k_2/k_3)^2$. Then, a normalization to the product $M_1M_2M_3=1$, or to the sum $\Sigma M_i=1$, allows the determination of the mean normalized TRM principal values M_1, M_2 and M_3. These are given in Table 3. Note that the choice of a normalization to the sum or to the product of M_i is not critical in this problem, since the angular change of vectors is governed by the ratios of the tensor eigenvalues, and not by their absolute values. The normalized TRM tensor $\mathbf{M}_{ij}$ is thus constructed and, after its inversion, an estimate of the magnetic field direction in each site is given by $H_i= \mathbf{M}^{-1}_{ij}J_j$ (i,j=1,2,3), where J_j are the cartesian components of the mean site TRM direction (Table 2). The field direction estimates obtained by this method are given in Table 3 and Fig.10b. The treatment applied to site H data is different, since for this site there were no AMS measurements. Here, the normalized principal susceptibilities k_i were first estimated from strain data according to the empirical correlation between strain and AMS principal values we have established previously (Cogné & Perroud 1987). Then the principal values M_1, M_2 and M_3 of the TRM anisotropy tensor were calculated in the same way as in the other sites.

A comparison of the field estimated by using the above relationship (Fig.10b) with the TRM mean site directions (Fig.10a) shows that this correction induces a significant clustering of the data. The magnetic field directions have a more Fisherian distribution than the TRM's, where large

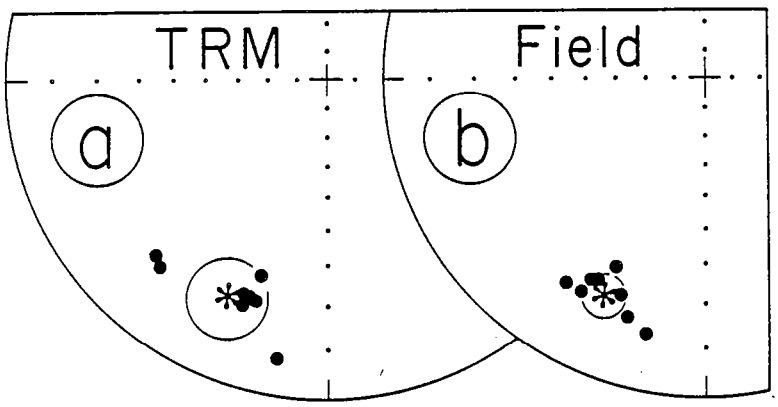

Fig. 10: (a) TRM mean-site directions and their mean (asterisk) with its circle of confidence (Table 2). (b) Magnetic field direction estimates, obtained by correcting TRM's from AMS induced deviations; asterisk: mean field direction with its circle of confidence. Stereographic projections in the lower hemisphere.

gaps appeared between points. This is accompanied by an increase of the Fisher (1953) parameter k value from 42 to 95 and a reduction of the α_{95} circle of confidence from 9 to 5.5° (Tables 2 and 3).

7. Discussion.

The above analysis and results point to the possibility of correcting TRM deviations induced by the anisotropy of magnetic susceptibility. In the granite of Flamanville, this improved the quality of palaeofield direction determination. However, two main points need to be discussed.

First, it is obvious that the formation mean directions themselves, (Tables 2 and 3) do not differ significantly . This means that in this particular case, the overall mean TRM direction is quite a good estimation of the magnetic field direction and therefore, the usefulness of the correction could appear questionable. In fact, this situation arises from the variations of the anisotropy directions around the granite body that make the deflections of TRM symmetric around the true magnetic field direction. The schematic Fig.9 is particularly illustrative of this phenomenon. Furthermore, it is clear that this situation is rather exceptional and that a constant direction of anisotropy plane should, in the general case, induce a systematic deflection of a rock formation mean magnetization and therefore, spurious results in the determination of the paleofield direction. A limited sampling area in the granite of Flamanville, for example near sites A and B or site C, would have produced the same kind of error.

A second and more important point rests on the examination of the final distribution of palaeofield estimations. Although the data are clustered by the correction, a slight scatter in declination remains (Fig.10b). If this scatter is considered as significant, two different causes can be conceived : (a) The first one could be an underestimation of the TRM anisotropy eigenvalue ratios M_1/M_2 and M_2/M_3, which would lead to an undercorrection of TRM deviations. As a matter of fact, the evaluation of the ratios M_1/M_2 and M_2/M_3 is based upon the assumption of a temperature independence of the principal susceptibility ratios k_1/k_2 and k_2/k_3 (Cogné 1987). The thermal dependence of these ratios was envisaged theoretically, but the thermal increase of the intrinsic susceptibility x_0 by a factor 100 was found to be accompanied by an increase of only a few percent of the apparent susceptibility ratios. This actually leads to a slight underestimation of M_1/M_2 and M_2/M_3 derived from the room temperature k_1/k_2 and k_2/k_3. However, this slight difference is not thought to be of real significance with respect to other sources of dispersion in susceptibility measurements, remanent magnetization measurements etc... (b) A second mechanism which could explain the remaining dispersion, is that of a deformation of the granite at temperatures lower than the blocking temperature of remanence. For all the above analysis, it has been assumed that the TRM was imprinted on the anisotropic material, after the end of plastic deformation processes. Although this hypothesis, which is quite difficult to verify, is well supported by the results of the present study, the possibility of strain occuring below the 500°C temperature range of TRM acquisition cannot be excluded. Such a sub-blocking temperature deformation should probably result in an increase of TRM deviations towards the foliation plane, as has been shown for CRM in deformed redbeds (Cogné & Perroud 1985), or for TRM in rhyolitic tuffs (Rosenbaum 1986). The proposed correction would therefore be unable to remove that part of deviation associated with strain acting after TRM acquisition. However, there is no tectonic event postdating Carboniferous

intrusion of the granite of Flamanville, and some structural features such as high temperature radial joints (i.e. perpendicular to the foliation planes), or the lack of crystallographic fabric in quartz (D. Gapais, pers. comm.) support the hypothesis that the most significant part of plastic strain associated with its emplacement occured at high temperatures, probably well above the Curie point of magnetite. It seems therefore that if a sub-blocking temperature strain exists, it is of minor importance.

With the evidence to hand, it is not possible to state categorically what is responsible for the dispersion of the magnetic field direction estimations that remains after the applied correction. Nevertheless this dispersion appears minor with respect to the initial dispersion of TRM mean site directions. Therefore TRM deviations are considered to be conveniently accounted for, and the quadratic relationship between TRM anisotropy eigenvalue ratios and principal susceptibility ratios provides a satisfactory method for removing them.

In conclusion this study has shown that (a) TRM acquired by anisotropic rocks can be significantly deviated by AMS from the magnetic field direction, in this case towards the k_1k_2 magnetic foliation plane. It is therefore important to check for the anisotropy of magnetic susceptibility when carrying out palaeomagnetic studies on rock units within deformed regions of orogenic belts. (b) If magnetic carriers of remanence are predominantly multidomain magnetite, the measurement of AMS allows a rapid estimate of the TRM anisotropy tensor. This provides an easy way to correct for TRM deviations and allows an unbiased magnetic field direction estimation from such deviated TRM's. If verified on other examples of anisotropic rock units, such results should allow us to extend the field of palaeomagnetic investigations within deformed regions of orogenic belts.

Acknowledgements: this work was supported by French Institut National des Sciences de l'Univers (INSU). This is a contribution of L.P. CNRS n° 4661.

Site	N	Bulk	k1			k2			k3			%An
		x10^{-2} SI	Int.	D/I(°)	a/b(°)	Int.	D/I(°)	a/b(°)	Int.	D/I(°)	a/b(°)	
A	7	0.521±0.200	1.115±0.020	65.5/14.0	4/4	1.035±0.004	207.0/72.0	6/3	0.849±0.018	333.0/11.0	5/4	31.0
B	4	0.671±0.300	1.099±0.022	243.0/ 4.0	29/8	1.019±0.008	136.0/76.5	25/7	0.882±0.026	334.5/13.0	19/5	24.5
C	11	0.636±0.090	1.083±0.010	10.0/33.0	6/3	1.016±0.008	172.0/56.0	6/3	0.901±0.008	274.5/ 8.0	3/2	20.0
D	8	0.605±0.207	1.072±0.025	2.5/34.0	17/10	1.032±0.007	167.0/55.0	17/8	0.896±0.026	267.5/ 7.5	13/3	19.5
E	10	0.758±0.096	1.088±0.023	357.0/38.0	7/4	1.019±0.010	157.0/50.5	8/5	0.892±0.019	259.5/10.0	7/2	22.0
F	10	0.459±0.095	1.077±0.016	340.5/45.0	5/5	1.017±0.005	131.5/41.0	6/4	0.906±0.018	235.0/15.0	6/3	19.0
G	14	0.544±0.112	1.061±0.009	342.0/35.0	9/3	1.019±0.006	126.0/49.0	10/3	0.920±0.008	239.0/18.5	8/3	15.0
I	9	0.571±0.150	1.088±0.006	297.0/54.0	10/4	1.046±0.010	102.0/35.0	10/5	0.865±0.011	197.0/ 7.0	5/4	26.0

Table 1. Normalized site mean susceptibilities in the granite of Flamanville. Each principal susceptibility is given with its standard deviation (σ), and the semi-angles (a and b) of the 95% confidence ellipse (after Jelinek, 1978). D/I state for declination/ inclination. Anisotropy percentage is defined as %An=(k1/k3-1)x100%. Bulk susceptibility is (k1+k2+k3)/3, where ki are the principal susceptibilities of the unnormalized mean tensor of each site.

Site	n/N	De	I	k	α_{95}
A	11/11	221.0	15.0	70	5.5
B	4/9	225.5	16.0	112	8.5
C	6/14	190.0	7.5	164	5.5
D	8/13	198.0	25.0	86	6.0
E	9/14	200.5	17.0	86	5.5
F	9/13	201.0	19.0	77	6.0
H	11/12	198.0	19.0	196	3.0
I	11/13	199.5	19.0	111	4.5
Mean	8	204.0	17.5	42	9.0

Table 2. Site mean Characteristic Remanent Magnetization directions in the Flamanville granite. n/N: number of entries in the statistics/ number of demagnetized specimens; De: declination, I: inclination, k, α_{95}: parameters of the Fisher (1953) statistics.

Site	M_1	M_2	M_3	Field direction	
				De	I
A	1.263	1.087	0.729	210.0	15.0
B	1.257	1.072	0.742	214.0	15.5
C	1.180	1.038	0.816	192.0	11.5
D	1.172	1.070	0.798	205.5	26.0
E	1.195	1.045	0.800	209.5	19.5
F	1.169	1.040	0.822	208.0	20.0
H	1.147	1.094	0.797	201.0	19.0
I	1.198	1.107	0.754	198.0	14.5
Mean N=8	De=205.0	I=18.0	k=95	α_{95}=5.5	

Table 3. M_1, M_2, M_3 are the eigenvalues of the TRM anisotropy tensor, calculated from $M_1/M_2=(k_1/k_2)^2$, $M_2/M_3=(k_2/k_3)^2$ and $M_1M_2M_3=1$. The field directions are estimated from TRM directions of Table 2, through the inverse TRM anisotropy tensor; they are given as De: declination, I: inclination. The formation mean fied direction is given with the k and α_{95} Fisher (1953) statistics parameters.

References.

Brun, J.P., 1981. Instabilités gravitaires et déformation de la croute continentale. Application au développement des domes et des plutons, thèse, Rennes, 197pp.

Cogné, J.P., 1987. TRM deviations in anisotropic assemblages of multidomain magnetite, submitted to Geophys. J. R. astr., Soc.

Cogné, J.P. & Perroud H., 1985. Strain removal applied to paleomagnetic directions in an orogenic belt : the Permian red slates of the Alpes Maritimes, France, Earth Planet. Sci. Lett., 72, 125-140.

Cogné, J.P., Perroud, H., Texier, M.P. & Bonhommet, N. 1986. Strain reorientation of hematite and its bearing upon remanent magnetization, Tectonics, 5, 5, 753-767.

Cogné, J.P. & Perroud, H., 1987. Anisotropy of magnetic susceptibility as a strain gauge in the Flamanville granite, Phys. Earth planet. Int., in press.

Dunlop, D.J., 1972. Magnetic mineralogy of unheated and heated red sediments by coercivity spectrum analysis, Geophys. J. R. astr. Soc., 27, 37-55.

Fisher, R.A., 1953. Dispersion on a sphere, Proc. Roy. Soc. London, A 217, 295-305.

Flinn, D., 1965. On the symmetry principle and the deformation ellipsoid, Geol. Mag., 102, 36-45.

Fuller, M.D., 1963. Magnetic anisotropy and palaeomagnetism, J. geophys. Res., 68, 293-309.

Hext, G.R., 1963. The estimation of second-order tensors with related tests and designs, Biometrika, 50, 353-373.

Jelinek, V., 1978. Statistical processing of anisotropy of magnetic susceptibility measured on groups of specimens, Studia Geoph. et Geod., 22, 50-62.

Kligfield, R. & Channel, J.E.T., 1981. Widespread remagnetization of Helvetic limestones, J. geophys. Res., 86, 1888-1900.

Ledru, P. & Brun, J.P., 1977. Utilisation des fronts et des trajectoires de schistosité dans l'étude des relations entre tectonique et intrusion granitique : exemple du granite de Flamanville (Manche), C. R. Acad. Sci. Paris, 285, Sér. D, 1199-1202.

Martin, N.R., 1953. The structure of the granite massif of Flamanville, Manche, North-West France, Quarterly J. geol. Soc. of London, 432, CVIII, 4, 311-341.

Nagata, T., 1961. Rock magnetism, Maruzen, Tokyo, 350pp.

Noltimier, H.C., 1971. Determining magnetic anisotropy of rocks with a spinner magnetometer giving in-phase and quadrature data output, J. geophys. Res., 76, 4849-4854.

O'Reilly, W., 1984. Rock and mineral magnetism, Chapman & Hall, New-York, 220pp.

Perroud, H., 1985. Synthèse des résultats paléomagnétiques sur le Massif Armoricain, Hercynica, I, 1, 65-71.

Ramsay, J.G., 1967. Folding and fracturing of rocks, Mc Graw-Hill, New-York, 568pp.

Rosenbaum, J.G., 1986. Paleomagnetic directional dispersion produced by plastic deformation in a thick Miocene welded tuff Southern Nevada : implications for welding temperatures, J. geophys. Res., 91, 12,817-12,834.

Schmidt, P.W. & Clark, D.A., 1985. Step-wise and continuous thermal demagnetization and theories of thermoremanence, Geophys. J. R. astr. Soc., 83, 731-751.

Senanayake, W.E. & MacElhinny, M.W., 1981. Hysteresis and susceptibility characteristics of magnetites and titanomagnetites: interpretation of results from basaltic rocks, Phys. Earth planet. Int., 26, 47-55.

Senanayake, W.E. & MacElhinny, M.W., 1982. The effects of heating on low-temperature and hysteresis properties of basalts, Phys. Earth planet. Int., 30, 317-321.

Stacey, F.D. & Banerjee, S.K., 1974. The physical principles of rock magnetism, Elsevier, Amsterdam, 195 pp.

Stephenson, A., Sadikun, S. & Potter, D.K., 1986. A theoretical and experimental comparison of the anisotropies of magnetic susceptibility and remanence in rocks and minerals, Geophys. J. R. astr. Soc., 84, 185-200.

Thellier, E. & Thellier, O., 1959. Sur l'intentisté du champ magnétique terrestre dans le passé historique et géologique, Ann. Géophys., 15, 3, 285-376.

Uyeda, S., Fuller, M.D., Belshé, J.C. & Girdler, R.W., 1963. Anisotropy of magnetic susceptibility of rocks and minerals, J. geophys. Res., 68, 279-291.

Van Der Voo, R. & Klootwijk, C.T., 1972. Paleomagnetic reconnaissance study of the Flamanville granite with a special reference to the anisotropy of its susceptibility, Geol. en Mijn., 51, 609-617.

Van der Voo, R. & Channel, J.E.T., 1980. Paleomagnetism in orogenic belts, Rev. Geophys. Space Phys., 18, 2, 455-481.

Vidal, P., 1980. L'évolution polyorogénique du Massif Armoricain : apport de la géochronologie et de la géochimie isotopique du Strontium, Mém. Soc. Géol. Minéral. Bretagne, 21, 162pp.

Zijderveld, J.D.A., 1967. AC demagnetization of rocks : analysis of results, in : Methods in Palaeomagnetism, pp. 254-287, eds Collinson, D.W., Creer, K.M. & Runcorn, S.K., Elsevier, New-York.

ANNEXE 4.

J.P. COGNE. **Experimental and numerical modeling of IRM rotation in deformed synthetic samples.** Accepté à Earth Planet. Sci. Lett.

EXPERIMENTAL AND NUMERICAL MODELING OF IRM ROTATION IN DEFORMED SYNTHETIC SAMPLES.

J.P. COGNE. C.A.E.S.S. Laboratoire de Géophysique Interne, Campus de Beaulieu, 35042 Rennes Cédex

Summary

The effect of strain upon isothermal remanent magnetization (IRM) carried by hematite particles embedded in a plasticine matrix has been investigated. Magnetized artificial hand samples were deformed by simple coaxial shortening. After deformation, the hand-samples were cut into 8-15 specimens and each specimen's IRM measured. Hence a mean IRM direction was obtained for each shortening step. The main results are: (1) When the initial direction of IRM is parallel to the shortening axis (λ_3) the hand-sample mean IRM stays parallel to λ_3 during deformation. However, individual magnetization directions are deflected towards the flattening plane, and thus the specimen directions are scattered by strain. This is accompanied by a significant decrease of magnetization intensity. (2) In contrast, when the initial direction of IRM is perpendicular to λ_3, the shortening results in a clustering of specimen magnetization directions, the mean direction being unchanged. This is accompanied by a slight increase of magnetization intensity. (3) In all other cases, where initial IRM direction makes an intermediate angle with shortening direction, deformation induces a deviation of each specimen IRM toward the flattening plane. This results in an overall deflection of hand-sample mean IRM. The amount of rotation increases with strain intensity. Changes of grouping and intensity depend on the initial angle between IRM and λ_3, defining a continuum in behavior between IRM directions being either parallel to λ_3 or perpendicular to λ_3. Finally, it is shown that all the experimental changes in IRM due to deformation (direction, grouping, intensity) can be modeled by a passive marker rotation of hematite planar particles.

1. Introduction.

Folding of rock units is important in paleomagnetism because it causes a primary natural remanent magnetization (NRM) to be deflected away from its original direction. Up to now, unfolding methods have mainly relied on (bedding) tilt corrections (rotation of a layer to the horizontal about its strike line). Through comparison of data from sites with various bedding attitudes, this allows a test of the age of magnetization. This test, proposed by Graham [1], has recently been improved, to take into account more complex fold geometries (plunging fold axes, superimposed folds, etc..) that are common within orogenic belts [2,4]. Application of these methods is reasonable if it can be assumed that the rock unit under consideration has been tilted by a sequence of rigid-body rotations, without any change of magnetization direction in the bedding reference frame. Internally deformed (strained) rocks have usually been avoided in paleomagnetism, because strain-induced particle rotations, amongst other mechanisms, are suspected to perturb the direction of magnetization [5,9].Moreover, some recent works have shown that strain -induced rotations of magnetization could lead to wrong interpretations of the fold test [10,12]. However, the effects of strain upon

remanent magnetization are poorly understood and so it would be useful to describe them. To this purpose, we recently studied the paleomagnetism of deformed Permian redbeds in the Alpes-Maritimes (France) [13]. The sense and amount of deviations of pretectonic paleomagnetic vector were found to be coherent with respect to strain directions and intensities. Using X-ray texture goniometry, these deviations were shown to be controlled by strain-induced progressive reorientations of hematite particles [14]. By using computer models of strain- induced passive rotation [15] of hematite platy minerals, we have shown that such a mechanism accounts for both magnetization deviations and hematite texture development in the Alpes- Maritimes redbeds [16].

Very few results of experimental shortening of magnetized bodies have yet been published. Kodama and Cox [17] studied the effect of constant volume deformation upon the IRM carried by magnetite needles embedded in a kaolinite matrix. However, the deformation was achieved by a discontinuous mechanism at the sample scale, with rigid blocks translating along conjugate sets of faults. This resulted in a decrease of IRM intensity, due to the loss of magnetic fractions involved in the fault zones, without any change in overall IRM direction. In contrast, Ozima [18] studied plastically deforming discs of magnetized Cu-Co alloy. He observed a significant deviation of IRM, which was interpreted as resulting from the rotation of Co ellipsoidal particles. Recently, Anson and Kodama [19] observed a shallowing of magnetization during compaction of synthetic sediments comprised of kaolinite and either equidimensional or acicular magnetite. They show that electrostatic forces induce a clumping of magnetite grains along the clay grains and that magnetization rotation is thus controlled by the reorientation of clay grains during compaction. Morash and Bonhommet [20] reported some preliminary results of experimental shortening of hematite-bearing Plasticine samples, showing that IRM systematically deviates towards the flattening plane. We decided to extend and complete these experiments, in order to describe some characterisric effects of strain- induced rotation of magnetic particles upon remanent magnetization, within a continuously deforming medium.

2. The model.

A non-magnetic modelling paste (violet Plasticine manufactured by Harbutt Ltd, England) was chosen as the model matrix, and hematite as the magnetic carrier. Hematite particles are platelets about 50 μm large, with a shape ratio (basal plane normal: basal plane length) of 1:20 to 1:30. Such a model material allowed us (a) to work with simple experimental conditions, at room temperatures and pressures and under low stresses ; (b) to obtain a continuous deformation at the sample scale, that is, to avoid fault formation within the samples ; (c) to homogeneously disperse the magnetic particles within the matrix.

The artificial samples were made of Plasticine + 5% in weight of hematite powder. The samples were given a saturation IRM (typical intensity of 10 Am^{-1}) in a field of 1 T. The deformation was performed with a simple coaxial press made of a single screw-jack and two plexiglas plates. The sample was placed between the plates, without confining pressure. As the jack advances, the sample is shortened in one direction and allowed to stretch perpendicular to the shortening direction, i.e.deformation is an axisymmetric, coaxial shortening. In order to facilitate the extension and avoid barrelling, the contact surfaces between the sample and the plates were lubricated. The

continuity and homogeneity of strain was checked by tracing a pattern of square markers on the sample faces and observing their change during shortening. Strain was observed to be homogeneous up to 50% shortening, but experiments were continued until 70% shortening, assuming that any cracks that appear above 50% shortening are concentrated at the boundaries. The results obtained corroborate this assumption.

The results presented here were obtained from two sets of experiments. In the first set, the sequence of operations was as follows :

1. Hematite particles were uniformly dispersed within a hand sample of Plasticine (about 150 cm^3). This sample was then cut to form a parallelepiped.

2. IRM was acquired in a known direction in the sample. In order to simplify the description of the results, the terms declination, inclination, horizontal and vertical directions will be assumed to be relative to the sample reference frame.

3. The sample was vertically shortened up to a given percentage, computed as $(l_o-l_f)/l_o x100$, where l_o (l_f) is the initial (final) length of the sample in the shortening direction.

4. Each hand sample was cut into 8-15 cubes about 15mm on a side. The magnetization directions and intensities of the cubes were measured. The IRM direction after deformation is calculated by a Fisher [21] mean of the cube magnetizations measured from one hand sample.

The result of such a sequence is a hand sample mean IRM direction which was acquired in a given field direction, and subjected to an amount of shortening. The sequence is repeated from (1) to (4) with a fixed initial field direction, and progressively increasing shortening steps. This has been repeated with four different field directions with initial inclinations, I_o, of 0^o, 30^o, 60^o and 85^o, and null declination. Since the IRM is acquired by initially isotropic samples, this set is named "initially isotropic".

In the second set of experiments, the sequences of operations was as follows :

1. An isotropic hand-sample was made.

2. Deformation of this sample by a 30% vertical shortening.

3. IRM acquisition by the anisotropic sample.

4. Horizontal shortening in the direction of the magnetic field declination.

5. Cutting the hand-sample in specimens and measuring the N specimen magnetizations.

As in the first set of experiments, this sequence was repeated for one given field direction, with increasing amounts of shortening. This was performed with four field directions (inclinations, I_H, of 0^o, 40^o, 70^o and 90^o, and null declinations). This set of experiments is referred to as the "initially 30% compacted" set.

Finally, these results are compared to the results obtained by numerical simulation of these sequences. The numerical simulation has already been described and discussed by Cogné et al. [16]. Briefly, N (1000) planar particles are assumed to follow a model of passive planes [15,22]. Each particle bears a micromoment with an orientation and intensity which depend on the field direction with respect to the particle reference frame through a magnetic anisotropy tensor (oblate with kmax/kmin = 100 and kmax = kint plane within the basal particle plane); the resultant magnetization (direction, intensity, clustering) is computed by vectorial sum of the N

micromoments. A magnetization can be given to the initially isotropic population, or after an initial shortening, and the population can then be deformed with various homogeneous strain tensors. During deformation, the micromoments rotate with the grain, without changing their coordinates in the particle frame. After each deformation sequence, the resultant magnetization can be computed. This allows us to simulate the experimental modelling sequences.

3. Results.

3.1. Samples initially isotropic.

The IRM acquired by isotropic samples is parallel to the applied field (Fig.1). During progressive vertical shortening (up to 70%). The initially horizontal (I_o=0°) IRM stays horizontal (Fig.1). Intermediate initial inclinations (I_o=30° and I_o=60°) show a significant progressive shallowing, that is, a rotation away from the shortening axis. The fluctuations in declination are not thought to be significant, they are most probably caused by the initial experimental uncertainties, since the experimental procedure was designed to have a good control of orientations with respect to the horizontal plane and not the vertical plane. The initially steeply-inclined direction (I_o=85°) does not show any significant deviation, except in the highest shortening steps (70%). A more detailed and complete comparison of IRM and shortening amount and direction is shown in Fig.2a. Since the applied strain is axisymmetric, the change in IRM direction is represented in two dimensions, with inclination as a function of percentage of shortening. The experimental points are compared with the curves obtained numerically (solid lines). It is obvious that rotation of IRM increases progressively with strain intensity for the intermediate initial inclinations (I_o=30° and 60°), and that the observed IRM behavior closely follows the predicted one. There is a clear difference in the size of the α_{95} circles of confidence (drawn as error bars in Fig.2a) between the results for IRM directions initially inclined at 0° (perpendicular to λ_3, the shortening axis) or 85°(subparallel to λ_3). This shows that the deformation tends to cluster the data when magnetization is perpendicular to the shortening direction, whereas it tends to scatter them when the initial magnetization direction is parallel (or close) to the shortening direction. Between these extreme angular relationships, the changes in IRM clustering are less clear. However, the data for an initial inclination of 60°,(closer to λ_3), are more scattered than the data for an IRM initially inclined at 30°.

According to the model of platelet rotations during shortening, and because the easy magnetization direction is within the basal plane of hematite, the clustering or scattering effect of strain on measured remanent magnetization directions of the artificial samples can be explained as a result of a clustering or scattering of hematite particles that carry the most significant part of IRM. If verified, such a mechanism should induce variations not only of the grouping of specimen IRM's, but also of IRM intensities. In order to smooth the intensity variations between the measured specimens of given deformed hand-samples, the total magnetic moment M of each hand-sample has been calculated as the vector sum of the N measured specimen IRMs, and then reduced to magnetic intensity per unit volume. The initial IRM intensity, Mo, by which the intensities M are normalized, has been obtained by averaging the intensity of the 4 initially isotropic samples. The changes of M/Mo with vertical shortening for various initial inclinations are shown

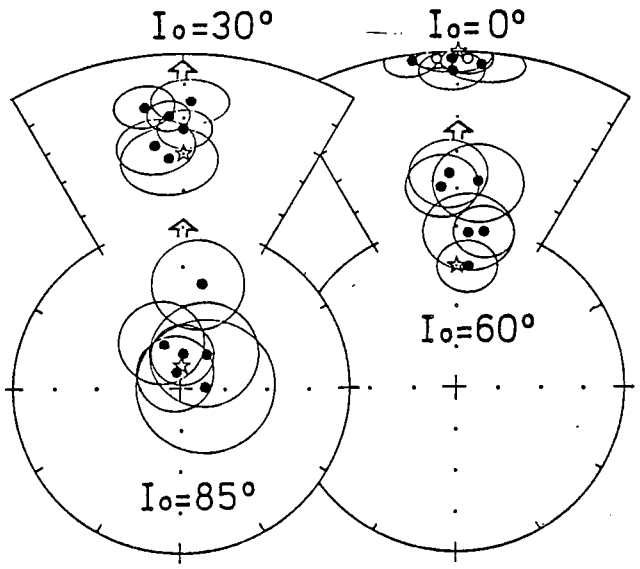

Fig.1: Initially isotropic set. Equal area projections of mean IRM direction evolution (open arrows) with increasing vertical shortening; stars: applied field= IRM initial directions.

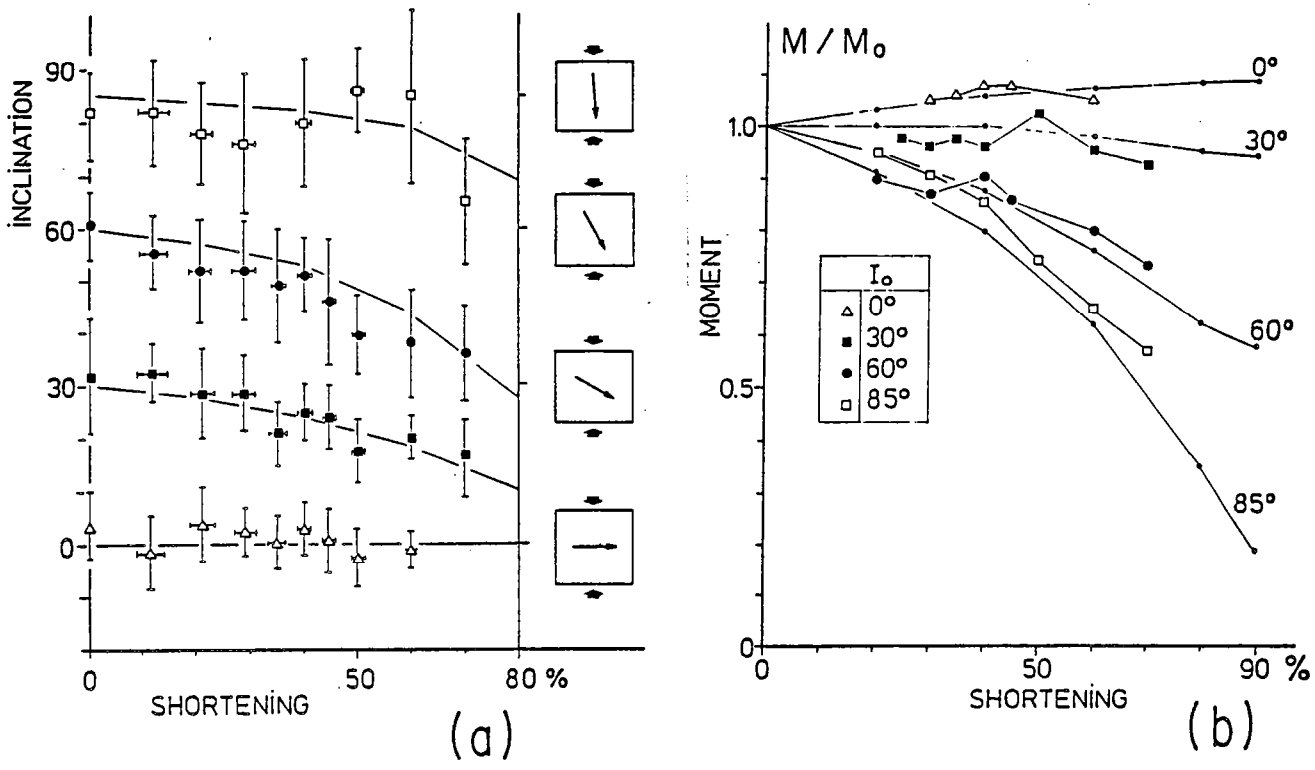

Fig.2: Initially isotropic set.(a): IRM inclination vs. vertical shortening percentage; the column at right illustrates the angular relations between the shortening direction (large arrow) and the initial IRM direction (long arrow). (b):normalized IRM intensity vs. shortening percentage; thin curves and little dots: numerical simulation results.

in Fig.2b. As expected, IRM intensity significantly decreases with increasing strain, when initial directions of magnetization and shortening are close to each other (I_o=60° and 85°); for I_o=0°, the shortening results in a slight increase of IRM intensity. Here too, the experimental points closely follow the numerical curves.

3.2. Samples Initially 30% compacted.

When the magnetic field is applied parallel (I_H=0°) or normal (I_H=90°) to the initial fabric plane (taken as the horizontal reference) IRM is acquired parallel to the field (Fig.3). In the intermediate field inclinations, the magnetization is significantly shallowed towards the initial fabric plane : for I_H=40°, I_{IRM}=25°, for I_H=70°, I_{IRM}=60°. Horizontal shortening results in a behavior of IRM similar to that of the previous set of samples. When the initial IRM direction is parallel to one of the deformation axes (I=0° parallel to λ_3, I=90° parallel to $\lambda_1 = \lambda_2$), the mean direction is not deviated. However, while the initial IRM directions parallel to λ_3 (I= 0°) are scattered by strain, IRM perpendicular to λ_3 (I=90°) are clustered by strain. Applying a progressive horizontal shortening in the direction of IRM declination to the intermediately inclined magnetizations induces a deviation of the mean IRM towards the incremental flattening plane. This results in an increase in inclination while the declination remains stable. The size of the α_{95} circles of confidence depends on the initial angle between IRM and λ_3. The magnetization acquired in I_H=40°, which is closer to λ_3 than a magnetization acquired in I_H=70°, has on the average greater dispersions.

Although the main characteristics of IRM behavior in this set of experiments appear to be similar to the initially isotropic one, some slight differences are apparent. First, the dispersion in declination of the intermediate inclinations seems to be less important than in the previous case. A possible reason for this could be that the initial fabric of the samples, which induces an initial preferred orientation of hematite platelets, causes the IRM acquisition to be more accurate and homogeneous. Secondly, the deviation of IRM acquired in the 40° inclined field (I_{IRM}=25°) appears to be greater than the similar curve of the initially isotropic set (I_o=60° of Fig.2a). The initial preferred orientation of hematite is thought to be responsible for an increase of the deformation effects upon the remanent magnetization.

4. Interpretation and conclusions.

The comparison with the numerically simulated effects of strain-induced passive rotations of hematite platelets, shows that such a mechanism conveniently accounts for the results obtained from the sets of experiments on artificial samples. In order to explain the various effects of this single mechanism upon measurable magnetization directions, intensities, and clustering at the hand-sample scale, we can propose the following interpretation. The high magnetocrystalline anisotropy of hematite creates an easy magnetization direction within its basal plane, and a very hard magnetization direction parallel to its normal (typical k_{max}/k_{min} in the range of 100 ; [23]). The most significant part of magnetization will therefore be the vector sum of particle micromoments of hematites which have their basal plane near the magnetic field direction, and the contribution of hematites having their basal plane normal to the field will be negligible.

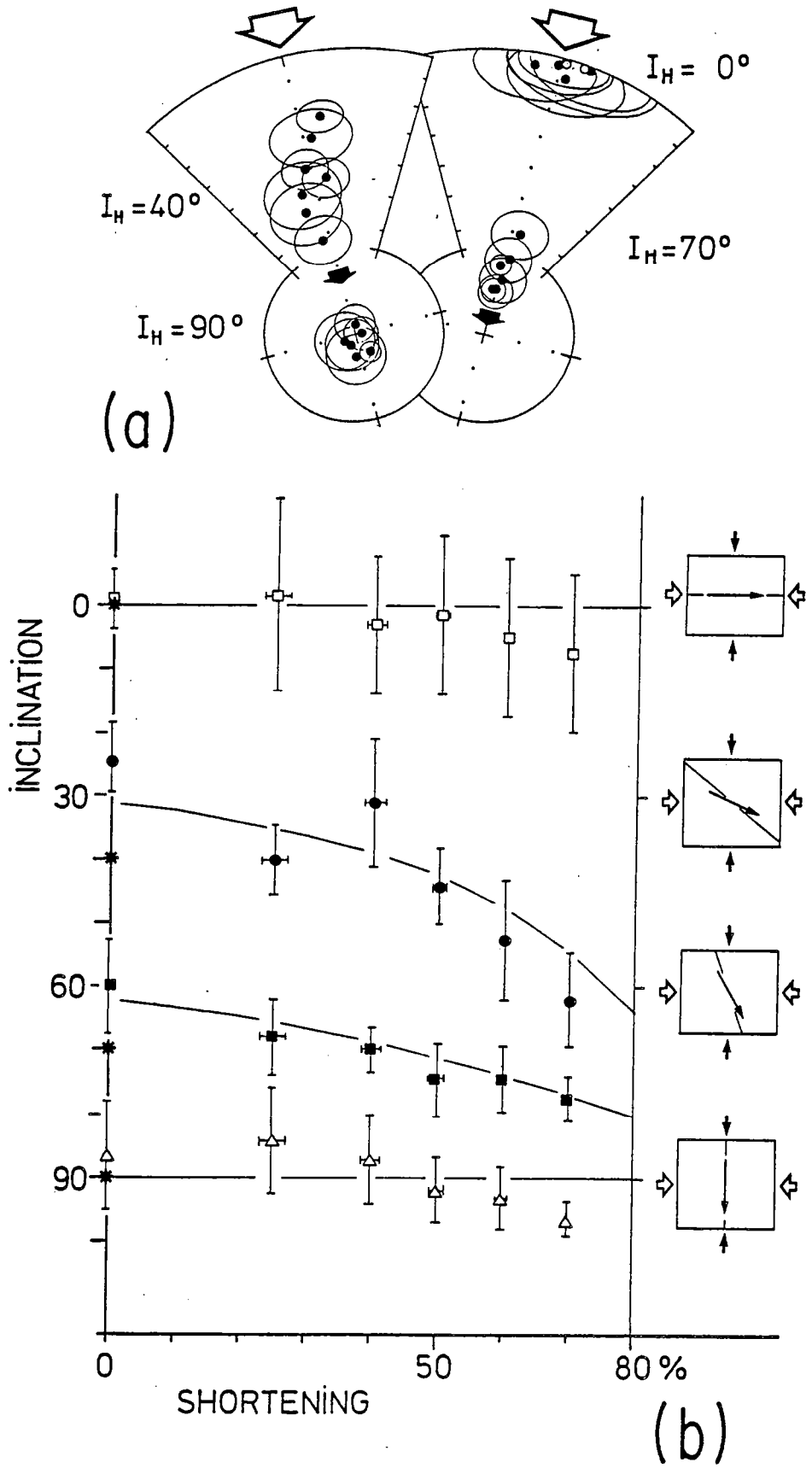

Fig.3: Initially 30% compacted set. (a): same as in Fig.1; in this case, the horizontal shortening (large open arrows) induces an increase in inclination (little closed arrows). (b): same as in Fig.2a; scale of inclinations has been inverted for comparison with Fig.2a; asterisks are the field directions; squares in the right column are an illustration of relationships between pre-IRM compaction (little arrows), field (thin lines), IRM (long arrows) and shortening (large open arrows) directions.

Then, the rotation of hematite platelets induced by strain, causes a rotation of these micromoments which in turn control the behavior of the net measurable resultant magnetization. This produces the results we described above. (a) When the shortening direction is perpendicular to the initial direction of magnetization (I_0=0° in Fig.2; I_0=90° in Fig.3) that part of hematite which carries the significant part of IRM is already oriented within the flattening plane, and thus micromoments are not deviated. Only these micromoments which have slight departure in a solid angle around the initial field direction are reoriented by a few degrees; this behavior produces the slight increase in magnetization intensity at the hand-sample scale, the clustering of measured specimen magnetizations, and the stability of mean magnetization direction during deformation. (b) In the other extreme case, the shortening is applied parallel to the initial IRM direction (I_0=0° in Fig.3), and thus, the involved hematite particles are initially at great angles from the flattening plane. Their rotation induces a rotation of micromoments more or less symmetrical around λ_3 and produces the observed decrease in intensity of IRM. At the measurable specimen scale, the IRM direction will generally be deflected towards the flattening plane in a random way, depending upon the amount of hematite having been rotated in a sense or another; however, a sufficient sampling of specimens should display an undeflected mean direction of magnetization at the hand-sample scale; this accounts for the undeflected mean IRM we observed at the hand-sample scale, together with the progressively increasing dispersion of individual measured IRM at the specimen scale. (c) In all the other cases of intermediate angles between λ_3 and initial IRM direction, the hematite particles involved in IRM undergo, on the average, an identical rotation. The more or less homogeneous rotation of micromoments thus results in a net rotation of resultant IRM towards the flattening plane. Note however that the closer the initial IRM inclination is to the direction of λ_3, the greater its dispersion and intensity decrease during strain.

In conclusion, the general effects of strain-induced hematite particle rotations upon remanent magnetization have been characterized. In natural rock units, if such a mechanism holds, we will observe the same kind of natural remanent magnetization behavior. This has been observed in the Alpes-Maritimes red beds [13] as well as with the preliminary results obtained from the Central Brittany red series [16]. In the present work,as well as in the cited ones, we have shown that a synthetic description of strain and magnetization relationships can be done. It is therefore inferred that removing strain from deviated remanent magnetizations should be possible, providing a detailed strain and magnetization interrelationships study is performed. This should allow the extension of paleomagnetic investigations towards the deformed external zones of orogenic belts, where metamorphism is of low grade.

Acknowledgements.

Preliminary investigations and results of colleague A. Morash helped the realization of the present experiments. P. Cobbold provided helpful comments on the conception of the model as well as on an early draft of this paper. This is a contribution of CAESS (L.P. CNRS n° 4661)

REFERENCES.

1 J.W. Graham, The stability and significance of magnetism in sedimentary rocks, J. Geophys. Res. 54, 131-167, 1949.

2 W.D. Mc Donald, Net tectonic rotation, apparent tectonic rotation and the structural tilt correction in paleomagnetic studies, J. Geophys. Res. 85, 3659-3669, 1980.

3 H. Perroud and P. R. Cobbold, L'aimantation rémanente comme marqueur de la déformation :Exemple d'un pli à axe incliné dans les séries rouges siluro dévoniennes à Cabrillanes, Asturies, Bull. Soc. Géol. France 26, 1, 169-184, 1984.

4 N. Bonhommet, P. R. Cobbold, H. Perroud, and H. Richardson, Paleomagnetism and cross-folding in a key area of the Asturian arc (Spain), J. Geophys. Res. 86, 1873-1887, 1981.

5 C. Van den Ende, Palaeomagnetism of Permian red beds of the Dome de Barrot (S. France), Thesis, 171 pp., Utrecht, 1977.

6 R. Kligfield, W. H. Owens, and W. Lowrie, Magnetic susceptibility anisotropy, strain, and progressive deformation in permian sediments from the Maritim Alps (France), Earth Planet. Sci. Lett. 55, 181-189, 1981.

7 H. Perroud, Relations paléomagnétisme et déformation: exemple de la région de Cabo de Penas (Espagne), C. R. Acad. Sci. Paris 294, 45-48, 1982.

8 R.A. Facer, Folding, strain and Graham's fold test in palaeomagnetic investigations, Geophys. J. R. Astr. Soc. 72, 165-171, 1983.

9 J.G. Rosenbaum, Paleomagnetic directionnal dispersion produced by plastic deformation in a thick Miocene welded tuff, southern Nevada: implications for welding temperatures, J. Geophys. Res. 91, 12817-12834, 1986.

10 K.P. Kodama, The effect of deformation on the fold test, Eos Trans. Amer. Geophys. Union, 268, 1986a

11 K.P. Kodama, Effect of flexural slip on Fisherian distributions: Implications for the fold test, Eos Trans. Amer. Geophys. Union, 67, 924, 1986b

12 B.A. Van der Pluijm, Grain-scale deformation and the fold test. Evaluation of syn-folding remagnetization, Geophys. R. Lett., 14, 155-157, 1987

13 J.P. Cogné and H. Perroud, Strain removal applied to paleomagnetic direction in an orogenic belt : the Permian red slates of the Alpes Maritimes, France, Earth Planet. Sci. Lett. 72, 125-140, 1985.

14 J.P. Cogné and D. Gapais, Passive rotation of hematite during deformation : a comparison of simulated and natural redbeds fabrics, Tectonophysics 121, 365-372, 1986.

15 A. March, Mathematische Theorie der Regelung nach der Korngestalt bei Affiner Deformation, Z. Krist. 81, 285-297, 1932.

16 J.P. Cogné, H. Perroud, M. P. Texier, and N. Bonhommet, Strain reorientation of hematite and its bearing upon remanent magnetization, Tectonics 5, 753-767, 1986.

17 K.P. Kodama and A. Cox, The effects of constant volume deformation on the magnetization of an artificial sediment, Earth Planet. Sci. Lett. 38, 436-442, 1978.

18 M. Ozima, Effects of a plastic deformation on the remanent magnetization of Cu-Co alloy, Earth and Planet. Sci. Lett., 47, 121-123, 1980.

19 G.L. Anson and K.P. Kodama, Compaction-induced inclination shallowing of the post- depositional remanent magnetization in a synthetic sediment, Geophys. J. R. astron. Soc., 88, 673-692, 1987.

20 A. Morash and N. Bonhommet, Deviation of I.R.M. during simple shortening experiments, Abstr. 4th IAGA Sci. Assem. Edinburgh, 113-12, 252, 1981.

21 R.A. Fisher, Dispersion on a sphere, Proc. R. Soc. London, Ser. A 217, 295-305, 1953.

22 W.H. Owens, Mathematical model studies on factors affecting the magnetic anisotropy of deformed rocks, Tectonophysics 24, 115-131, 1974.

23 S. Uyeda, M. D. Fuller, J. C. Belshé, and R. W. Girdler, Anisotropy of the magnetic susceptibility of rocks and minerals, J. Geophys. Res. 68, 279-292, 1963.

ANNEXE 5.

J.P. COGNE, H. PERROUD, M.P. TEXIER and N. BONHOMMET. **Strain reorientation of hematite and its bearing upon remanent magnetization.** Tectonics 5, 5, 753-767, 1986.

TECTONICS, VOL. 5, NO. 5, PAGES 753-767, SEPTEMBER 1986

STRAIN REORIENTATION OF HEMATITE AND ITS BEARING UPON REMANENT MAGNETIZATION

J. P. Cogné, H. Perroud, M. P. Texier and N. Bonhommet

CAESS, Laboratoire de Géophysique Interne, Université de Rennes 1, France

Abstract. Using a computer-based numerical model, we suggest that passive reorientation of hematite planar particles induced by strain perturb significantly the remanent magnetization carried by the hematite. The evolution of its direction and dispersion in a progressively increasing strain can be correlated with the evolution of passive lines. In real rocks, the amount of reorientation can be approched by measuring one of the three following tensors: strain tensor, orientation tensor of some hematite cristallographic axes, or magnetic susceptibility tensor. From examples taken in the Maritime Alps and in Brittany, we emphasize the possible correlations between these tensors (orientation of principal axes and axial ratios). Finally, we use our best estimate of strain to correct the paleomagnetic results by the strain removal technique we have already used in the Maritime Alps (Cogné and Perroud, 1985). When applied to the preliminary paleomagnetic results obtained from Ordovician deformed redbeds of Brittany, it allows to recover a conclusive primary magnetization direction, although the characteristic magnetizations appear post-folding with respect to the classical fold test.

Paper number 6T0090.
0278-7407/86/006T-0090$10.00

INTRODUCTION

Amongst ferric oxides, fine-grained hematite is one of the most common carriers of remanent magnetization. In red sediments, the coloration, which is associated with hematite, is generally believed to be secondary [Van Houten, 1973; Collinson, 1965], that is, post-depositional. The growth of hematitic minerals in an ambiant magnetic field leads to a chemical remanent magnetization and establishes the most significant part of the magnetic signal from redbeds. Its stability against demagnetizing factors (time, temperature, or magnetic fields) allows the magnetic record to remain stable for very long periods of time, and thus it is very valuable for paleomagnetic purposes. However, we have to consider the very strong shape anisotropy of tabular hematite, together with the alignment of the easy axis of magnetization in the basal plane. Therefore, the question arises of the paleomagnetic effect of any deformations the rock unit has undergone during its geological history, before or after the magnetization acquisition. In effect, how does strain affect the remanent magnetization? According to deformation theory, we should expect rotations of hematite grains induced by strain. Our point in this paper will be first to theoretically model this

problem, by the way of a computer-based simulation using the "passive deformation" concept of March [1932]. This will allow the fabric development of hematite to be simulated, together with its associated magnetization. Then we will try to compare these results with observations from red formations we have studied recently. In the Permian red beds from the Maritime Alps, an attempt will be made to correlate paleomagnetic vectors deviations, as described previously [Cogné and Perroud, 1985], with the strain-induced hematite fabrics estimated using X ray texture goniometry. In the last part, preliminary paleomagnetic results from the deformed Ordovician red beds of central Brittany are discussed. In that example, the anisotropy of the magnetic susceptibility was used to control the hematite preferred orientations. We will conclude by reviewing the possibilities and limitations of paleomagnetic results from red formations from orogenic belts.

THE MODEL

The aim of the computer model is to simulate the effects of hematite particles reorientation under strain, specifically (1) the distribution of these particles, estimated by the preferred orientations of some cristallographic axes and (2) the orientation of the magnetic micromoments and their resultant. The simulation is based upon the strain response of a finite number (< 1000) of planar particles. The initial conditions are the following:

1. Hematite grains are modelled as platelets, each being characterized by a cartesian frame where Z is the c axis and XY is the basal plane of hematite.

2. The initial coordinates of the Z axis of each particle in the reference frame of the system are generated by sampling random numbers from the random function of the calculator. The uniformity of the lines distribution derived from this sampling has been checked by calculating their orientation tensor. Several test runs did not show any systematic departure from an isotropic orientation tensor of the initial populations. The orientation of the particle X axis in the plane perpendicular to Z is generated in the same manner.

3. The grains are assumed to rotate without changing shape. The rotation of each grain follows the material lines and planes strain response model [March, 1932; Owens, 1973, 1974], by applying the strain tensor to X (material line) and the inverse strain tensor to Z (pole to material plane).

4. The strain is homogeneous over all the sample population.

5. All the directionnal features of the model (orientation of particle, magnetization, etc.) are referenced to an external coordinate system. To simplify the expression of the results, this reference frame will be considered as being the geographic system (north-east-vertical) allowing the use of terms such as horizontal/vertical directions, compaction, inclination, etc.

Hematite Fabric Simulations

In order to compare simulated with natural hematite fabrics, it has been necessary to compute the distribution of poles to {104} form. As a matter of fact, in hematite the {104} reflection has the maximum relative X ray diffracted intensity, and thus X ray texture goniometry measurements are more accurate and generally done on these planes [Siddans, 1980 ; Hrouda et al.,1985]. Cristallographic parameters of hematite show that the 6 poles to {104} lie on a cone of 38.84° half aperture angle, around the c axis. Therefore, for each particle of the simulation, six {104} poles were generated, the first in the XZ plane of the particle frame at an angle of 38.84° from Z, the five others by successive 60° rotations around Z.

For each state of incremental strain applied to the population, the simulated hematite fabric is specified by the calculation of the weighted orientation tensor (WOT) [Cobbold and Gapais, 1979] either for the c axes or for the poles to {104}. This tensor derives from the classical Scheidegger [1965] orientation tensor by weighting the direction cosines products and squares of each vector by the quadratic elongation of strain in this direction. If the WOT is computed on deformed populations of material lines having a uniform initial distribution in the unstrained state, its eigenvalues are the principal quadratic extensions and it is therefore equal to the strain tensor. This is obviously not the case for the {104} normals which are attached to material lines and planes but are not material lines themselves. Moreover, an isotropic orientation tensor (three equal eigen-

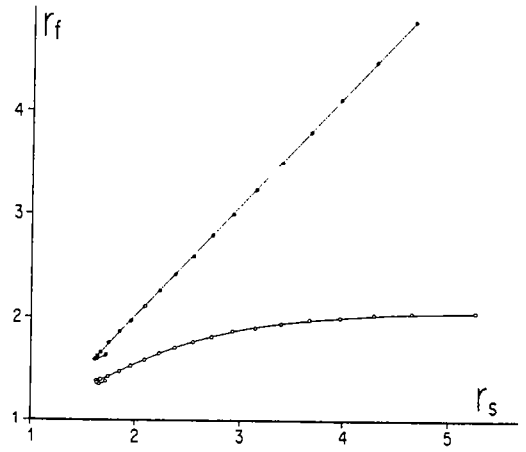

Fig. 1. Hematite texture development; curves of fabric intensity (rf) vs total strain intensity (rs) resulting from the strain simulation (see text). Closed symbols, c axes fabric; open symbols, {104} normals fabric.

values) is obtained from distribution of lines on a cone of about 57° half aperture angle [Woodcock, 1977]. From the conical position of {104} normals around the c axes, an alignment of hematite basal planes will result in a conical distribution of the axes with a half aperture angle of about 40°. This accounts for the low eigenvalues ratios reported below.

To illustrate the working of the simulation, the results from a sample run are detailed here. The choosen strain history is first a 30% compaction (30% shortening along the vertical axis of the reference frame), then followed by regular incremental strain steps. The incremental strain ellipsoid is oblate with an axial ratio $\lambda_1/\lambda_3 = \lambda_2/\lambda_3 = 1.1$ and the minimum elongation axis horizontal. This results in a progressive coaxial deformation which may be described by the classical path of the finite strain ellipsoid shape in a Flinn [1965] diagram (see, for examples Ramsay and Huber [1983, p. 186]; Graham [1978]) from an initially oblate ellipsoid towards the prolate shape then a return to the oblate field when the shortening increases. The reorientation of the simulated hematite platelets resulting from this history has been checked by computing the weighted orientation tensors of both c axes and {104}normals after each incremental strain step.

The relationships between these tensors and the total strain tensor at each step are illustrated in Figure 1 where intensity paramaters ($r = \lambda_1/\lambda_2 + \lambda_2/\lambda_3 - 1$; Watterson [1968]) of fabric (rf) is drawn as a function of strain intensity (rs). As expected from the WOT theory together with the material lines and planes strain response model and the uniform distribution of the initial population, the orientation tensor of the c axes distribution at the strained state is identical to the total strain tensor. This results in the equality of the intensities values rs and rf, obvious in Figure 1. The shape of the curve for the {104} normals is quite different. As noted above, no linear correlation exists between the two tensors, and eigenvalues ratios are lower than strain, leading to the shallow slope of the rf vs. rs curve in Figure 1. Nevertheless, the increase in the hematite reorientation results in a notable increase in the fabric intensity of {104} normals in the 1 to 5 strain intensity range. Thus, in natural rocks such a progressive reorientation, if present, should be detected.

Magnetization Behaviour Simulations

The model has been used to simulate magnetization deviations induced by the rotation of platelets bearing micromoments. For this simulation, the following conditions are assumed:

1. Each particle bears a micromoment having length and orientation determined by the coordinates of the "direction of applied field" in the particle frame through the classical magnetic susceptibility tensor.

2. This tensor may be described by a hard magnetization direction parallel to the Z axis of the particle frame and an isotropic susceptibility in the XY plane (i.e., the basal plane of the particle). The choosen susceptibility ratio is kmax/kmin=100, in the range of magnetocrystalline anisotropy of hematite [Uyeda et al., 1963].

3. Due to the low susceptibility of hematite, magnetic interactions between the grains are regarded as negligible [see Owens, 1974; Hrouda et al., 1985].

4. As in the material lines and planes strain response model, the particles are assumed not to change in shape and length, the micromoments are assumed to rotate with the grain without changing their coordinates in the particle frame. For the same reason, possible stress effects on

magnetic micromoment at the grain scale are not taken into account.

The resultant magnetization is calculated by the vector sum of all the micromoments of the population. To estimate the variations in the homogeneity of the magnetization within the population of grains during deformation it should have been possible to consider the variations in modulus of the resultant vector, considered as the remanence intensity. Nevertheless, Fisher [1953] statistics appear to be a more convenient tool to illustrate the simulated remanence deviations and cluster, because it can be more easily compared with the usual dispersion parameters of natural data distributions. It has been noted above that the initial population distribution tends to uniformity for a sufficiently high number of particles (1000). This may be not the case for more small populations of, for example, 100 particles where some random departure from homogeneity are observable. When applying a "magnetic field" this results in random slight deviations of the resultant magnetization from the field direction. Repeating the simulation on several such samples, one would expect to obtain a dispersion of sample resultants, but the overall mean direction should converge towards the applied field direction. In practice, the initial population of 1000 particles has been divided in 10 samples of 100 particles. Each sample provides a resultant by vector summation and at each strain step the Fisher statistics have been computed on the 10 sample resultants.

The simulated effects of passive rotation of planar particles under strain upon the magnetization directions and cluster have been investigated in the following conditions: successive coaxial increments of strain (same incremental strain as in the previous part, with an horizontal shortening axis) have been applied to both initially isotropic and anisotropic (30% compacted) populations. In both cases, the evolution of a magnetization acquired by the population prior to the deformation (after the compaction in the anisotropic case) has been studied for three different orientations of the magnetic field. The three field directions are : horizontal, with a direction parallel to the λ_3 shortening axis of incremental strain ; inclination of 30°, with a declination parallel to λ_3 ; vertical. Results of the magnetization simulation are as follows:

Horizontal field. When applying a horizontal field to the population, the resultant magnetization of the 1000 particles is parallel to the field direction in both isotropic and compacted populations. In the latter the distribution is slightly better clustered but not significantly. During the whole simulation of shortening parallel to the magnetization direction, the resultant direction remains unchanged. It is only the dispersion of the 10 sample magnetization directions that is affected. In a plot of the Fisherian k value, normalized to the initial ko value, as a function of total strain intensity rs (Figure 2), we observe a very rapid decay of k with increasing rs. This decay is in the range of 70% at the rather low strain intensity of 2. A further observation can be made on the initially compacted population (Figure 2). In this case, the superimposition of the horizontal shortening upon the initial compaction ellipsoid leads in the first stages to a decay in the total strain intensity. This gives the particular shape of the corresponding k/ko vs. rs curve, and it is very important to point out that a dramatic decay of almost 60% of the k value appears while strain intensity stays unchanged.

The third curve in Figure 2 is quite different in its principle. This curve, rearranged from the curves described in a previous analysis of paleomagnetic data dispersions in the Maritime Alps [Cogné and Perroud, 1985, Figure 8, p. 133] gives the evolution of the dispersion parameter (k) of a Fisherian population of passive vectors under a coaxial flattening strain, the shortening axis of which is in the direction of the population mean. The nearly complete superposition of this curve with the one resulting from the model, shows that the dispersion of sample magnetizations induced by planar particles reorientations in the conditions of simulation is similar to the dispersion of passive lines.

30° inclined field. Horizontal shortening in the direction of a 30° inclined magnetization has effects on both orientation and cluster of the magnetization resultants. The curves of k/ko vs. rs show a pattern similar to those of Figure 2 with a 60% decrease of k for rs= 2 and 80% for rs= 5. This means that even for angles of 30° between shortening axis and magnetization direction, the scattering effect of strain cannot be neglected. The

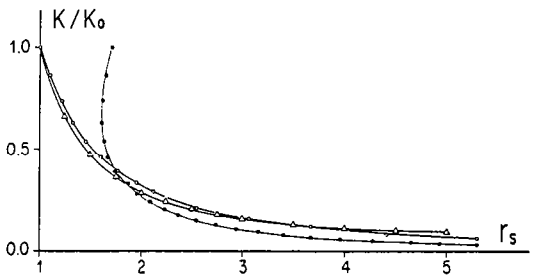

Fig. 2. Simulation of hematite magnetization deviations; evolution of the Fisherian dispersion parameter (k), normalized to its initial value (k0), vs. total strain intensity (rs). The shortening axis in this case is parallel to the initial resultant magnetization. Open circles, initially isotropic population; closed circles, initially 30% compacted population; open triangles, evolution of a Fisherian distribution of passive vectors in the same conditions.

second effect is an important deviation of the magnetization mean directions (Figure 3). This deviation from the initial direction becomes significant at the third increment in the initially isotropic population (Figure 3, left), i.e., for a strain intensity, rs= 1.33. In both the isotropic and anisotropic initial population the total deviation of the mean directions is in the range of 25°-30° for rs= 5.5. In the initially compacted population (Figure 3, right), the initial anisotropy leads to a shallowing of the magnetization direction away from the applied field, illustrating the well known shallowing effect of compaction. Then, superposition of strain leads to a total deviation of about 20° from the initial field direction for rs= 5.

Vertical field. Both isotropic and compacted populations were given a vertical magnetization. As expected, reorientation of particles under horizontal shortening does not produce any deviation of this magnetization. Evolution of the sample magnetization clustering, expressed by the curves k/ko vs. rs, show an important increase of k/ko during shortening (k/ko= 2.1- 2.2 for rs= 5). The significance of this increasing in natural rocks needs to be discussed. When working on undeformed, isotropic materials, measurements of magnetization leads to a mean direction which is characterized by a variance and a circle of confidence. These statistical parameters give the degree of accuracy in the estimation of the true paleomagnetic direction. This incertitude is always present and is due to all the experimental factors in the data acquisition procedure. Thus we may assume that intrinsic dispersion of magnetization within a sample is not detectable if it is lower than the experimental dispersion. Therefore, if in certain deformation conditions, strain induces an improvement in the micromoments alignment, this will certainly not be detectable due to the range of experimental error.

In summary, the results of the simulation described here show that in the case of a shortening direction close to the magnetic one, the passive rotation of planar particles results in a passive rotation of the micromoment resultants. This results in an increase in the dispersion of the resultants, but does not affect the mean direction of the sample magnetizations. When angle between shortening direction is larger (at least up to 30°), we may have both significant scattering effect, and additionally a net deviation of the resultant magnetizations. Although not truly passive themselves, these resultants exhibit large deviations in the range of true passive vectors deviations. This implies that in nature we can expect a high scatter of the data when the angle between shortening direction and the pa-

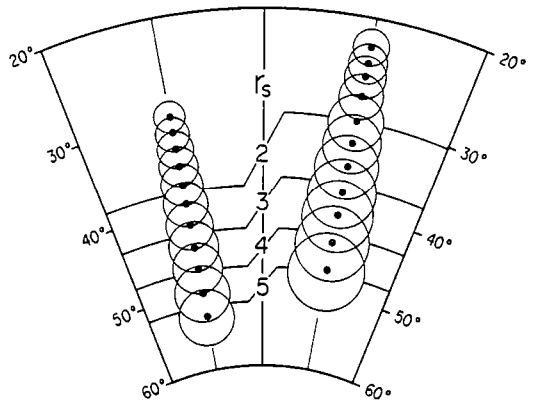

Fig. 3. Hematite magnetization deviations; progressive deviation, due to strain, of the magnetization acquired in a 30° inclined field. (left) Initially isotropic population; (right) initially 30% compacted population; note the shallowing of the initial magnetization due to the initially anisotropic fabric. Circles are the 95% circles of confidence. Stereographic projection.

leomagnetic one is small. An increase of this angle should result in an increase in the deviation of the mean paleomagnetic direction with a diminution in the scattering. The amount of deviation appears to depend strongly upon the amount of hematite particle rotation. Therefore, the understanding of magnetic mineral fabric development is a critical step of the analysis of the effects of strain upon remanent magnetization in natural rocks.

THE MARITIME ALPS RED BEDS

The red beds of the Maritime Alps form the upper part of the Permian cover of the Argentera crystalline massif. Excellent strain markers provided by green elliptical reduction spots have made these series the subject of numerous studies on strain, fabric, and anisotropy of magnetic susceptibility [Graham, 1978; Siddans, 1980; Kligfield et al., 1981, 1983; Siddans et al., 1984]. Mainly strained in the alpine orogeny [Siddans, 1979], these series are folded with WNW-ESE trending axes, and exhibit a strain gradient from south to north [Graham, 1978] accompagnied by a progressive cleavage development. Metamorphism and textures have been studied by Siddans [1980] who shows that the main mechanism of cleavage development is provided by illite recrystallisation in low grade metamorphism. The evolution of the susceptibility anisotropy tensor with increasing strain has been described by Kligfield et al. [1981, 1983]. The authors conclude that the progressive reorientation of ultrafine hematite particles is expressed by the similarities in shape and axes orientations of the strain and the magnetic susceptibility anisotropy ellipsoids. Furthermore a logarithmic correlation is found between principal susceptibility differences and principal strains. Hematite particle rotations induce a scattering of the magnetization directions carried by the redbeds. Our analysis of the paleomagnetic data dispersion [Cogné and Perroud, 1985] has shown a consistency between the sense and amount of paleomagnetic direction deviations and the direction and intensity of total strain. This may be briefly summarized as follows. In the sites where there is a low angle between the shortening direction and the mean NRM direction, the paleomagnetic directions are widely dispersed. The scatter increase with strain intensity in a manner similar to passive line behavior. When the angle between the shortening direction and the mean paleomagnetic one is large, the whole site direction population is deviated toward the cleavage plane, without noticeable change in grouping (compared to the usual grouping of paleomagnetic directions in similar rock type).

These observations lead us to assume a material linelike (passive line) behavior of the magnetization vectors. Thus, the strain removal technique, using the inverse strain tensor of each site, was used to undeform both bedding plane and paleomagnetic vectors of the sites, allowing us to recover a formation mean paleomagnetic direction not significantly different from the Stable Europe Permian direction determined by Van den Ende [1977] within the undeformed part of the Dome de Barrot formation [Cogné and Perroud, 1985].

In an effort to correlate magnetization deviations with hematite rotations, the preferred orientation of hematite cristallographic lattices was studied by X ray diffraction goniometry on samples from 8 sites where strain is homogeneous at the site scale. Measurements and data processing were done at the Laboratoire de Géologie Structurale, Université de Rennes following the procedure described by Gapais [1979]. For the reasons noted above, the measurements were made on poles to {104} form and the expected pole figures must have small circle distributions if hematite basal planes are aligned with each other. From the pole figures we have selected four typical results (Figure 4). Strain increases from the upper left to lower right corners in the figure. First is the compactionnal stage (site A) in the southern part of the Dome de Barrot. Although rather weak, hematite fabric is obvious, with a small circle distribution around the normal to bedding. The two following pole figures were obtained on sites showing early stages of cleavage development. In both sites superimposition of horizontal shortening upon the preexisting bedding fabric provides total strain ellipsoids of constriction shape with long axis horizontal. In site B (North Dome de Barrot) cleavage is not yet present and the pole figure is represented in the bedding plane projection. In site C (South Tinée Valley) cleavage is of pencil type. Corresponding pole figure is represented in the cleavage plane, with trace of bedding (So) indicated. In both figures, we observe inter-

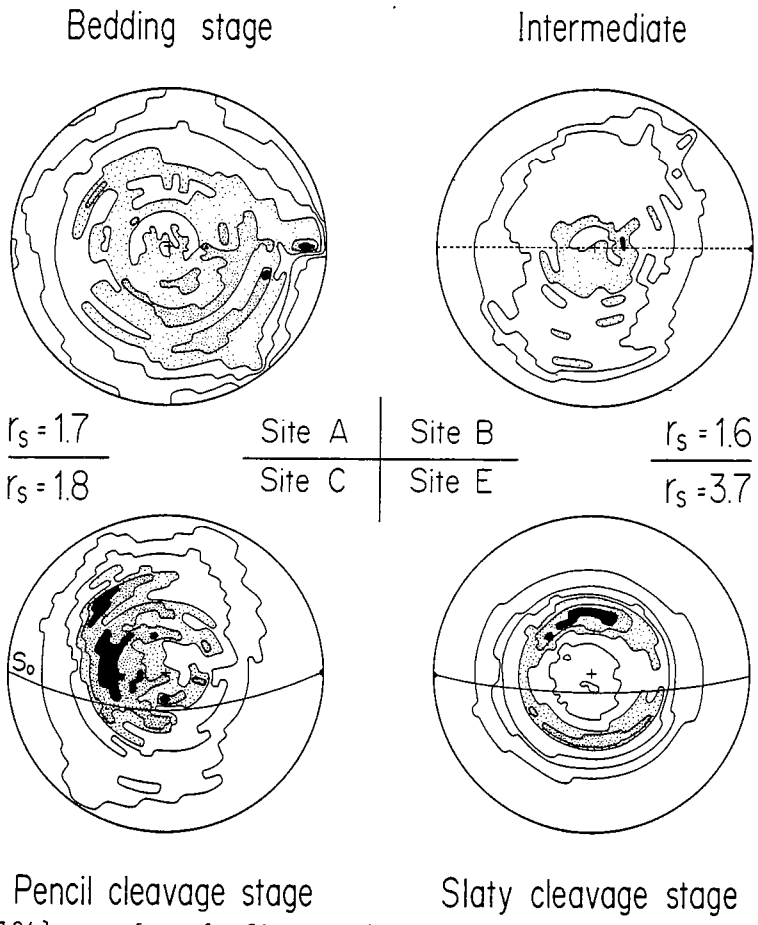

Fig. 4. {104} normals pole figures obtained by X ray texture goniometry in 4 sites of the Maritime Alps red beds. Location of the sites of Cogné and Perroud [1985, Figure 1, p. 127]. Equal area projections. Plane of projection is bedding (So) in sites A and B, cleavage (Sl) in sites C and E (trace of So indicated). Dashed line in site B is the λ_1 λ_2 incremental strain plane. Contours (in multiples of uniform distribution): site A, 0.5- 1.0- 1.2- 1.4- 1.6; site B, 1.0- 1.2- 1.4- 1.6; site C, 1.0- 1.2- 1.3- 1.35- 1.4; site E, 1.0- 1.5- 1.8- 2.0- 2.1- 2.2.

mediate fabrics expressed by the elongated pattern of the points, between normal to bedding and normal to cleavage (or λ_3 axis of incremental strain in site B). In the fourth stage (site E in the Tinée Valley), strain ellipsoids are flattened in the well developed slaty cleavage. The pole figure shows a well- defined small circle distribution around the normal to cleavage. This expresses the strong preferred orientations of hematite basal planes within the cleavage plane.

In order to examine the relationships between finite strain and hematite progressive reorientation suggested by the {104} pole figures, the strain intensities (rs) of each of the eight sites studied have been compared to the fabric intensities (rf) derived from the eigenvalues ratios of the {104} normals weighted orientation tensors (Figure 5). One can note that hematite fabric intensities increase in a manner roughly similar to that corresponding to rigid rotation of planar particles in a material planes strain response model as described above. For comparison, hematite fabrics were simulated using this model, from the finite strain data of the eight sites. The obtained intensity parameters are drawn in Figure 5 (open squares). The similarity in the slopes of the curves for simulated and experimental results shows that the increase in hematite fabric intensities is

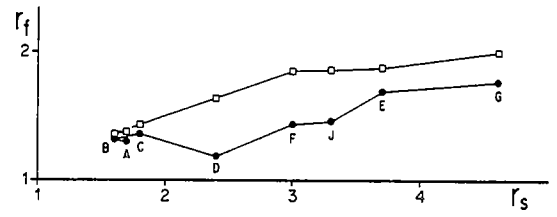

Fig. 5. Fabric intensity (rf) vs strain intensity (rs). Closed circles, from the {104} normals texture goniometry measurements of the eight studied sites in the Alpes Maritimes red beds (see Cogné and Perroud [1985] for site locations); open squares, simulated fabrics using the strain data of the same sites.

similar to the increase in the simulated fabric intensities. This suggests that a model of passive reorientation of planar particles can be used to describe the observed relationships between fabric and strain within the red beds studied. Unfortunately, the very small dimensions of hematite grains (ultrafine pigment) did not allow any microscopic observation of the deformation mechanisms of hematite fabric development. In particular, probable mechanisms such as dynamic recrystallization or intracrystalline slip cannot be seen. Nevertheless, without knowing the physical processes involved, the above analysis suggests that passive rigid rotation of planar particles adequately describes the main characteristics of observed hematite fabric development within these red beds.

Simulating such a passive rotation with a set of particles bearing micromoments, it has been shown above that a shortening applied in the direction of the magnetic resultant induces a passive linelike behavior of the magnetization. This behavior is similar to the one we described in our previous paleomagnetic study of the Maritime Alps redbeds [Cogné and Perroud, 1985]. We therefore argue that the idea of a strain removal technique based upon this behavior is valid.

PONT-REAN FORMATION, SOUTH OF RENNES, BRITTANY

The red beds of the Pont-Réan Formation are found underlying the "Grès Armoricain" in central Brittany and are inferred to be Cambro-Trémadocian. Lateral equivalents are found in several places in the Armorican Massif, and a paleontologically-based Arenig age was found in the Ancenis area, in the Moulin de Chateaupanne formation [Cavet et al., 1979]. In our study area (Figure 6), the red beds have suffered a penetrative deformation during the Hercynian orogeny, resulting in ESE-WNW folding accompanied by the development of subvertical axial planar cleavage. As observed in the field, the stretching lineation trends parallel to the bedding-cleavage intersection. In contrast, the Moulin de Chateaupanne

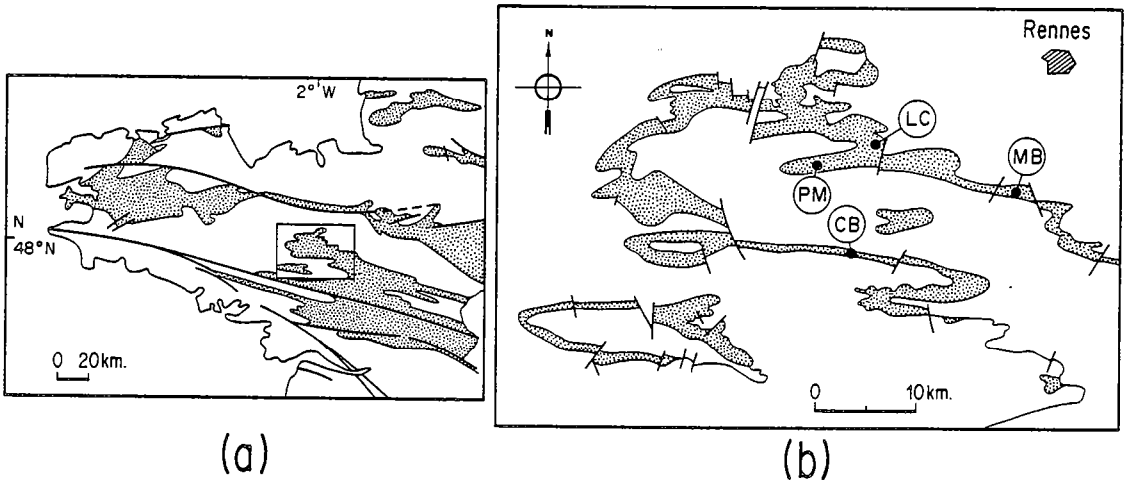

Fig. 6. (a) Geological setting of the studied area in the Armorican Massif (western France); dotted areas, paleozoic sediments. (b) Location map of the sampling sites in the Pont-Réan formation (dotted area).

TABLE 1. Mean Structural and Susceptibility Data for the Pont-Rean Formation

Site	So		Sl		λ_1	λ_2	λ_3	k	r	kmax		kmin		kmax/kint	kint/kmin
	S	Di	S	Di						De	I	De	I		
PM	56	33	91	80	1.206	1.096	0.756	0.22	1.55	74	12	345	3	1.029	1.023
MB	66	28	88	86	1.449	1.115	0.619	0.37	2.10	86	1	176	1	1.040	1.036
CB	280	56	101	86	1.618	1.471	0.420	0.04	3.60	99	11	8	4	1.030	1.092
LC	135	22	69	86	1.392	0.928	0.774	2.50	1.70	254	22	undefined		1.053	1.029

So and Sl are the bedding and cleavage planes. Their orientations are defined by S (strike) and Di (dip). λ_i are the eigenvalues of the strain tensor, with $\lambda_1\lambda_2\lambda_3 = 1$. k and r describe the shape [Flinn, 1965] and intensity [Watterson, 1968] of strain tensor. The orientation of principal susceptibility axes (kmax,kmin) is given by De (declination) and I (inclination). For comparison, strain Z axis is the pole of Sl while X axis is at the So/Sl intersection.

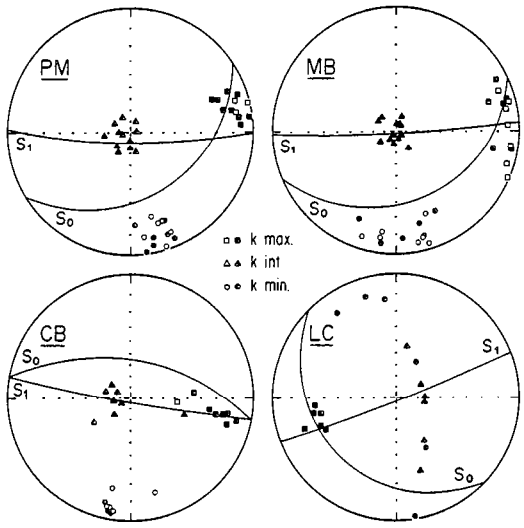

Fig. 7. In Situ directions of principal susceptibilities with bedding (So) and cleavage (S1) planes traces (downward hemisphere). Closed symbols, downward inclinations; open symbols, upward inclinations. Stereographic projections.

formation has not been deformed. We have recently paleomagnetically studied it and we will use the result [Perroud et al., 1986] as a reference in the undeformed state for the present study.

The mean strain ellipsoid of each site has been estimated using the Rf/ Φ method of Dunnet [1969], by measuring the axial ratio of elliptical reduction spots. Then, assuming a constant volume deformation (i.e. $\lambda_1 \lambda_2 \lambda_3 = 1$), the principal longitudinal strains, $\lambda i = 1+ei$ (i=1,2,3), are determined. In this study, we have estimated the hematite particles orientation distribution through the anisotropy of the magnetic susceptibility. Measurements were done at the C.F.R., Gif sur Yvette, using an improved Digico anisotropy delineator and the corrected calibration procedure [Hrouda et al., 1983]. Results are shown in Table 1 and Figure 7. It appears that all magnetic axes are strongly orientated, except in site LC where only the maximum susceptibility (k max) axis is well defined. Correlation between strain and susceptibility ellipsoids is excellent:

Principal directions. In site LC, where the rock shows a pencil structure, we found kmax at the intersection between the bedding and cleavage planes; In other sites, the minimum axis (kmin) is close to the cleavage plane pole, and kmax close to the regional stretching lineation direction. It should be noticed however, that where the strain intensity is the smallest (site PM, rs= 1,55) kmax significantly deviates towards the bedding plane, indicating the existence of a pre-orogenic magnetic anisotropy (deposition or compaction).

Shape of the ellispoids. Using Flinn diagrams [Flinn, 1965], we have reported both strain and susceptibility ellipsoids axial ratios (Figure 8, top). Although the absolute values of these ratios are quite different, it can be noticed that the representating points are similarly distributed in both cases; CB has a definitive oblate tensor, while the other sites, which are less deformed, are distributed over the plane strain line. Site LC, however, which shows the pencil structure, is in both cases in the prolate tensor field.

Principal values. After Kligfield et al.[1983], we have tried to correlate the principal strain ($\varepsilon i = \ln(1+ei)$) and principal susceptibility differences ($Mi = (ki-ko)/ko$, $ko = (kmax.kint.kmin)^{1/3}$). We have obtained (Figure 8, bottom) a strong positive correlation $\varepsilon i = 10.67 Mi - 0.01$ ($r = 0.95$). The slope of the best fit line is

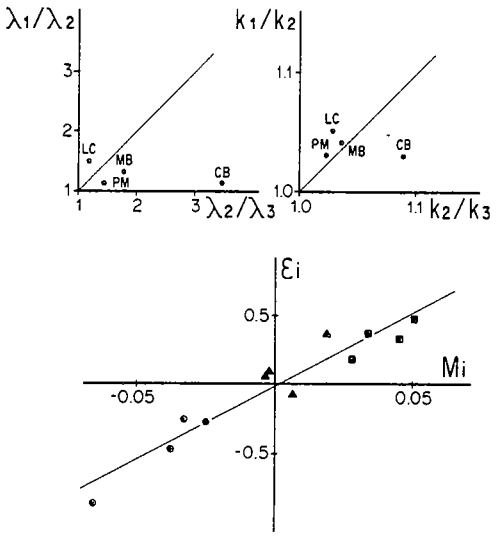

Fig. 8. (top) Flinn diagrams for strain (top left) and susceptibility (top right) ratios. Lower: mean logarithmic principal strains (i) vs mean principal susceptibility difference (Mi). Same symbols for kmax, kint, kmin as in Figure 7. The line represents the best fitted line over the experimental points.

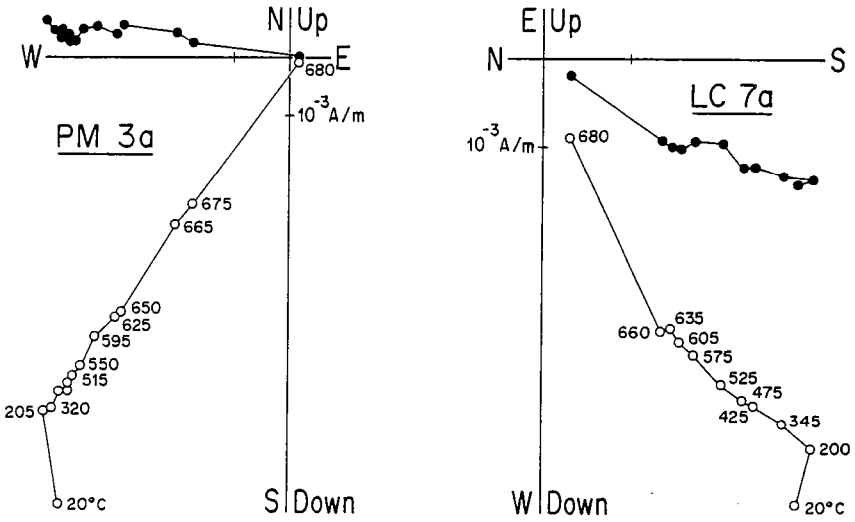

Fig. 9. Thermal demagnetization results in Zijderveld [1967] in situ orthogonal projections. Open symbols, projection of the vector end-points onto the vertical plane; closed symbols, projection onto the horizontal plane. Temperature in °C is indicated.

very different from the Kligfield et al. result (25.65), but the correlation seems to apply well in both cases. The difference in slope could be due to the rock type or perhaps also in a part to the calibration of the apparatus.

In conclusion to this part, we want to point out that strain and susceptibility tensors are correlated, and thus both can be used to estimate the deformation. This can be very useful when no clear markers of deformation can be found. We next consider how this deformation affects the remanent magnetization (RM).

Six samples from each site were subjected to stepwise thermal demagnetization up to 680°C, using a Schonstedt nonmagnetic oven. Remanent magnetization measurements were done with a computer-assisted spinner magnetometer (Schonstedt DSM-1). Results were displayed in Zijderveld diagrams (Figure 9) and characteristic magnetizations graphically interpreted. The results are given in Table 2. The clearest results are from site PM. We obtained here a very good univectorial decay of the magnetization toward the origin (Figure 9, left) characterized by a sharp decrease of intensity near the Curie point of hematite. Apart from a small parasitic component removed by the first heating step, no evidence of secondary components is seen. A few samples from site MB show a similar behavior. Unfortunately, other samples from this site were either unstable during demagnetization or remagnetized in the present-day earth's field. Therefore, a reliable average was not obtained on site MB. However, we will see later that the two individual directions obtained are quite compatible with site PM site-mean. Finally, the two other sites reveal a more complex magnetization (Figure 9, right). An intermediate temperature component can be obtained by line-fitting between 200°and 600°C. It has a southwest declination and shallow downward inclination. Then from 600°to 680° C, the magnetization remains unchanged defining a "stable end point". The first component is widely found in paleomagnetic studies of Paleozoic rocks in the Armorican Massif [Perroud et al., 1986]. It has also been described for the Moulin de Chateaupanne formation and interpreted as an Hercynian partial overprint. The question arises of how well this overprint has been cleaned before the RMs reach the end points. We will discuss this again in the light of the final results. The average of the end points is the best estimate we have of the characteristic magnetization directions in both sites LC and CB.

In situ (not corrected for tilt) site-mean directions are reasonnably clustered (Figure 10) but the overall mean (D=244° , I=63°) is not interpretable as syn- or post tectonic magnetization; we do not know any field direction similar to this one, in the Armorican Massif, since the

TABLE 2. Mean Magnetization directions Obtained in the Pont-Rean Formation

Site	N	IS D	IS I	k	α_{95}	TC D	TC I	Undeformed D	Undeformed I	k	α_{95}
PM	6	284	55	213	5	223	67	257	78	171	5.0
LC	6	223	61	168	5	224	39	215	48	109	6.5
CB	5	217	63	23	16	348	57	210	61	14	21.0
Mean	3	244	63	19	-	251 (k=5)	68	219	63	22	-
MB											
2a	-	267	53	-	-	228	54	239	67	-	-
3	-	279	55	-	-	233	61	272	73	-	-

These results correspond to the high temperature components, and are shown as in situ (IS), tilt-corrected (TC) and after inverse deformation. N is the number of specimens used in the statistics; k and α_{95} are Fisherian parameters for dispersion; D and I state for declination and inclination.

Hercynian orogenesis. On the other hand, it is not far from the result of the undeformed Moulin de Chateaupanne formation (shown in Figure 10, SRTC), which has been assigned an Ordovician age. However, tilt correction disperses the data. So, without further analysis, we are not able to deduce from this study any solid conclusion. Note that a similar situation was described by us in the case of the Maritime Alps. We have therefore decided to apply the inverse deformation algorithm introduced there to the directions of magnetization and to the bedding planes. Tilt correction using the unstrained bedding plane leads to the final estimate of the site mean directions, mentioned in Table 2. We observe that the clustering is improved, compared with that after the ordinary tilt correction, and at least as good as before any correction. A comparison with the Moulin de Chateaupanne Ordovician magnetization (Figure 10, SRTC) shows a good consistency. We think therefore that the inverse deformation procedure is truly worthwile in this case. It allows us to recover a primary magnetization which we would have rejected otherwise.

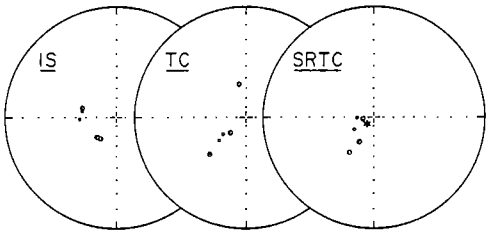

Fig. 10. Stereographic projections of the site-mean magnetization directions (large dots) and magnetization directions of individual samples from site MB (little dots), after thermal cleaning. IS, in situ directions; TC, tilt corrected directions; SRTC, directions after strain removal and tilt correction using the unstrained bedding plane. The star is the Ordovician magnetization direction in the Moulin de Chateaupanne formation [Perroud et al., 1986].

In spite of this optimistic conclusion, reasons for the final dispersion of the results can be discussed. Directions obtained through indisputable univectorial magnetization are much closer to the Ordovician reference direction than those obtained from multicomponent magnetizations. We can therefore suspect that incomplete resolution of the components has biased such directions, pulling them toward the intermediate temperature component direction, that is toward shallower inclinations. This is particularly plausible for site CB, which has a large within-site dispersion. It is possible

that chemical leaching could help to resolve this question, so further work is planned on these red beds, involving a larger number of sampling sites.

CONCLUSIONS

Based upon the passive behavior model, our hematite reorientations simulations have pointed out the large deviations that strain can induce on the magnetization carried by the particles. These deviations are characterized by a scattering of the micromoment resultants when the shortening direction is close (up to 30°) to the magnetic one, and a net rotation of the micromoment resultant toward the strain plane otherwise.

When working on naturally deformed rocks, the problem is to estimate the mechanism and amount of hematite reorientation. X ray texture goniometry and anisotropy of magnetic susceptibility are convenient tools for this purpose. In the Maritime Alps red beds, the preferred orientation of hematite {104} normals appears to be controlled by strain in a manner similar to the strain response in material planes model. In most sites hematite rotations can be considered as responsible for the anomalous scattering of the paleomagnetic data. This dispersion is shown to be similar to the dispersion of passive lines. In the Pont-Réan formation, the effects of strain upon hematite orientation have been checked using magnetic susceptibility anisotropy measurements. Here too, the similarities between strain and susceptibility ellipsoids in shape and in axes length and direction may be interpreted in terms of a reorientation of hematite grains. Paleomagnetic data analysis has shown the existence of a stable, steeply dipping magnetization component with little, within-site dispersion (except in one site where the dispersion is likely due to an incomplete separation of the components). This high, within-site consistency was to be expected, considering the large angle between the shortening axis and the magnetization direction. Moreover, we met here the same paradoxal situation as in the Maritime Alps; tilt correction tends to disperse data which are not interpretable as magnetizations acquired post folding. In both cases, we tried to recover the initial pretectonic paleomagnetic direction by removing the strain using the inverse strain tensor, as determined in each site. For the preliminary results obtained in the Pont-Réan formation as well as in the Maritime Alps, this treatment renders the data interpretable in terms of pretectonic magnetizations.

To conclude this analysis, we would like to emphasize the interest we find to compare strain, crystallographic fabric and magnetic susceptibility tensors. Strain removal technique allows the use of many more rock units in our paleomagnetic research. It may lead to a better precision of the paleogeographic reconstructions and to a better understanding of the deformation kinematics and mechanisms. The correlations between these tensors are our best chance to estimate with confidence the finite deformation in many rocks. Our positive attempts in inverse deformation of paleomagnetic data suggest that this way is potentially rich in information. However, we have to temper this optimistic view by the following considerations: when the intensity of deformation becomes too high, the technique of strain removal used here is probably not applicable. Our approach uses largely a theoretical deformation model (March passive behavior) which is probably not valid for very large strains. Moreover, extensive remagnetizations will generally appear. Furthermore, although red beds are commonly choosen for paleomagnetic investigations, we cannot extend our conclusions for hematite reorientations to other rock types. But we feel that our studies, together with parallel work by others (see, for example, Kligfield et al. [1983]) open new fields for paleomagnetic applications. And finally, we strongly stress that assessing the deformation state of the rock is essential in routine paleomagnetic analysis, especially when working within an orogenic belt. Ignoring this aspect will lessen the reliability of the results.

Acknowledgments. We thank C. Laj for its permission to use the Digico anisotropy delineator at the C.F.R., Gif/Yvette. D. Gapais has provided helpful comments on an earlier draft of this paper, and C. M. Marshall had corrected the English of this final version. This is a contribution of CAESS (L.P. 4661, CNRS).

REFERENCES

Cavet, P., J. J. Chauvel, H. Lardeux, and J. Blaise, Paléozoique du domaine

ligérien entre Ancenis et Chalonnes, Bull. Soc. Geol. Miner. Bretagne, C11, 61-65, 1979.

Cobbold, P. R., and D. Gapais, Specification of fabric shapes using an eigenvalue method: Discussion, Geol. Soc. Am. Bull., 90, 310-312, 1979.

Cogné, J. P., and H. Perroud, Strain removal applied to paleomagnetic directions in an orogenic belt: The Permian red slates of the Alpes Maritimes, France, Earth Planet. Sci. Lett., 72, 125-140, 1985.

Collinson, D. W., Origin of the remanent magnetization and initial susceptibility of certain red sandstones, Geophys. J. R. Astron. Soc., 9, 203-217, 1965.

Dunnet, D. A., A technique of finite strain analysis using elliptical particles, Tectonophysics, 7, 117-136, 1969.

Fisher, R. A., Dispersion on a sphere, Philos. Trans. R. Soc. London, Ser. A, 217, 295-305, 1953.

Flinn, D., On the symmetry principle and the deformation ellipsoid, Geol. Mag., 102, 36-45, 1965.

Gapais, D., Orientations préférentielles de réseau et deformations naturelles, 3rd cycle thesis, 261 pp., Univ. de Rennes, Rennes, France, 1979.

Graham, R. H., Quantitative deformation studies in the Permian rocks of the Alpes-Maritimes, Proceedings of Symposium in Honour of Prof. J. Goguel, Mem. BRGM, 91, 219-238, 1978.

Hrouda, F., A. Stephenson, and L. Woltar, On the standardization of measurements of the anisotropy of magnetic susceptibility, Phys. Earth Planet. Inter., 32, 203-208, 1983.

Hrouda, F., H. Siemes, N. Herres, and C. Hennig-Michaeli, The relationship between the magnetic anisotropy and the c-axis fabric in a massive hematite ore, J. Geophys., 56, 174-182, 1985.

Kligfield, R., W. H. Owens, and W. Lowrie, Magnetic susceptibility anisotropy, strain and progressive deformation in Permian sediments from the Maritime Alps (France), Earth Planet. Sci. Lett., 55, 181- 189, 1981.

Kligfield, R., W. Lowrie, A. Hirt, and A. W. B. Siddans, Effect of progressive deformation on remanent magnetization of Permian redbeds from the Alpes Maritimes (France). Tectonophysics, 97, 59-85, 1983.

March, A., Mathematische theorie der regelung nach der korngestalt bei affiner deformation, Z. Kristallogr., 81, 285-297, 1932.

Owens, W. H., Strain modifications of angular density distributions, Tectonophysics, 16, 249-261, 1973.

Owens, W. H., Mathematical model studies on factors affecting the magnetic anisotropy of deformed rocks, Tectonophysics, 24, 115-131, 1974.

Perroud, H., M. Robardet, R. Van der Voo, N. Bonhommet, and F. Paris, Revision of the age of magnetization of the Montmartin redbeds, Normandy, France, Geophys. J. R. Astron. Soc., 80, 541-549, 1984.

Perroud, H., N. Bonhommet, and J. P. Thébault, Paleomagnetism of the Ordovician Moulin de Chateaupanne formation, Vendée, western France, Geophys. J. R. Astron. Soc., in press, 1986.

Ramsay, J. G. and M. I. Huber, The Technique of Modern Structural geology, vol.1, Strain Analysis, 307 pp., Academic, Orlando, Fla, 1983.

Scheidegger, A. E. On the statistics of the orientation of bedding planes, grain axes and similar sedimentological data, U.S. Geol. Surv. Prof. Pap., Ser. C, 525, 164- 167, 1965.

Siddans, A. W. B., Arcuate fold and thrust pattern in the subalpine chains of southeast France, J. Struct. Geol., 1, 117-126, 1979.

Siddans, A. W. B., Compaction, métamorphisme et structurologie des argilites permiennes dans les Alpes Maritimes (France), Rev. Geol. Dyn. Geogr. Phys., 22, 279-292, 1980.

Siddans, A. W. B., B Henry, R. Kligfield, W. Lowrie, A. Hirt, and M. N. Percevault, Finite strain patterns and their significance in Permian rocks of the Alpes Maritimes (France), J. Struct. Geol., 6, 339-368, 1984.

Uyeda, S., M. D. Fuller, J. C. Belshe, and R. W. Girdler, Anisotropy of the magnetic susceptibility of rocks and minerals, J. Geophys. Res., 68, 279-292, 1963.

Van den Ende, C., Paleomagnetism of Permian redbeds of the Dome de Barrot (S. France), thesis, 171 pp., Univ. of Utrecht, Utrecht, The Netherlands, 1977.

Van Houten, F. B., Origin of redbeds, a review 1961-1972, Ann. Rev. Earth Planet. Sci. Lett., 1, 38-61, 1973.

Watterson, J., Homogeneous deformation of the gneisses of Vesterland, southwest

Greenland, Bull. Groenl. Gron. Geol. Unders., 78, 1968.
Woodcock, N. H., Specification of fabric shapes using an eigenvalue method, Geol. Soc. Am. Bull., 88, 1231-1236, 1977.
Zijderveld, J. D. A., Demagnetization of rocks: analysis of results, in Methods in Paleomagnetism, edited by D. W. Collinson, K. M. Creer and S. K. Runcorn, pp. 254-286, Elsevier, New York, 1967.

N. Bonhommet, J. P. Cogné, H. Perroud, and M. P. Texier, CAESS, Laboratoire de Géophysique Interne, Institut de Géologie, Université de Rennes 1, Campus de Beaulieu, 35042 Rennes Cedex, France.

(Received June 12, 1985;
revised January 16, 1986;
accepted February 3, 1986.)

ANNEXE 6.

J.P. COGNE, D. GAPAIS. **Passive rotation of hematite during deformation : a comparison of simulated and natural redbeds fabrics.** Tectonophysics, 121, 365-372, 1986.

Tectonophysics, 121 (1986) 365—372
Elsevier Science Publishers B.V., Amsterdam — Printed in The Netherlands

Letter Section

Passive rotation of hematite during deformation: a comparison of simulated and natural redbeds fabrics

J.P. COGNÉ and D. GAPAIS

Centre Armoricain d'Etude Structurale des Socles, (L.P. C.N.R.S., Université de Rennes), Campus de Beaulieu, 35042 Rennes Cedex (France)

(Received July 29, 1985; revised version accepted October 24, 1985)

ABSTRACT

Cogné, J.P. and Gapais, D., 1986. Passive rotation of hematite during deformation: a comparison of simulated and natural redbeds fabrics. *Tectonophysics*, 121: 365—372.

A simulation model is used to generate pole figures assuming strain-induced passive rotation of hematite crystals. Comparison of simulated and natural hematite fabrics allows us to distinguish between dominant passive rotation and other grain-scale deformation mechanisms. Two natural examples are discussed: redbeds from the French Maritime Alps and Pyrenean redbeds. Fabrics indicate that passive rotation is the dominant reorientation mechanism of primary hematite grains during progressive deformation of redbeds.

INTRODUCTION

When carrying out paleomagnetic studies of redbeds within tectonised regions important questions arise about possible deviations of primary magnetic vectors due to strain-induced, hematite preferred orientations (e.g. Kligfield et al., 1983; Cogné and Perroud, 1985). Removing such deviations is a critical step in paleomagnetic analyses, requiring knowledge of grain-scale deformation mechanisms responsible for actual hematite fabrics. Methods of strain removal (see Cogné and Perroud, 1985) will yield the true primary magnetic orientation only if hematite grains behave like passive markers rotating during progressive deformation. Indeed, this is the only particular case where total strain and fabric ellipsoids are expected to be identical (March, 1932; Owens, 1973; Tullis, 1976).

Passive rotation is commonly invoked to account for preferred orientation patterns of planar particles (e.g. phyllosilicates) within low-grade metamorphic rocks (Tullis, 1976; Oertel, 1983). However it probably combines with other mechanisms such as recrystallisation, intracrystalline slip, or primary metamorphic growth, whose contribution to the bulk fabric is generally difficult to estimate (Siddans, 1976; Le Corre, 1979).

X-ray texture goniometry or magnetic anisotropy techniques provide good

0040-1951/86/$03.50

tools for fabric analysis of planar magnetic particles such as hematite. In this paper, the former technique has been used to check hematite reorientation mechanisms within two sets of samples from the Permian redbeds of the Maritime Alps and the Pyrenean Permo-Triassic redbeds. Reduction spots present in the rocks provided good independent measurements of the total strain. Numerical simulations of hematite fabrics are used to estimate and discuss deviations from a model of passive reorientation.

NUMERICAL SIMULATIONS

Although possible in massive hematite ore (Hrouda et al., 1985), direct, accurate measurements of hematite *C*-axis fabrics are in general difficult because of the very low intensity of the corresponding X-ray diffraction peak. Due to the relatively low fraction of hematites in redbeds, we measured poles to {104} form of crystallographic planes which yield maximum diffracted intensities. For each hematite crystal, the six normals to {104} are distributed on a cone of 38.84° half-aperture angle around the *C*-axis. This accounts for the need for numerical simulations for the quantitative interpretation of pole figures; a direct comparison between strain and orientation tensors of {104} pole figures is not possible, in contrast to the case of *C*-axis distributions.

The model used here is based upon March's model (1932) of passive reorientation of planar particles. It consists of N ($\leqslant 1000$) planar particles, each characterized by a direct Cartesian frame where Z is the *C*-axis and XY is the basal plane of hematite. The six poles to {104} planes are attached to each particle, with a conical distribution around the *C*-axis. When applying a strain to the whole population, each particle is free to rotate passively, following the passive plane behaviour model. For each state of strain it is possible to generate a {104} pole figure and to compute the corresponding weighted orientation tensor W.O.T. (Cobbold and Gapais, 1979) which quantifies the degree of axes alignment. From the theory of the W.O.T., derived from the Scheidegger (1965) orientation tensor, an isotropic tensor (three equal eigenvalues, $S_1 = S_2 = S_3$) will be obtained for a perfect 57° half-aperture conical distribution of lines. Consequently, the conical distribution of {104} poles will result in low eigenvalue ratios, even for a high degree of hematite basal plane alignment. This accounts for the low fabric intensities reported below.

HEMATITE FABRIC RESULTS

Texture goniometry measurements were carried out at the University of Rennes (see Gapais and Brun, 1981 for details on data processing and representation). Results are given in the form of {104} pole figures and associated computed weighted orientation tensors.

The redbeds of the Maritime Alps

The red series of the Maritime Alps form the upper part of the Permian cover of the Argentera Crystalline Massif. Numerous elliptical green reduction spots provide good strain markers all along the regional strain gradient which characterizes the deformation of the redbeds in the area (Graham, 1978). Thus, all successive stages of increasing finite strain can be analysed, from a compactional sedimentary fabric (in the Dome de Barrot, southern outcrop) up to a well developed slaty cleavage with a flattened strain ellipsoid (northern Tinée Valley). In the intermediate stages, the finite strain ellipsoid is of the constriction type, due to the superimposition of a vertical flattening fabric (cleavage) upon the horizontal bedding fabric. This exceptional sequence has given rise to many studies about strain (Graham, 1978), susceptibility anisotropy (Henry, 1973; Kligfield et al., 1981, 1983), cleavage development (Siddans, 1980) and deviations of paleomagnetic vectors (Cogné and Perroud, 1985). In the present study, hematite fabrics have been measured in eight samples distributed along the strain gradient. Strain has been estimated at each site by measuring axial ratios of reduction spots. Results are described in detail by Cogné and Perroud (1985). Three typical {104} pole figures are shown in Fig. 1, together with simulated pole figures for similar finite strain ellipsoids and assuming passive rotation of hematite. The "undeformed" compactional stage (Fig. 1a) is characterized by a weak fabric with a small-circle distribution of poles around the normal to the bedding. This expresses a slight, preferred orientation of hematite basal planes within the bedding plane and reveals the anisotropic character of the initial material. The superposition of a subhorizontal shortening (subvertical $\lambda_1\lambda_2$ incremental strain plane) results in a constriction type finite strain ellipsoid ($K_s > 1$, Fig. 1b). The reorientation of hematite basal planes towards the cleavage plane is indicated by the elongated pattern of the pole distribution in both passive rotation model and experimental data. In the ultimate stages (Fig. 1c) of increasing strain, hematite basal planes are strongly orientated within the cleavage, as shown by the quasi-perfect small-circle pattern of {104} poles distribution about the shortening direction. Variations of pole distribution with increasing strain are quite similar for the simulated and natural fabrics. This clearly suggests that fabrics result from the progressive reorientation of the basal planes of primary hematite grains with progressive deformation.

Using the strain data of the eight sites studied, we have generated the expected fabrics for strictly passive planar hematite reorientation. The comparison of intensity parameter ($r = \lambda_1/\lambda_2 + \lambda_2/\lambda_3 - 1$; $\lambda_1 > \lambda_2 > \lambda_3$ = principal values: Watterson, 1968) for strain and for both simulated and natural fabrics is shown in Fig. 2. As expected, the fabric intensities (r_f) are rather low compared with strain intensities (r_s). Nevertheless, what is remarkable is the high degree of similarity in the slopes of the r_f/r_s curves for simulated and natural fabrics. This identity is better seen when reporting the simulated

368

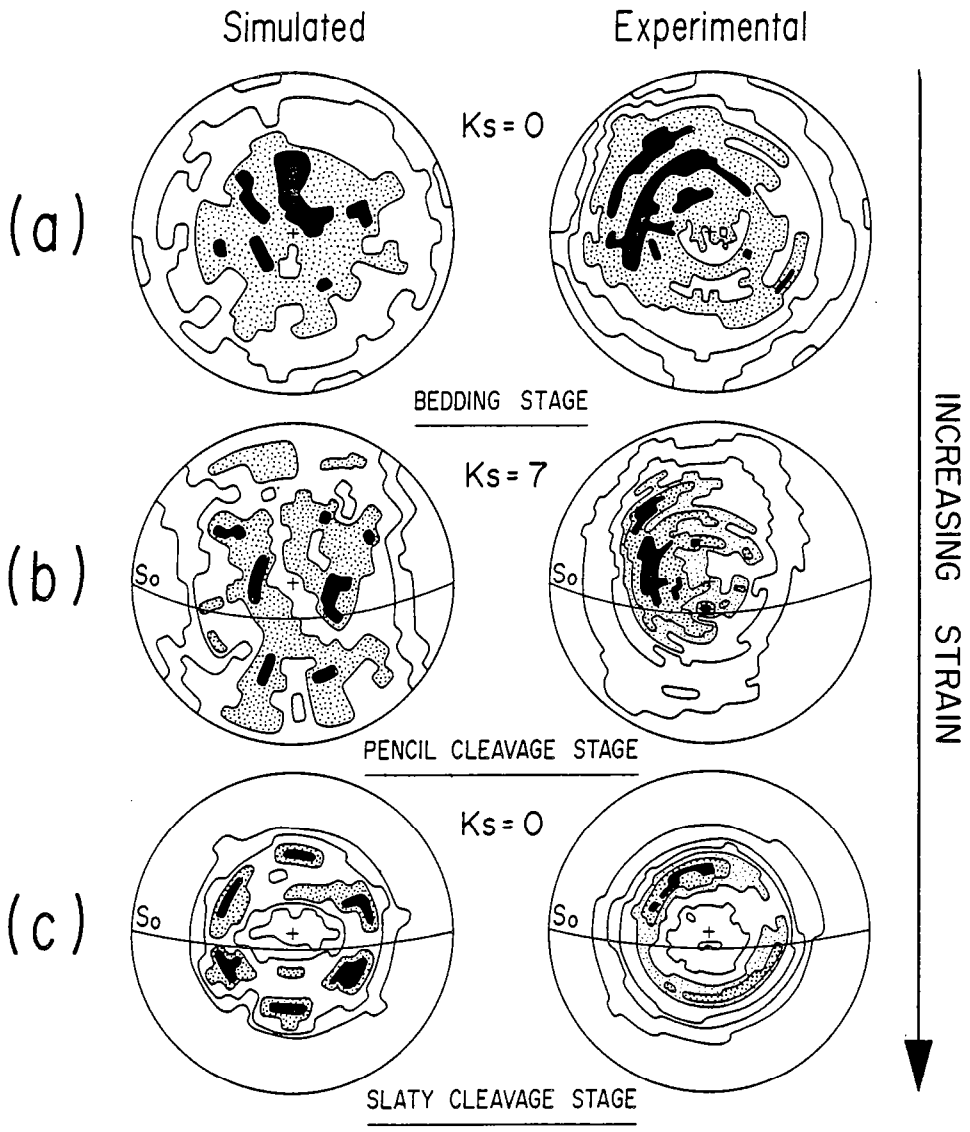

Fig. 1. Simulated (left) and natural (right) {104} axes pole figures for three increasing strain stages. K_s is the strain ellipsoid shape $(\lambda_1/\lambda_2 - 1)/(\lambda_2/\lambda_3 - 1)$ parameter (Flinn, 1965). Planes of projection are bedding for the two uppermost figures, cleavage with bedding trace indicated (S_o) for the others. Equal-area projections. Contours: Left (in % of poles in 1% of the hemisphere surface). (a) 0.5—0.8—1.1—1.4; (b) 0.7—0.9—1.1—1.3; (c) 1.0—1.4—1.7—2.0. Right (in multiples of uniform distribution): (a) 0.5—1.0—1.2—1.4—1.6; (b) 1.0—1.2—1.3—1.35—1.4; (c) 1.0—1.5—1.8—2.0—2.1—2.2.

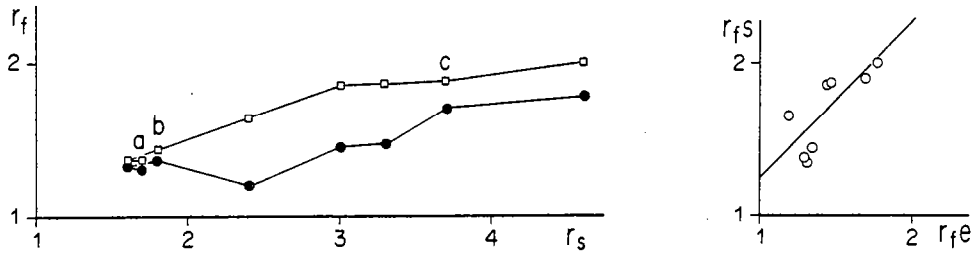

Fig. 2. Fabric intensities (r_f) vs. strain intensities (r_s) for natural (closed circles) and simulated (open squares) {104} preferred orientations from the redbeds of the Maritime Alps. *a*, *b* and *c* refer respectively to the pole figures drawn in Fig. 1a, b and c.

Fig. 3. Correlation between natural (r_fe) and simulated (r_fs) fabric intensities. The slope of the best fit line is 0.982 with a correlation factor of 0.756.

fabric intensities (r_fs) vs. the experimental one (r_fe) (Fig. 3). We obtain a rather good linear correlation ($r = 0.756$) with a slope very close to 1 (0.983). In other words, there is no difference in the way hematites have actually reorientated within these redbeds and a strain induced passive rotation of planar particles. Differences in absolute values of fabric intensities can be the results of different unknown factors such as (1) weakness of signal/noise ratios in texture goniometry measurements, (2) low fraction of randomly orientated hematites in shadow zones, (3) low fraction of non-planar hematite in the population (specularite?). Nevertheless, our results clearly show that the major mechanism of hematite reorientation in these redbeds is of the passive rotation type.

The Pyrenean redbeds

Six sites, located near the Col du Somport, have been sampled in the Permo-Triassic Pyrenean redbeds. Situated at the southern border of the Pyrenean Primary Axial Zone, these series show the characteristic southerly overturned folding of the South Pyrenean Zone (Choukroune, 1976). The axial planar slaty cleavage, developed during the main Pyrenean phase, dips moderately towards the north. As in the Maritime Alps, reduction spots allowed the strain to be measured in the field.

Paleomagnetic studies have been done on the Permo-Triassic redbeds all along the Pyrenean Chain. They have shown that the Permo-Triassic primary magnetization component is often overprinted by several remagnetizations related to tectonic events starting during the late Jurassic (Schott, 1985). This point is important for the interpretation of hematite fabric data.

In contrast to the red formations of the Maritime Alps, strain ellipsoids are all of the flattening type. Nevertheless, strain intensities show variations in the range of 1.9—3.7. That is, a correlation between strain and fabric intensities should be detected if present. {104} pole figures show a shape

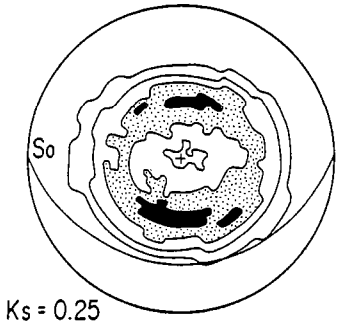

Fig. 4. Typical example of {104} pole figure from the Pyrenean red series. Plane of projection is cleavage with bedding trace indicated (S_o). K_s is the shape parameter of the strain ellipsoid (Flinn, 1965). Equal area projection. Contours (in multiples of uniform distribution): 1.0—1.25—1.5—1.7.

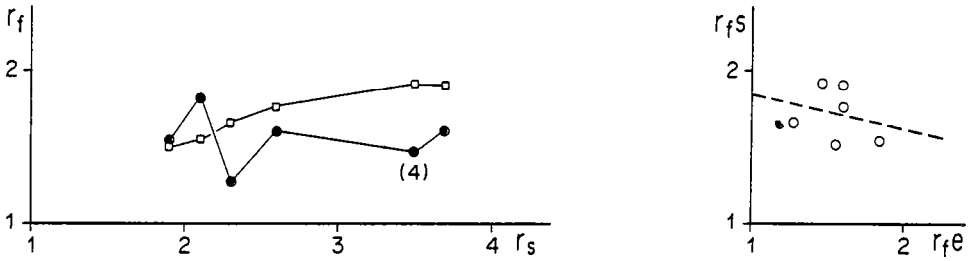

Fig. 5. Fabric intensities (r_f) vs. strain intensities (r_s) for natural (closed circles) and simulated (open squares) {104} preferred orientations from the Pyrenean redbeds. Number 4 on the curve refers to the pole figure drawn in Fig. 4.

Fig. 6. Intensities of natural (r_fe) vs. simulated (r_fs) hematite fabrics for the Pyrenean redbeds. Dotted line is obtained from linear regression.

similar to that in the most deformed sites of the Maritime Alps (Fig. 4). {104} poles are distributed on a well defined cone, centered on the normal to the cleavage. However, important differences with previously described data are found in the curves of strain intensities vs. fabric intensities (Fig. 5) and in the plots of simulated vs. natural fabric intensities (Fig. 6). In the former, the slope of the curves does not fit anymore (Fig. 5). The calculated correlation between simulated and natural fabric intensities (Fig. 6) supports conditions of parameters independence ($r = -0.235$). This implies that passive rotation can no longer be invoked as the major mechanism responsible for the development of hematite preferred orientations. The lack of correlation between the parameters could be explained by processes such as dissolution—crystallisation and/or dynamic recrystallisation of hematite. The observation of polished sections in reflected light did not provide any microstructural evidence for such processes, although numerous

quartz veins in the redbeds indicate fluid circulations during the cleavage development. Nevertheless, paleomagnetic analysis of these rocks (Schwarz, 1963; Cogné, 1983) has revealed an important overprinting of the primary magnetic direction by a secondary one, which is suspected to be syn- to post-tectonic in age. As this component is carried by fine hematite particles (pigment), this strongly supports the idea of hematite neoblasts formation during the deformation history of these series.

CONCLUSIONS

Although the conical distribution of hematite {104} normals gives rise to difficulties in direct comparisons between principal strains and the weighted orientation tensor eigenvalues, texture goniometry has proved helpful in explaining the behaviour of hematite during deformation.

With the help of a passive behaviour simulation, we have shown that in the Permian redbeds of the Maritime Alps, the reorientation of primary diagenetic hematites during progressive deformation is mainly achieved by passive rotation. In such rocks, strain removal to recover the primary paleomagnetic directions should be valid.

In the Pyrenean red formations of the Col du Somport, passive rotation is probably accompanied by the formation of new hematite grains during deformation. This is independently borne out by paleomagnetic evidence of secondary magnetization overprinting events taking place during the Pyrenean orogenesis.

REFERENCES

Choukroune, P., 1976. Strain patterns in the Pyrenean Chain. Philos. Trans. R. Soc. London, Ser. A, 283: 271—280.

Cobbold, P.R. and Gapais, D., 1979. Specification of fabric shapes using an eigenvalue method: discussion. Geol. Soc. Am. Bull., 90: 310—312.

Cogné, J.P., 1983. Etude paléomagnétique et déformation inverse de l'aimantation de séries naturelles déformées. Thèse 3ème cycle, Rennes, 108 pp.

Cogné, J.P. and Perroud, H., 1985. Strain removal applied to paleomagnetic directions in an orogenic belt: the Permian red slates of the Alpes Maritimes, France. Earth Planet. Sci. Lett., 72: 125—140.

Flinn, D., 1965. On the symmetry principle and the deformation ellipsoid. Geol. Mag., 102: 36—45.

Gapais, D. and Brun, J.P., 1981. A comparison of mineral grain fabrics and finite strain in amphibolites from Eastern Finland. Can. J. Earth. Sci., 18 (6): 995—1003.

Graham, R.H., 1978. Quantitative deformation studies in the Permian rocks of the Alpes-Maritimes. Proc. Symp. in honour of Prof. J. Goguel. Mem. Bur. Rech. Geol. Min., 91: 219—238.

Henry, B., 1973. Studies of microtectonics, anisotropy of magnetic susceptibility, and paleomagnetism of the Permian Dome de Barrot (France): paleotectonic and paleosedimentological implications. Tectonophysics, 17: 61—72.

Hrouda, F., Siemes, H., Herres, N. and Hennig-Michaeli, C., 1985. The relationship between the magnetic anisotropy and the *c*-axis fabric in a massive hematite ore. J. Geophys., 56: 174—182.

Kligfield, R., Owens, W.H. and Lowrie, W., 1981. Magnetic susceptibility anisotropy, strain, and progressive deformation in permian sediments from the Maritime Alps (France). Earth and Planet. Sci., Lett., 55: 181—189.

Kligfield, R., Lowrie, W., Hirt, A. and Siddans, A.W.B., 1983. Effect of progressive deformation on remanent magnetization of Permian Redbeds from the Alpes Maritimes (France). Tectonophysics, 97: 59—85.

Le Corre, Cl., 1979. L'évolution typologique et texturale des roches argilo- silteuses au cours de la schistogenèse. Notion de trajectoire de fabrique. Bull. Mineral., 102: 273—281.

March, A., 1932. Mathematische Theorie der regelung nach der korngestalt bei affiner deformation. Z. Kristallogr., 81: 285—297.

Oertel, G., 1983. The relationship of strain and preferred orientation of phyllosilicate grains in rocks — a review. Tectonophysics, 100: 413—417.

Owens, W.H., 1973. Strain modifications of angular density distributions. Tectonophysics, 16: 249—261.

Scheidegger, A.E., 1965. On the statistics of the orientation of bedding planes, grain axes and similar sedimentological data. U.S. Geol. Surv., Prof. Pap., 525C: 164—167.

Schott, J.J., 1985. Paleomagnetism in the Pyrenean Realm: a review. 3rd E.U.G. Meet., Strasbourg, April 1985 — Terra Cognita, 5: 139.

Schwarz, E.J., 1963. A paleomagnetic investigation of Permo-Triassic redbeds and andesites from the Spanish Pyrenees. J. Geophys. Res., 68, 10: 3265—3271.

Siddans, A.W.B., 1976. Deformed rocks and their textures. Philos. Trans. R. Soc. London, Ser. A, 283: 43—54.

Siddans, A.W.B., 1980. Compaction, metamorphisme et structurologie des argilites permiennes dans les Alpes-Maritimes (France). Rev. Géogr. Phys. Géol. Dyn., 22: 279—292.

Tullis, T.E., 1976. Experiments on the origin of slaty cleaveage and schistosity. Geol. Soc. Am. Bull., 87: 745—753.

Watterson, J., 1968. Homogeneous deformation of the gneisses of Vesterland, Southwest Greenland. Grønl. Geol. Unters. Bull., 78.

ANNEXE 7.

J.P. COGNE, H. PERROUD. **Strain removal applied to paleomagnetic directions in an orogenic belt : the permian red slates of the Alpes Maritimes,France.** Earth Planet.Sci. Let. 72, 125-140, 1985

Earth and Planetary Science Letters, 72 (1985) 125–140
Elsevier Science Publishers B.V., Amsterdam – Printed in The Netherlands

[5]

Strain removal applied to paleomagnetic directions in an orogenic belt: the Permian red slates of the Alpes Maritimes, France

Jean-Pascal Cogné and Hervé Perroud

C.A.E.S.S., Laboratoire de Géophysique Interne, Institut de Géologie, Université de Rennes I, Campus de Beaulieu, 35042 Rennes Cedex (France)

Received May 24, 1984
Revised version accepted October 2, 1984

Detailed investigations of relationships between strain and directions of characteristic remanent magnetization (ChRM) have been conducted on the Permian red series of the Alpes Maritimes, France. The analysis of the results obtained by structural and paleomagnetic studies on 14 sites leads to the following observations: in most sites, the mean direction of the strain shortening axis is close to the expected Permian paleomagnetic direction. In this case we observe a large scatter of the ChRM directions within each site, which is interpreted as an increase of an initial dispersion due to strain. Moreover this dispersion more or less increases with strain intensity. In other cases, where the angle between the shortening axis and the paleomagnetic direction is high, the whole population is deflected towards the cleavage (XY) plane. These observations lead us to assume a material line-like behaviour of the ChRM vectors and consequently an attempt has been made to recalculate these directions by strain removal. These calculations give positive results at two levels: (1) a statistically significant improvement in the clustering of the within-site distributions, and (2) after tilt correction, using unstrained bedding planes, a significant improvement in the clustering of the between-site distribution. The formation mean direction, after strain removal, is in good agreement with known Permian results for stable Europe.

1. Introduction

Since Runcorn [1] first demonstrated the opening of the Atlantic, using paleomagnetic data from North America and Europe, paleomagnetic methods have been widely used, mainly on a large scale, to contribute to the understanding of (1) the relative motions of the continents, and (2) apparent polar wander. More recently, attention moved towards the margins of the large plates, in order to understand the interactions between them. An increasing number of paleomagnetic studies has been done within the orogenic belts themselves, providing new constraints on tectonic evolution of mountain belts [2]. However, some special problems of deformation, metamorphism or overprinting arise in such areas, and great care is required in the interpretation of the data [3]. Up to now, the widely used "structural corrections" are in fact the familiar tilt corrections introduced by Graham [4] who compared the dispersion of data before and after rotation of the bedding plane about its strike line. More complex developments of this method have been applied for plunging fold axes [5,6] or fault rotations and have been reviewed by MacDonald [7], but all of them involve rigid rotations of blocks in which it is assumed that there is no plastic strain. However, strain has been considered as responsible for anomalous results, which show negative fold tests even though the magnetization is probably pretectonic [8] or as an alternative explanation to syntectonic remagnetization for scattered data [9]. For these reasons, penetratively deformed rocks are generally regarded as unsuitable for paleomagnetic work and very few quantitative studies have been carried out on this problem.

Nevertheless some laboratory experiments have

0012-821X/85/$03.30

been done on various synthetic samples, to study the magnetization behaviour during progressive strain. Kodama and Cox [10] did not show any coherent bias of the remanence with respect to the shortening axis; these results are thought to be due to the nature of the artificial sediment itself (kaolinite matrix) which showed a discontinuous deformation behaviour at the sample scale. On the other hand, Ozima [11] observed that "compressional plastic deformation of a Cu-Co alloy (...) resulted in a systematic rotation of remanent magnetization (IRM at H = 0.1 T) away from the axis of compression with increasing degree of the deformation". Morash and Bonhommet [12], working on hematite in a homogeneous plasticine matrix, obtained systematic rotation of the resultant IRM, the angle of rotation being close to that predicted for a macroscopic material line. Similarly, Blow and Hamilton [13] observed a significant shallowing of detrital remanent magnetization, acquired by tank redepositions of silty clay grade sediments during compactional loading. This can be attributed to vertical shortening. In this context, it would seem sensible to study the remanence behaviour in natural deformed series. The results presented here provide a tentative answer to the first question that can be asked: is there any coherent effect of plastic deformation on pretectonic remanent magnetization; in other words, does the pretectonic remanence behave like a macroscopic material line (see Appendix 1) during deformation?

To investigate this particular problem, the studied series must (a) have a pretectonic magnetization that can be recovered by magnetic analysis; (b) have good natural strain gauges in sufficient quantity.

Permian red shales and slates covering the Argentera Massif (Alpes Maritimes, France) have been chosen because they satisfy the above requirements (Fig. 1). A thick Permian sequence of sediments forms the autochthonous cover of the Argentera crystalline massif. The upper part (1 km thick) consists of red sandstones (Barrot Formation). A slight unconformity below the Werfenian quartzites points to a slight pre-Triassic deformation [14] but the main phase is of Alpine age [15]. Open to isoclinal folds show axial planar slaty cleavage. These red slates contain many ellipsoidal reduction spots and these good quality strain markers have been widely used in previous tectonic studies. Graham [16] made the first quantitative strain study in this area, revealing that strain increases from south to north. Interrelationships of deformation, metamorphism and textures were studied by Siddans [17] who concluded that illite recrystallisation during low-grade metamorphism was the predominant mechanism of cleavage development. Relationships of magnetic fabric and strain were investigated by Henry [18] and Kligfield et al. [19,20]. Paleomagnetic analysis has been done by Van Den Ende [8] within the undeformed part of the Dôme de Barrot. He determined a mean paleomagnetic direction for these series ($D = 205.5°$, $I = -13.5°$, $\alpha_{95} = 2.6°$) of Permian age and thus, the magnetization is actually pretectonic (prealpine), at least in the undeformed part of the formation.

2. Sampling and field measurements

Two sets of sites were sampled in the Barrot Formation (Fig. 1). The first set (group I) of nine sites (A to J) is distributed in the Dôme de Barrot [2] and along the Tinée [6] and Roya [1] valleys. Here the strain intensity increases from south to north. The other set (group II) of six sites (P1 to P6) is distributed throughout the two limbs and hinge of a 50-m-wide anticline (Fig. 2), in the Vionène valley, the most deformed part of this area (asterisk in Fig. 1c). In this fold, the finite strain intensity is roughly constant, but there are variations in the geometrical relationships of the bedding plane and principal directions of strain.

The scale of the sites was selected to ensure a good homogeneity of strain and bedding dip in each site, and was generally about 2 m × 2 m. 145 cores were drilled and oriented in-situ, and cut in the laboratory to yield 250 specimens. Field structural measurements were made at each site as follows: the axial ratios of the elliptical reduction spots were measured on at least two sets of perpendicular natural planes, as close as possible to the principal strain planes. Measurements of cleavage plane and lineations (bedding-cleavage inter-

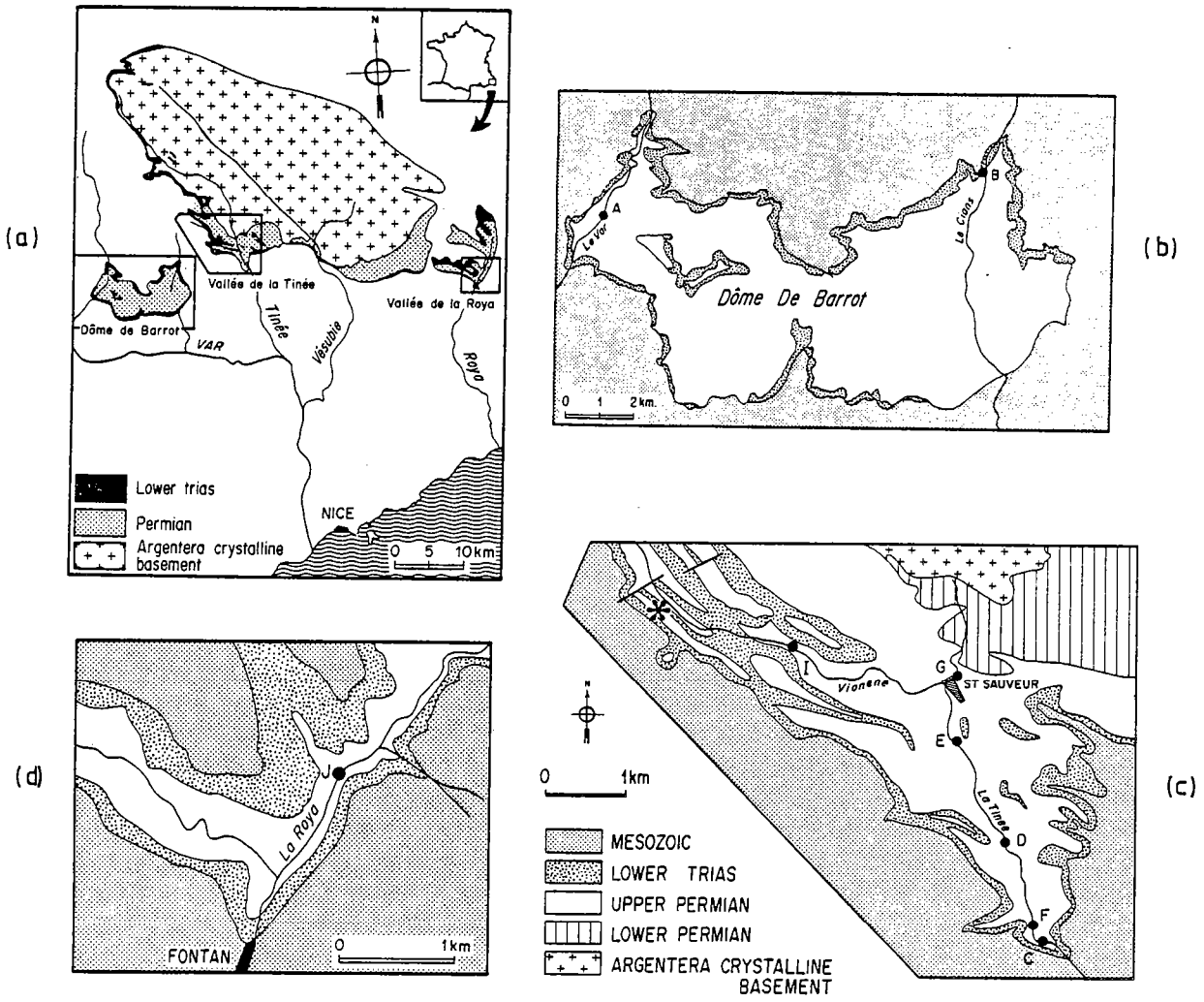

Fig. 1. (a) Location map of the main outcrops of Permian red shales and slates in the Alpes Maritimes. Sampling sites in (b) the Dôme de Barrot, (c) The Tinée and Vionène valleys, (d) the Roya valley. Asterisk in (c): group II sites.

section, stretching, etc.) give the orientation of the principal strain axes. In the most deformed sites, some difficulties arise with the determination of a bedding plane; as a matter of fact, the development of the slaty cleavage tends to erase the bedding plane and this surface may not be detectable in some times. Fortunately, the bedding trace is always marked by some green "reduction bands" on the other available planes (cleavage, joint planes, etc.). Plots of these traces on a stereogram give a mean bedding plane at every site studied.

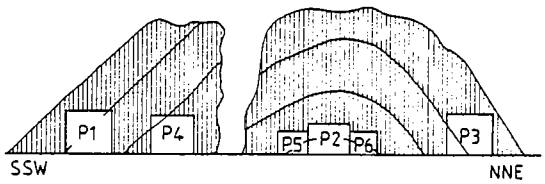

Fig. 2. Schematic cross-section through the fold in the Vionène valley showing the structural emplacements of the sites P1 to P6 (group II).

3. Strain analysis—results

Results of structural and strain measurements are summarized in Table 1. They allow us to determine a mean bedding plane and a mean strain tensor at each site as follows. The measurements of the axial ratios of the elliptical reduction spots are plotted on either a R_f/ϕ diagram [21,22] or a simple long-axis/short-axis diagram, depending on the angular fluctuations that may exist between the long axis and a reference line; this yield a mean strain ratio for each studied plane. Then, if we suppose no volume change ($\lambda_1 \cdot \lambda_2 \cdot \lambda_3 = 1$) we can calculate the elongation $\lambda_1 \geqslant \lambda_2 \geqslant \lambda_3$ along each axis. On the other hand, considering the cleavage plane as the XY finite strain plane, its pole is the orientation of minimum elongation axis Z and the stretching lineation is the maximum elongation axis X; the intermediate axis Y is orthogonal to the others to form a right-handed cartesian frame.

The results obtained here (Table 1) are consistent with previous ones obtained in this area [15,16,19,20]. In the undeformed southern part of the Dôme de Barrot (site A), ellipsoids are slightly flattened in the bedding ($\lambda_1 = \lambda_2 > \lambda_3$). Towards the north, strain intensity increases (Fig. 3). In the northern part of the Dôme de Barrot (site B), although cleavage is not present, ellipsoids are prolate ($\lambda_1 > \lambda_2 = \lambda_3$) with long axes trending about N110°; in the southern Tinée valley (site C) cleavage development, superposed upon a compactional fabric, produces a pencil structure and ellipsoids are prolate, with long axes parallel to bedding/cleavage intersection; moving towards the north, ellipsoids are flattened in the slaty cleavage, first triaxial ($\lambda_1 > \lambda_2 > \lambda_3$) with X parallel to the bedding/cleavage intersection (site F), then oblate ($\lambda_1 = \lambda_2 > \lambda_3$; sites D and E). Finally the ellipsoids return to a triaxial shape, with X parallel to the down-dip stretching lineation within the cleavage, in the most deformed sites (G, I). The Roya valley site(J) shows an intermediate stage of this sequence, equivalent to site F. The six sites of the fold show the most deformed state, similar to those of sites G and I.

From the strike and dip of axial planar slaty cleavage we can see that the Z-axis is generally subhorizontal with a general trend SSW-NNE, which is more or less parallel to the Permian paleomagnetic direction of the Dôme de Barrot.

TABLE 1

Mean orientations and strain

Sites	Bedding		Cleavage		X-axis		Principal strains		
	S	D	S	D	D	I	λ_1	λ_2	λ_3
A	181	10	–	–	–	–	1.193	1.193	0.702
B	242	5	–	–	305	5	1.368	0.855	0.855
C	72	25	90	90	90	8	1.478	0.869	0.778
D	105	30	285	64	–	–	1.339	1.339	0.558
E	46	45	264	61	–	–	1.546	1.546	0.418
F	96	37	102	90	102	4	1.915	1.063	0.491
G	340	26	295	78	324	66	2.629	1.143	0.346
I	317	26	295	67	353	13	2.098	1.499	0.318
J	73	46	276	44	89	11	1.643	1.369	0.444
P1	131	39	291	87	89	82	2.072	1.480	0.326
P2	149	15	300	82	72	79	1.789	1.361	0.410
P3	317	72	131	80	272	74	2.002	1.310	0.381
P4	139	39	299	87	91	84	1.894	1.388	0.380
P5	116	20	300	82	20	82	1.789	1.361	0.410
P6	304	23	300	82	17	82	1.789	1.361	0.410

S, D: strike, dip of bedding and cleavage planes, D, I: declination, inclination of X-axis.

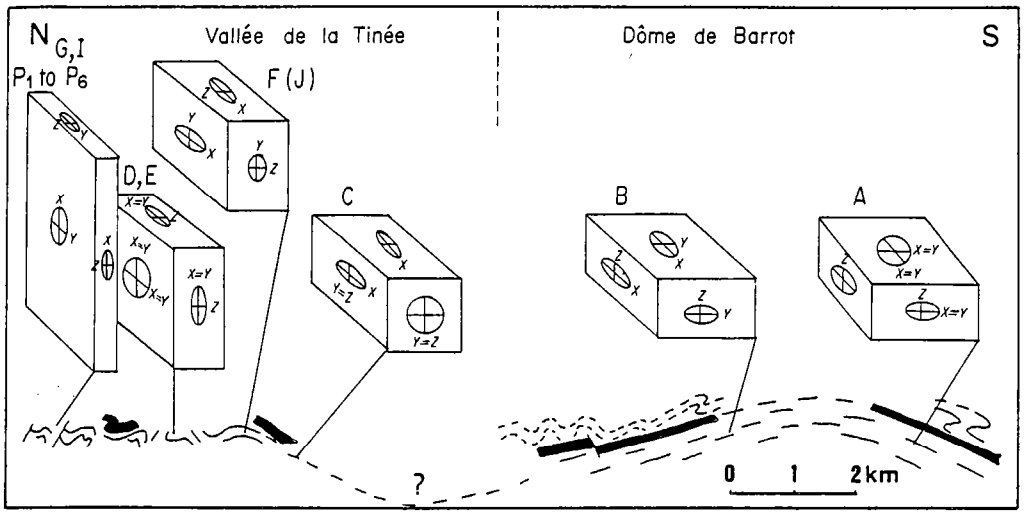

Fig. 3. Schematic cross-section through the Dôme de Barrot and the Tinée outcrops, with block-diagrams illustrating the increasing strain stages (after Graham [16]).

4. Paleomagnetic analysis

4.1. Laboratory techniques and measurements

All the magnetic measurements have been done with a computer-assisted Schonstedt DSM-1 spinner magnetometer of sensitivity $\sim 10^{-4}$ A m^{-1}. Progressive isothermal remanent magnetization (IRM) acquisition experiments have been performed with a Brucker BE-10 electromagnet (maximum field 1.25 T). Thermal demagnetization procedures have been carried out with a Schonstedt TSD-1 non-magnetic furnace in a mu-metal shield with a very low residual field of about 10 nT. For chemical demagnetization, samples were prepared by drilling a 1-cm diameter hole in order to increase the leaching surface [23,24]. On the other hand, uniform leaching of the sample was helped by the presence of cleavage planes that provided good diffusivity. The samples were then immersed in HCl in individual receptacles and left in a field-free space during increasing time steps. This was performed at room temperature and required a total time ranging from 600 to 1150 hours of leaching.

4.2. NRM

All 250 specimens were submitted to a short-period viscosity test [25]. 83% have a short-period viscosity coefficient lower than the 20% limit we have chosen as the maximum allowed value for our paleomagnetic investigations.

In-situ NRM directions are somewhat scattered but do not appear to show any significant present-day field overprinting (Fig. 4).

Tilt correction does not induce any improvement in these distributions either in the gradient population (group I) or in the fold (group II). So we have here an apparent paradox: on the one hand NRM directions are closed to the expected Permian direction (SW declination and shallow) and therefore should be considered as pretectonic; but on the other hand, tilt correction does not improve these distributions, which is normally characteristic of syn- to post-tectonic magnetizations. One possible reason for this is strain.

4.3. Thermal demagnetization

Thermal demagnetizations were carried out on 76 specimens and have shown single (Fig. 5a) or double (Fig. 5b) component NRM behaviour. In

130

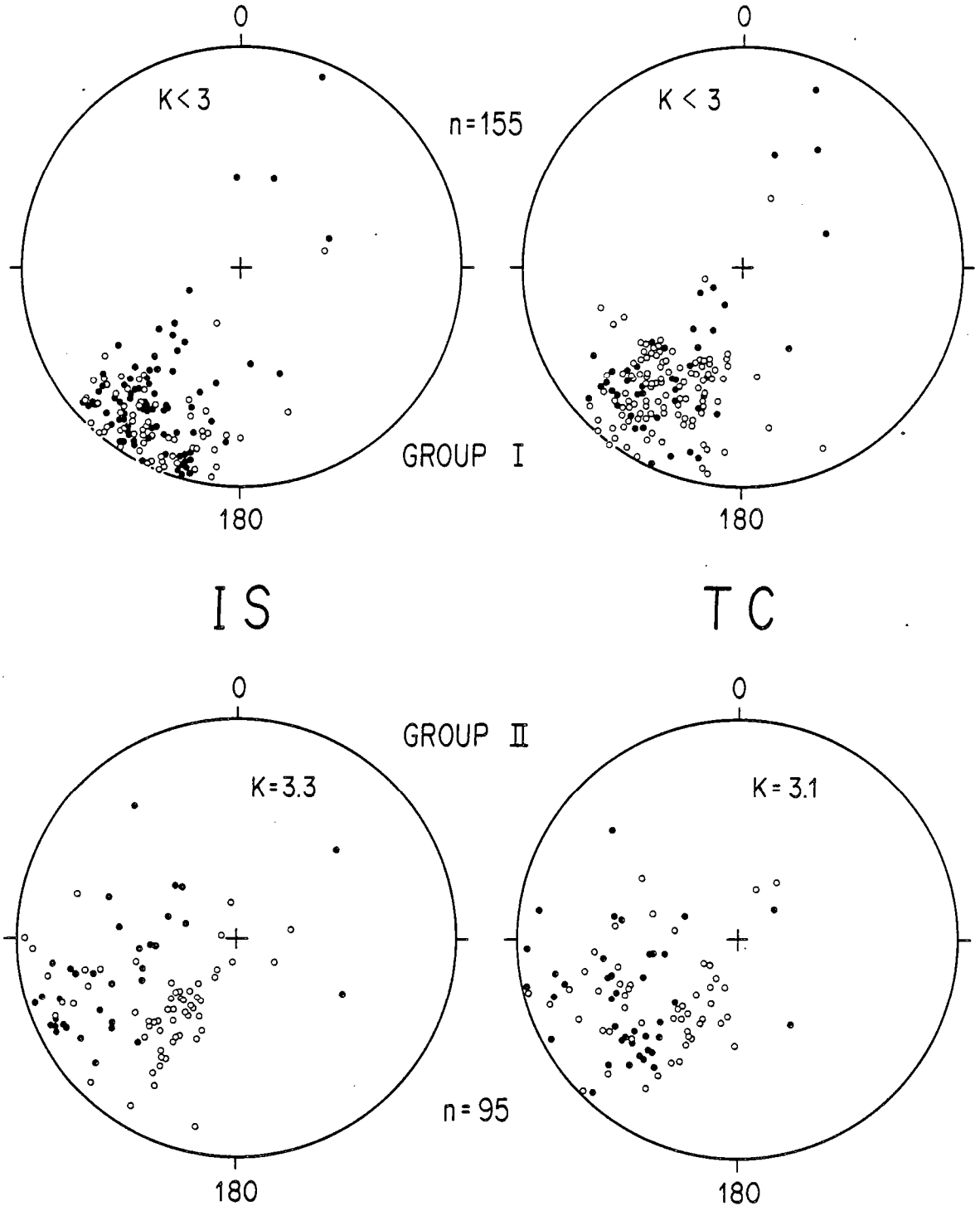

Fig. 4. NRM directions of the specimens of group I (top) and group II (bottom). IS: in-situ (left); TC: tilt-corrected (right). Open symbols: negative inclinations. Closed symbols: positive inclinations. Stereographic projections.

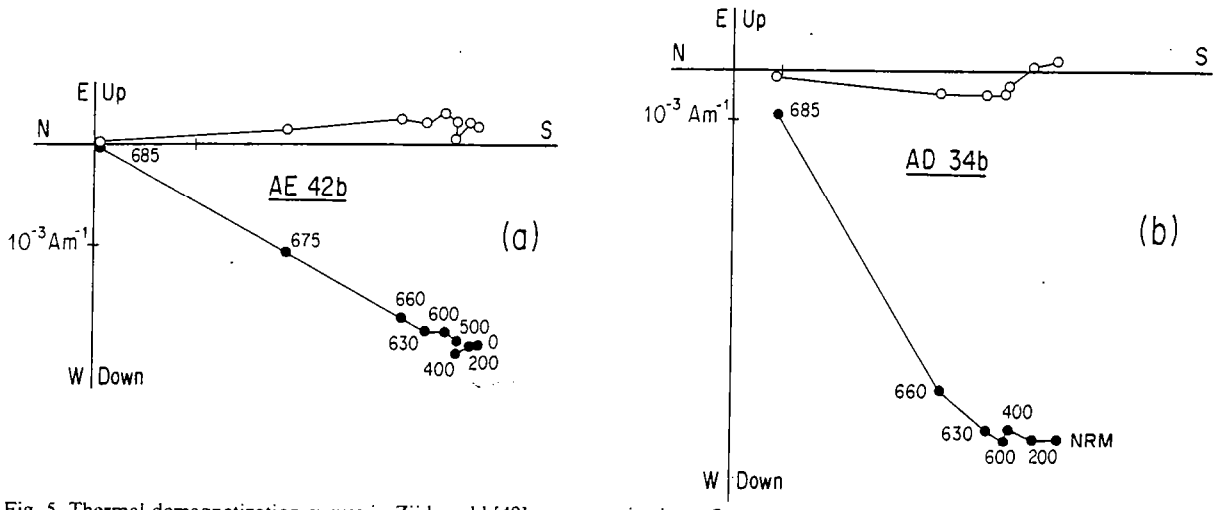

Fig. 5. Thermal demagnetization curves in Zijderveld [40] vector projections. Open symbols: projection of the vector end-points onto the vertical plane. Closed symbols: projection onto the horizontal plane. Temperature in °C is indicated.

the latter case, it was often impossible to separate the two components by this technique because of a nearly complete overlapping of the unblocking temperature spectra. This kind of data was treated by the great circle method [26]. Another problem especially present in the most deformed sites, was the appearance of strong viscous magnetization components in the higher-temperature steps of the procedure, that conceal the characteristic magnetization. Some IRM acquisitions performed on unheated and heated specimens [27] show the presence of a low-coercivity magnetic carrier (magnetic or maghemite) after annealing and an absence of this phase in the fresh specimens. Thus we appear to have magnetite production during the heating process as described by Dunlop [28]. When these mineralogical modifications occurred, we rejected the results from further consideration.

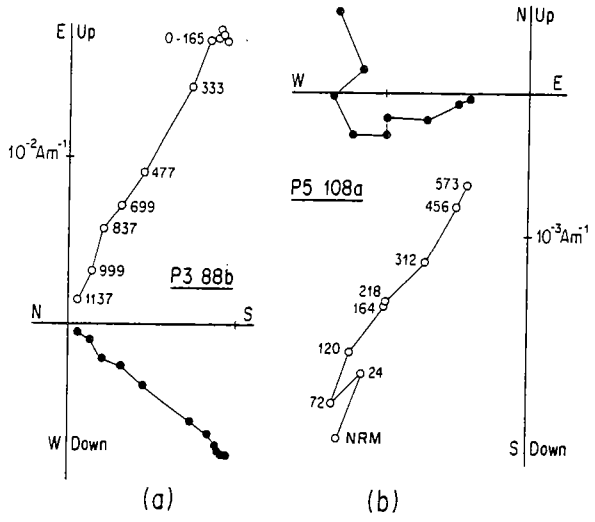

Fig. 6. Chemical demagnetization curves. Cumulative time of leaching is indicated in hours. Same conventions as in Fig. 5.

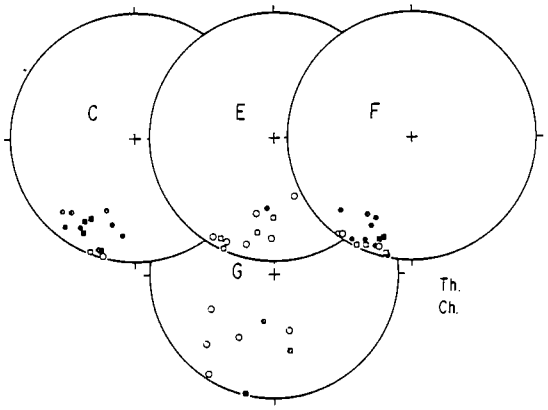

Fig. 7. In-situ ChRM directions obtained by thermal (circles) and chemical (squares) demagnetization in four sites of group I. Same conventions as in Fig. 4.

4.4. Chemical demagnetization

In order to isolate a characteristic component and to avoid mineralogical changes during heating, chemical demagnetization by hydrochloric acid was performed on 82 specimens. In this case, too, we observe either single (Fig. 6a) or double (Fig. 6b) component behaviour, but here the two components appear to be clearly separated during leaching. IRM acquisitions done on pairs of leached and non leached specimens [27] show that more than 90% of the magnetization is carried by a very high-coercivity phase, fine-grained hematite, so the NRM of these rocks is probably of chemical origin [29–31].

4.5. Summary of data obtained by demagnetization

Three kinds of magnetic behaviour have been recovered:

(1) Thermal demagnetization led to determination of remagnetization planes for each treated specimen (sites A and I). In this case, the mean direction of the site is determined by the intersection of the great circles, and an "ellipse of confidence" [32] is calculated. The very poor intersection determination from these great circles for site I (see Table 2) render this site unusable.

(2) Characteristic remanent magnetization (ChRM) directions have been isolated either by thermal demagnetization (site J) or by chemical demagnetization (sites P1 to P6) or by the two techniques (sites C, E, F, G). In the latter case the populations obtained by the two techniques are nearly identical (Fig. 7).

(3) When both ChRM directions and great circles have been determined (sites B and D), we have two estimates of the mean paleomagnetic direction of the site, one by Fisher statistics on the ChRM directions, and the other by great circles intersection. A final mean direction is calculated by averaging these two estimates.

TABLE 2

In-situ (IS) and tilt-corrected (TC) mean directions after chemical and thermal demagnetization

Sites	N	IS		TC		k	α_{95}
		D	I	D	I		
A	9	195	−4	194	−6	(p = 15	r = 9)
B	11	213	−15	212	−12	21	13.0
C	14	205	10	205	−8	39	6.5
D	15	215	10	216	−18	22	10.0
E	12	193	−9	208	−29	15	11.5
F	16	204	5	206	−29	50	5.3
G	8	202	−7	202	11	4	29.5
(I	7	223	31	-	-	p = 35	r = 9)
J	9	211	−1	222	−29	14	14.0
P1	8	210	0	207	−40	4	30.0
P2	12	207	−26	202	−39	25	9.0
P3	9	210	−57	217	13	50	7.5
P4	7	242	−2	246	−39	25	9.0
P5	8	235	13	234	−5	10	18.5
P6	8	232	4	234	26	10	18.5
Group I (A–J)	8 k = 45, α_{95} = 8.5	205	−1.5	208 k = 24.5, α_{95} = 11.5	−15		
Group II (P1–P6)	6 k = 7.5, α_{95} = 26	224	−11	224 k = 6, α_{95} = 29.5	−15		

k, α_{95}: parameters of Fisher statistics; p, r: 1/2 angles of the "ellipse of confidence". The results of the site I are not taken into account in the calculation of the means.

5. Results—analysis of the ChRM directions

5.1. Group I (gradient sites)

From the results obtained by demagnetization (Table 2), two main conclusions can be drawn. First, the within-site dispersions remain rather high after demagnetization, with always low values of k. This contrasts with the results obtained on undeformed beds [8]. Although these directions look like Permian magnetizations, tilt corrections do not produce any improvement in the between site dispersion.

The fact that the regional trend of shortening axis (Z) of the strain ellipsoid is subhorizontal in a SSW direction (i.e., more or less parallel to the pretectonic magnetization vector for the undeformed part of the series (Dôme de Barrot)) suggests that the large observed within-site dispersion represents an increase of the initial dispersion, due to a shortening the axis of which is close to the mean of the vectors population.

To check this interpretation, the paleomagnetic data have been compared with a simple numerical model. The modeling conditions are as follows:

(1) The calculations are done on fictitious sets of vectors, each having a Fisherian distribution characterized by the usual statistical parameters (k, α_{95}) [33].

(2) We apply an axisymmetric strain to the vectors.

(3) The shortening axis is exactly parallel to the initial mean direction of each population.

(4) The vectors behave as material lines under strain (see Appendix 1).

(5) Strain intensity, estimated by the parameter $r = \lambda_1/\lambda_2 + \lambda_2/\lambda_3 - 1$ [41] is incremented by regular coaxial steps until $r = 5$.

(6) At each strain step, the mean of each population is recalculated with its statistical parameters.

These calculations performed on four populations with different initial value of k (14.5, 39, 70, and 125) give the following results:

(1) The mean direction of each population stays parallel to the Z axis.

(2) There is a rapid decay of the Fisher k parameter with increasing r (Fig. 8). In other words, the dispersion of a vectors population under these conditions becomes rapidly large, even for relatively small strain intensities.

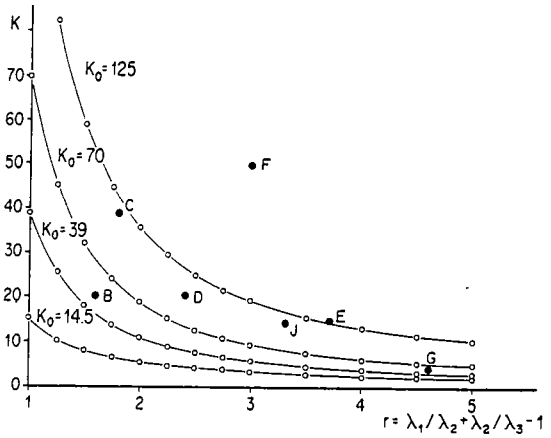

Fig. 8. Curves of modeled behaviour of Fisher's k parameter as a function of strain intensity r [41]. Black dots are real parameters of the group I sites.

With one exception (site F), the real paleomagnetic and structural data for each of the eight sites B to J show a good fit with calculated curves for an initial population of k parameters in the range 50–100, which is the usual value for this kind of rock. In nature, there is probably seldom any true parallelism between pretectonic mean direction of magnetization and shortening axis, and moreover the strain is not uniaxial. Nevertheless, this model may explain the within-site dispersions.

5.2. Group II (fold sites)

Although chemical demagnetization allowed us to isolate a stable component for each treated specimen, the dispersions remain very high except for site P3 (Table 2; Fig. 9). In this field, characteristics and intensities of strain are more or less identical from site to site but we have variations in the angles between the strain axes and the bedding plane, in other words, variables angles between the shortening axis and the pretectonic magnetization. It is possible to find, as before, a coherent attitude of paleomagnetic data with respect to strain directions. Comparison of the data shows that in sites P1 and P4 from the southern limb (see Fig. 2).

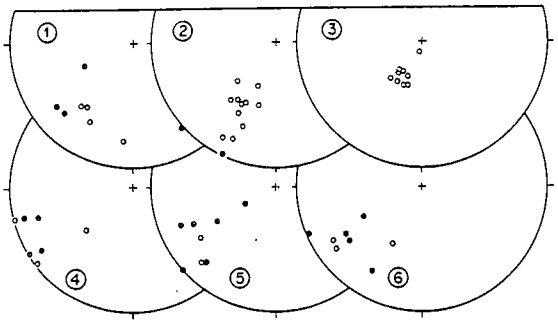

Fig. 9. In-situ ChRM directions obtained by chemical demagnetization in the six group II sites. Same conventions as in Fig. 4.

there exists a large scatter of paleomagnetic data (with k values respectively 4 and 7), as well as in sites P2, P5, P6 from the hinge; this high scatter is consistent with the low angle between the Z-axis and the expected mean pretectonic magnetization direction, as observed in the group I sites; in contrast, in site P3 of the northern limb, where this angle is much higher, scatter remains small in the observed state ($k = 50$), but there is a deviation of the whole population away from the shortening axis, towards steep upwards inclinations.

As mentioned above, a simple tilt correction does not bring any improvement in the clustering of the site-mean directions. This is due to the fact that the site-mean directions of the two limbs bypass each other during unfolding (Fig. 10). This type of situation is classically attributed to a syn-

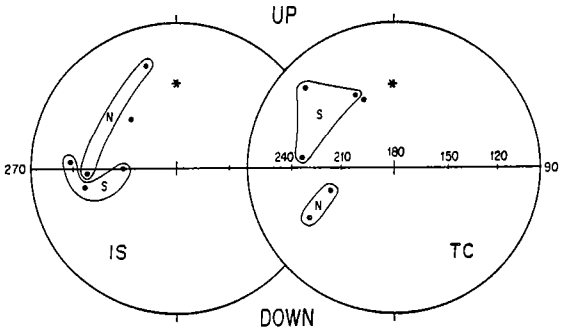

Fig. 10. Site-mean ChRM directions of group II in a vertical stereographic projection. Dots are contoured depending on their southern (S) or northern (N) limb site position. IS: in situ; TC: tilt-corrected; asterisk: recent field axis (reverse polarity). Closed symbols in the southern hemisphere.

tectonic origin of magnetization. However, this cannot be the case here, because the Tertiary age of the deformation would imply a remagnetization field close to the Tertiary field and yet somewhere between the directions of the two limbs, which is not at all the case. Instead the directions are distributed around a Permian field direction. We suggest therefore that strain induces a deviation of the initial magnetization. In a general way, strain has to be considered as an alternative interpretation for magnetic data which show this kind of by-passing upon unfolding.

5.3. Conclusions

(1) When it is possible to isolate a stable ChRM direction in each specimen, these directions are generally scattered within the deformed sites.

(2) This dispersion shows an increase with strain when the shortening direction is close to the paleomagnetic one.

(3) When the angle between the Z-axis and the theoretical pretectonic mean paleomagnetic direction is higher, the within-site dispersion seems to remain unaffected, but the whole population is deviated towards the cleavage (XY) plane.

Thus the behaviour of the paleomagnetic vectors population studied here is similar to the behaviour of passive vectors under strain. In order to test this hypothesis, and to recover a mean paleomagnetic direction consistent with the Permian direction of Stable Europe, the effects of strain have been removed from each ChRM direction.

6. Strain removal

6.1. Principle

The analysis of deformation is a geometrical description of the transformation from an initial state to a deformed state. This description, which is totally independent of the mechanism and the path of deformation, is mathematically decomposed into (a) strain (i.e., changes in relative positions of points, (b) rigid-body rotation, and (c) rigid body translation. The latter is generally not

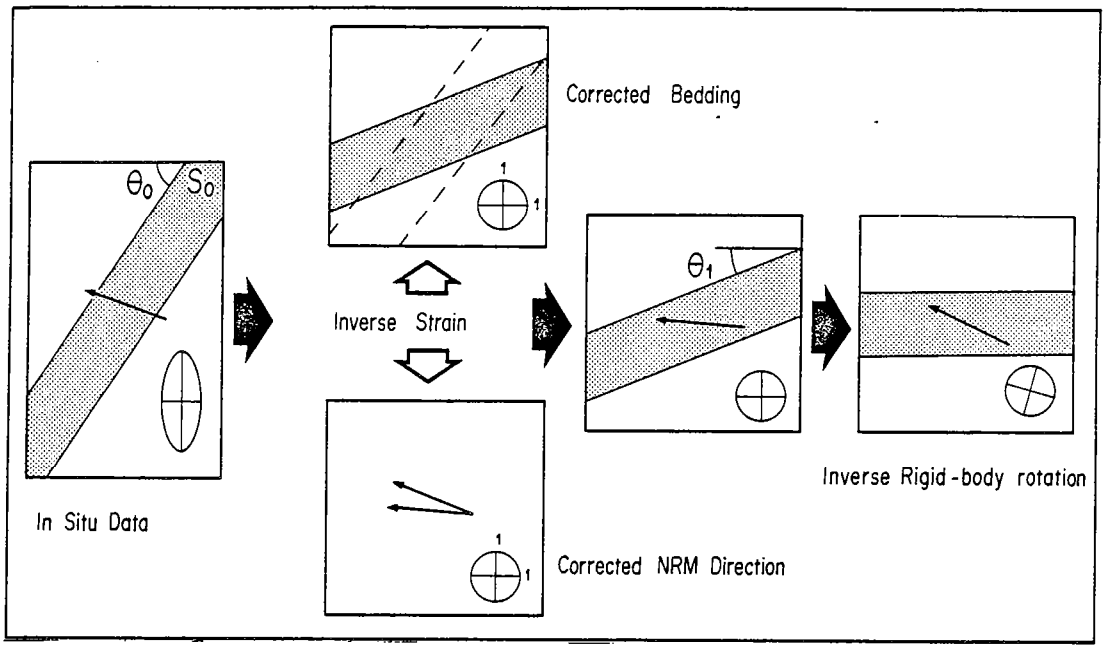

Fig. 11. Schematic sketch of strain removal. From the in-situ paleomagnetic and strain data, both vectors and planes are corrected for strain. Then the inverse rigid-body rotation is done by tilt correction from the unstrained bedding plane.

easy to detect and does not affect paleomagnetic vectors; therefore, it will no longer be considered here. Consequently, total deformation has been removed from the ChRM vectors in two steps (Fig. 11):

(1) First, according to theoretical relationships

TABLE 3

Mean-site and mean-group directions after strain removal and tilt correction from the unstrained bedding plane with the results of the test $k_2 > k_1$

Sites	N	D	I	k	α_{95}	k_{SR}/k_{IS}	F	Test
A	9	194	−11	($p=15$	$r=9$)			
B	4	213	−12	36	13.0	1.70	4.28	?
C	14	194	−8	67	4.9	1.73	1.92	?
D	7	204	−9	82	5.0	4.45	2.69	+
E	12	180	−11	78	4.9	5.03	2.05	+
F	16	196	−16	351	2.0	7.02	1.84	+
G	8	204	−1	44	8.5	9.78	2.48	+
J	9	196	−16	45	7.8	3.08	2.29	+
P1	8	205	−7	125	5.0	31.25	2.48	+
P2	12	208	−11	193	3.0	7.72	2.05	+
P3	9	221	6	115	5.0	2.30	2.29	+
P4	7	217	−9	174	4.5	10.23	2.69	+
P5	8	218	−0.5	96	5.7	9.60	2.48	+
P6	8	217	7	107	5.5	10.70	2.48	+
Group I	8	198.0	−10.5	59	7.5			
Group II	6	214.5	−2.5	65.5	8.0			

k_{SR}/k_{IS}: k ratios for strain removed and in-situ directions; F: value of the Fisher-Snedecor table at the 5% level for the $2(N-1)$, $2(N-1)$ degrees of freedom.

136

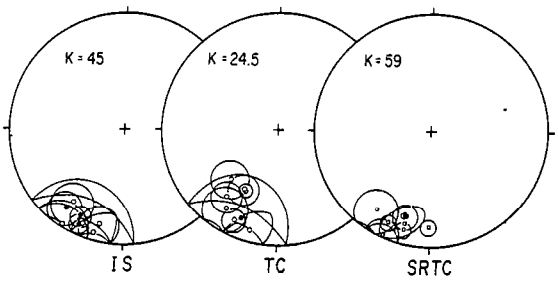

Fig. 12. Group I: site-mean directions with their circles of confidence. IS: in-situ; TC: tilt-corrected; SRTC; after strain removal and tilt correction from the unstrained bedding plane. The Fisher k parameters refer to the between-site dispersions.

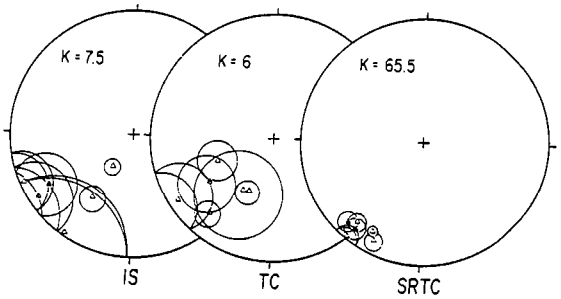

Fig. 13. Group II: site-mean directions with their circles of confidence. Same abbreviations and conventions as in Fig. 12.

between initial and final positions of a passive line under strain (see Appendix 1) the inverse strain tensor S^{-1} has been used to recalculate the initial direction of the ChRM of each specimen, without any rigid-body rotation.

(2) The mean strike and dip of the bedding plane of each site has always been determined by using surfaces with no rheological contrast with the layers where reduction spots were measured. In this case, bedding plane can be considered as a passive plane during deformation and thus, the observed strike and dip of these planes is the result of the superposition of a rotationnal part due to strain and a rigid-body rotation. Consequently, the strain was also removed from the bedding plane (see Appendix 1). The residual strike and dip of the recalculated plane (so-called "unstrained bedding plane") was considered as the part of rigid-body rotation which is associated with the total deformation. Inverse rigid-body rotation of the ChRM vectors was then performed by bringing the recalculated bedding plane of the site to the horizontal with a classical tilt correction (rotation about the strike line, of an angle equal to the dip).

Mean directions of the two groups are given in Table 2 for in-situ and tilt-corrected directions and in Table 3 after strain removal and tilt correction from the unstrained bedding plane. These data for the three stages are illustrated Fig. 12 for group I and in Fig. 13 for group II.

6.2. *Effect of strain removal on within-site dispersions*

Strain removal performed on ChRM vectors induces a general displacement of each vector towards the Z-axis of the site. Because in most of our sites the Z-axis is close to the mean of the paleomagnetic vector population there is a general decrease of the within-site dispersions (Table 3). For the sites distributed along the gradient (group I), the improvement in the clustering, reflected by the k_2/k_1 ratios, begins to be significant in a statistical sense after the pencil structure stage (site C), and increases towards the north with the strain intensity. The increase of the k_2/k_1 ratios, due to the increase of the inverse strain intensities applied to the directions, is to be related to the general decrease of the k values of observed in-situ ChRM directions along the gradient (group I), reported above. For the six sites of the fold (group II), the improvement in the within-site clustering is always statistically significant but one can notice that the value of the k_2/k_1 ratios depends upon the angle between the strain axes and the paleomagnetic direction (site P3: 2.3, site P1: 31.2)

The behaviour of the vector populations under strain removal is illustrated by the reduction of the circles of confidence in Figs. 12 (SRTC) and 13 (SRTC).

Starting from within-site distributions, which were in some cases almost unsuitable for paleomagnetic purposes, strain removal allows us to improve these distributions, and this first step of the treatment may be considered as quite positive.

6.3. *Between-site dispersion*

The second step which consists of a tilt correction from the unstrained bedding plane of each

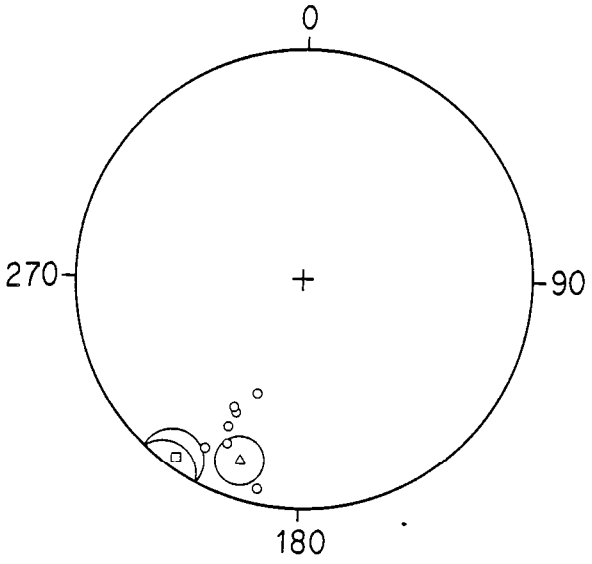

Fig. 14. Group I (triangle) and group II (square) means compared with seven Permian directions (circles) recalculated for the Argentera sites from the poles of Stable Europe [34].

site, gives us further control on the directions recovered by strain removal. Comparison of the site-mean statistics at the three-different stages (Tables 2 and 3) for group I and II shows an improved clustering of the directions after this inverse rigid-body rotation. This improvement is statistically significant with respect to simple tilt correction for group I data (k goes from 24 to 59; $n = 8$) and to both in-situ and tilt-corrected data for group II (k from 7 and 6 to 65; $n = 6$). Furthermore, the mean paleomagnetic directions from the two groups (Fig. 14) show a very good fit with the directions recalculated for the Alpes Maritimes red bed location using the seven most reliable Permian poles of Stable Europe, as reviewed by Van der Voo et al. [34].

This second step of the treatment appears to be positive for the clustering of the between-site distributions as well as for the improvement of the paleomagnetic direction accuracy. It is also the most significant since it is not controlled as strongly as the first step by the shortening axis.

7. Summary of the analysis

The observations arising from this study are the following:

(1) The "primary" chemical remanent magnetization acquired by the Permian red beds of the Alpes Maritimes before deformation undergoes an important deviation during the Alpine deformation of these rocks.

(2) This deviation shows a coherence with respect to the strain axes that is reflected by (a) a large scatter of the within-site populations of paleomagnetic vectors, which increases with strain intensity, when the angle between the shortening Z-axis and the initial mean direction of the population is low; (b) a deviation of the whole population when this angle is higher.

(3) The deviation which can tentatively be correlated with hematite reorientations during deformation, as shown by texture goniometry [27], shows similarities with macroscopic material lines behaviour. Therefore, an attempt has been made to recalculate pretectonic directions of magnetization by strain removal using the theoretical equations for deformation involving passive lines and planes.

Recalculating each individual ChRM direction by using the inverse strain tensor determined at each sampling site, we obtain positive results at two levels: (a) First, the particular relationships between the Z-axis and mean paleomagnetic direction lead to an improvement in the clustering of the population at the site and thus, to an improvement in the site mean direction; (b) after inverse rigid-body rotation by tilt correction from the undeformed bedding plane, the overall mean directions of the two groups of sites show good consistency with known Permian paleomagnetic directions of Stable Europe [34], with good statistical quality parameters.

8. Discussion

Strain removal technique applied to remanent magnetization vectors [35,36] has been partly used by Kligfield et al. [20] on their data obtained from the same rocks. These authors observe an important improvement in the within-site clustering of the ChRM directions during strain removal. Based on the fact that under inverse strain, passive markers inevitably move towards the shortening

Z-axis, they conclude to a probably large computing effect.

In our opinion, the most important observations are (a) the coherence of the angular deviation of the ChRM vectors with respect to the strain axes directions and intensity, and (b) the agreement with the inferred initial magnetization direction. Therefore, the strain may be considered as responsible for the scatter of the data. Thus, the observed improvement in the within-site distributions during strain removal may no longer be regarded as only a computing effect, even if there is a possible over correction, as far as we cannot be sure of the exact passive behaviour of the vectors. On the other hand, the decomposition of total deformation into strain and rigid-body rotation is a geometrical notion which is not necessary related to the natural processes involved in folding and cleavage development. Therefore, strain removal techniques should include inverse rigid-body rotation. This is only with this second step which has shown positive results in the improvement of between-site distributions, that the treatment may be regarded as fully positive. These results lead us to assume that strain measured in the field gives us a good estimation of the corrections to apply to the ChRM vectors.

In spite of all the points that are to be investigated, these promising results show that it seems possible to use paleomagnetic directions as markers not only of rigid rotations and translations of plates or microplates, but also when plastic deformation occurs.

Acknowledgements

We thank Dr. P.R. Cobbold for helpful discussions.

This is a contribution of L.P. C.N.R.S. No. 4661; the work was supported by the French CNRS and Institut National d'Astronomie et de Géophysique through the National Research Project ATP Geodynamique.

Appendix 1

Macroscopic material line behaviour under strain [37]

A material line is defined to join two material points P_1 and P_2 the vector positions of which are, in a convenient cartesian coordinate system, r_1 and r_2. Thus the line is defined by the vector difference:

$$l = r_1 - r_2$$

The change in position of points P_1 and P_2 under a homogeneous strain (neglecting rigid-body rotation and translation) leads to new vector positions r_{f_1} and r_{f_2} related to the initial r_{i_1}, r_{i_2} by (f: final, i: initial):

$$r_f = S \cdot r_i,$$

where S is a symmetric (strain) tensor. The material line joining the two points is then defined by the vector difference:

$$l_f = r_{f_1} - r_{f_2} = S \cdot r_{i_1} - S \cdot r_{i_2}$$
$$= S \cdot (r_{i_1} - r_{i_2}),$$
$$l_f = S \cdot l_i$$

So the change in length and coordinates of a material line is directly related to its initial length and coordinates and to the strain tensor S.

With respect to the chosen coordinate system, the cartesian components of S are (using the summation convention):

$$S_{ij} = a_{ik} \cdot a_{jm} \cdot S'_{km} \qquad (i, j, k, m = 1, 2, 3)$$

where S' is the matrix of the three eigenvalues of S and is of the form:

$$S' = \begin{bmatrix} 1+e_1 & 0 & 0 \\ 0 & 1+e_2 & 0 \\ 0 & 0 & 1+e_3 \end{bmatrix}$$

e_i: elongation along each axis and a_{ij} are the direction cosines of the three eigenvectors in the chosen reference frame.

Knowing the coordinates of the vector defining a material line in the deformed state, the initial coordinates can be calculated in the same way by using the inverse strain tensor:

$$l_i = S^{-1} \cdot l_f$$

where

$$S_{ij}^{-1} = a_{ik} \cdot a_{jm} \cdot S'^{-1}_{km} \qquad (i,j,k,m = 1,2,3)$$

Material plane behaviour [38,39]

We define n_i (n_f) as the normal to the initial (final) plane and l_i (l_f) as a vector within the initial (final) plane.

l and n are at right angle, thus their scalar product is:

$$n_i \cdot l_i = n_f \cdot l_f = 0$$

from equations above, we have $l_f = S \cdot l_i$ so:

$$n_i \cdot l_i = n_f \cdot S \cdot l_i$$

$$n_i = S^T \cdot n_f$$

where S^T is the transpose of S; S is a symmetrical tensor, therefore:

$$n_i = S \cdot n_f$$

So initial coordinates of the normal to a passive plane are recovered by multiplying the strain tensor to the final (observed) normal coordinates.

References

1 S.K. Runcorn, Paleomagnetic comparisons between Europe and North America, Proc. Geol. Assoc. Can. 8, 77–85, 1956.

2 R. Van der Voo and J.E.T. Channel, Paleomagnetism in orogenic belts, Rev. Geophys. Space Phys. 18 (2), 455–481, 1980.

3 H. Perroud, Contribution a l'étude paléomagnetique de l'arc ibéroarmoricain, Bull. Soc. Geol. Mineral. Bretagne C, XIV, 1–114, 1982.

4 J.W. Graham, The stability and significance of magnetism in sedimentary rocks, J. Geophys. Res. 54, 131–167, 1949.

5 N. Bonhommet, P.R. Cobbold, H. Perroud and A. Richardson, Paleomagnetism and cross-folding in a key-area of the Asturian arc (Spain), J. Geophys. Res. 86. 1873–1887, 1981.

6 H. Perroud and P.R. Cobbold, L'aimantation rémanente comme marqueur de la déformation: example d'un pli a axe incliné dans les séries rouges siluro-dévoniennes a Cabrillanes, Asturies (Espagne), Bull. Soc. Geol. Fr. XXVI, 1, 169–184, 1984.

7 W.D. MacDonald, Net tectonic rotation and the structural tilt correction in paleomagnetic studies, J. Geophys. Res. 85, 3659–3669, 1980.

8 C. Van den Ende, Paleomagnetism of Permian red beds of the Dôme de Barrot (S. France), 171 pp., Thesis, Utrecht, 1977.

9 H. Perroud, Paleomagnetism of Paleozoic rocks from the Cabo de Penas, Asturia, Spain, Geophys. J. R. Astron. Soc. 75, 201–215, 1983.

10 K.P. Kodama and A. Cox, The effects of constant volume deformation on the magnetization of an artificial sediment, Earth Planet. Sci. Lett. 38, 436–442, 1978.

11 M. Ozima, Effects of a plastic deformation on the remanent magnetization of Cu-Co alloy, Earth Planet. Sci. Lett. 47, 121–123, 1980.

12 A. Morash and N. Bonhommet, Deviation of I.R.M. during simple shortening experiments, Abstr. 4th IAGA Sci. Assem. Edinburgh, 113-12, 252, 1981.

13 R.A. Blow and M. Hamilton, Effect of compaction on the acquisition of a detrital remanent magnetization in fine-grained sediments, Geophys. J. R. Astron. Soc. 52, 13–23, 1978.

14 R.H. Graham, Wrench faults, arcuate fold patterns and deformation in the southern French Alps, Proc. Geol. Assoc. 89, 125–142, 1978.

15 A.W.B. Siddans, Arcuate fold and thrust pattern in the Subalpine Chain of Southeast France, J. Struct. Geol. 1 (2), 117–126, 1979.

16 R.H. Graham, Quantitative deformation studies in the Permian rocks of the Alpes Maritimes, Proc. Symp. in Honour of Prof. J. Goguel, Mem. B.R.G.M. 91, 219–238, 1978.

17 A.W.B. Siddans, Compaction, métamorphisme et structurologie des argilites permiennes dans les Alpes Maritimes (France), Rev. Geol. Dynam. Géogr. Phys., 22, 279–292, 1980.

18 B. Henry, Studies of microtectonics, anisotropy of magnetic susceptibility and paleomagnetism of the Permian Dôme de Barrot (France). Paleomagnetic and paleosedimentological implications, Tectonophysics 17, 61–72, 1973.

19 R. Kligfield, W.H. Owens and W. Lowrie, Magnetic susceptibility anisotropy, strain and progressive deformation in Permian sediments from the Maritime Alps (France), Earth Planet. Sci. Lett. 55, 181–189, 1981.

20 R. Kligfield, W. Lowrie and A. Hirt, Effect of progressive deformation on remanent magnetization of Permian Red Beds from the Alpes Maritimes (France), Tectonophysics 97, 59–85, 1983.

21 D. Dunnet, A technique of finite strain analysis using elliptical particles, Tectonophysics 7, 117–136, 1969.

22 D. Dunnet and A.W.B. Siddans, Non-random sedimentary fabrics and their modifications by strain, Tectonophysics 12, 307–325, 1971.

23 J.K. Park, Acid leaching of red beds and the relative stability of red and black magnetic components, Can. J. Earth Sci. 7, 1088–1092, 1970.

24 S.G. Henry, Chemical demagnetization: methods, procedures and applications through vector analysis, Can. J. Earth Sci. 16, 1832–1841, 1979.

25 E. Thellier and O. Thellier, Sur l'intensité du champ magnétique terrestre dans le passé historique et géologique, Ann. Geophys. 15(3), 285–376, 1959.

26 H.C. Halls, A least-squares method to find a remanence direction from converging remagnetization circles, Geophys. J. R. Astron. Soc. 45, 297–304, 1976.

27 J.P. Cogné, Etude paleomagnétique et déformation inverse de l'aimantation de séries naturelles déformées, 108 pp., Thèse 3e cycle, Rennes, 1983.
28 D.J. Dunlop, Magnetic mineralogy of unheated and heated red sediments by coercivity spectrum analysis, Geophys. J. R. Astron. Soc. 27, 37–55, 1972.
29 J.G. MacPherson, Genesis of variegated red beds in the fluviatil Aztec siltstone (late Devonian) southern Victoria Land, Antarctica, Sediment. Geol. 27, 2, 119–142, 1980.
30 R.D. Elmore and R. Van der Voo, Origin of hematite and its associated remanence in the Copper Harbour conglomerate (Keweenawan), Upper Michigan, J. Geophys. Res. 87, 10918–10928, 1982.
31 T.R. Walker, E.E. Larson and R.P. Hoblitt, Nature and origin of hematite in the Moenkopi Formation (Triassic) Colorado Plateau: a contribution to the origin of magnetism in red beds, J. Geophys. Res. 86, 317–333, 1981.
32 M. Westphal, Analyse statistique de directions non-orientées, Pageoph, 119, 80–81, 1981.
33 R.A. Fisher, Dispersion on a sphere, Proc. R. Soc. London, Ser. A 217, 295–305, 1953.
34 R. Van der Voo, J. Peinado and R.S. Scotese, A paleomagnetic reevaluation of Pangea reconstructions, Geodynamics 12, 11–26, 1984.
35 J.P. Cogné, N. Bonhommet and P.R. Cobbold, Pretectonic magnetization obtained by strain removal EGS-ESC Meet., Leeds, August 1982, EOS Trans. Am. Geophys. Union 63, 51, 1982.
36 J.P. Cogné, Pretectonic direction of magnetization recovered by strain removal, The example of a fold in red sediments of the Alpes Maritimes (France), 2nd EUG Meet., Strasbourg, March 1983, Terra Cognita 3, 107, 1983.
37 P.R. Cobbold, Compatibility equations and the integration of finite strain in two dimensions, Tectonophysics 39, T1–T6, 1977.
38 W.H. Owens, Strain modifications of angular density distributions, Tectonophysics 16, 249–262, 1973.
39 M.N. Percevault, Problème inverse en déformation finie. Applications au segment hercynien de Bretagne centrale, 137 pp., Thèse 3e cycle, Rennes, 1983.
40 J.D.A. Zijderveld, Demagnetization of rocks: analysis of results. in: Methods in Paleomagnetism, D.W. Collinson, K.M. Creer and S.K. Runcorn, eds., pp. 254–286, Elsevier, Amsterdam, 1976.
41 J. Watterson, Homogeneous deformation of the gneisses of Westerland, Southwest Greenland, Grønl. Geol. Unters. Bull. 78, 1968.

ANNEXE 8.

J.P. COGNE. **Paleomagnetic direction obtained by strain removal in the Pyrenean Permian redbeds at the "Col du Somport" (France).** Earth Planet. Sci. Lett., 85, 162-172, 1987.

Earth and Planetary Science Letters, 85 (1987) 162–172
Elsevier Science Publishers B.V., Amsterdam – Printed in The Netherlands

[4]

Paleomagnetic direction obtained by strain removal in the Pyrenean Permian redbeds at the "Col du Somport" (France)

J.P. Cogné

C.A.E.S.S., Laboratoire de Géophysique Interne, Université de Rennes 1, Campus de Beaulieu, 35042 Renes Cedex (France)

Received February 17, 1987; revised version accepted June 17, 1987

In order to investigate the possibility and limitations of paleomagnetic works within strained regions, a paleomagnetic study, related with strain analysis has been conducted in the deformed Pyrenean Permian redbeds in the "Col du Somport" area. Paleomagnetic sampling together with strain estimates have been conducted in 6 sites through a fold. The results obtained by measuring the orientation and axial ratios of elliptical reduction spots show that (1) the shale beds have undergone a penetrative strain, (2) the sandy beds can be regarded as tectonically unstrained with reduction spots flattened in the bedding, showing that they recorded the compaction. It is shown that the total strain recorded in the slaty beds probably results from the superimposition of tectonic strain upon the compaction fabric. The paleomagnetic study shows that the primary pretectonic magnetization is widely overprinted by a secondary syn- or post-tectonic magnetic component. As both components appear to be carried by hematite pigment, their separation using classical demagnetization procedures has been difficult. A characteristic remanent magnetization (ChRM) has however been determined, when possible, as the hardest component in demagnetization curves. Then, the ChRM direction distributions are represented in stereographic density plots. Although these ChRM directions exhibit a clear tendency towards SE declinations and shallow inclinations, characteristic of Permian paleomagnetic field direction for the Iberian plate, the tilt correction does not induce a clustering of these directions. Strain is inferred to be responsible for this situation. Assuming that both pretectonic magnetization directions and bedding planes closely follow the material plane and line strain response model of March [1], an attempt has been made to remove the effect of strain upon the remanent magnetization. It is shown that when using a reconstructed tectonic strain tensor (i.e., the total strain tensor as measured in the field, corrected for an estimated compaction) we obtain a significant clustering of ChRM directions. The computation of the relevant VGP, gives a pole position (210.5° E, 42.0° N) compatible with the reference APWP for the Iberian plate. It is therefore inferred that the strain removal technique is a usable tool in order to obtain paleomagnetic results within such strained rocks.

1. Introduction

The use of paleomagnetic methods to help the understanding of ancient plate motions as well as of geodynamic evolution of some orogenic zones, is based upon the assumption of a time stability of the remanence acquired at a given age until now. The deformation, sensu-lato, whose effects are especially crucial in orogenic belts, is well admitted to cause deviations of primary (pretectonic) magnetization direction in folded or fractured rocks. Since Graham [2] has proposed the fold test to determine pre- or post-tectonic acquisition age of remanence in folded series, some developments of the simple tilt correction have been done, to take into account plunging axis folds [3], non-cylindrical folds [4] or superposed folds [5]. However, all the proposed techniques consist of more or less complicated rotations, assuming only a rigid-body rotation part in the total deformation, and cannot deal with internally deformed, or strained, rocks [6,7].

In order to investigate rock magnetism properties and remanent magnetization behaviour in naturally deformed series, we recently conducted some studies in deformed red slates. The first one dealt with the Permian red shales and slates of the Alpes Maritimes (France). In these rocks, we showed a nearly material-line behaviour of the deviated pretectonic direction of magnetization under strain [8]. It has been shown that these deviations are controlled by progressive hematite platelets reorientation during the cleavage development in these rocks [9] and, with the help of a

0012-821X/87/$03.50

numerical simulation, that passive rotation of platelets bearing micromoments may induce an actual material line-like behaviour of resultant magnetization [10]. In these series, we made an attempt to remove strain, using the strain data measured in the field. This allowed a reliable Permian paleomagnetic direction to be recovered, even though in-situ and tilt corrected directions were too scattered to be consistently interpreted.

In order to verify the assumptions of a material line behaviour of primary paleomagnetic vectors in such strained rocks, other paleomagnetic investigations related with structural analysis have been carried out in a fold from the Permian redbeds of the Pyrenean chain.

2. Geological setting and sampling sites

The studied area is situated at the "Col du Somport" (0.5° W, 42.8° N), at the southern border of the "Axial Primary Zone" of the Pyrenean chain (Fig. 1a). An Autunian age is inferred from the paleontologically based age of lateral equivalent formations at the "Sierra del Cadi" [11]. Here, the red series show ESE-WNW trending asymmetrical folds, slightly recumbent to the south, characteristic of the fan-shaped cross section of the chain (Fig. 1b) [12]. The location of this area, southwards of the North Pyrenean Fault System, which is suspected to be the limit between the Iberian and European plates during the Cretaceous opening of the Bay of Biscaye [14], points to its Iberian belonging. These structural observations are controlled by the paleomagnetic data obtained by Schwarz [15] on the Permian andesites of the Rio Aragon, a few kilometers south of the Col du Somport area. Paleomagnetic vectors have a shallow inclination with a SSE declination, characteristic of Permian and Permo-Triassic data

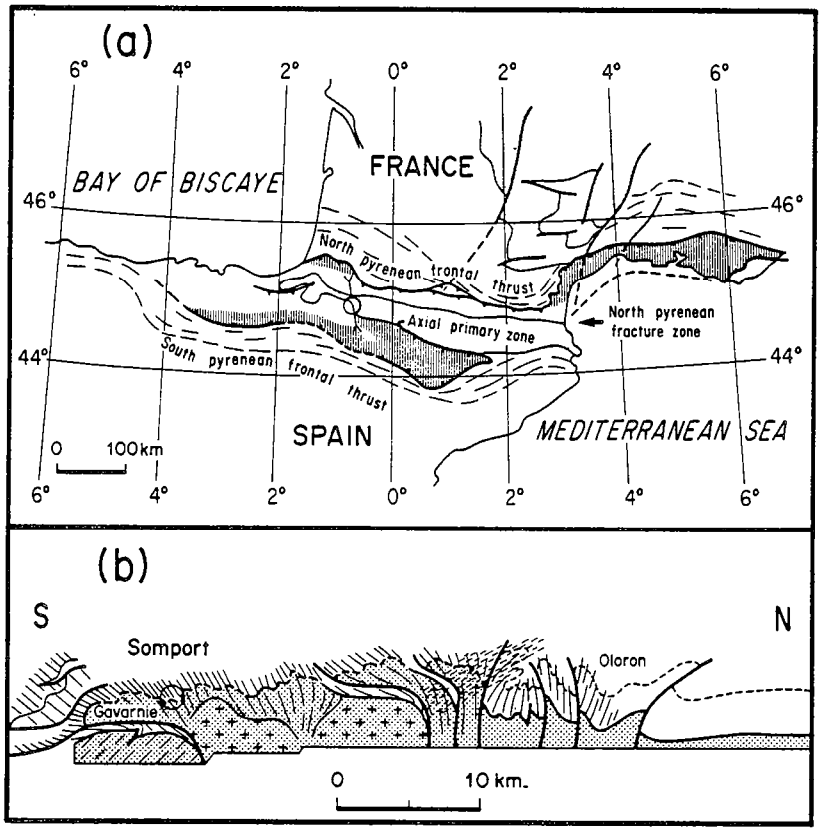

Fig. 1. (a) Schematic structural map of the Pyrenean chain (after Choukroune [12]). The Somport area is circled, and the emplacement of the cross-section of Fig. 1b is indicated. Pointed area: Hercynian basement. Hatched area: Secondary Eocene "décollé". (b) Schematic N-S cross-section through the axial zone (after Choukroune [13]). The Somport structural emplacement is indicated.

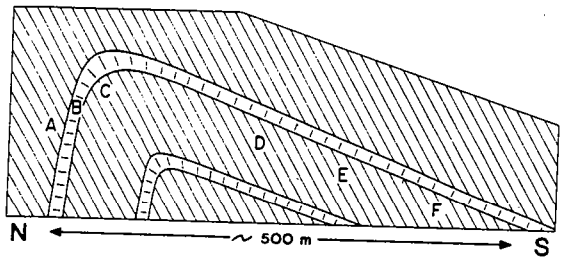

Fig. 2. Schematic cross-section through the folded red formation showing the structural position of the six sites studied.

for the Iberian plate [16,17]. The major Pyrenean phase is responsible for the axial planar northerly dipping slaty cleavage development in these redbeds.

66 cores were drilled and oriented in 6 sampling sites (A to F; Fig. 2), along the N157 roadside on about 500 m of cross section under the Col du Somport. Three sites (A, B, C) are situated in a southern steeply dipping limb, the others in a northern long slightly dipping limb. Samples of site B were drilled in a fine-grained red sandstone bed, about one meter thick, the others from the slaty mudstones. The area of the sites, generally 1–10 m^2, was chosen in order to ensure a good homogeneity of the strain (see Ramsay [18]) within each site.

3. Strain estimates

The red series studied are mainly mudstone slates with alternance of some sandstone beds which underline the bedding plane. The well-developed slaty cleavage which affects the muddy beds, exhibits a large refraction at the sandy beds interface. In these beds, cleavage becomes of fracture type and the sedimentary fabric appears to remain unaffected by the tectonic strain. At each site, a mean strain tensor has been estimated by measuring in the field the orientation and axial ratios of elliptical green reduction spots and little quartz pebbles, on natural fracture planes as close as possible to the principal strain planes. It is to be noted that when both strain markers are present in the same measurement plane, their mean axial ratios are, on the average, identical. From the measurements on at least two sets of perpendicular strain planes, and assuming no volume change (i.e. $\lambda_1\lambda_2\lambda_3 = 1$), the principal strains λ_i

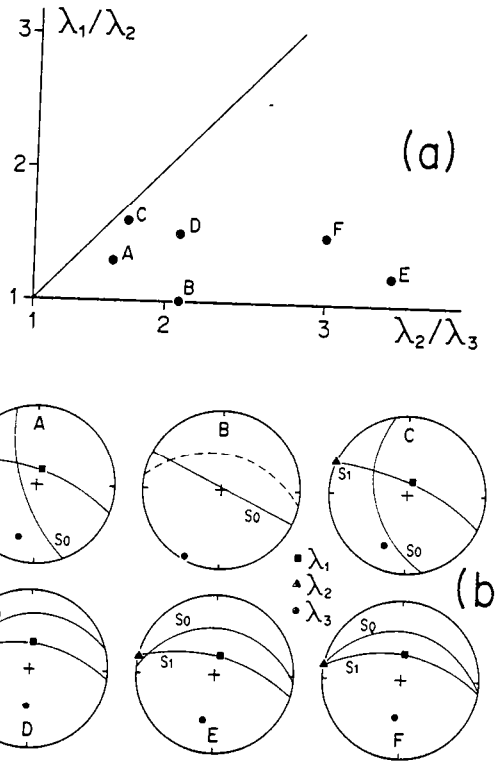

Fig. 3. (a) Flinn [19] diagram for the strain data of the 6 sites studied. (b) Stereoplots of bedding (S_0), cleavage (S_1) and strain principal axes. Stereographic projections in the lower hemisphere.

and related strain parameters are computed. The results are listed in Table 1 and shown in Fig. 3.

In the slates, the ellipsoids are flattened in the cleavage plane, with the maximum elongation axis (λ_1) parallel to the stretching lineation which has, on the average, a 90° pitch in the cleavage. The ellipsoids are triaxial, with a shape parameter K [19] lower than 1, and intensities r [20] ranging from 1.9 to 3.7. In contrast, the sandstone bed of site B shows oblate ellipsoids ($\lambda_1 = \lambda_2 > \lambda_3$), flattened in the bedding, which underline the preserved sedimentary fabric. The shape and orientation of elliptical reduction spots as well as the non-penetrative fracture-type cleavage, show that these sandy beds can be regarded as tectonically unstrained and that only the compaction is reponsible for the shape of the reduction spots.

A very important observation arises from these results: one can note that strain intensities and ellipsoid shapes show variations with the site location in the southern (A, C) or northern (D, E, F)

TABLE 1

Mean structural data for the sites of the Somport area

Site	S_0		S_1		α	X		λ_1	λ_2	λ_3	K	r
	strike	dip	strike	dip		D	I					
A	160	65	287	66	110	17	66	1.395	1.072	0.670	0.558	1.9
B	297	88	277	49	–	–	–	1.281	1.281	0.609	0	2.1
C	166	40	292	70	95	22	70	1.633	1.020	0.600	0.886	2.3
D	254	19	274	51	33	4	51	1.678	1.119	0.533	0.546	2.6
E	274	28	282	62	34	12	62	1.715	1.429	0.408	0.145	3.7
F	278	25	277	52	27	7	52	1.890	1.260	0.421	0.369	3.5

Notes: S_0 and S_1 are the bedding and cleavage planes; their orientations are defined by strike and dip. α is the angle between pole to cleavage and pole to bedding. The orientation of the principal elongation axis X is defined by D (declination) and I (inclination). λ_i are the eigenvalues of the strain tensor, with $\lambda_1\lambda_2\lambda_3 = 1$. K and r describe the shape [19] and intensity [20] of the strain ellipsoid.

limb of the fold. More precisely, the lower the angle between pole to cleavage and pole to bedding, the greater the strain intensity and the lower the shape parameter (Table 1). In other words, when compaction and tectonic shortening axes are close to each other, the total strain ellipsoid recorded by the elliptical markers are more flattened, and with a greater intensity, than when this angle is higher. It is thus inferred that the strain measured in the field results from the superimposition of the tectonic strain upon a noticeable compactional fabric. It will be shown that recovering the tectonic part of total strain is a critical point in order to remove its effects upon pretectonic remanent magnetization.

4. Paleomagnetic analysis

All the magnetic measurements have been done with a computer-assisted Schonstedt DSM-1 spinner magnetometer of sensitivity 10^{-9} A m^2. Progressive IRM acquisition experiments were done with a Brucker BE-10 electromagnet (maximum field 1.25 T). A Schonstedt TSD-1 non-magnetic furnace was used for thermal demagnetization procedures. Chemical demagnetizations were carried out following the classical procedures [21,22]: samples immerged in HCl in individual closed recipients were prepared by drilling a 1 cm diameter hole in order to increase the leaching surface, and let in a field-free space during increasing time steps. This was performed at room temperature and required a total leaching time ranging from 500 to 1000 hours.

The 127 specimens of this study were submitted to a short-period viscosity test [23]. 94% have a viscosity coefficient lower than the 20% value we have chosen as the maximum allowed for our paleomagnetic investigations. The NRM intensities are rather low, ranging from 10^{-3} to 10^{-1} A m^{-1}. The NRM directions are widely scattered. The density plots of the in-situ directions (Fig. 4, up) reveal a bipolar distribution, with one northerly steeply dipping maximum and one subhorizontal southeast maximum. Tilt-correcting these directions (Fig. 4, down) induces a scattering of

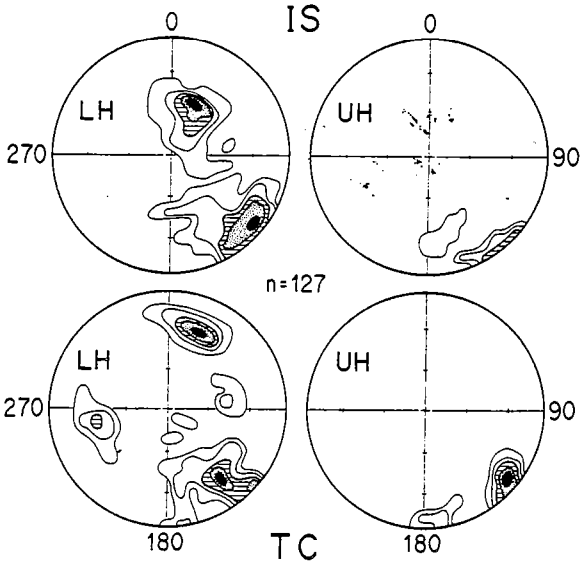

Fig. 4. Density plots of the NRM directions of the Somport redbeds. Upper: in-situ (IS); lower: tilt-corrected (TC); left: lower hemisphere (LH); right: upper hemisphere (UH). Contours are 1, 2, 3.5, 5 and 8% of the data in 1% of the hemisphere surface. Equal-area projections.

the first group, that can thus be thought to be post-tectonic remagnetizations. On the other hand, this does not improve the SE directions distribution, although they can be thought to be characteristic of the Iberian Permian paleomagnetic direction, and therefore, antetectonic in age. We can thus suspect both effects of remagnetization, and of strain upon the pretectonic magnetization directions.

Both thermal and chemical stepwise demagnetization techniques were used as an attempt to separate the contributions of the two groups of magnetization. 80 specimens were demagnetized thermally and 36 specimens by hydrochloric acid leaching. The NRM evolution during demagnetization can be summarized site by site as follows:

—All the specimens of the sandy bed of site B exhibit linear demagnetization paths in the Zijderveld [24] diagrams (Fig. 5a) in thermal as well as in chemical demagnetization. The unblocking temperatures are high, near the Curie point of hematite (Fig. 5a, left). This reveals a single magnetization component, whose southeasterly striking is characteristic of the Iberian Permian paleomagnetic direction.

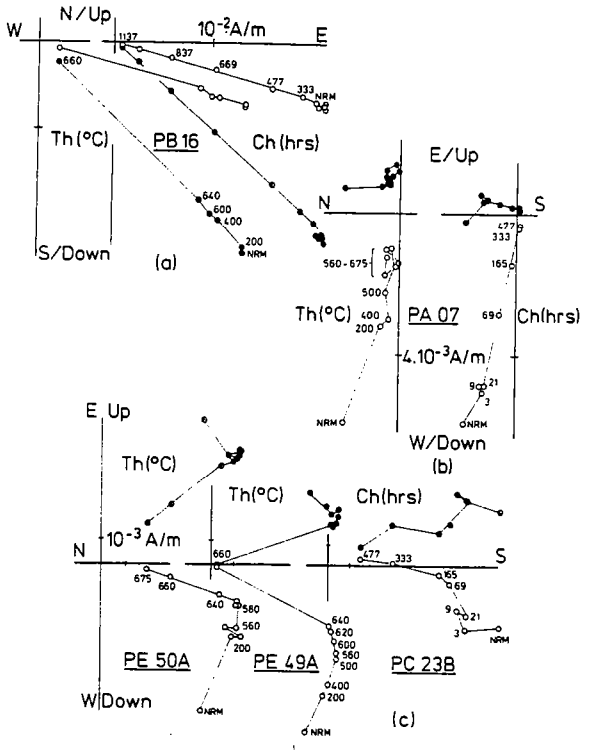

Fig. 5. Thermal (Th) and chemical (Ch) demagnetization curves in Zijderveld [24] vector projections. Demagnetization steps are indicated in °C and hours of leaching (hours). Closed (open) symbols: projection onto the horizontal (vertical) plane. (a) (b) (c): see text.

—In sites A and F (Fig. 5b), a north to northeasterly steeply dipping component predominates. Although in some cases, the demagnetization curves do not converge towards the origin (see, for example, Fig. 5b specimen PA 07), they suggest a nearly total overprinting of the pretectonic magnetization by a secondary magnetization component. Such directions appear consistent with the Cretaceous and Lower Tertiary remagnetizations as described by Schott [17] through the whole Pyrenean chain.

—In the three other sites (C, D, E; Fig. 5c), the demagnetization curves clearly show the presence of at least these two components. Thermal demagnetization was the most successful mean of separating them (Fig. 5c, specimen PE 50A). However, the least stable component has unblocking temperatures as high as 600 °C, sometimes higher, which may partially overlap the high unblocking temperature spectra of the hardest component. This results in some cases in an incomplete separation of the components, as can be seen in Fig. 5c, specimen PE 49A. In most cases, the chemical demagnetization by acid leaching did not allow a good separation of the components (Fig. 5c, specimen PC 23B). This kind of situation could arise either from a bad penetration of HCl into the specimen, or from identical magnetic carriers for both magnetization components.

Isothermal remanent magnetization (IRM) acquisition experiments were performed on pairs of leached and unleached specimens from the same core. The curves obtained (Fig. 6) are typical of red series, with the predominance of high coercivities in the fresh specimen, which are thought to be characteristic of the ultrafine red hematite pigment [25]. After acid leaching, this phase tends to disappear, and a lower coercivity phase (0.1–0.3 T) remains, which seems to be unaffected by leaching in HCl. The low coercivities could be due either to magnetite or to large specularite hematite. However, the comparison of the magnetization intensities acquired at 1.25 T, shows that the dissolved phase, the pigment, bears more than 98% of the IRM acquired by the fresh specimens. Since a similar NRM percentage is carried by the

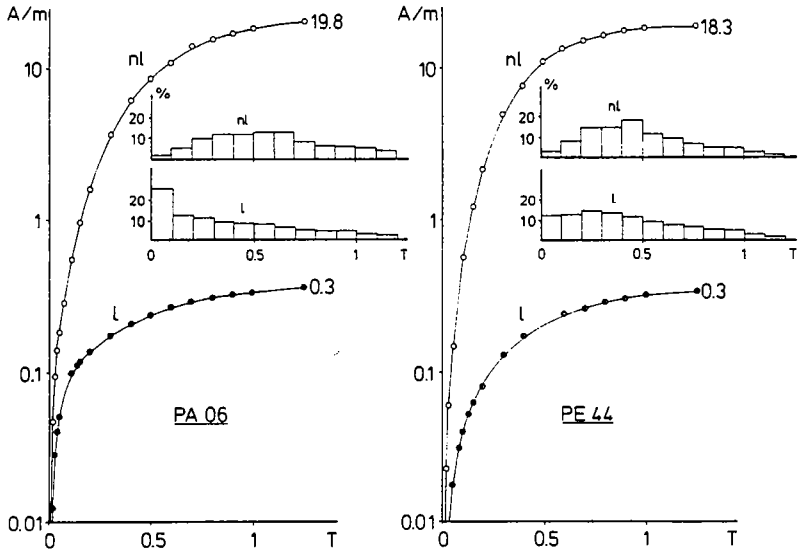

Fig. 6. IRM acquisition curves for pairs of leached (l) and nonleached (nl) specimens of samples PA 06 and PE 44. The IRM intensity acquired at the 1.25 T field is indicated at the endpoint of the curves. Inset: coercivity spectra.

dissolved phase (Fig. 5), it is thought that the lower coercivity phase has probably a negligible contribution to the total NRM of these rocks.

From these experimehts, as well as from the similarities between chemical and thermal demagnetization curves, it is thus inferred that NRM is predominantly carried by a single magnetic mineral, the red hematite pigment. This explains the difficulties encountered in separating NRM components which show a nearly to complete overlapping of both unblocking temperature and solubility spectra.

5. Results of the paleomagnetic analysis

From the above comments, it appears that the straight portions of demagnetization curves in Zijderveld [24] diagrams are not necessarily well resolved single NRM components, and that there exists a real possibility of measuring the vectorial sum of two components simultaneously demagnetized. It is therefore unappropriate to classify the isolated components in groups depending upon their unblocking temperature ranges or solubility spectra, and to treat them following the classical Fisher [26] analysis. Another reason to avoid the Fisher's statistics is that the strain can disperse data initially clustered, and a population can loose its Fisherian distribution. A classical Fisherian analysis could lead to reject some data which show anomalous direction, although the anomaly itself is significant with respects to the strain. In the present study, this is complicated by the fact that magnetization components are suspected to be poorly separated, and it was often impossible to decide if one component direction resulted from a strain-induced deviation or from a partial overprint, or a composition of both effects. Therefore, in order to avoid an a-priori interpretation of the components, we have preferred to define, whenever possible, a characteristic remanent magnetization (ChRM) as the last component in the demagnetization curves. The ChRM are then interpreted, not on a site-by-site basis, but all together in the same projections. It is assumed that if the whole strain removal technique is valid, only the part of pretectonic directions should cluster, all the other directions (secondary and overprinted components) should be dispersed by the treatment. To have a better vision of the distributions of points, density plots of these directions are used. From the 116 demagnetized specimens, 38 were rejected, since it was not possible to determine a stable ChRM component. The following analysis is thus done on 78 magnetization directions.

The density plots of the ChRM directions are shown in Fig. 7, as in-situ (up) and tilt corrected

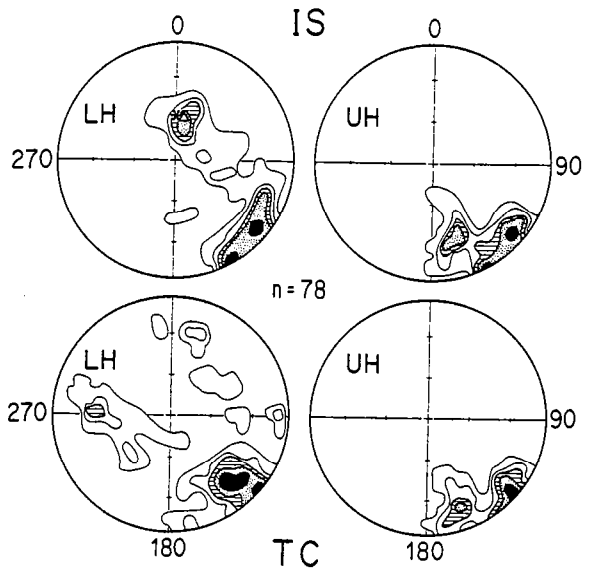

Fig. 7. Density plots of the 78 ChRM directions isolated by demagnetization. Upper: in-situ (IS); lower: tilt-corrected (TC); left: lower hemisphere (LH); right: upper hemisphere (UH). Same contours and projections as in Fig. 3. In the upper left projection, star is the normal present-day dipole field direction, open triangle is the mean strain λ_1 axis of the five slates sites.

(down). The in-situ directions show a large scatter which draws approximately a great circle containing the present-day dipole field axis. A first group of data clusters near the normal dipole field direction, as shown by a submaximum of density. The tilt correction using the classical procedure as described by Graham [2], disperses the data of this first group (Fig. 7, down), which are thus inferred to be post-tectonic in age. Furthermore, one can note that, in the in-situ projection, the maximum of this first group is slightly deviated from the dipole towards the λ_1-axis of the strain (see Fig. 7). This could illustrate the effect of anisotropy due to the cleavage development upon the post-tectonic magnetization acquisition.

At the other end of the girdle drawn in the in-situ projections (Fig. 7, up) by intermediate (probably unresolved) magnetization directions, a more important group of directions shows south-easterly declinations, with shallow, negative and positive inclinations. The classical tilt correction does not induce any significant improvement in the distribution of this population, and submaxima which are observable in-situ, remain scattered after this procedure. However, such declinations and inclinations are only compatible with Permian paleomagnetic directions known for the Iberian plate, and therefore should be pretectonic in age. The absence of effects of tilt correction could be partly explained by the fact that the fold axis trends subhorizontal in an ESE direction, that is, close to the remanent magnetization directions. Nevertheless, even in this case, unfolding should appreciably cluster pretectonic magnetization directions if they are dispersed by rigid rotations only.

As in the case of the Alpes Maritimes redbeds, where a similar situation was described [8], the strain is inferred to be responsible for the failure of the fold test. A further observation may be done about the remanent magnetization declinations. As a matter of fact, if the magnetization were Permian, it should present a declination around 160°. But we observe that remanent magnetization declinations trend 120–140°, as well in-situ as tilt corrected, that is between the expected declination (160°) and the cleavage plane direction (100–110°). This is in good agreement with the expected behavior of remanent magnetization vectors in such strained rocks [10].

6. Strain removal

Here as in the case of the Alpes Maritimes redbeds, an attempt has been made to correct the magnetization vectors using the inverse strain tensor determined from field measurements. Assuming that both ChRM vectors and bedding plane closely follow the material lines and planes strain response model of March [1], strain removal is done in two steps [8]. First, each ChRM direction is corrected by using the inverse strain tensor of the relevant site. On the other hand, the bedding plane tilt, as observed in the field is decomposed into two parts, a rigid-body rotation, and a strain-induced rotation; the strain is therefore removed from the bedding plane in a similar way. The strain removal of the paleomagnetic vectors is then achieved by a tilt correction using the unstrained bedding plane. Some remarks must be done about this treatment. First, the final orientation of a material line within a homogeneously strained volume does not depend upon the strain history, but only upon the initial orientation of the line and the finite strain tensor. Therefore the

folding style does not interfer with the strain removal technique, providing that corrections are made at a scale where strain is homogeneous, and that the total strain itself is accurately determined. This accuracy is limited by the fact that the treatment is made at the site scale, in a discrete manner. In particular, the rigid-body rotation within a site, which is estimated from the tilt of the undeformed bedding plane, is not fully constrained for the rotations about vertical axes. To summarize, we can say that, compared to an ideal undeforming method, the strain removal applied here is of the same simplifying level as the classical tilt correction of Graham [2] with respect to more elaborated unfolding methods [3–5] taking into account the fold geometry.

Results of this treatment are shown in Fig. 8, where the density plots are drawn in vertical E-W projections for a better visualization, since the changes in the distributions of points are expected to be around the horizontal plane. For comparison, Fig. 8a shows the tilt corrected directions as in Fig. 7 (lower). The strain removal technique, applied by using the strain tensor directly determined from the elliptical markers measurements in the field, leads to the results of Fig. 8b. It

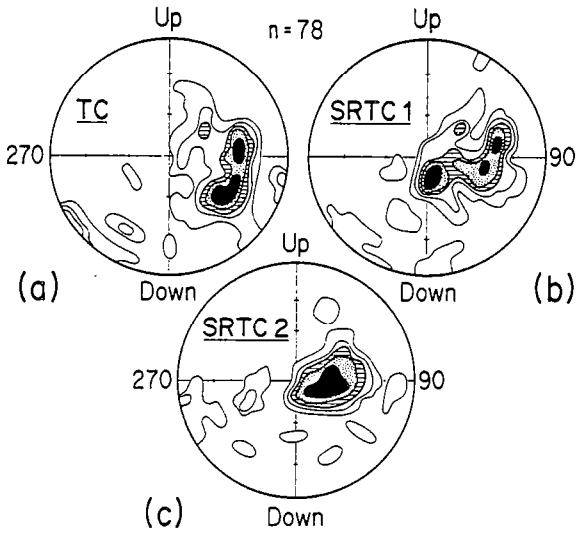

Fig. 8. Density plots of ChRM directions in vertical E-W projections in the upper hemisphere. (a) Tilt-corrected (TC) data. (b) SRTC1: data after strain removal and tilt correction from the unstrained bedding plane, using strain tensors directly derived from the field measurements. (c) SRTC2: same treatment, but using strain tensors corrected for the compaction. Same contours and projections as in Fig. 3.

is clear from this figure, that the treatment does not bring any improvement in the dispersion of the ChRM's. Thus, in a first approach, this could be interpreted as a failure of the procedure. However, a more careful analysis of the dispersion of Fig. 8b has shown that the southernmost directions belong to the northern limb sites of the studied fold, and the easternmost directions to the southern limb sites. And, whereas the first group seems to be overcorrected, the latter is undercorrected. Two main reasons for this situation can be evoked: (a) a bad estimation of the rigid body rotation part of the total deformation, in particuliar, as it was noted above, of the rotations about vertical axes, which are not recovered by the unstraining method we propose; (b) a bad estimation of the tectonic strain which induces the ChRM deflections. This last hypothesis is corroborated by the remarks we made about the strain distribution within the fold limbs: it has been shown that there is a relation between the total strain intensity (greater in the northern limb than in the southern one) and the angle between λ_3 and the pole to bedding in each site. This has been interpreted as resulting from the superimposition of the tectonic strain upon a noticeable compactional fabric. Since ChRM is carried by ultrafine pigment which is generally believed to form in-situ, during or after diagenesis [27], it can be thought that the time of primary magnetization acquisition is situated between the two main strain events of compaction and deformation. On the other hand, reduction spots appear to have recorded both events. Therefore an estimation of the tectonic part of the total strain tensor has been made by removing its compactional part.

Formally, if we express the total strain tensor **S** (determined from elliptical markers measurements in the field) as:

$$\mathbf{S} = \mathbf{T} \cdot \mathbf{C}$$

where **T** is the tectonic strain tensor, and **C** the compaction tensor, we estimate **T** as

$$\mathbf{T} = \mathbf{S} \cdot \mathbf{C}^{-1}$$

then **T** is used to correct ChRM, as described above. In each site, the tensor **C** has been constructed with eigenvalue ratios $\lambda_1/\lambda_2 = 1$ and $\lambda_2/\lambda_3 = 2$, the order of magnitude of eigenvalue ratios of site B, with the compaction direction

normal to the bedding plane.

Another problem is to improve the corrections applied to site B data. As described, the sandy bed does not show any internal deformation induced by the folding of the rock unit. Therefore, ChRM directions have not been changed with respects to the bedding reference frame and in the previous treatment, site B data were only corrected by a simple tilt correction. However, in all the other sites, bedding tilt was always measured at sandy and pelitic beds interface as it was for the site B. The bedding plane of site B can thus be considered as a passive material plane, like in the other sites, and its actual attitude, as resulting from a rigid body rotation and a rotation induced by the strain of the plastically deforming pelitic matrix in which it is embedded. In order to remove this strain induced rotation an estimated strain tensor was constructed at this place by averaging the nearly homogeneous strain data (intensity and direction; see Fig. 3) of sites A and C which are the nearest to site B. Then the rigid body inverse rotation was done by a classical tilt correction, by using the undeformed bedding plane tilt, as in the other sites. During these rotations, ChRM directions remain fixed within the bedding reference frame.

The results obtained by correcting ChRM directions using the estimated tensor **T** are illustrated in Fig. 8c. It is clear from this figure that the paleomagnetic directions cluster to form a single density maximum. It is thus inferred that the most significant part of the dispersion observed in Fig. 8b was actually induced by a bad estimation of the tectonic strain in each site, and the insufficiency of a simple tilt correction for site B data.

The density contours of the maximum in Fig. 8c show that these directions have a nearly Fisherian distribution. We can thus calculate their mean direction and compare it with the mean of the same specimen directions in the in-situ and simply corrected situations. We obtain:

in-situ:

$D_m = 140.0°$ $I_m = -2.5°$

$k = 12$ $\alpha_{95} = 6°$ $N = 50$

tilt-corrected:

$D_m = 142.0°$ $I_m = 7.5°$

$k = 12$ $\alpha_{95} = 6°$ $N = 50$

undeformed:

$D_m = 157.5°$ $I_m = 1.5°$

$k = 28$ $\alpha_{95} = 4°$ $N = 50$

These results can be summarized as follows: (a) there is no change in grouping induced by tilt correction; (b) tilt corrected data strike too much to the east with regards to the known Iberian Permian paleomagnetic directions; (c) the removal of tectonic strain induces a clustering of directions. The computation of the relevant VGP's gives:

tilt-corrected: 226.5°E, 32.0°N

undeformed: 210.5°E, 42.0°N

As a final control on the recovered paleomagnetic direction, these VGP's are compared with the available apparent polar wander path (APWP) of the Iberian plate from the Upper Carboniferous to the Lower Jurassic (after the compilation by Schott [17]) (Fig. 9). The VGP calculated after the classically tilt corrected data is broadly away from this APWP. In contrast, the undeformed ChRM directions give a VGP which appears compatible with the Lower Permian published results. Overall, the strain removal technique not only improves the clustering of the paleomagnetic mean direction at the formation scale (which could have been interpreted as being only a computing effect), but also allows us to obtain results of geodynamic significance.

7. Summary and conclusion

The analysis of the results obtained by structural and paleomagnetic studies on 6 sites distributed in both limbs of the fold shows that at least two magnetization components are carried by the red hematite pigment. The recovering of primary pretectonic magnetization by the mean of demagnetization techniques has been difficult, due to the large remagnetization of these rocks, probably when or shortly after the Carboniferous deformation occurred. However, the characteristic remanent magnetization directions distribution has been globally interpreted by analysing their density path. This shows a grouping of ChRM's towards SE directions, which can be a-priori thought to be Permian, and therefore pretectonic in age. The effect of strain upon these directions is two-

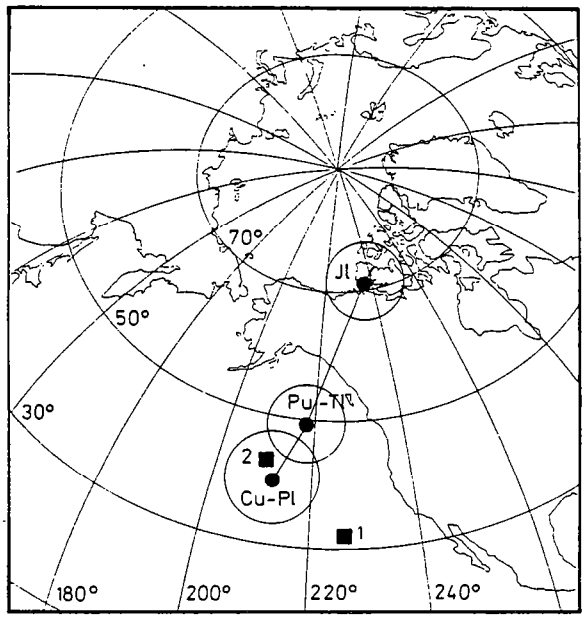

Fig. 9. Squares: virtual geomagnetic poles from the present study (*1*: after the tilt-corrected data; *2*: after the correction for strain (SRTC2 in Fig. 7c)). Circles: Iberian apparent polar wander path (after the compilation by Schott [17]). *Cu*: Upper Carboniferous; *Pl*: Lower Permian; *Pu*: Upper Permian; *Tl*: Lower Trias; *Jl*: Lower Jurassic.

fold: first, they show a non-positive fold test, mainly due to a significant scatter of the directions in inclination, after tilt correction. This strain-induced change in angular relationships between magnetization and bedding has already been described in previous studies in such redbeds. Secondly, ChRM declinations appear deviated towards the east by a significant amount of about 20–40°. This is in good agreement with expected sense and amount of magnetization deviations, when the initial angle between the pretectonic magnetization and the strain shortening axis is in the range of 40–50°. Although the relationships between strain and deviated magnetization directions are less precise and less well documented than in the Alpes Maritimes redbeds, it has been assumed that global behaviour of remanent magnetization closely approaches the material line strain response model of March [1], as it has been shown in other natural series [8] and in analogic simulations [28], as well as numerical ones [10].

We therefore decided to use the strain removal technique we previously proposed [29,30], in order to test the hypothesis of a passive line behaviour of remanent magnetization vectors. Applied to the paleomagnetic directions of this study, this technique did not bring an improvement in the vectors distribution, when using the strain tensors directly derived from the elliptical markers measurements. Nevertheless, it has been shown that the observed anomalies in the corrected directions can be explained by a bad estimation of the actual tectonic strain undergone by each site. The strain tensors have thus been corrected from a compactional part estimated from the measurements of site B elliptical reduction spots.

The strain removal, using these corrected tensors, induces a clustering of the paleomagnetic directions. Although they can appear as somewhat complicated, the proposed improvements do not question the basic hypothesis of a nearly material line behaviour of ChRM. However, they put forward the need of an extreme care in analysing the deformation and paleomag... vectors relationships. The recovered mean paleomagnetic direction then gives a VGP which well fits the Permian part of the Iberian APWP. It is thus concluded that the strain removal technique has proven helpfull in recovering a mean pretectonic direction of magnetization in a series which has suffered a significant strain, and where the structural corrections classically used in mountain belts should have given a non positive fold test and, without other controls, false geodynamic results. It is therefore argued that paleomagnetic studies are possible within strained regions, under the condition of a carefull analysis of strain, NRM components and directions, and their interrelationships. Although the limitations of the method are not currently known, such results, if verified on other examples, should open new fields of paleomagnetic investigations within strained regions of orogenic belts.

References

1 A. March, Mathematische Theorie der Regelung nach der Korngestalt bei affiner Deformation, Z. Kristallogr. 81, 285–297, 1932.

2 J.W. Graham, The stability and significance of magnetism in sedimentary rocks, J. Geophys. Res. 54, 131–167, 1949.

3 H. Perroud and P.R. Cobbold, L'aimantation rémanente comme marqueur de la déformation: exemple d'un pli à axe incliné dans les séries rouges siluro-dévoniennes à Cabrillanes, Asturies (Espagne), Bull. Soc. Géol. Fr. 26, 1, 169–184, 1984.

4 W.D. MacDonald, Net tectonic rotation, apparent tectonic rotation, and the structural tilt correction in paleomagnetic studies, J. Geophys. Res. 85, 3659–3669, 1980.
5 N. Bonhommet, P.R. Cobbold, H. Perroud and A. Richardson, Paleomagnetism and cross-folding in a key area of the Asturian Arc (Spain), J. Geophys. Res. 86, 1873–1887, 1981.
6 R. Van der Voo and J.E.T. Channel, Paleomagnetism in orogenic belts, Rev. Geophys. Space Phys. 18, 2, 455–481, 1980.
7 R.A. Facer, Folding, strain and the Graham's fold test in paleomagnetic investigations, Geophys. J.R. Astron. Soc. 72, 165–171, 1983.
8 J.P. Cogné and H. Perroud, Strain removal applied to paleomagnetic directions in an orogenic belt: the Permian red slates of the Alpes Maritimes, France, Earth Planet. Sci. Lett. 72, 125–140, 1985.
9 J.P. Cogné and D. Gapais, Passive rotation of hematite during deformation: a comparison of simulated and natural redbeds fabrics, Tectonophysics 121, 365–372, 1986.
10 J.P. Cogné, H. Perroud, M.P. Texier and N. Bonhommet, Strain reorientation of hematite and its bearing upon remanent magnetization, Tectonics 5, 753–768, 1986.
11 G. Lucas, Le grès rouge du versant nord des Pyrénées. Essai sur la géodynamique de dépots continentaux du Permien et du Trias, 267 pp., Thèse, Toulouse, 1985.
12 P. Choukroune, Structure et évolution tectonique de la zone Nord-Pyrénéenne, Mem. Soc. Géol. Fr. 127, 1–116, 1976.
13 P. Choukroune, Strain patterns in the Pyrenean Chain, Philos. Trans. R. Soc. London, Ser. A 283, 271–280, 1976.
14 P. Choukroune, X. Le Pichon, M. Seguret and J.C. Sibuet, Bay of Biscay and Pyrénées, Earth Planet. Sci. Lett. 18, 109–118, 1973.
15 E.J. Schwarz, A paleomagnetic investigation of Permo-Triassic redbeds and andesites from the Spanish Pyrenees, J. Geophys. Res. 68, 10, 3265–3271, 1963.
16 J.D.A. Zijderveld and R. Van der Voo, Les données paléomagnétiques et leur implication sur l'histoire structurale du Golfe de Gascogne, in: Histoire Structurale du Golfe de Gascogne, Publ. Inst. Fr. Pét. 22, II.1–II.23, 1971.
17 J.J. Schott, Paléomagnetisme des séries rouges du Permien, du Trias et du Crétacé inférieur dans les chaines pyrénéo-cantabrique et nord-ouest ibérique. Implications géodynamiques, 382 pp., These, Strasbourg, 1985.
18 J.G. Ramsay, Folding and Fracturing of Rocks, 568 pp., McGraw-Hill, New York, N.Y., 1967.
19 D. Flinn, On the symmetry principle and the deformation ellipsoid, Geol. Mag. 102, 36–45, 1965.
20 J. Watterson, Homogeneous deformation of the gneisses of Vesterland, southwest Greenland, Gronl. Geol. Unters. Bull. 78, 1968.
21 S.G. Henry, Chemical demagnetization: methods, procedures and applications through vector analysis, Can. J. Earth Sci. 16, 1832–1841, 1979.
22 J.K. Park, Acid leaching of redbeds and the relative stability of the red and black magnetic components, Can. J. Earth Sci. 7, 1088–1092, 1970.
23 E. Thellier and O. Thellier, Sur l'intensité du champ magnétique terrestre dans le passé historique et géologique, Ann. Géophys. 15, 3, 285–376, 1959.
24 J.D.A. Zijderveld, Demagnetization of rocks: analysis of results, in: Methods in Paleomagnetism, D.W. Colinson, K.M. Creer and S.K. Runcorn, eds., pp. 254–286, Willey, New York, N.Y., 1967.
25 D.J. Dunlop, Magnetic mineralogy of unheated and heated red sediments by coercivity spectrum analysis, Geophys. J.R. Astron. Soc. 27, 37–55, 1972.
26 R.A. Fisher, Dispersion on a sphere, Proc. R. Soc. London, Ser. A 217, 295–305, 1953.
27 F.B. Van Houten, Origin of redbeds, a review 1961–1972, Annu. Rev. Earth Planet. Sci. 1, 39–61, 1973.
28 A. Morash and N. Bonhommet, Deviation of IRM during simple shortening experiments, Abstr. 4th IAGA Sci. Assem., Edinburgh, I13-12, 252, 1981.
29 J.P. Cogné, N. Bonhommet and P.R. Cobbold, Pretectonic magnetization obtained by strain removal, EGS-ESC Meet., Leeds, EOS Trans. 63, 51, 1982.
30 J,.P. Cogné, Pretectonic direction of magnetization recovered by strain removal. The example of a fold in red sediments of the Alpes-Maritimes (France), 2nd EUG Meet. Strasbourg, Terra Cognita 3, 107, 1983.

ANNEXE 9.

Déformation, anisotropie de susceptibilité magnétique et paléomagnétisme des séries rouges de la formation de Pont-Réan (Bretagne centrale, France).

Déformation, anisotropie de susceptibilité magnétique et paléomagnetisme des séries rouges de la Formation de Pont-Réan (Bretagne centrale, France).

1. Introduction.

L'étude conjointe de la déformation, de l'anisotropie de susceptibilité magnétique et du paléomagnétisme des séries rouges du Sud de Rennes (Formation de Pont-Réan) a été entreprise dans le but d'une part, de documenter la caractérisation des effets de la déformation interne sur l'aimantation rémanente antétectonique, et d'autre part de vérifier l'applicabilité de l'algorithme de déformation inverse des aimantations proposé précédemment (Cogné & Perroud, 1985).

La formation rouge de Pont-Réan marque le début de la sédimentation paléozoique dans la région du sud de Rennes. Elle repose en discordance sur les schistes Briovériens et passe de manière continue à la formation des Grès Armoricains. Bien que non datée avec précision, elle est considérée comme étant d'age Cambro-Trémadocien. Cependant un age Arenig a été proposé pour l'équivalent latéral de la formation du Moulin de Chateaupanne (Région d'Ancenis; Cavet et al., 1979) et un age radiométrique de 473 ± 15 MA par méthode U-Pb sur les intercalations volcaniques dans la formation du Cap de la Chèvre, Presqu'ile de Crozon (Bonjour et al., 1987), également considérée comme équivalent latéral de la formation de Pont-Réan. Il semble par conséquent raisonnable de supposer un age Ordovicien Inférieur pour cette dernière.

La zone des synclinaux du Sud de Rennes (Fig.1) a fait l'objet d'études structurales détaillées (Le Corre, 1978; Le Théoff, 1977; Crambert, 1981; entre autres). Celles-ci ont montré que le plissement hercynien est accompagné d'une déformation pénétrative marquée par le développement d'une schistosité de plan axial subverticale d'orientation E-W (Le Corre, 1978). La présence de marqueurs tels que les galets déformés du conglomérat de base (Le Théoff, 1977) ou les taches de réduction elliptiques (Crambert, 1981) ont permis de quantifier la déformation totale en de nombreux points et de mettre en évidence un gradient de la déformation du NW vers le SE de la structure. Cela a conduit Percevault et Cobbold (1982), par le biais d'une déformation inverse tridimensionnelle, à attribuer la structuration de la région à un cisaillement dextre d'échelle crustale. Une interprétation identique a été proposée par Barbotin (1987) sur la base de l'étude des trajectoires de déformation de tout le domaine Centre Armoricain.

Enfin, un travail récent de Ballard et al. (1986) et Brun (comm. pers.), basée sur l'étude des discordances Briovérien-Paléozoique, des variations d'épaisseur de la formation de Pont-Réan et du Grès Armoricain, des faciès conglomératiques de base etc.. a conduit ces auteurs à proposer un contexte distensif de la région pendant la sédimentation des séries rouges du Sud de Rennes. Le dépot se serait alors effectué sur une suite de blocs Briovériens basculés entre failles normales, délimitant des petits bassins de section triangulaire (Fig.1d). Il faut noter qu'à proximité de ces failles normales, le plan de dépot peut présenter un pendage synsédimentaire de 10° à 20° vers le centre du bassin. On verra que ce point a probablement une influence non négligeable sur la distribution finale des directions d'aimantation primaire.

Du point de vue paléomagnétisme, l'étude de 3 échantillons a permis à Duff (1979) de montrer l'existence d'une composante d'aimantation à forte

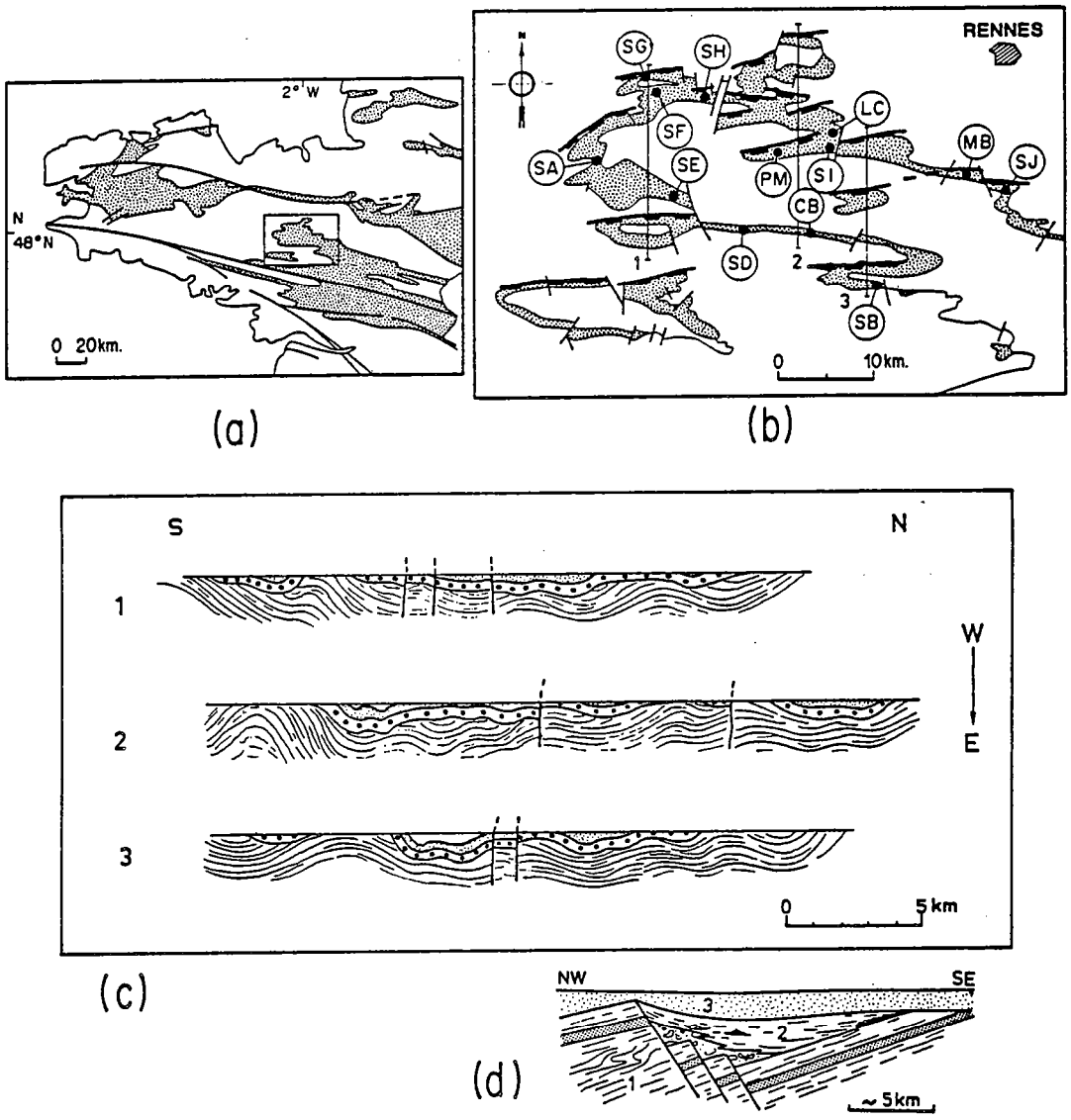

Fig.1: (a) Carte de situation de la zone étudiée; aire pointillée: sédiments paléozoiques. (b) Localisation des sites d'échantillonnage; aire pointillée: formation rouge de Pont-Réan. Les traits gras indiquent les failles normales synsédimentaires (voir texte). Traits fins n° 1 à 3: coupes de la Fig.1c. (c) Coupes schématiques à travers les synclinaux du Sud de Rennes (d'après Le Corre, 1978). (d) Coupe schématique donnant la structure des bassins sédimentaires lors du dépot de la formation de Pont-Réan (d'après Ballard et al., 1986); 1: Briovérien, 2: Formation de Pont-Réan, 3: Formation du Grès Armoricain.

inclinaison dans ces séries. Ces fortes inclinaisons sont caractéristiques du champ magnétique Ordovicien du Massif Armoricain (cf. la compilation de Perroud, 1985). Cela nous a permis de suspecter a priori l'existence d'une aimantation rémanente antétectonique dans ces séries.

L'étude présentée ici reprend et complète l'étude préliminaire effectuée sur 4 sites (Texier, 1985; Cogné et al., 1986). Au total, 13 sites distribués autour de la structure synclinale ont été échantillonnés (Fig. 1b). Dans le but d'étudier les effets de la déformation interne homogène sur l'aimantation antétectonique à l'échelle de chaque site, la taille de ceux-ci est limitée au volume dans lequel on peut considérer la déformation comme homogène. Les critères de terrain d'homogénéité de la déformation sont (a) des surfaces initialement planes restent planes (plan de stratification par exemple) (b) des surfaces initialement parallèles restent parallèles. 177 carottes (2.5 cm de diamètre, 5 à 10 cm de long) ont été forées et orientées sur le terrain à l'aide de compas magnétiques et solaires. Parallèlement à cet échantillonnage, les mesures structurales (orientation et pendage des plans de stratification (S_0) et de schistosité (S_1), linéation..) ont été faites sur chaque site. Au moins un échantillon contenant des taches de réduction elliptiques (de taille généralement millimétrique) a été prélevé sur chaque site, sauf SH, dans le but de quantifier la déformation interne.

2. Déformation interne et anisotropie de susceptibilité magnétique.

2.1. TECHNIQUES ET MESURES.

Sur chaque site le tenseur de déformation totale a été défini de la manière suivante. La normale à S_1 est assimilée à la direction principale d'élongation minimum λ_3, et S_1 au plan principal $\lambda_1 \lambda_2$. La linéation d'étirement mesurée sur le terrain correspond à la direction principale d'élongation maximum λ_1. Dans tous les sites étudiés, celle-ci est confondue avec la linéation d'intersection S_0/S_1. Ceci correspond avec les observations de Le Corre (1978) et le Théoff (1977). Compte-tenu de la petite taille des taches de réduction elliptiques, leurs rapports axiaux ont été mesurés sur des agrandissements photographiques des sections suivant les plans principaux de déformation des échantillons. A partir des mesures, et en supposant un changement de volume nul ($\lambda_1 \lambda_2 \lambda_3 = 1$), les valeurs principales $\lambda_i = 1+e_i$ ($i=1,2,3$) sont déterminées. Notons que j'ai préféré déterminer le rapport axial moyen de chaque section par une moyenne arithmétique des rapports axiaux, plutôt que par la méthode des abaques Rf/Φ de Dunnet (1969). Ceci permet en effet de calculer un écart-type sur les rapports axiaux moyens d'un plan donné, et par la suite, de fournir une estimation des barres d'erreur sur les valeurs principales λ_1, λ_2 et λ_3 de la déformation totale d'un échantillon donné.

Les mesures d'anisotropie de susceptibilité magnétique ont été effectuées pour une part sur l'appareil Digico du CFR, Gif-sur-Yvette (échantillons des 4 sites de l'étude préliminaire) et d'autre part (sites SA à SJ) sur l'appareil Digico du laboratoire de paléomagnétisme de Rennes, en tenant compte de la correction de procédure de calibration proposée par Hrouda et al. (1983). Des tests ont été faits, qui n'ont pas montré de différences significatives entre les résultats obtenus sur des échantillons mesurés sur ces deux appareils. A partir des mesures de N specimens par site, le tenseur moyen d'anisotropie de susceptibilité magnétique est calculé d'après la statistique tensorielle de Jelinek (1978). Brièvement, le tenseur moyen est estimé par la somme des N tenseurs normalisés (normalisation à l'invariant $k_{11}+ k_{22}+ k_{33}$: somme des termes diagonaux). Le calcul de la matrice de

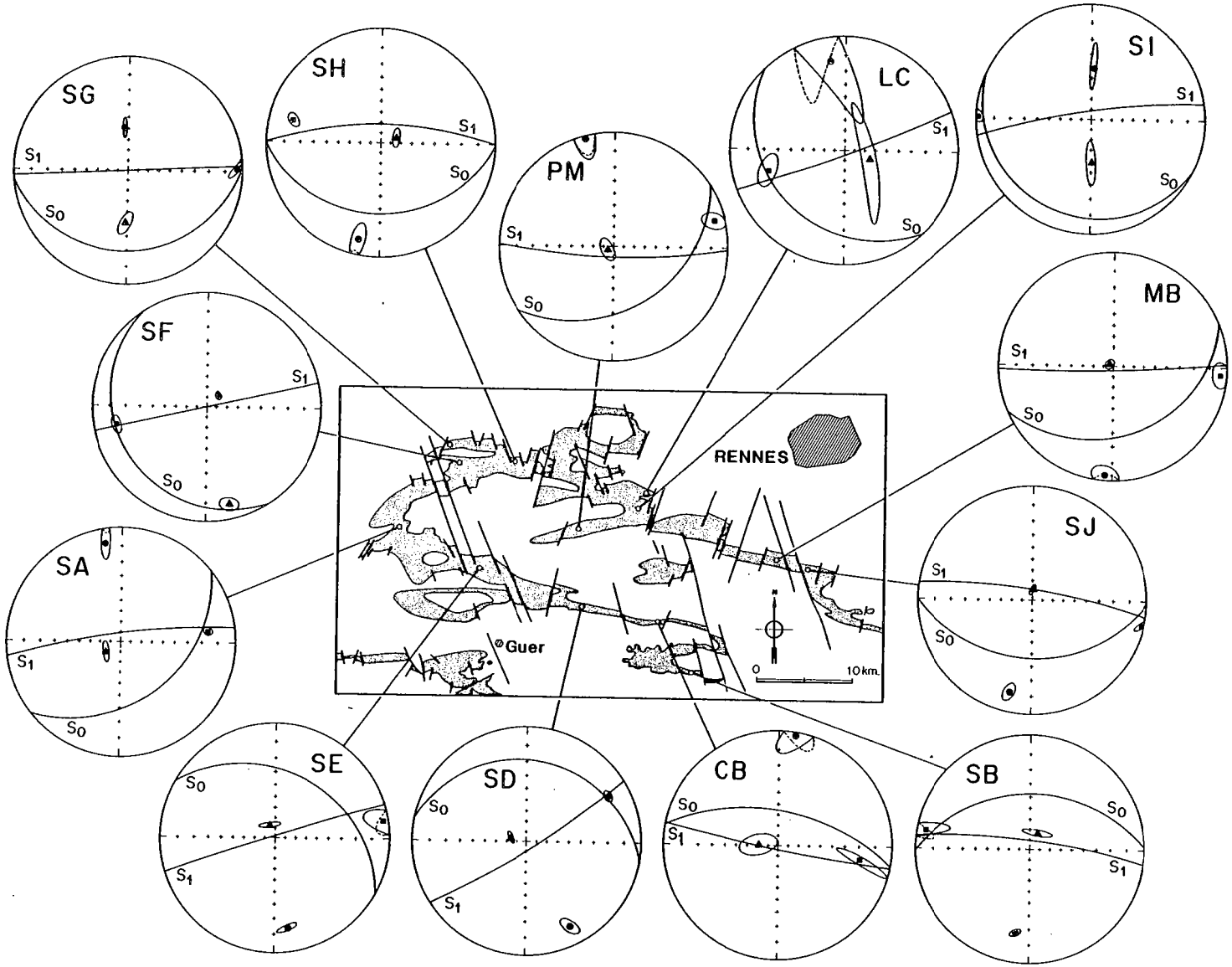

Fig.2: Projections stéréographiques dans l'hémisphère inferieur des directions structurales et d'anisotropie de susceptibilité magnétique. S_0: Plan de stratification; S_1: plan de schistosité. Les susceptibilités principales, avec leurs ellipses de confiance à 95%, sont: carrés: k_1 (max), triangles: k_2 (int), ronds: k_3 (min).

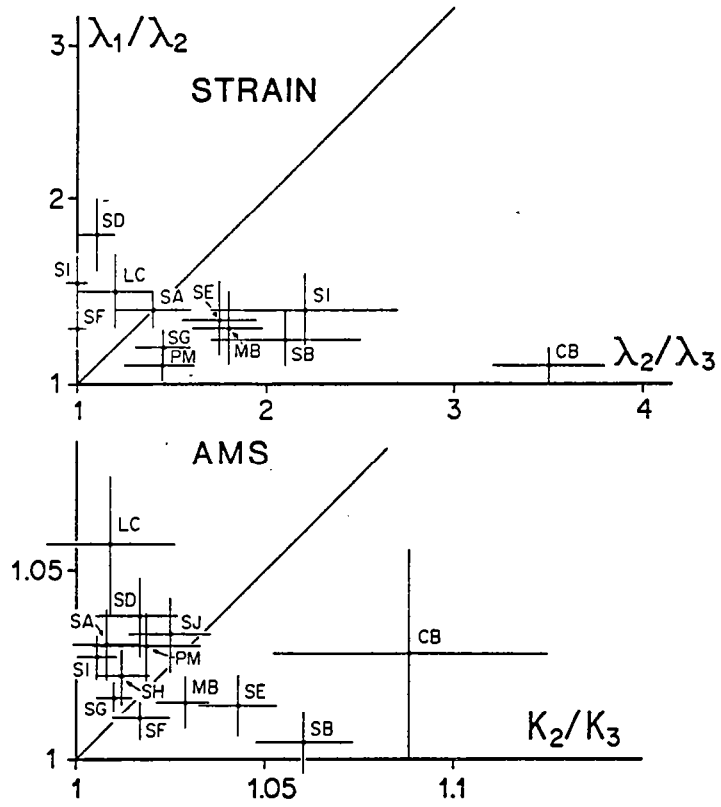

Fig.3: Diagrammes de Flinn (1965) des données de déformation (Strain) et d'anisotropie de susceptibilité magnétique (AMS).

covariance attachée à cette somme permet une estimation de l'écart-type sur les valeurs propres du tenseur moyen, et également le calcul d'ellipses de confiance (pour une probabilité donnée) analogues aux cercles de confiance de la statistique de Fisher pour les vecteurs.

2.2. RESULTATS.

Les estimations moyennes de déformation interne et d'anisotropie de susceptibilité magnétique sont données Tables I et II et illustrées Fig. 2 et 3. Du point de vue des directions (Fig.2) on peut noter que la susceptibilité maximum k_1 montre en général une bonne coincidence avec l'intersection du plan de schistosité (S_1) et du plan de stratification (S_0), c'est à dire, avec la linéation observée sur le terrain. La susceptibilité minimum est généralement proche du pole de la schistosité, λ_3. Il existe toutefois des exceptions (sites SG, SI) où k_3 et k_2 ont des directions intermédiaires entre les poles de S_0 et S_1. Ceci peut être interprété comme la marque de fabriques magnétiques intermédiaires entre la fabrique initiale due à la compaction et la fabrique développée par la déformation tectonique. Cette interprétation est corroborée par les données exceptionnelles du site SF où, contrairement à tous les autres sites, l'axe de susceptibilité minimum est proche du pole de la stratification, bien qu'une schistosité soit déjà mesurable sur le terrain. Notons enfin que pour ce site, ainsi que pour le site LC où la taille des ellipses de confiance autour de k_2 et k_3 montre que ceux-ci sont pratiquement non définis dans le plan k_2k_3, cette fabrique magnétique correspond à un débit en crayon de la roche.

La forme des ellipsoides et l'intensité de la déformation et de l'anisotropie de susceptibilité sont illustrées sur les diagrammes de Flinn (1965) de la Fig.3. Les points se répartissent dans les champs de constriction et d'aplatissement, aussi bien pour la déformation que pour l'anisotoropie de susceptibilité. Les intensités sont généralement faibles, r 2.5 et %An 5% pour la majorité des sites. Par ailleurs, les intensités les plus fortes sont atteintes par des points situés dans le champ de l'aplatissement. Ceci est en bon accord avec les résultats de Crambert (1981). Une différence notable existe entre la forme des ellipsoides de déformation et d'anisotropie de susceptibilité. Les elliposides d'anisotropie de susceptibilité magnétique apparaissent en effet plus constrictifs que les ellipsoides de déformation. Cependant, compte tenu de la faiblesse des intensités, de faibles variations de l'axe intermédiaire (λ_2 ou k_2 normalisé) autour de l'unité peuvent etre responsables de variations significatives des valeurs relatives λ_1/λ_2 et λ_2/λ_3 d'une part, et k_1/k_2 et k_2/k_3 d'autre part.

Afin d'établir, si elle existe, une relation entre déformation et anisotropie, il parait préférable de comparer la longueur des axes plutot que les rapports axiaux. Suivant en cela la relation empirique établie par Kligfield et al. (1981, 1983) dans les séries rouges des Alpes Maritimes, on a donc reporté les susceptibilités normalisées ("principal susceptibility differences" $Mi=(k_1-k_0)/k_0$; $k_0=(k_1.k_2.k_3)^{1/3}$) en fonction des "déformations naturelles" ($\varepsilon i= \ln(\lambda i)$) (Fig.4). La correlation entre ces paramètres apparait bonne (r=0.943) et la droite de régression $\varepsilon i=13.6Mi-0.04$ passe pratiquement par zéro. Cela signifie que, malgré les différences observées en diagramme de Flinn, les variations des tenseurs d'anisotropie sont, dans l'ensemble, reliées aux variations des tenseurs de déformation. La remarque faite ci-dessus au sujet de la forme des ellipsoides dans les diagrammes de Flinn est justifiée par la répartition des axes intermédiaires (λ_2 et M_2: triangles) autour de zéro dans la Fig.3.

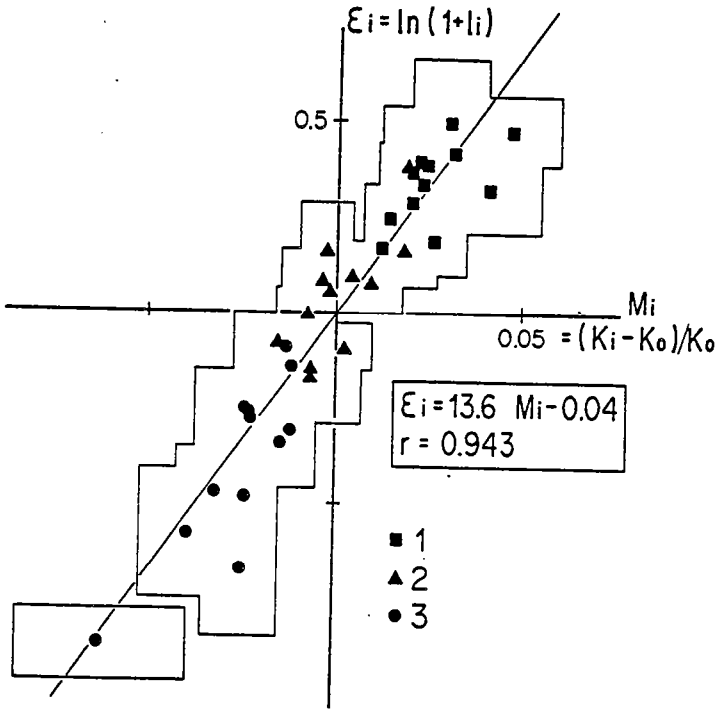

Fig.4: Susceptibilités principales normalisées (M_i) en fonction des "strains naturels" (ε_i). La droite de régression est tracée et son équation est donnée. Symboles: voir Fig.2.

Finalement, l'ensemble des ces observations peut être interprété de manière classique en terme de déformation progressive: une fabrique sédimentaire initiale développe une anisotropie dont l'ellipsoide est de révolution autour de λ_3. Ce stade n'est pas observé dans le cas présent, mais est attesté par la position de k_3 perpendiculairement à S_0 dans le site SF. Au cours de la déformation tectonique, le raccourcissement subhorizontal fait passer l'ellipsoide de déformation totale dans le champ de la constriction. Puis, avec l'augmentation de l'intensité de la déformation, les ellipsoides repassent dans le champ de l'aplatissement. Ceci est accompagné par le développement de la susceptibilité maximale k_1 suivant l'intersection S_0/S_1 et par un réajustement progressif de la susceptibilité minimale k_3 depuis la normale à S_0 (site SF) jusqu'à la normale à S_1 (sites SA, SB, SD, SE, SH, SJ, PM, MB, CB) en passant par des fabriques intermédiaires (sites LC, SG, SI).

Sans entrer dans le détail, ce point ayant déjà fait l'objet d'études plus poussées (Le Théoff, 1977; Le Corre, 1978; Crambert, 1981; Percevault, 1983; Barbotin, 1987), on peut remarquer que les intensités de déformation et de fabrique magnétique sont plus fortes vers le SE (sites SB, CB) que vers le NW (site SF en particulier, où la fabrique magnétique est encore dominée par la fabrique sédimentaire). Ce gradient a déjà été interprété en terme de cisaillement dextre transcurrent d'importance crustale, affectant toute la couverture sédimentaire de la Bretagne Centrale.

3. Analyse paléomagnétique.

3.1. A.R.N.

Les intensités de l'aimantation rémanente naturelle (Fig.5 à gauche) sont globalement comprises entre 10^{-2} et 10^{-3} Am^{-1}, valeurs classiques pour les séries rouges. Ces intensités, assez faibles, sont cependant suffisantes pour permettre l'analyse de l'aimantation par les techniques de désaimantation, et la mesure au magnétomètre spinner Schonstedt DSM-1 (sensibilité $10^{-4}Am^{-1}$). Les directions d'ARN, représentées en diagramme de densité Fig.5, montrent un étalement des points entre des directions SSW faiblement inclinées et des directions WSW à très forte inclinaison. Il n'apparait pas de trainage significatif des directions d'ARN vers la direction actuelle du champ magnétique du dipole axial centré. D'une manière générale, et compte tenu des données paléomagnétiques connues pour le Massif Armoricain (Perroud, 1985), la distribution globale des directions d'ARN pour la formation de Pont-Réan peut etre interprétée comme résultant de la réaimantation partielle de directions primaires ordoviciennes fortement inclinées, dans le champ magnétique carbonifère SW faiblement incliné (réaimantation hercynienne largement connue dans la chaine varisque).

3.2. DESAIMANTATIONS

Dans le but de séparer les différentes composantes d'aimantation et de tenter d'isoler une composante primaire antétectonique dans chaque site, l'analyse vectorielle de l'aimantation au cours de désaimantations thermiques progressives a été effectuée.

Le comportement de l'aimantation au cours des désaimantations s'est en général révélé assez simple. Deux types de courbes de désaimantation ont été obtenues (Fig.6). (1) D'une part, lorsque l'ARN présente initialement de fortes inclinaisons, l'aimantation décroit progressivement avec la température, sans changement de direction (Fig.6a). Dans ce cas, l'aimantation est donc univectorielle. On peut remarquer que les températures de blocage se répartissent en 2 groupes: déblocage progressif d'une partie de

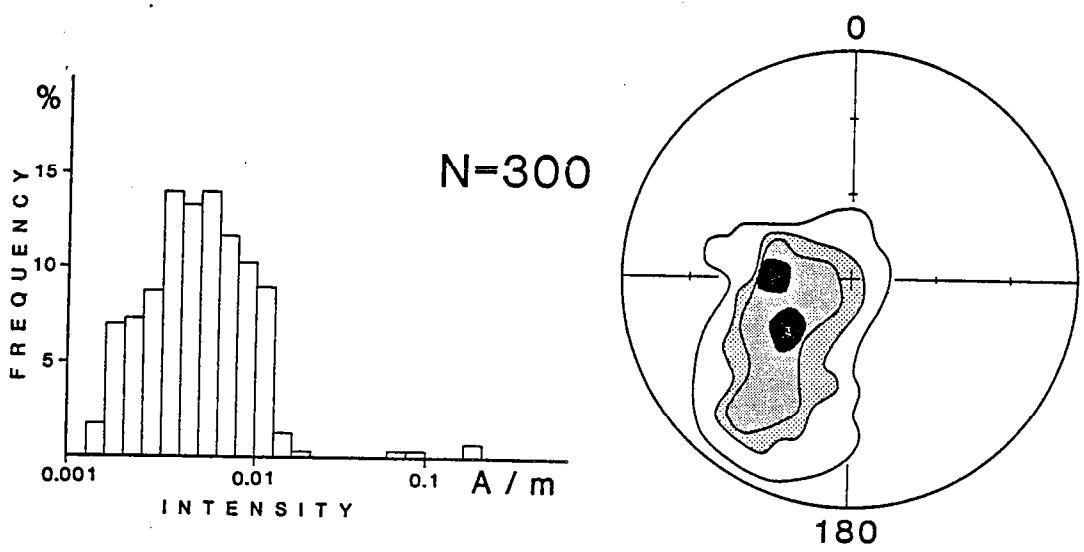

Fig.5: ARN: gauche: histogramme de fréquence des intensités; droite: diagramme de densité des directions. Projection à aire équivalente dans l'hémisphère inférieur. Contours: 1- 2.5- 5 et 10% des données dans 1% de la surface de l'hémisphère.

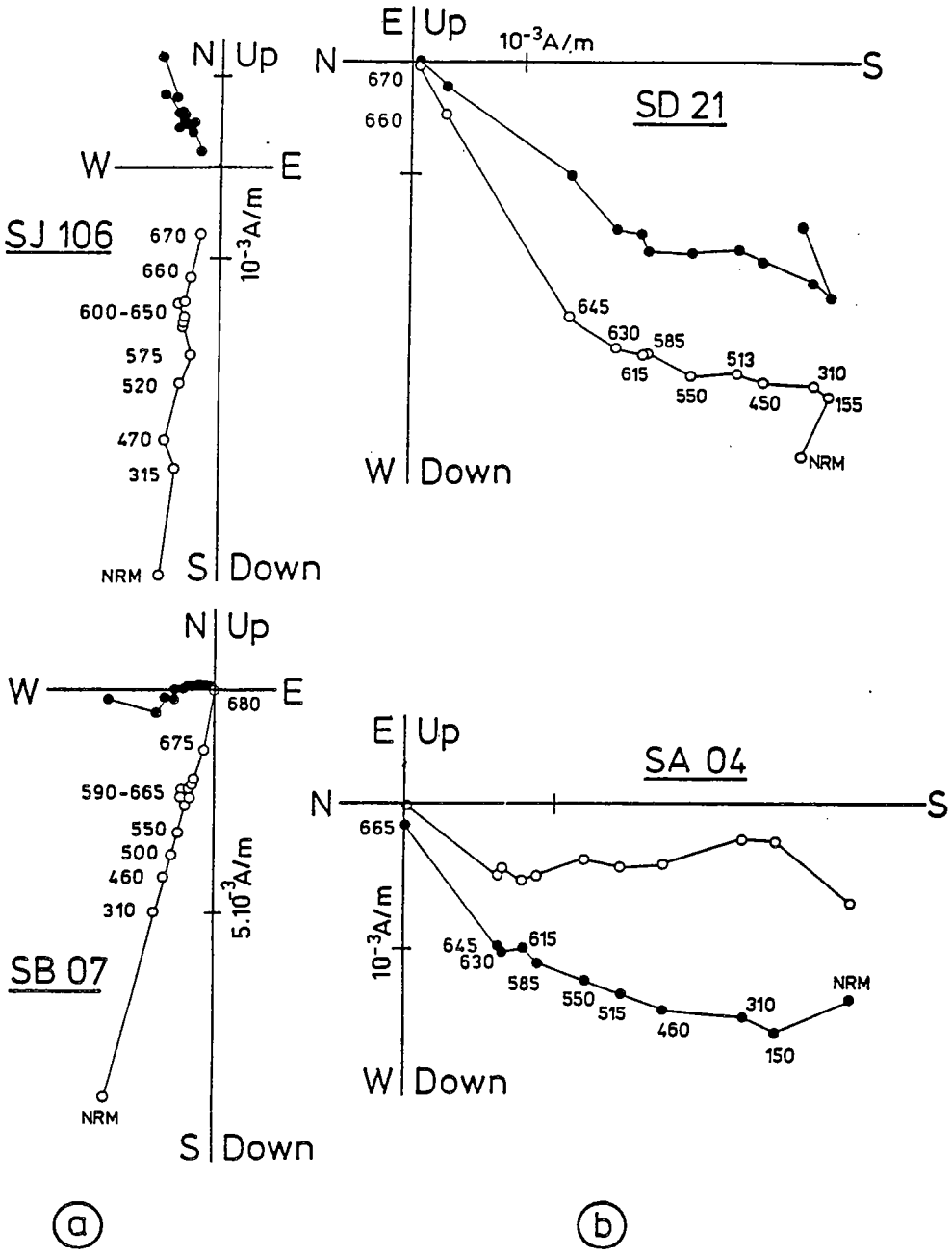

Fig.6: Désaimantations thermiques en projections orthogonales de Zijderveld (1967). Symboles fermés (ouverts): projection sur le plan horizontal (vertical). (a) et (b): voir texte.

l'aimantation entre 20 et 600°C, puis stabilité de 600 à 650°C et enfin décroissance finale de l'aimantation entre 660 et 680°C, température de Curie de l'hématite. (2) Le deuxième type de comportement a été observé principalement sur les échantillons présentant des ARN à inclinaison faible ou intermédiaire vers le SW. Il est caractérisé par la présence de deux composantes d'aimantation (Fig. 6b): une composante basse température (BT), qui se désaimante jusqu'à 600°C; elle présente des déclinaisons S à SSW et des inclinaisons faibles à intermédiaires. La désaimantation se termine par la mise en évidence d'une composante haute température (HT), de température de déblocage 640-650°C, d'inclinaison plus forte et de déclinaison W à SW. La bonne séparation de ces deux composantes n'est pas toujours assurée, ainsi qu'il est montré sur l'exemple de la Fig.6b, specimen SA04.

La séparation en deux composantes BT et HT a été obtenue sur 5 sites (SA, SD, SH, SI, et LC); une seule composante fortement inclinée et couvrant la quasi-totalité du spectre de température, a été mise en évidence sur les autres sites.

La répartition bimodale du spectre de température plaide en faveur d'au moins deux phases de porteurs magnétiques. Les courbes d'acquisition d'aimantation rémanente isotherme (ARI) effectuées par Texier (1985) n'ont cependant mis en évidence qu'un seul type de minéral magnétique, de coercivité élevée, typique de l'hématite. L'étalement des températures de blocage des composantes BT est compatible avec l'hématite pigment, les hautes températures correspondraient alors à de l'hématite plus grossière, voire de la specularite. Les composantes BT faiblement inclinées pourraient résulter de la remobilisatin du pigment, plus sensible à la circulation des fluides, durant l'orogenèse hercynienne, et seraient donc réellement secondaires.

4.Analyse des directions d'aimantation rémanente.

4.1.COMPOSANTES BASSE TEMPERATURE.

Comme il a été dit ci-dessus, la composante BT n'a été isolée que sur 5 sites. Les directions moyennes in-situ (IS) et corrigées du pendage (CP) sont données Table III et illustrées Fig.7. Avant correction de pendage, celles-ci possèdent une déclinaison assez homogène d'environ 200°, mais montrent d'importantes variations en inclinaison. La correction de pendage ne regroupe pas la distribution inter-site. De plus, bien que l'on ne possède des données BT que sur un seul site du flanc sud du synclinal (site SD), on peut remarquer que cette direction moyenne croise les directions des sites du flanc nord (SA, SH, LC) au cours du déplissement. Une application classique du test de plissement nous conduirait donc à interpréter ces aimantations comme étant syntectoniques. Cependant les études paléomagnétiques des séries rouges des Alpes-Maritimes (Cogné & Perroud, 1985) ou des Pyrénées (Cogné, 1987a) ont montré que les critères classiques d'évolution des groupements de vecteurs paléomagnétiques au cours du déplissement perdent toute signification dans les roches déformées. Le caractère syntectonique des composantes BT n'est donc pas absolument démontré ici. Plusieurs hypothèses peuvent etre émises pour expliquer la dispersion de ces composantes et son évolution lors de la correction de pendage:

1. Mauvaise séparation de ces composantes d'aimantation et des composantes HT fortement inclinées. Ceci est probable dans le cas du site I, dont l'inclinaison est anormalement forte par rapport aux autres sites, bien que la déformation y soit analogue.

2. Acquisition d'une aimantation post tectonique par des roches anisotropes. En effet, le plan de schistosité subvertical S_1 est en moyenne

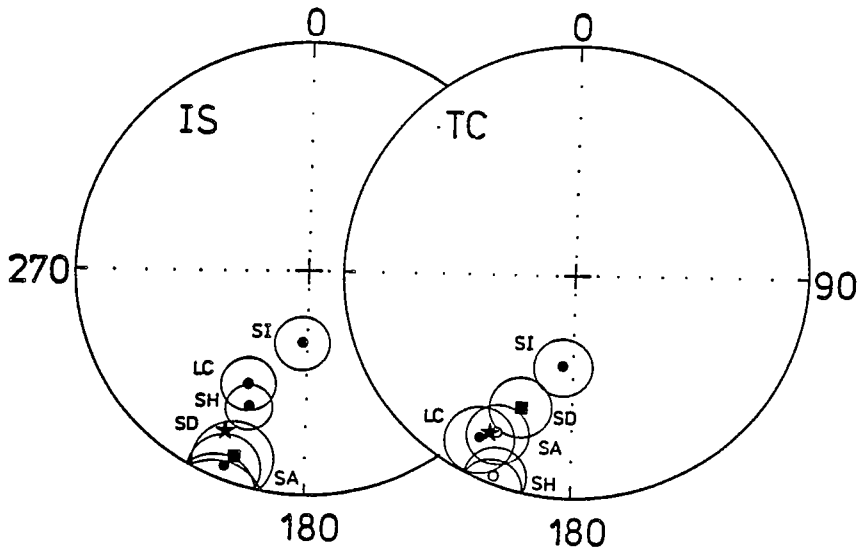

Fig.7: Directions moyennes intra-site des composantes BT (basse température) avec leurs cercles de confiance. IS: in-situ; TC: corrigées du pendage (tilt-corrected). Etoile: direction du champ magnétique du dipole axial centré Carbonifère (Perroud, 1985). Symboles fermés (ouverts): projection dans l'hémisphère inférieur (supérieur). Projections stéréographiques.

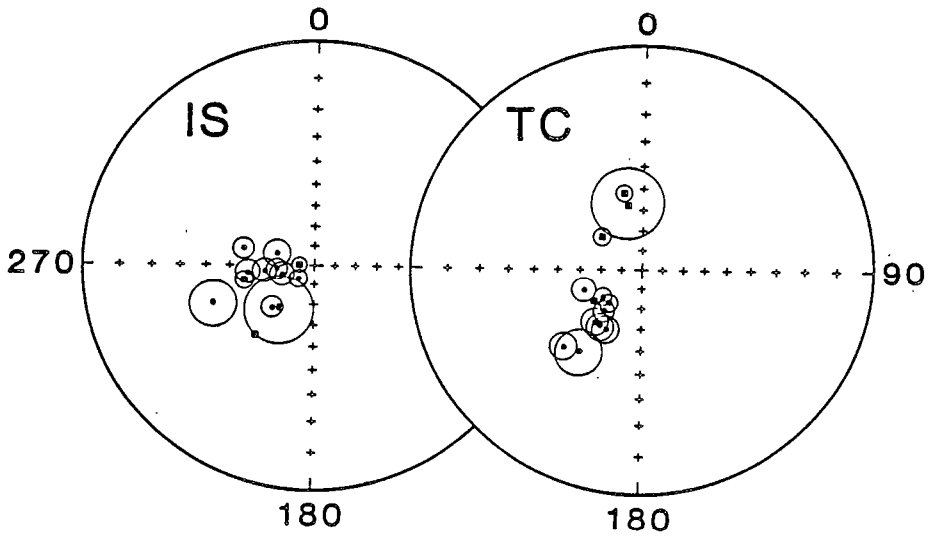

Fig.8: Directions moyennes intra-site des composantes HT (haute température) avec leurs cercles de confiance. Carrés: directions moyennes des sites du flanc sud. Memes abréviations et conventions que dans la Fig.7.

perpendiculaire aux déclinaisons des aimantations BT. L'effet de l'anisotropie serait donc essentiellement sensible sur les inclinaisons.

3. Acquisition syntectonique de l'aimantation au cours du plissement hercynien. L'aimantation serait alors acquise par un matériau déjà anisotrope et continuant à se déformer. On ne peut donc pas tenter de corriger les effets de la déformation comme on l'a proposé pour les aimantations antétectoniques (Cogné & Perroud, 1985), car on ne peut connaitre avec exactitude le taux de déformation subi par ce type d'aimantation, acquise au cours de la déformation progressive.

4. Enfin, en toute rigueur, on ne peut écarter l'hypothèse d'une aimantation antétectonique déviée par la déformation, dans la mesure où les critères de déplissement n'ont plus de signification.

Cependant, sur la base de leur affinité avec la direction du champ dipole carbonifère du Massif Armoricain (étoile, Fig.7), on admettra que les composantes BT isolées ici sont probablement des réaimantations hercyniennes, sans toutefois pouvoir déterminer leur age syn- ou post- tectonique sensu-stricto, ni par conséquent, calculer de direction moyenne de cette aimantation.

4.2. COMPOSANTES HAUTE TEMPERATURE.

Les moyennes intrasite des composantes d'aimantation haute température sont données table IV et illustrées Fig.8 in-situ (IS) et après correction de pendage classique (CP, ou TC pour "tilt- corrected"). Comme il a été noté plus haut, ces directions présentent de fortes inclinaisons, avec des déclinaisons W à SW. De telles directions sont tout à fait similaires aux directions paléomagnétiques des séries rouges Ordoviciennes de la formation de Chateaupanne ($D=228^{o}$, $I=81^{o}$; Perroud et al., 1986), ou du Massif de Thouars ($D=186^{o}$, $I=81^{o}$; Perroud & Van Der Voo, 1985). Par ailleurs, elles se démarquent nettement de la direction du champ du dipole axial centré actuel. Dans la mesure où l'on ne connait pas de fortes inclinaisons du champ magnétique depuis l'Ordovicien dans le Massif Armoricain (Perroud, 1985), l'hypothèse que l'on a bien isolé la composante d'aimantation rémanente antétectonique primaire dans ces séries est retenue.

L'examen des données, Table IV et Fig.8, amène immédiatement deux remarques :

1. A l'échelle de chaque site, les composantes d'aimantation sont extrèmement bien groupées, exception faite des sites CB et SA sur lesquels je reviendrai ultérieurement. Les paramètres k de la statistique de Fisher sont fréquemment supérieurs à 100, parfois à 200 et, pour le site SD, à 1000. Ces valeurs, courantes dans les roches volcaniques où l'aimantation thermorémanente fossilise le champ magnétique de manière instantanée, peuvent etre considérées comme anormalement élevées pour une série sédimentaire, où l'ordre de grandeur de k pour 1 site est en général 50 à 100 (Cf. Perroud et al., 1986; Van den Ende, 1977; Schott, 1985; pour quelques études de séries rouges).

2. La deuxième remarque concerne la comparaison des distributions inter-site in-situ et après correction de pendage (Fig.8). Il est évident que la correction de pendage induit une dispersion de la population assez bien groupée in-situ, dispersion liée à la divergence des aimantations en fonction de leur position structurale dans le flanc sud ou dans le flanc nord du synclinal. En utilisant les critères de déplissement classiques, cette évolution est considérée comme caractéristique d'une aimantation

post-tectonique. Il y a donc là anomalie du comportement des aimantations anté-tectoniques vis à vis du déplissement.

Cependant l'interprétation de ces anomalies est aisée, si l'on se réfère aux analyses des effets de la déformation interne sur l'aimantation antétectonique, effectuées d'après les résultats de modèles analogiques (Cogné, 1987b) ou numériques (Cogné et al., 1986) et d'études paléomagnétiques de séries rouges déformées (Cogné & Perroud, 1985; Cogné, 1987a). On a ici un exemple supplémentaire de la cohérence globale des déviations de l'aimantation induites par la déformation interne. L'interprétation proposée est schématisée Fig.9. A partir de couches supposées subhorizontales et ayant une aimantation subverticale (Fig.9a), la déformation interne provoque le développement d'une schistosité de plan axial durant le plissement. Du fait de l'angle élevé entre direction de raccourcissement (subhorizontale) et direction paléomagnétique initiale (fortement inclinée), la déviation de l'aimantation rémanente vers le plan d'aplatissement (Fig.9b) se traduit par les deux faits observés. (1) A l'échelle du site où la déformation est homogène, la déviation de l'aimantation se fait sans dégradation du groupement des aimantations mesurables, comme c'était le cas dans les séries rouges des Alpes Maritimes (Cogné & Perroud, 1985). Au contraire, la déformation tend à réduire les dispersions naturelles, de manière analogue à ce qui a été observé lors de la déformation expérimentale d'échantillons synthétiques (Cogné, 1987b). Le groupement intrasite anormal décrit ci-dessus apparait donc comme un résultat de la déformation interne sur l'aimantaiton rémanente. (2) L'aimantation rémanente étant initialement proche du plan d'aplatissement, sa déviation vers celui-ci provoque un regroupement inter-site des directions sur l'ensemble de la série plissée, comme indiqué sur le schéma de la Fig.9b. Ceci explique le bon groupement in-situ des directions moyennes, et la dispersion inévitable produite par la simple correction de pendage (Fig.9c).

Ici, comme dans les autres cas précédemment étudiés, la déviation de l'aimantation rémanente mesurable peut etre attribuée à une rotation des micromoments élémentaires, et par conséquent des minéraux magnétiques qui les portent, vers le plan d'aplatissement. Ce mécanisme de rotation des particules d'hématite est, de plus, attesté par les données d'anisotropie de susceptibilité magnétique. On a pu en effet constater que l'orientation préférentielle de l'hématite, mesurée par l'anisotropie de susceptibilité, est controlée par la déformation totale de la roche. Ceci est observé aussi bien pour les spécimens présentant une aimantation secondaire (signe d'une remobilisation chimique de l'hématite, liée à la déformation) que pour les spécimens n'en présentant pas. Il parait donc raisonnable d'attribuer la réorientation de l'hématite primaire portant l'aimantation antétectonique, à des rotations.

A la lumière de cette interprétation, les faibles groupements des directions d'aimantation dans les sites SA et CB apparaissent anormaux vis à vis du comportement global. Cependant, les composantes haute température dans ces 2 sites (Fig.10) montrent une distribution allongée depuis de fortes inclinaisons de direction W vers une direction SW de moindre inclinaison. Il se pourrait donc que les composantes d'aimantations ordoviciennes et hercyniennes aient été mal séparées lors des désaimantations, comme il a été montré, par exemple, Fig. 6b. Dans la mesure où il s'agit probablement ici de composantes d'aimantations intermédiaires, d'une part la mauvaise qualité de

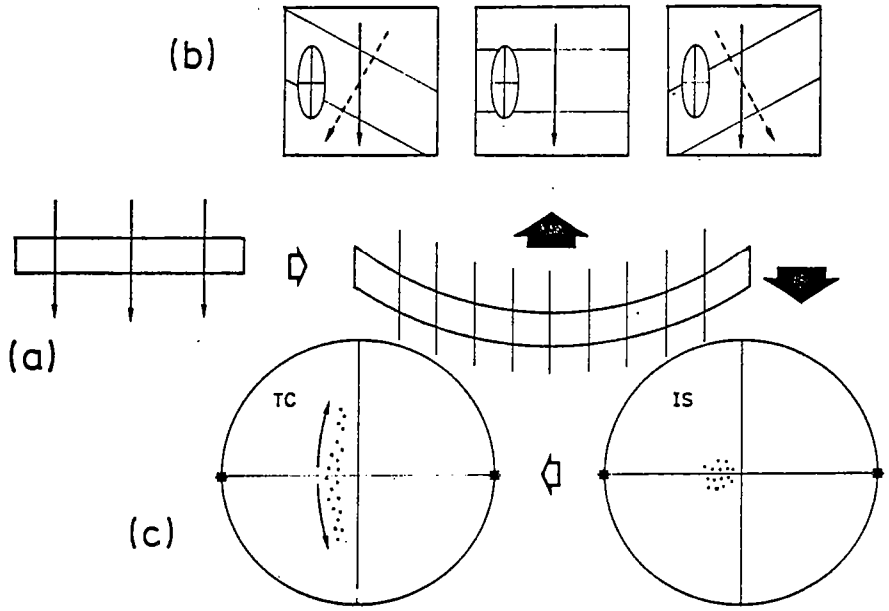

Fig.9: Schéma interprétatif des effets de la déformation interne sur l'aimantation primaire dans les schistes rouges de la formation de Pont-Réan. (a), (b) et (c): voir texte.

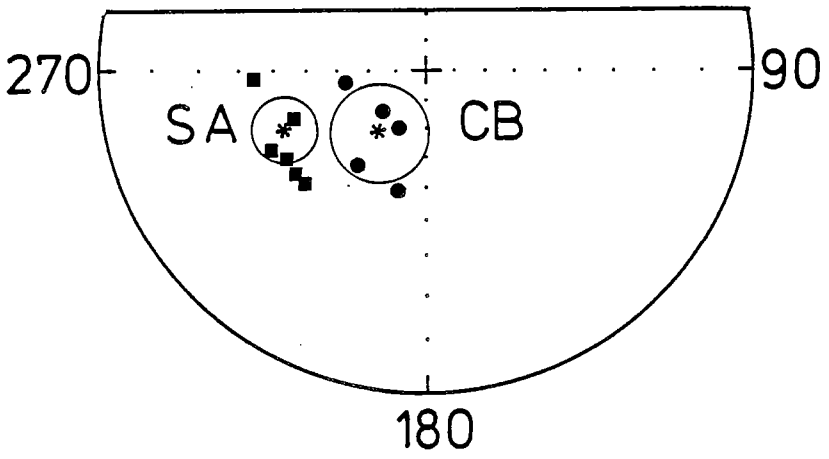

Fig.10: Composantes HT des sites SA et CB et leurs moyennes (astérisques) en projection stéréographique dans le repère in-situ.

leur groupement n'interfere pas avec l'interprétation proposée ci-dessus, et d'autre part, j'ai été amené à les éliminer de la suite de cette étude.

5. Déformation inverse des aimantations rémanentes antétectoniques.

A partir de l'analyse des déviations de l'aimantation rémanente antétectonique, le problème qui se pose est donc de tenter une détermination fiable de la direction du champ magnétique de l'époque d'acquisition de cette aimantation. L'analyse des résultats faite ci-dessus montre que les déviations de l'aimantation vers le plan d'aplatissement et la qualité des groupements sont compatibles avec les déviations subies par les lignes passives suivant le modèle de March (1932). En fait, il est difficile de vérifier avec exactitude, d'après l'état final, le caractère passif de l'aimantation. Cependant, si l'on fait à priori l'hypothèse de ce comportement et si l'on effectue une déformation inverse en utilisant cette hypothèse, le résultat de la déformation inverse doit la valider ou l'infirmer.

5.1. TECHNIQUE DE DEFORMATION INVERSE DES AIMANTATIONS.

Le principe de la technique utilisée à déjà été détaillé (Cogné & Perroud, 1985). Brièvement, elle repose sur les points suivants: l'orientation finale d'une ligne passive ne dépend pas de l'histoire de la déformation progressive, mais uniquement de son orientation initiale et de la déformation totale. par conséquent, on peut décomposer cette dernière en deux composantes: une composante de déformation interne, et une composante de rotation rigide (la troisième composante, la translation rigide, n'intervient pas dans le problème posé). Tout le problème revient donc à estimer ces deux composantes. En ce qui concerne la déformation interne, son estimation est relativement aisée, pour peu que l'on possède de bons marqueurs. La rotation rigide totale est par contre plus difficile à définir. Jusqu'à présent, le plan de stratification est admis comme un bon marqueur de la paléo-horizontale. Cependant si l'on considère que ce plan s'est lui-meme comporté comme un plan passif, il est nécessaire de dédéformer celui-ci, avant d'utiliser son pendage comme estimation de la rotation rigide. Il faut noter qu'à l'échelle d'un site de déformation homogène, le pendage de la stratification dédéformée ne fournit une estimation que de la composante de rotation autour d'un axe horizontal. Les rotations possibles autour d'axes verticaux ne sont par conséquent pas quantifiables par cette technique. Dans le cas présent, on peut cependant estimer que les fortes inclinaisons de l'aimantation rendent l'effet de ces dernières négligeable.

Pour résumer, la déformation inverse totale des directions d'aimantation s'effectue en deux étapes: (1) dédéformation du vecteur aimantation par le tenseur inverse de déformation interne; (2) rotation rigide inverse par correction de pendage de la stratification, après déformation inverse de cette dernière.

5.2. ESTIMATION DU TENSEUR DE DEFORMATION INVERSE.

En ce qui concerne la déformation inverse des aimantations rémanentes de la formation de Pont-Réan, les mesures d'anisotropie de susceptibilité ont été mises à profit pour améliorer l'estimation de la déformation interne en chaque site sur les 2 plans suivants. (1) La précision de l'orientation des carottes prélevées par les méthodes d'échantillonnage paléomagnétique d'une part, et le traitement statistique des mesures d'anisotropie de susceptibilité d'autre part, autorisent à penser que la détermination des directions des susceptibilités principales (k_1,k_2,k_3) se fait avec une très

bonne précision. Considérant que les directions des susceptibilités principales sont globalement confondues avec les directions principales de déformation sur l'ensemble des sites étudiés, on admettra que les écarts angulaires constatés sur certains sites résultent principalement d'erreurs et d'imprécisions des mesures des plans et linéations effectuées à la boussole sur le terrain. Par conséquent, le tenseur de déformation utilisé sur chaque site pour corriger les directions d'aimantation aura pour vecteurs propres les directions des susceptibilités principales mesurées en laboratoire (Table II). (2) Un raisonnement analogue a été tenu pour les valeurs propres du tenseur de déformation; d'un coté, les mesures de rapports axiaux des taches de réduction ont été effectuées sur des blocs de petite taille, et la représentativité de ces mesures par rapport à la déformation moyenne d'un site n'est pas assurée. Par contre, l'échantillonnage des spécimens paléomagnétiques est plus étendu et possède une meilleure représentativité statistique de l'anisotropie moyenne d'un site donné. Ici également, on peut estimer que les valeurs propres des tenseurs mesurés sont globalement corrélées (cf. Fig.4) sur l'ensemble des sites, et que les écarts observés à l'échelle de chaque site sont principalement dus à l'imprécision des mesures de déformation.

On a donc redéfini, sur chaque site, des valeurs principales de déformation, à partir de la droite de correlation générale $\varepsilon i = 13.6 Mi - 0,04$ et des données moyennes d'anisotropie de susceptibilité magnétique.

5.3. RESULTATS.

Contrairement au cas des Alpes Maritimes, la déformation inverse n'a pas été effectuée ici sur chacun des specimens de chaque site, mais sur la direction moyenne du site. Ceci est simplement du au fait que dans les Alpes Maritimes, les relations entre direction de raccourcissement et direction moyenne d'aimantation provoquaient une forte dispersion intrasite de cette dernière. Il était par conséquent nécessaire, avant de considérer l'évolution des groupements inter- site, de récupérer une moyenne intrasite bien définie. Dans le cas présent de la formation de Pont-Réan, la définition de la moyenne à l'intérieur de chaque site est suffisamment bonne pour rendre cette étape intermédiaire inutile.

Les directions moyennes d'aimantation rémanente antétectonique après déformation inverse sont données Table IV et comparées Fig.11 avec les distributions In-Situ et corrigées du pendage par la correction classique. On constate que le traitement de déformation inverse permet d'obtenir un bon groupement des directions d'aimantation. Le paradoxe du comportement de l'aimantation lors de la simple correction de pendage se trouve donc levé, et l'hypothèse d'une aimantation antétectonique est validée. Le bon accord entre la direction moyenne à l'état dédéformé (Table IV) avec les directions d'aimantation Ordoviciennes connues dans le Massif Armoricain, permet de plus d'argumenter la validité et l'applicabilité de la technique de déformation inverse de l'aimantation dans les séries rouges déformées de la formation de Pont-Réan.

Cependant, un examen plus approfondi des directions d'aimantation dédéformées (Fig.11 SRTC) permet d'identifier 2 groupes de directions bien distincts. L'un composé de 7 sites (PM, SB, SD, SE, SF, SG, et SI) montre des inclinaisons supérieures à 70°, l'autre composé des 4 sites restants (LC, MB, SH et SJ) a des inclinaisons inférieures à 60°. Par référence avec les données paléomagnétiques connues, ces dernières paraissent un peu trop faibles. Ceci a pour effet de donner un allongement N-S au nuage de points.

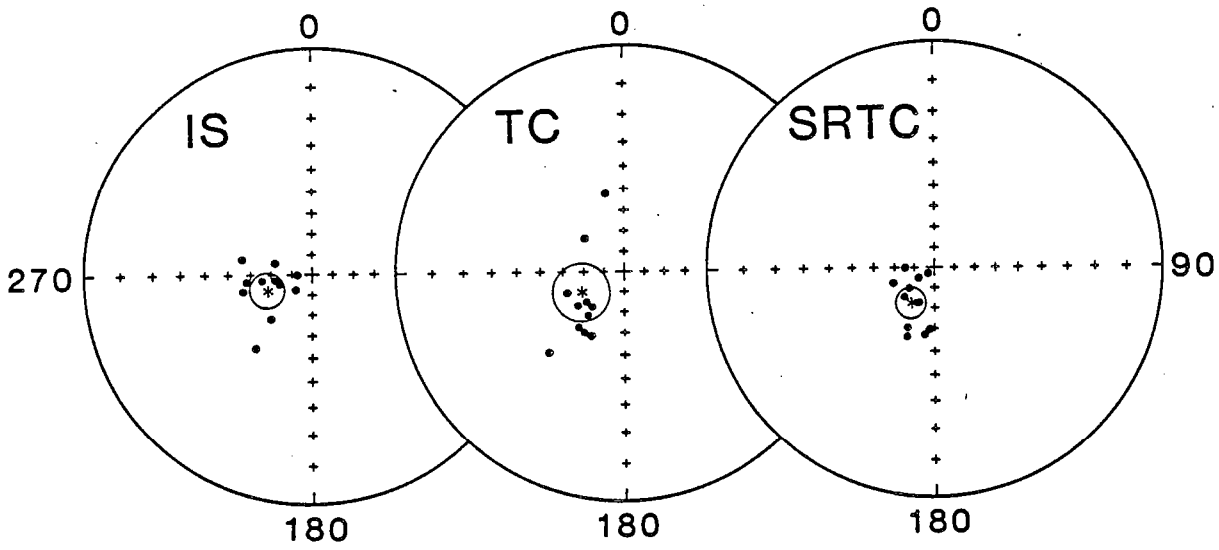

Fig.11: Directions moyennes HT et leurs moyennes intersites (astérisques). IS: In situ; TC: après correction de pendage; SRTC: après déformation inverse et correction de pendage de la stratification dédéformée.

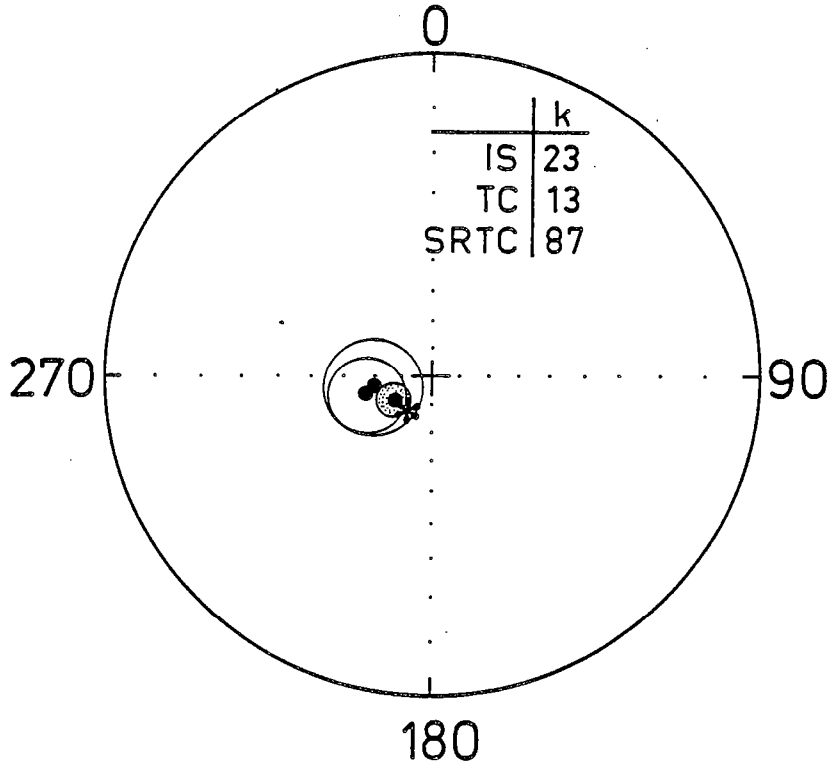

Fig.12: Moyennes pour les 7 sites retenus de cette étude. IS, TC, SRTC: voir fig.11. Les paramètres de groupement k sont indiqués.

Une première hypothèse pour expliquer cet allongement serait de supposer que l'on a ici un effet de surcorrection des directions d'aimantations, qui montreraient alors une tendance vers l'axe de raccourcissement 3, globalement horizontal et de direction N-S. Cependant, les intensités de déformation dans ces 4 sites ne diffèrent pas significativement des intensités de déformation dans les autres sites (Table I). Il n'existe donc pas à priori de raison particulière pour qu'une surcorrection de déformation interne se produise ici et n'affecte pas les autres sites. Une deuxième hypothèse pourrait etre une appréciation erronée de la rotation rigide inverse, estimée par le pendage de la stratification dédéformée. En effet, comme indiqué en introduction, Ballard et al. (1986) ont mis en évidence une sédimentation de la formation rouge sur des blocs Briovérien basculés par failles normales dans un contexte distensif de la région. A proximité des failles normales, le plan de sédimentation peut avoir eu initialement un pendage non négligeable, de l'ordre d'une quinzaine de degrés ou plus, vers le centre du bassin. Il se trouve précisément que les 4 sites (LC, MB, SH, SJ) incriminés ici se situent à proximité de telles failles (cf. Fig.1), que leur écart moyen à l'autre groupe est d'une quinzaine de degrés, et que le sens de cet écart est compatible avec l'orientation et le pendage des failles normales.

Ces considérations m'amènent à conclure que les données de ces 4 sites sont effectivement anormales par rapport à l'autre groupement. Notons toutefois que si cette interprétation est la bonne, l'anomalie de la correction appliquée à ces aimantations n'est pas directement liée à l'algorithme de déformation inverse, mais aux conditions de sédimentation de la formation, et à l'hypothèse, généralement admise mais difficile à controler, du plan de stratification comme marqueur de la paléo horizontale. Le caractère anormal des directions paléomagnétiques de ces 4 sites me conduit par conséquent à les éliminer de l'estimation finale de la direction moyenne d'aimantation.

On retiendra donc, sur la base des 7 sites restants, les directions moyennes d'aimantation suivantes (Fig.12) :

In Situ	D_m=254°	I_m=67°	k= 23	α_{95}= 13°	
Corrigé du pendage	D_m=258°	I_m=70°	k= 13	α_{95}= 17°	N=7
Dédéformé	D_m=235°	I_m=75°	k= 87	α_{95}= 6.5°	

C'est cette dernière direction d'aimantation dédéformée que l'on retiendra comme étant la direction d'aimantation caractéristique antétectonique des séries rouges de la Formation Ordovicienne de Pont-Réan. On remarquera enfin que la direction moyenne retenue est identique à la direction du champ dipole Ordovicien (astérisque sur la Fig.12) recalculée pour le lieu 48°N, 2.5°W (Perroud, 1985).

6. Conclusions

On peut résumer les principaux résultats de cette étude de la manière suivante:

1. La déformation interne des séries rouges de la Formation de Pont-Réan est accompagnée par le développement d'une anisotropie de susceptibilité magnétique. Leurs tenseurs sont corrélés tant du point de vue de leurs vecteurs propres que de leurs valeurs propres. On peut donc considérer que la déformation interne controle la fabrique magnétique. Compte tenu de la préservation d'une aimantation rémanente antétectonique dans la plupart des sites, et donc de l'hématite qui la porte, l'orientation préférentielle de

l'hématite est interprétée comme résultant globalement d'un mécanisme de rotation.

2. Les effets de la déformation interne sur l'aimantation rémanente antétectonique correspondent exactement à ce que l'on pouvait prévoir d'après les modèles analogiques et numériques (Cogné, 1987b; Cogné et al., 1986), et l'analyse globale du problème (Cogné et Perroud, 1987). Du fait de l'angle initialement fort entre direction de raccourcissement et direction d'aimantation, la déviation de celle-ci se fait sans dispersion de l'aimantation à l'intérieur d'un site de déformation homogène, mais avec au contraire un effet probable de resserrement de ces directions. Pour la meme raison, la distribution inter-site se trouve regroupée à l'état déformé.

3. La technique de déformation inverse appliquée à ces directions d'aimantation s'est révélée efficace. Aucune surcorrection significative, liée à l'approximation des vecteurs aimantation comme lignes passives, n'a été observée. Cela signifie que cette approximation est une hypothèse de travail correcte dans l'étude paléomagnétique de séries rouges modérément déformées, comme cela était suggéré par les résultats des études précédentes (Cogné & Perroud, 1985; Cogné, 1987a).

Finalement, l'étude détaillée des relations aimantation/déformation a permis de déterminer une direction d'aimantation antétectonique bien controlée, sur une série déformée que l'analyse paléomagnétique classique aurait nécessairement rejetée.

Site	S_0 D	S_0 P	S_1 D	S_1 P	L De	L I	λ_1	λ_2	λ_3	K	r
SA	51	35	262	81	79	18	1.400	1.000	0.714	1.00	1.80
SB	269	38	277	80	278	7	1.486	1.189	0.566	0.23	2.35
SD	280	19	57	82	59	13	1.527	0.848	0.771	8.00	1.90
SE	299	30	252	88	71	23	1.472	1.090	0.623	0.46	2.10
SF	146	13	77	90	257	12	1.191	0.916	0.916	-	1.30
SG	87	20	87	90	87	0	1.278	1.065	0.730	0.45	1.65
SH	90	26	270	71	90	0	-	-	-	-	-
SI	112	9	261	81	262	4	1.339	0.864	0.864	-	1.55
SJ	90	37	278	79	97	5	1.652	1.180	0.513	0.31	2.70
MB	66	28	88	86	89	12	1.449	1.115	0.619	0.37	2.10
PM	56	33	91	80	95	22	1.206	1.096	0.756	0.22	1.55
LC	135	22	69	86	247	20	1.392	0.928	0.774	2.50	1.70
CB	280	56	101	86	101	0	1.618	1.471	0.420	0.04	3.60

Table I: Données structurales moyennes des sites de la formation de Pont-Réan. Les plans de stratification (S_0) et de schistosité (S_1) sont repérés par D: direction, et P: pendage (dans la direction D+90°). La linéation (L) est repérée par De: déclinaison, I: inclinaison vers le bas. λ_1, λ_2 et λ_3 sont les valeurs propres du tenseur de déformation interne, déduites des mesures des rapports axiaux des taches de réduction. K: paramètre de forme, $K=(\lambda_1/\lambda_2-1)/(\lambda_2/\lambda_3-1)$; r: paramètre d'intensité, $r=\lambda_1/\lambda_2+\lambda_2/\lambda_3-1$.

Site	N	Bulk	k1			k2			k3			%An
		$x10^{-3}$ SI	Int.	D/I(°)	a/b(°)	Int.	D/I(°)	a/b(°)	Int.	D/I(°)	a/b(°)	
SA	32	0.126	1.023±0.006	82.5/15.5	3/2	0.992±0.003	235.0/72.5	10/3	0.984±0.005	350.5/ 8.0	10/3	3.9
SB	19	0.149	1.022±0.005	100.0/ 4.5	15/3	1.017±0.004	24.5/72.0	15/3	0.960±0.008	189.0/17.0	4/2	6.4
SD	32	0.143	1.030±0.007	60.0/12.0	4/2	0.992±0.003	282.5/74.0	6/2	0.977±0.008	152.5/10.0	6/3	5.4
SE	23	0.125	1.023±0.003	81.0/ 3.0	11/6	1.008±0.005	338.0/76.5	11/2	0.968±0.005	171.5/13.5	6/2	5.7
SF	25	0.115	1.012±0.003	258.5/13.0	5/3	1.002±0.003	166.5/ 6.1	5/4	0.985±0.004	46.0/74.5	4/3	2.7
SG	22	0.115	1.014±0.002	89.0/ 3.5	6/2	0.997±0.001	181.5/40.0	10/4	0.988±0.003	355.0/49.0	9/2	2.6
SH	23	0.109	1.018±0.003	284.0/13.5	5/3	0.997±0.004	71.0/73.0	10/3	0.984±0.003	182.0/ 8.5	10/4	3.4
SI	15	0.113	1.020±0.003	271.0/ 1.0	4/3	0.993±0.003	180.0/49.0	20/4	0.987±0.002	1.5/41.0	20/3	3.3
SJ	20	0.076	1.029±0.005	103.0/ 2.0	4/1	0.997±0.005	3.5/79.0	5/2	0.973±0.005	193.5/10.0	5/3	5.8
MB	15	0.104	1.019±0.005	98.0/ 2.5	7/4	1.004±0.003	350.0/83.0	6/4	0.976±0.005	188.5/ 7.0	7/5	4.4
PM	13	0.146	1.026±0.003	74.5/ 6.5	7/4	0.996±0.006	244.0/83.0	12/6	0.978±0.008	344.5/ 1.0	12/5	4.9
LC	6	0.110	1.040±0.011	255.0/21.0	12/6	0.984±0.007	109.0/65.0	55/7	0.976±0.009	350.0/13.0	55/7	6.6
CB	8	0.154	1.046±0.016	99.0/19.0	19/3	1.018±0.012	273.5/71.0	19/10	0.936±0.020	8.5/ 2.0	13/6	11.8

Table II. Susceptibilités moyennes normalisées dans la formation de Pont-Réan. Les susceptibilités principales sont données avec leurs écarts types (σ), et les angles d'ouverture (a et b) des ellipses de confiance à 95%. D/I: declinaison/ inclinaison. Le pourcentage d'anisotropie est défini par %An=(k1/k3-1)x100%. "Bulk": susceptibilité définie par $(k_1+k_2+k_3)/3$, où k_i sont les susceptibilités principales du tenseur moyen non normalisé de chaque site.

Site	N	IS De	IS I	CP De	CP I	k	α_{95}
SA	7	201	3	204	-14	43	9
SD	5	200	6	201	25	49	11
SH	7	202	23	200	- 2	58	8
SI	5	183	54	186	45	41	12
LC	6	206	31	208	10	44	10

Table III: Directions moyennes des composantes d'aimantation basse température isolées sur 5 sites. N: nombre d'entrées dans la statistique de Fisher (1953). Directions repérées par De: déclinaison, I: inclinaison (positive vers le bas, négative vers le haut). Is: in-situ, CP: après correction de pendage; k: paramètre de groupement de la statistique de Fisher, α_{95}: 1/2 angle d'ouverture du cone de confiance à 95%.

Site	n/N	In-Situ De	In-Situ I	Déplissé De	Déplissé I	Dédéformé De	Dédéformé I	k	α_{95}
SA*	6/8	248	40	216	42	-	-	34	10
SB	7/8	272	82	347	51	268	75	268	4
SD	7/8	218	46	234	62	202	70	1008	2
SE	8/8	257	56	310	64	231	85	178	4
SF	7/8	229	79	233	66	233	74	211	4
SG	8/8	263	71	220	62	227	69	115	5
SH	7/8	254	73	209	55	188	56	103	6
SI	8/8	264	65	249	60	251	67	100	5
SJ	7/9	289	70	214	55	184	60	79	7
MB	9/9	264	58	220	56	205	57	79	6
PM	6/6	284	55	223	66	238	81	213	4
LC	6/6	223	61	224	40	202	54	168	5
CB*	5/6	217	63	348	57	-	-	23	16
Mean	11/13	254	67	237	64	213	70		
		k=29	α_{95}=8	k=13	α_{95}=13	k=35	α_{95}=8		

Table IV. Moyennes intrasites des composantes Haute Température des Séries rouges de la Formation de Pont-Réan. n/N: nombre d'entrées dans la statistique/ nombre d'échantillons analysés. De,I: déclinaison, inclinaison.(*) Sites rejetés pour le calcul de la moyenne inter-site (Mean). k, α_{95}: Paramètres de groupement de la statistique de Fisher.

REFERENCES

Ballard, J. F., J. P. Brun, and J. Durand, La discordance Briovérien-Paléozoique inferieur en Bretagne centrale: signature d'un épisode de distension ordovicienne, C. R. Acad. sci. Paris, 303, 1327-1332.

Barbotin, E., Trajectoires de déformation finie et interprétation cinématique, Thèse, 154 pp., Rennes, 1987.

Bonjour, J. L., J. J. Peucat, J. J. Chauvel, F. Paris, and J. Cornichet, A middle Arenigian radiometric age for the Paleozoic transgression in West Brittany, France, (abstr.), 4th E. U. G. Meeting, Strasbourg, Terra Cognita, 7, 250, 1987.

Cavet, P., J. J. Chauvel, H. Lardeux, and J. Blaise, Paléozoique du domaine ligérien entre Ancenis et Chalonnes, Bull. Soc. géol. Minér. Bretagne, 11, 61-65, 1979.

Cogné, J. P., Paleomagnetic direction obtained by strain removal in the Pyrenean Permian redbeds at the "Col du Somport" (France), accepté à Earth Planet. Sci. Lett., 1987a.

Cogné, J. P., Experimental and numerical modeling of IRM rotation in deformed synthetic samples, accepté à Earth and Planet. Sci. Lett., 1987b.

Cogné, J. P., and H. Perroud, Strain removal applied to paleomagnetic direction in an orogenic belt : the Permian red slates of the Alpes Maritimes, France, Earth Planet. Sci. Lett., 72, 125-140, 1985.

Cogné, J. P., and H. Perroud, Unstraining paleomagnetic vectors: the current state of debate, Eos Trans. (in press)

Cogné, J. P., H. Perroud, M. P. Texier, and N. Bonhommet, Strain reorientation of hematite and its bearing upon remanent magnetization, Tectonics, 5, 753-767, 1986.

Crambert, S., Déformation totale dans les schistes rouges Cambro- Tremadocien de Bretagne centrale, Mém. D.E.A., 31pp., Rennes, 1981.

Duff, B. A., The paleomagnetism of Cambro- Ordovician redbeds, the Erquy spillites series and the Tregastel- Ploumanac'h granite complex, Armorican Massif (France and the Channel Islands), Geophys. J. R. astr. Soc., 59, 345-365, 1979.

Dunnet, D., A technique of finite strain analysis using elliptical particles, Tectonophysics, 7, 117-136, 1969.

Fisher, R. A., Dispersion on a sphere, Proc. R. Soc. London, A217, 295-305, 1953.

Flinn, D., On the symmetry principle and the deformation ellipsoid, Geol. Mag., 102, 36-45, 1965.

Hrouda, F., A. Stephenson, and L. Woltar, On the standardization of measurements of the anisotropy of magnetic susceptibility, Phys. Earth Planet. Int., 32, 203-208, 1983.

Jelinek, V., Statistical processing of anisotropy of magnetic susceptibility measured on groups of specimens, Studia Geoph. Geod., 22, 50-62, 1978.

Kligfield, R., W. H. Owens, and W. Lowrie, Magnetic susceptibility anisotropy, strain, and progressive deformation in permian sediments from the Maritim Alps (France), Earth Planet. Sci. Lett., 55, 181-189, 1981.

Kligfield, R., W. Lowrie, A. M. Hirt, and A. W. B. Siddans, Effect of progressive deformation on remanent magnetization of Permian redbeds from the Alpes Maritimes (France), Tectonophysics, 97, 59-85, 1983.

Le Corre, C., Approche quantitative des processus synschisteux. L'exemple du segment Hercynien de Bretagne Centrale, Thèse, 381pp., Rennes, 1978.

Le Theoff, B., Marqueurs ellipsoidaux et déformation finie. Application aux synclinaux de Bretagne Centrale et aux "mantled gneiss domes" de Kuopio (Finlande), Thèse, 96 pp., Rennes, 1977.

March, A., Mathematische Theorie der Regelung nach der Korngestalt bei Affiner Deformation, Z. Krist., 81, 285-297, 1932.

Percevault, M. N., Problème inverse en déformation finie. Application au segment hercynien de Bretagne Centrale, Thèse, 137 pp., Rennes, 1983.

Percevault, M.N., and P.R. Cobbold, Mathematical removal of regional ductile strains in central Brittany : evidence for wrench tectonics, Tectonophysics, 82, 317-328, 1982.

Perroud, H., Synthèse des résultats paléomagnétiques sur le Massif Armoricain, Hercynica, 1, 65-71, 1985.

Perroud, H., and R. Van der Voo, Paleomagnetism of the late Ordovician Thouars Massif, Vendée, Western France, J. Geophys. Res., 90, 4611-4625, 1985.

Perroud, H., N. Bonhommet, and J. P. Thébault, Paleomagnetism of the Ordovician Moulin de Chateaupanne formation, Vendée, Western France, Geophys. J. R. Astr. Soc., 85, 573-582, 1986.

Schott, J.J., Paléomagnétisme des séries rouges du Permien et du Trias et du Crétacé inférieur dans les chaines pyrénéo cantabrique et nord-ouest ibérique. Implications géodynamiques, Thèse, 382 pp., Strasbourg, 1985.

Texier, M.P., Anisotropie de susceptibilité magnétique. Corrélation avec la déformation. Application aux schistes rouges de la série de Pont-Réan, Mém. D.E.A., 36 pp., Rennes, 1985.

Van den Ende, C., Palaeomagnetism of Permian red beds of the Dome de Barrot (S. France), Thesis, 171 pp., Utrecht, 1977.

Zijderveld, J.D.A., Demagnetization of rocks : analysis of results, in Methods in Paleomagnetism, edited by D. W. Collinson, K. M. Creer and S. K. Runcorn, pp. 254-286, Elsevier, New-York, 1967.

ANNEXE 10.

J.P. COGNE, H. PERROUD. **Unstraining paleomagnetic vectors: the current state of debate.** Eos Trans., 68, 34, 705, 1987.

Reproduit avec l'aimable autorisation de l'American Geophysical Union.

Eos, Vol. 68, no. 34, Pages 705, 711–712, August 25, 1987

Unstraining Paleomagnetic Vectors: The Current State of Debate

Jean-Pascal Cogné and Hervé Perroud

Centre Armoricain d'Etudes Structurales des Socles,
Laboratoire de Géophysique Interne,
Université de Rennes,
Rennes, France

Introduction

One of the main goals of paleomagnetic studies is to produce evidence for ancient continent displacements and thus produce paleogeographical reconstructions of the earth in the geological past. To achieve this goal, paleomagnetists use the direction of remanent vectors as measured in rocks to derive latitudinal and azimuthal data, according to the model of the Earth magnetic field (EMF). One of the many difficulties faced by these researchers is the determination of whether the rock deformation may have altered the original paleomagnetic direction. If so, the paleomagnetists must correct the effect of such a deformation. Obviously, this aspect is of secondary importance in cratonic areas where beds lie flat or are gently folded, and in earlier times, most paleomagnetic studies were conducted in such areas. However, it now appears that we cannot avoid work within orogenic belts if we want to resolve geodynamic problems [*Van der Voo and Channel,* 1980]. It therefore became necessary to examine more carefully the interaction between magnetizations and deformation. During the last decade, several teams have conducted research efforts in this direction.

Our aim in this paper is first to review the results of such work, and second, to present our analysis of the difficult problem of internal deformation (strain) effects upon remanent magnetization. In this latter part, we shall argue the possibility of correcting paleomagnetic vectors within strained rocks.

Historical Review

A rock volume under stress may undergo three types of permanent transformations [*Ramsay,* 1967]:

- a whole translation, which, on a local scale, is of no consequence for paleomagnetism;
- a rigid body rotation; or
- a change of relative position of particles within the rock volume, which changes the shape of the body.

This third type of transformation is named internal deformation, or strain.

The first attempt to correct the effects of deformation upon paleomagnetic direction was concerned only with the rigid body rotation. This was *Graham*'s [1949] classic tilt correction, which consists of a rotation of the bedding around the strike line back to the horizontal. The comparison of magnetization dispersion before and after the correction allows determination of the relative chronology between the magnetization acquisition and folding ages. In a structural point of view, this treatment should apply strictly in the case of concentric folds with a horizontal axis, without any strain. However, it was widely used in different situations until paleomagnetists began to work in orogenic belts, where the strong need for more elaborate unfolding methods appeared. As an example, the discrepancy between net and apparent tectonic rotation due to plunging fold axes and/or faulting is emphasized by *MacDonald* [1980] on the basis of various theoretical cases. In a paleomagnetic study of the Asturian arc (Spain), *Bonhommet et al.* [1981] successfully recovered a pretectonic magnetization direction by applying two successive inverse rotations in an area deformed by two interfering folding phases. In a similar way, *Perroud and Cobbold* [1984] took structural history into account to correct the magnetization directions in an inclined axis fold hinge in the redbeds of the San Pedro formation (Asturias, Spain). *Courtillot et al.* [1986] used remagnetization that occurred between two phases of folding in a fold of Hercynian age in the Montagne Noire (France) to determine the shape of the structure prior to the remagnetization. All these studies have in common the assumption that only rigid body rotations are involved in the folding processes of the studied rock unit. However, the need for assessing the lack of strain is mentioned in each of them.

The possibility that folding processes may alter the initial angular relationship between the magnetic vector and the bedding plane has been cited by *Graham* [1949], *Tarling* [1971], and *Facer* [1983], among others. For this reason, strongly deformed series were generally avoided for paleomagnetic studies. In fact, the first attempts to correlate magnetic vector deviations with the amount of shortening in magnetized bodies originate in the wide problem of "inclination error" due to compaction in sedimentary rocks. Simultaneously, *Kodama and Cox* [1978] and *Blow and Hamilton* [1978] presented the results of experimental studies on the effects of compaction of artificial sediments upon the inclination of detrital remanent magnetization. Kodama and Cox did not obtain any coherent bias of their magnetization with respect to the compression axis. This was explained by the brittle deformation mechanism in their samples, in which shortening had been achieved by undeformed blocks gliding along two conjugate fault sets. On the other hand, Blow and Hamilton showed systematic deflections of the magnetization away from the compaction axis, and the amount of deflection was

0096–3941/87/6834/705$01.00

related to both initial inclination and degree of compaction. *Ozima* [1980] obtained the same kind of results by shortening magnetized Cu-Co alloy disks. *Morash and Bonhommet* [1981] used hematite-bearing plasticine samples to show that isothermal remanent magnetization (IRM) deviates toward the flattening plane during coaxial shortening experiments with various initial angular relationships and increasing deformation steps.

In parallel with these laboratory simulations, studies of deformed rocks were developed. One case, dealing with the Permian red slates from the Alpes-Maritimes (France), was the subject of efforts of different teams. These series, whose red coloration is due to the hematite pigment, contain some zones of decoloration that are named reduction spots. These green reduction spots are generally assumed to develop spherically in isotropic media, and if a deformation occurs, they become ellipsoidal. This characteristic allows quantification of the strain within deformed redbeds by measurement of axial ratios and principal directions. In the Alpes-Maritimes, *Graham* [1978] used these elliptical green reduction spots to demonstrate the presence of a strain gradient from the south to the north. The first paleomagnetic results were obtained by *Van den Ende* [1977], who observed that when cleavage appears, the tilt correction leads to incoherent results. He proposed that this was caused by strain. In a study of finite strain, magnetic susceptibility, and remanent magnetization in the same deformed beds, *Lowrie and Kligfield* [1981] concluded that remanent vectors are too scattered by the strain to be suitable for paleomagnetic purposes.

In contrast, *Cogné et al.* [1982] and *Cogné* [1983] found a good agreement between the paleomagnetic vectors deviations and principal strain directions, consistent with experiments by *Morash and Bonhommet* [1981]. They therefore introduced a new correction for these deviations that uses the inverse strain tensor determined at each site. The correction consists of applying the inverse strain tensor to first, the magnetic vector and second, to the bedding plane. In fact, the apparent bedding is caused by the superimposition of a strain-induced rotation upon the rigid body rotation. Finally, the initial direction of magnetization is recovered by a tilt correction using the unstrained bedding plane. This treatment is primarily based upon a strain response model known as *March*'s [1932] passive deformation theory. *Kligfield et al.* [1983] attempted to correct magnetization vectors by using this strain removal technique, but they did not correct for bedding strain–induced distortions. They concluded that this treatment is not valid because the inverse strain inevitably produces a deflection of the magnetization toward the finite strain Z axis of each site. A careful examination of strain and magnetic vector relationships allowed *Cogné and Perroud* [1985] to show that magnetic vector deviations were similar to strain-induced passive line deviations. They found that the strain removal technique allows the elimination of the anomalous within-site dispersion of magnetizations, elimination of the between-site dispersion of mean paleomagnetic directions along a fold, and recovery of a reliable Permian paleomagnetic pole. They therefore decided to use this technique in other situations and obtained successful results in Ordovician redbeds from Brittany [*Cogné et al.*, 1986].

More recently, *Lowrie et al.* [1986] acknowledged the need for correcting the bedding plane for strain before any rigid body rotation, but they did not agree to the application of inverse strain to paleomagnetic vectors. In another example from the Alpine Helvetic Nappes, *Hirt et al.* [1986] analyzed the effect of intense strain upon remanent magnetization. They found a girdle distribution of vectors that they interpreted as resulting from a heterogeneous horizontal simple shear rotating the remanent vectors as passive line markers.

Finally, some numerical models and simulations have been proposed to aid in understanding the interactions between strain and natural remanent magnetization. *Rochette* [1983] used a two-dimensional numerical model to characterize the deviations of magnetizations acquired by anisotropic materials in which the magnetic minerals show preferred orientation distribution or by isotropic populations that later undergo some preferred orientation development processes. By using three-dimensional numerical simulation, *Cogné et al.* [1986] showed that the passive rotation of platy hematites, each bearing a micromoment, produces a nearly passive line behavior of the net resultant magnetization of the population. They argued that the strain removal technique applied to paleomagnetic vectors should be valid if the deformation mechanism of hematite is achieved mainly by a passive rotation of hematite platelets during the cleavage development. This has been verified in the case of the Alpes Maritimes redbeds by *Cogné and Gapais* [1986], who showed that the preferred orientation development of hematite, estimated by X ray texture goniometry, is conveniently described by a passive rotation mechanism.

Discussion

Lowrie et al. [1986], who were mentioned previously, defended their opinion that the strain removal technique that we have proposed is not valid and leads to an overcorrection of the vectors. In the remainder of this paper, we shall try to show first, that their argument is based upon some statements that are not supported by the results of the published case histories and second, that a careful and complete analysis of the relationships of magnetization and deformation provides the basis of our method. We shall demonstrate the validity of the treatment in the cases that we have studied and show that this technique should be used more widely.

Analysis of the Effects of Strain Upon Remanent Magnetization

When a rock unit contains visible deformed objects, such as fossils, ooliths, reduction spots, etc., it is easy to use these strain markers to estimate the strain state by applying the tectonic and microtectonic techniques of strain analysis [e.g., *Ramsay*, 1967; *Means*, 1976; *Ramsay and Huber*, 1983]. Where such markers are rare, some strain-induced physical properties modification can be used. There are principally two techniques that allow the quantification of mineral-preferred orientations: the X ray diffraction method and the anisotropy of magnetic susceptibility (AMS) measurements. Although the first one has been the subject ot numerous studies and has allowed empirical relationships to be

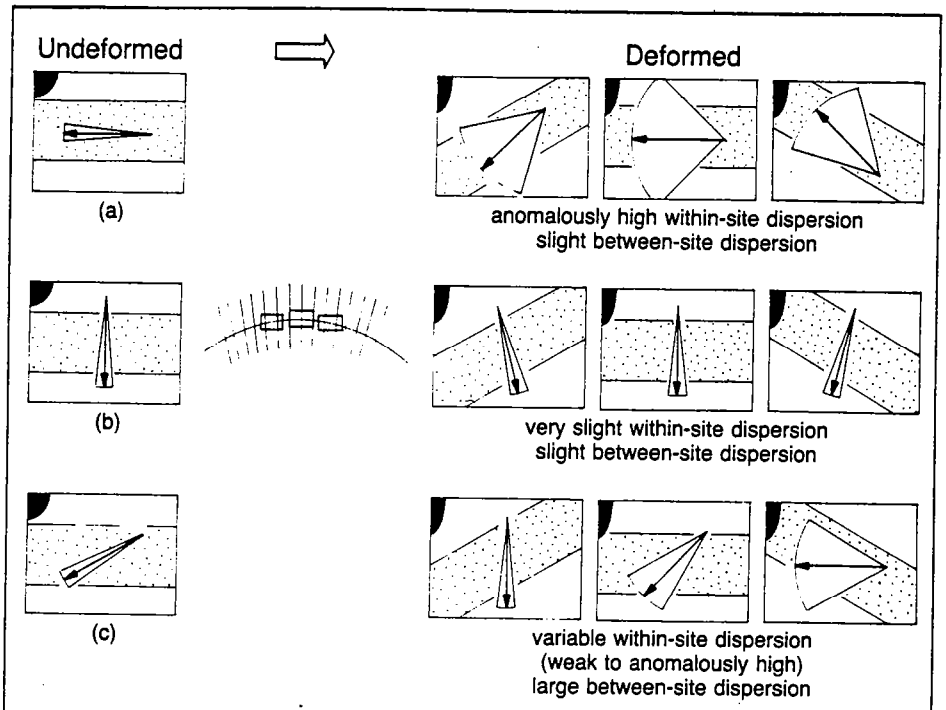

Fig. 1. Schematic drawing of two-dimensional characteristics of paleomagnetic vectors distributions resulting from gently folding rock units with cleavage development. Examples are given for different initial angular relationships between mean paleomagnetic direction, bedding plane, and strain axes. The direction of the paleomagnetic vectors is assumed to be perpendicular to the fold axis. These sketches result from observations of naturally deformed series and from numerical and analog simulations. Cases illustrated in (*a*) and (*c*) find their analogy in the Alpes-Maritimes redbeds [*Cogné and Perroud,* 1985], while the case in (*b*) is found in the Pont-Rean formation redbeds [*Cogné et al.,* 1986].

found between mineral fabrics and finite strain [*Tullis and Wood,* 1975; *Siddans,* 1976; *Wood and Oertel,* 1980; *Miller and Christie,* 1981; *Gapais and Brun,* 1981], its practical application and interpretation are rather difficult. On the other hand, the AMS technique provides a rapid means of estimating the degree of preferred orientation of magnetic minerals. The magnetic fabric of a rock is mathematically expressed by a second-order symmetrical Cartesian tensor, analogous to the strain tensor. A large body of literature shows that these two tensors are related, in the direction of their axes and in the magnitude of their principal values, in several rock types from different deformed regions [*Wood et al.,* 1976; *Rathore,* 1979, 1980; *Kligfield et al.,* 1981, 1983; *Hrouda,* 1982; and others]. However, the quantitative relationships between the magnitudes of strain and AMS principal axes must be established for every rock type, and a minimum amount of classical strain markers is generally needed. Nevertheless, a systematic check of the strain state by the AMS method is desirable when performing paleomagnetic studies in folded rocks within orogenic belts.

For the studies summarized above, it seems that there is a consensus about the effect of homogeneous strain upon the remanent magnetization. This can be described as one dominant phenomenon, the deviation of the magnetization vector of a given rock volume from its original direction toward the flattening plane or away from the shortening axis. This is described by analog models [*Blow and Hamilton,* 1979; *Ozima,* 1980; *Morash and Bonhommet,* 1981] and by numerical models and simulations [*Rochette,* 1983; *Cogné et al.,* 1986], as well as by studies of natural remanent magnetization in deformed rocks [*Cogné and Perroud,* 1985; *Hirt et al.,* 1986]. It has been shown that this deviation in the redbeds is controlled by the strain rotation of micromoment-bearing hematite platelets [*Cogné et al.,* 1986; *Cogne and Gapais,* 1986]. The problem now is to understand how this phenomenon interferes with the distribution of the magnetic vectors. As this is highly dependent upon the geometrical configuration of the initial magnetization and main axes of deformation, we will try to envision it in several situations in the theoretical case of homogeneous strain. These situations are schematized in Figure 1.

Let us first consider the case, in which the strain-shortening axis is parallel to the initial direction of magnetization. If parallelism is strict, the direction of magnetization theoretically should not be deviated. However, the resultant magnetization in rock samples is the average of population of micromoments that present a natural dispersion. Therefore each micromoment will be deviated by the shortening. If the sampling is adequate, the resultant magnetization will stay unchanged, while the dispersion of micromoments will increase with increasing strain. With this effect, we should theoretically observe a decreasing of the magnetization intensity. In fact, this observation seems difficult to realize in nature, since intensity is monitored primarily by other parameters (magnetic mineralogy, iron oxides concentration, and so on). This strain-induced within-site scattering has been described by *Kligfield et al* [1983] and related to strain intensity by *Cogné and Perroud* [1985] in the case of the Alpes Maritimes redbeds. It is very important to point out that this scattering effect of strain is not a characteristic phenomenon but is specifically a consequence of the particular relationships that exist between

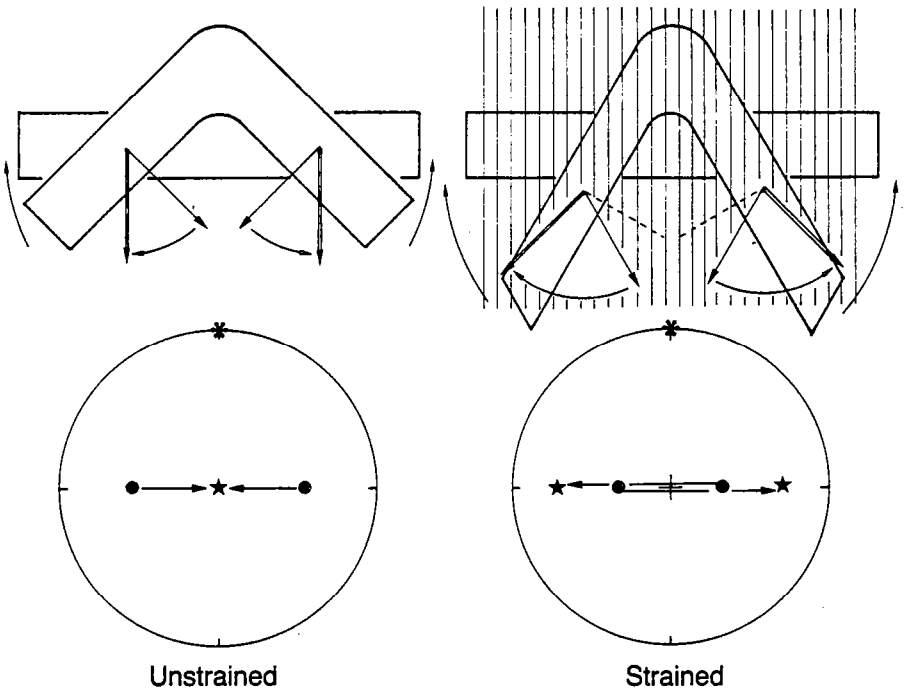

Fig. 2. Schematic illustration of the bypass effect caused when the classical tilt correction is applied to strain beds bearing an initially vertical magnetization. (left) Folding by rigid body rotation. The angular relationship of bedding and magnetization is not altered, and the tilt correction clusters the vectors around their initial direction. (right) The strain induces a rotation of the vectors from their initial tilted attitude (dashed lines) toward the cleavage plane (light vertical lines). During the classical unfolding, the deviated in situ magnetic vectors (single arrows) bypass each other, and the tilt-corrected data (double arrows) can be as scattered as in situ. These situations are shown below in stereoplots as in situ (dots) and tilt corrected (stars); asterisks indicate the fold axes.

the direction of magnetization and the strain-shortening axis in this rock unit.

If we now consider the case in which the pretectonic direction of magnetization is initially parallel to either the intermediate or the maximum elongation axis, the simulations of *Cogné et al.* [1986] suggest not only that the mean magnetization of the site stays unchanged but also that the clustering of the measured vectors should increase. Although the clustering in nature cannot be observed beyond the minimum measurement error range, the directions of magnetization should present a grouping at least as good as that in the same but undeformed rock type. *Cogné et al.* [1986] observed this in the redbeds of the Pont-Rean formation (Brittany, France), where the magnetization is close to the steeply dipping cleavage plane.

From these two extreme cases, it can easily be deduced that intermediate angles between magnetization and strain axes will result in a deflection of the whole magnetization vector population toward the flattening plane and probably toward the elongation axis, with a scattering or a clustering of the population depending upon the "close" or "far" position of initial magnetization with respect to the shortening axis. What "close" and "far" mean exactly is not currently known, and furthermore, a rotating set of vectors can be close to the shortening axis in the first stages of deformation and later can be located far from it.

An important point, common to all these situations, is that if the bedding plane in each site behaves passively [*Cogné and Perroud,* 1985; *Lowrie et al.,* 1986], the strain will induce a rotation of this plane independently from the strain-induced rotation of the magnetic vectors. Therefore, in the general case, strain alters the angular relationships of bedding plane and magnetization, leading to inconclusive results in the classical fold test [*Graham,* 1949]. This was described first by *Van den Ende* [1978] and later by *Kligfield et al.* [1983] in the Permian Alpes-Maritimes red slates. Later authors found that the tilt-corrected remanent vectors lie on a great circle. In the same series, *Cogné and Perroud* [1985] show that the mean paleomagnetic direction from the two limbs of a fold bypass each other along this great circle during the classical tilt correction. This situation, which is generally considered to be characteristic of a syn-folding age of magnetization acquisition, has been shown here to be purely an effect of strain upon the pretectonic magnetization. This particular effect on the between-site distributions is illustrated in Figure 2. Note that in this figure, the fold axis is perpendicular to the initial direction of magnetization, an attitude that induces a great circle distribution of the tilt-corrected data from the strained beds (shown by the stars in the stereoplot, Figure 2). This distribution, which has been noted by *Kligfield et al.* [1983] in the Alpes-Maritimes redbeds (in which such a situation exists), is thus shown to arise from the particular angular relationships between magnetization and fold axis. However, the classically tilt-corrected vectors of strained beds cannot be expected to lie on a great circle in the general case. Another illustration of the strain-induced angular modification of magnetization with respect to the bedding appears in the Pont-Rean redbeds [*Cogné et al.,* 1986]. In these beds, the mean site directions are clustered more closely before the classical tilt correction than after, although the uncor-

rected mean paleomagnetic direction has no younger equivalent and cannot be interpreted as a remagnetization.

Is a Correction for Strain Possible?

From the analysis presented above, one can see that the effect of homogeneous plastic strain upon magnetization in hematite-bearing sediments can be described as a single phenomenon. The logical consequences of this phenomenon upon the distribution of paleomagnetic vectors can be envisioned as relationships between strain directions and initial mean paleomagnetic directions. We have shown here that the theoretically expected behavior of magnetization fits quite well with the small number of case histories in the literature, both in cases of naturally deformed series and in models and simulations. Since the magnetization distributions can be analyzed in the terms of a single mechanism, we can now ask whether it is possible, in our state of knowledge of this problem, to propose a correction of the paleomagnetic vectors for the effects of strain.

In our own paleomagnetic analysis of the Alpes-Maritimes redbeds, we have shown that the distribution of the observed magnetic vectors is globally similar to the effects that the strain would have on passive vectors. We therefore proposed to treat them as passive vectors, and we described a strain removal technique based upon the passive behavior concept [*Cogné et al.*, 1982; *Cogné and Perroud*, 1985]. As noted above, this method was successful at several levels: It reduced the strain-induced within-site dispersions, reduced the between-site dispersion after the tilt correction from the undeformed bedding plane, and recovered a mean paleomagnetism direction compatible with the one expected from the paleomagnetic reference pole.

This demonstration has been strongly criticized by *Kligfield et al.* [1983] and *Lowrie et al.* [1986]. Their main points are that inverse strain inevitably moves passive vectors toward the shortening Z axis of the strain and that this results in a clustering of the corrected paleomagnetic directions around the shortening axis. They conclude that the mean direction obtained loses its paleomagnetic significance because it mainly reflects the mean strain Z axis direction. We cannot agree with this argument. First, it seems well established that strain induces a deflection of the magnetization away from the Z axis. Therefore, whatever the unstraining method used, it should necessarily induce a rotation of magnetization towards this axis. Second, in the case of the Alpes-Maritimes, the directions of magnetization cluster around the site Z axis because in most sites, they were initially distributed around this direction. It can be shown that even if we do not correct the directions for strain, their within-site mean is close to the Z axis. A third point is that the shortening direction is roughly constant over the entire folded area. Therefore, if one considers that unstrained paleomagnetic vectors are the Z axis in each site, their between-site distribution should be grouped more completely before any tilt correction than after. Such behavior was not observed, but in contrast, we obtained a significant clustering of the mean site direction after the last step of the treatment, i.e., tilt correction from the unstrained bedding plane.

It is thus shown that the clustering effect of the strain removal technique is specifically due to the particular relationships between strain axes and pretectonic paleomagnetic direction in the case of the Alpes-Maritimes redbeds. It should furthermore be noted that this effect does not exist when this special angular relationship is not met (for example, see site P3 of *Cogné and Perroud* [1985] and the preliminary results obtained by *Cogné et al.* [1986] in the Pont-Rean redbeds formation). Therefore we strongly stress that the clustering in itself cannot be considered as a proof of the invalidity of the strain removal technique.

Nevertheless, we agree that although the strain removal technique appears basically correct in its principle, it is probably an approximation of the exact correction to be made, and therefore it needs some improvement. Two main issues remain:

- The results of numerical simulations [*Cogné et al.*, 1986] have shown that the deviations of magnetization toward the flattening plane, although large, may be not exactly equal to passive line deviations. However, it is not possible at present to state the consequences of this discrepancy categorically for the magnetization deviations within naturally deformed rocks.
- The second critical point is the accuracy with which the total deformation at each site is determined. As a matter of fact, the proposed strain removal technique is applied at a site scale (where strain is homogeneous), that is, in discrete points within an inhomogeneously deformed region. The compatibility between undeformed sites through the whole study area is thus not verified and cannot be used as a control on the undeformed state. In particular, the rigid body rotation within a site, which is estimated from the tilt of the undeformed bedding plane, is not fully constrained for the rotations about vertical axes. This problem is at the same level as the problem of improving the simple tilt correction of *Graham* [1949] to take complex fold geometries into account.

Conclusion

We can draw the following conclusions:

- Pretectonic remanent magnetization directions are deviated by strain. This implies that in strained rock units, the classical unfolding methods cannot be used as tests for the relative age of folding and magnetization acquisition.
- In deformed redbeds, the effects of strain-induced hematite rotations upon remanent magnetization have been globally characterized.
- The conclusion just mentioned allows us to propose a strain removal technique based upon the approximation that magnetizations behave as passive lines during deformation.
- It is only with new paleomagnetic investigations within strained regions that the limitations of this technique can be stated and improvements achieved. For now, the results obtained by using this technique lead us to consider it as an efficient approximation for recovering magnetization directions in moderately strained rock units.

References

Blow, R. A., and M. Hamilton, Effect of compaction on the acquisition of a detrital re-

manent magnetization in fine-grained sediments, *Geophys. J. R. Astron. Soc., 52,* 13, 1978.

Bonhommet, H., P. R. Cobbold, H. Perroud, and H. Richardson, Paleomagnetism and cross-folding in a key area of the Asturian arc (Spain), *J. Geophys. Res., 86,* 1873, 1981.

Cogné, J. P., Pretectonic direction of magnetization recovered by strain removal: The example of a fold in red sediments of the Alpes-Maritimes (France)(abstract), *Terra Cognita, 3,* 107, 1983.

Cogné, J. P., and H. Perroud, Strain removal applied to paleomagnetic direction in an orogenic belt: The Permian red slates of the Alpes Maritimes, France, *Earth Planet. Sci. Lett., 72,* 125, 1985.

Cogné, J. P., and D. Gapais, Passive rotation of hematite during deformation: A comparison of simulated and natural redbeds fabrics, *Tectonophysics, 121,* 365, 1986.

Cogné, J. P., N. Bonhommet, and P. R. Cobbold, Pretectonic magnetization obtained by strain removal (abstract), *Eos* Trans. AGU, 63, 51, 1982.

Cogné, J. P., H. Perroud, M. P. Texier, and N. Bonhommet, Strain reorientation of hematite and its bearing upon remanent magnetization, *Tectonics, 5,* 753, 1986.

Courtillot, V., P. Chambon, J. P. Brun, and P. Rochette, A magnetotectonic study of the Hercynian Montagne Noire, *Tectonics, 5,* 733, 1986.

Facer, R. A., Folding, strain and Graham's fold test in palaeomagnetic investigations, *Geophys. J. R. Astron. Soc., 72,* 165, 1983.

Gapais, D., and J. P. Brun, A comparison of mineral grain fabrics and finite strain in amphibolites from Eastern Finland, *Can. J. Earth Sci., 18,* 6, 995, 1981.

Graham, J. W., The stability and significance of magnetism in sedimentary rocks, *J. Geophys. Res., 54,* 131, 1949.

Graham, R. H., Quantitative deformation studies in the Permian rocks of the Alpes Maritimes, *Mem. BRGM, 91,* 219, 1978.

Hirt, A. M., W. Lowrie, and O. A. Pfiffner, A paleomagnetic study of tectonically deformed red beds of the Lower Glarus Nappe Complex, Eastern Switzerland, *Tectonics, 5,* 723, 1986.

Hrouda, F., Magnetic anisotropy of rocks and its application in geology and geophysics, *Geophys. Surv., 5,* 37, 1982.

Kligfield, R., W. H. Owens, and W. Lowrie, Magnetic susceptibility anisotropy, strain, and progressive deformation in permian sediments from the Maritim Alps (France), *Earth Planet. Sci. Lett., 55,* 181, 1981.

Kligfield, R., W. Lowrie, A. M. Hirt, and A. W. B. Siddans, Effect of progressive deformation on remanent magnetization of Permian redbeds from the Alpes Maritimes (France), *Tectonophysics, 97,* 59, 1983.

Kodama, K. P., and A. Cox, The effect of a constant volume deformation on the magnetization of an artificial sediment, *Earth Planet. Sci. Lett., 38,* 436, 1978.

Lowrie, W., and R. Kligfield, Effect of progressive deformation on the remanent magnetization of redbeds (abstract), *Eos* Trans. AGU, 62, 273, 1981.

Lowrie, W., A. M. Hirt, and R. Kligfield, Effects of tectonic deformation on the remanent magnetization of rocks, *Tectonics, 5,* 713, 1986.

McDonald, W. D., Net tectonic rotation, apparent tectonic rotation, and the structural tilt correction in paleomagnetic studies, *J. Geophys. Res., 85,* 3659, 1980.

March, A., Mathematische Theorie der Regelung nach der Korngestalt bei Affiner Deformation, *Z. Kristallogr., 81,* 285, 1932.

Means, W. D., *Stress and Strain,* Springer Verlag, New York, 1976.

Miller, D., and J. Christie, Comparison of quartz microfabric with strain in recrystallized quartzite, *J. Struct. Geol., 3,* 129, 1981.

Morash, A., and N. Bonhommet, Deviation of I.R.M. during simple shortening experiments, paper presented at the Fourth Scientific Assembly, Int. Assoc. Geomag. and Aeron., Edinburgh, U.K., 1981.

Ozima, M., Effects of a plastic deformation on the remanent magnetization of a Cu-Co alloy, *Earth Planet. Sci. Lett., 47,* 121, 1980.

Perroud, H., and P. R. Cobbold, L'aimantation rémanente comme marqueur de la déformation: Exemple d'un pli à axe incliné dans les séries rouges siluro dévoniennes à Cabrillanes, Asturies, *Bull. Soc. Geol. France, 26,* 169, 1984.

Ramsay, J. G., *Folding and Fracturing of Rocks,* McGraw-Hill, New York, 1967.

Ramsay, J. G., and M. I. Huber, *The Technique of Modern Structural Geology,* vol. 1, *Strain Analysis,* Academic, New York, 1983.

Rathore, J. S., Magnetic susceptibility anisotropy in the Cambrian slate belt of North Wales and correlation with strain, *Tectonophysics, 24,* 115, 1979.

Rathore, J. S., The magnetic fabric of some slates from the Borrowdale volcanic group in the English Lake District and their correlation with strain, *Tectonophysics, 67,* 207, 1980.

Rochette, P., Propriété magnétiques et déformation dans des roches sédimentaires alpines: Application au Dogger de la zone dauphinoise, 3rd cycle thesis, Univ. de Grenoble, Grenoble, France, 1983.

Siddans, A. W. B., Deformed rocks and their textures, *Philos. Trans. R. Soc. London Ser. A, 283,* 43, 1976.

Tarling, D. H., *Principles and Applications of Palaeomagnetism,* Chapman and Hall, New York, 1971.

Tullis, T., and D. Wood, Correlation of finite strain from both reduction bodies and preferred orientation of mica in slates from Wales, *Geol. Soc. Am. Bull., 86,* 632, 1975.

Van den Ende, C., Palaeomagnetism of Permian red beds of the Dome de Barrot (S. France), thesis, Rijksuniv. Utrecht, Utrecht, the Netherlands, 1977.

Van der Voo, R., and J. E. T. Channel, Paleomagnetism in Orogenic belts, *Rev. Geophys., 18,* 455, 1980.

Wood, D., and G. Oertel, Deformation in the Cambrian slate belt of Wales, *J. Geol., 88,* 285, 1980.

Wood, D. S., G. Oertel, J. Singh, and H. F. Bennett, Strain and anisotropy in rocks, *Philos. Trans. R. Soc. London Ser. A, 283,* 27, 1976.

Jean-Pascal Cogné *received his DEA degree in structural geology (1981) and his Doctorat es-Sciences (1987) from the University of Rennes. He is with the university's Laboratory of Geophysics.*

Hervé Perroud, *a senior researcher at the French National Agency for Scientific Research (Centre National de la Recherche Scientifique), received his DEA degree in geophysics (1978) and his Doctorat es-Sciences (1985) from the University of Rennes. He is currently on leave to work with the petroleum industry on programing supercomputers.*

Dans la même collection :

N°1 - H. MARTIN - Nature, origine et évolution d'un segment de croûte continentale archéenne : contraintes chimiques et isotopiques. Exemple de la Finlande orientale. 392 p., 183 fig., 51 tabl., 4 pl. (1985). 140F.

N°2 - G. QUERRE - Palingenèse de la croûte continentale à l' archéen : les granitoïdes tardifs (2,5-2,4 Ga) de Finlande Orientale. Pétrologie et géochimie. 226 p., 74 fig., 41 tabl., 3 pl.(1985). 85F.

N°3 - J. DURAND - Le Grès Armoricain. Sédimentologie. Traces fossiles. Milieux de dépôt. 150 p., 76 fig., 9 tabl., 19 pl. (1985). 55F.

N°4 - D. PRIOUR - Genèse des zones de cisaillement : Application de la méthode des éléments finis à la simulation numérique de la déformation des roches. 157 p., 106 fig., 7 tabl., (1985). 55F.

N°5 - V. NGAKO - Evolution métamorphique et structurale de la bordure sud-ouest de la "série de Poli". Segment camerounais de la chaîne panafricaine. 185 p., 76 fig., 16 tabl., 12 pl. (1986). 70F.

N°6 - J. DE POULPIQUET - Etude géophysique d'un marqueur magnétique situé sur la marge continentale sud-armoricaine. 159 p., 121 fig., 5 tabl. (1986). 55F.

N°7 - P. BARBEY - Signification géodynamique des domaines granulitiques. La ceinture des granulites de Laponie : une suture de collision continentale d'âge Protérozoïque inférieur (1.9-2.4 Ga). 324 p., 89 fig., 46 tabl., 11 pl. (1986). 115F.

N°8 - Ph. DAVY - Modélisation thermo-mécanique de la collision continentale. **233 p., 72 fig., 2 tabl. (1986). 95F.**

N°9 - Y. GEORGET - Nature et origine des granites peralumineux à cordiérite et des roches associées. Exemples des granitoïdes du Massif Armoricain (France) : Pétrologie et géochimie. **250 p., 140 fig., 67 tabl., (1986). 100F.**

N°10 - D. MARQUER - Transfert de matière et déformation progressive des granitoïdes. Exemple des massifs de l'Aar et du Gothard (Alpes centrales Suisses). **287 p., 134 fig., 52 tabl., 5 cartes hors-texte (1987). 120F.**

N°11 - J.S. SALIS -Variation séculaire du champ magnétique terrestre. Direction et Paléointensité sur la période 7.000 - 70.000 BP dans la chaîne des Puys. **190 p., 73 fig., 28 tabl., 1 carte hors-texte (1987). 90F.**

N°12 - Y. GERARD - Etude expérimentale des interactions entre déformation et transformation de phase. Exemple de la transition calcite-aragonite. **126 p., 42 fig., 3 tabl., 10 pl. (1987). 75F.**

N°13 - H. TATTEVIN - Déformation et transformation de phases induites par ondes de choc dans les silicates. Caractérisation par la microscopie électronique en transmission. **150 p., 50 fig., 1 tabl., 13 pl. (1987). 95F.**

N°14 - J.L. PAQUETTE - Comportement des systèmes isotopiques U-Pb et Sm-Nd dans le métamorphisme éclogitique. Chaîne Hercynienne et chaîne Alpine. **190 p., 88 fig., 39 tab., 2 pl. (1987). 95F.**

N°15 - B. VENDEVILLE - Champs de failles et tectonique en extension : modélisation expérimentale. **392 p., 181 fig., 1 tabl., 82 pl. (1987). 265F.**

N°16 - E. TAILLEBOIS - Cadre géologique des indices sulfurés à Zn, Pb, Cu, Fe du secteur de Gouézec-St-Thois : Dévono-Carbonifère du flanc Sud du Bassin de Châteaulin (Finistère). 195 p., 64 fig., 41 tabl., 8 pl. photo., 8 pl. h.texte. (1987).
110F.

N°17 - J.P. COGNE - Contribution à l'étude paléomagnétique des roches déformées. 204 p., 86 fig., 17 tabl., (1987).
90F.

BON DE COMMANDE

A retourner à :

Centre Armoricain d'Etude Structurale des Socles
Mémoires et documents du CAESS
Université de Rennes I - Campus de Beaulieu
35042 - RENNES Cédex (France).

NOM .....

ORGANISME .....

ADRESSE .....

Veuillez me faire parvenir les ouvrages suivants :

N°	Auteur	Nb Exemplaires	Prix Unitaire	TOTAL

Frais d'envoi :
1 volume : 15,00 F.

Total	
Frais d'envoi	
Montant total	

Veuillez établir votre chèque au nom de l'Agent Comptable de l'Université de Rennes I et le joindre au bon de commande.

Imprimé au CAESS

Dépot Légal

4 éme trimestre 1987

RESUME.

L'ensemble des travaux rassemblés dans ce mémoire constitue un essai de caractérisation des effets de la déformation interne sur l'aimantation rémanente des roches. Bien que le champ des investigations paléomagnétiques ait été récemment étendu aux zones déformées des plaques continentales, de tels effets sont actuellement mal connus. L'étude détaillée des relations entre aimantation et déformation interne apparait par conséquent nécessaire, dans le cadre du développement des méthodologies du paléomagnétisme en zone orogénique. Les principaux résultats obtenus sont les suivants :

- L'étude de la déformation interne, de l'anisotropie de susceptibilité magnétique (AMS) et du paléomagnétisme du granite de Flamanville (Normandie, France), montre que la déformation, liée à la mise en place du granite, controle le développement d'une forte fabrique magnétique. L'AMS, due à une orientation préférentielle de grains allongés de magnétite polydomaine, est accompagnée par une anisotropie d'acquisition de l'aimantation thermorémanente (ATR) du matériau déformé. Une relation quadratique simple a été établie entre ces 2 tenseurs. Cette relation, vérifiée par des tests expérimentaux, a été appliquée au cas du granite de Flamanville: le tenseur inverse d'anisotropie d'ATR, estimé par la mesure de l'AMS, permet de corriger les déviations de l'ATR, et de déterminer une direction de champ magnétique fiable.

- Le problème des effets d'une déformation interne postérieure à l'acquisition d'une aimantation a été abordé par le biais de simulations analogiques et numériques, et d'études paléomagnétiques de 3 formations rouges déformées (Alpes-Maritimes, Pyrénées, Bretagne). Il est montré que la rotation des porteurs magnétiques, induite par la déformation interne, et traduite par le développement de fabriques cristallographiques et magnétiques, produit une rotation de l'aimantation rémanente (à l'échelle du specimen mesurable) depuis sa direction initiale vers le plan d'aplatissement de la déformation. A partir de cette description, l'évolution de populations de vecteurs à l'échelle d'un site de déformation homogène peut etre prédite, en fonction des relations angulaires entre direction moyenne initiale de l'aimantation et directions principales de déformation. A l'échelle de la série plissée, la modification des relations angulaires aimantation/plan de stratification induit des anomalies de comportement vis-à-vis du test de pli.

- Il est finalement montré que les déviations de l'aimantation, dans les modèles et dans les séries rouges étudiées, sont proches des déviations de lignes matérielles suivant le modèle de March (1932). Il apparait donc possible d'effectuer une déformation inverse de l'aimantation, dans le but de déterminer la direction d'aimantation antétectonique à l'état non déformé.

Bien que tous les problèmes posés par la déformation interne en paléomagnétisme ne soient pas résolus, l'aspect positif des résultats obtenus ici permet d'envisager l'extension des investigations paléomagnétiques vers les zones modérément déformées des chaines de montagnes.

MOTS-CLES.

Paléomagnétisme, Déformation Interne, Anisotropie de Susceptibilité Magnétique, Anisotropie d'Aimantation Thermorémanente, Modèles, Déformation Inverse, Séries Rouges, Granite.

Editions du C.A.E.S.S.
Université de Rennes I
F-35042 RENNES Cedex